AN EVALUATION OF REMOTELY SENSED IMAGERY AS A DATA SOURCE FOR HYDROLOGICAL INFORMATION

Martin Jonathan France

Master of Philosophy

THE UNIVERSITY OF ASTON IN BIRMINGHAM

June 1991

The University of Aston in Birmingham

AN EVALUATION OF REMOTELY SENSED IMAGERY AS A DATA SOURCE FOR HYDROLOGICAL INFORMATION

Martin Jonathan France

Master of Philosophy

1991

In the field of hydrology, with increasing opportunities afforded by remote sensing for assessing and monitoring various components of the hydrological cycle it is important to recognise the current capabilities and appropriate applications of remotely sensed data. This thesis examines the use of Landsat MSS, Landsat TM and Panchromatic Aerial Photography at 1:50000 scale for their accuracy in delineating, mapping and measuring, morphometric parameters and landcover.

A review of morphometric parameters is presented, including the application of remotely sensed imagery for their assessment. The use of remotely sensed data in hydrological modelling is discussed. Technical details of each type of imagery are given. A sequence of image enhancement techniques is applied to both the Landsat TM and Landsat MSS data to evaluate optimal image enhancements for drainage network delineation and landcover discrimination.

Supervised and unsupervised automatic classification procedures are applied to the digital data for landcover classification. Different visual interpretation techniques are compared for drainage network and landcover interpretation.

Landsat TM is seen to exhibit considerable advantage over Landsat MSS for the interpretation of drainage networks. High correlation is found between Landsat TM catchment area interpretations and those derived from a 1:50000 scale map of the area. Basin length and mainstream length parameters also show correlation. Similar results are obtained for the aerial photography. A minimum catchment size of $30km^2$ is suggested for Landsat TM imagery, and a minimum lake size of 0.6ha. Broad landcover classifications using visual and automatic classification methods, and also by different interpreters, are seen to be in general agreement.

The important role of Geographic Information Systems and Digital Elevation Models (DEM's) in hydrology is discussed. A DEM is created for the research area and a classified Landsat TM image is vectorised and stored together with other data in a GIS.

Key phrases: Remote Sensing, Hydrology, Geographic Information Systems, Morphometric parameters, Landcover classification.

This thesis is dedicated to

Dr. W. Gordon Collins

without whose encouragement and support none of
this research would have been possible.

ACKNOWLEDGEMENTS

Firstly I would like to thank Dr. W.G. Collins, known by members of the Remote Sensing Unit with respect and affection as "The Doc". With his encouragement, inspirational optimism and the provision of various means of funding for three years, before receiving official funding, I was able to embark on this research. I am also very grateful for the opportunity to attend conferences in Florida, Holland and Kenya along with many other meetings and conferences in the U.K., which together provided a broad view of the remote sensing world.

I would also like to express sincere thanks to my supervisor Dr. Peter Hedges of the Civil Engineering Department, who has shown great patience during the protracted completion of my thesis.

My early image processing work was undertaken at various establishments due to a lack of facilities at Aston at the time. In this connection I would like to thank George and Pam Vass of NRSC, RAE, Farnborough; Alan Belward of Silsoe College, Bedford; Dave Williams and Angela Morrison of NERC, Swindon for their helpfulness. Thanks should also go to the Overseas Devlopment Administration for funding the image processing at Silsoe College.

I am grateful to Steve Dury and Martin Smith of the Remote Sensing Unit, Aston University, for their help respectively with field work and aerial photographic interpretation. Thanks must also go to Jez Halse for his assistance during field work.

I would like to thank the Hydrology and Water Management Working Group of the National Remote Sensing Centre for providing funding for this research.

I am thankful for the use of image processing and GIS facilities whilst working at Telespazio, Rome for which I thank Marcello Riccotilli. I am very grateful to the many friends and colleagues who made my stay in Italy such a pleasant one and would like to thank Pierluigi Adami, Fabrizio Pauri, Massimo Antoninetti, Marc Staljannsens, Raja Refk, Guido Boarelli, Achille Ciappa, Pasquale Lanciano, Anna Rita Gentile and Jim Wiggins amongst many others. In particular, I would like to thank Claudio Carboni for his assistance with data transfer from I^2S System 600 to ARC/INFO.

Since returning to the UK I have been able to pursue my research at the Institute of Hydrology in an environment with a wealth of hydrological knowledge and experience. I am grateful for the help and advice offered by several members of the staff. I would like to thank Rick Neale of NERC Computer Services for enabling the continuation of this work. A special thanks to Jan Norduijn for assistance with the statistical analysis of results.

My parents, brothers, relatives and friends, Ivan Filby in particular, deserve thanks for their encouragement and understanding over the course of this research. Finally, I am indebted to my wife Liza Mae, who has shown immense patience and provided endless encouragement and loving support during the past year as she adjusts to a foreign environment. I am also grateful for her help with some diagrams and typing.

CONTENTS

		Page
Title page		1
Summary		2
Dedication		3
Acknowledgements		4
List of Figures		12
List of Tables		22
Chapter 1	**INTRODUCTION**	27
Chapter 2	**PREVIOUS RELATED WORK IN REMOTE SENSING AND HYDROLOGY**	34
	2.1 General overview	34
	2.2 Morphometry	42
	2.3 Previous work on remote sensing and morphometry	58
	2.4 Previous work on remote sensing and hydrological modelling	65
	2.5 Summary	73
Chapter 3	**THE STUDY AREA**	76
	3.1 Introduction	76
	3.2 Physiography	80
	3.3 Geology	85
	3.4 Soil types	89
	3.5 Landcover	97

		Page
	3.6 Climate	101
	3.7 Field Survey	103
	3.8 Summary	105
Chapter 4	**DETAILS OF IMAGERY**	107
	4.1 Introduction	107
	4.2 The significance of historical remote sensing	107
	4.3 The physical basis of remote sensing	109
	4.4 Panchromatic aerial photography	112
	4.5 Landsat Multispectral Scanner (MSS) imagery	118
	4.6 Landsat Thematic Mapper (TM) imagery	123
	4.7 Summary of data types	130
Chapter 5	**IMAGE PROCESSING AND ENHANCEMENT**	132
	5.1 Introduction	132
	5.2 Image preprocessing	135
	5.2.1 Introduction	135
	5.2.2 Geometric correction	136
	5.2.3 Atmospheric correction	142
	5.3 Image enhancement	143
	5.3.1 Band selection	143
	5.3.2 Contrast enhancement (stretching)	150
	5.3.3 Density slicing	158

Page

5.3.4 Band ratios 160

5.3.5 Vegetation indices 163

5.3.6 Kauth Thomas or Tasselled Cap Transformation 164

5.3.7 Principal Components Analysis (PCA) 165

5.3.8 HSI colour space 166

5.3.9 Perspective view 167

5.3.10 Spatial filtering 168

5.4 Summary 174

5.5 Problems of image hardcopy consistency 176

Chapter 6 **AUTOMATIC CLASSIFICATION** 179

6.1 Introduction 179

6.2 Supervised classification 181

6.2.1 Training data 181

6.2.2 Classification methods 192

6.2.3 Smoothing 198

6.2.4 Geometric correction 200

6.2.5 Supervised classification of Landsat MSS data 201

6.3 Unsupervised classification 207

6.4 Summary 211

		Page
Chapter 7	**IMAGE INTERPRETATION AND DATA EXTRACTION**	213
	7.1 Introduction	213
	7.2 Aerial photography	214
	7.3 Colour transparencies of Landsat MSS and Landsat TM imagery	223
	7.3.1 Landsat MSS imagery	224
	7.3.2 Landsat TM imagery	226
	7.4 "On screen" image interpreation	230
	7.5 1:50000 & 1:250000 Ordnance Survey sheets	237
	7.6 Summary	240
Chapter 8	**QUANTITATIVE RESULTS AND ANALYSIS**	242
	8.1 Introduction	242
	8.2 Morphometric details of the hydrological features	243
	8.2.1 Drainage network details for the main research area	243
	8.2.2 Drainage network ordering	255
	8.2.3 Catchment specific drainage network details	263
	8.2.4 Areal morphometric parameters	269
	8.3 Landcover information	277
	8.4 Classification accuracy	281
	8.5 Identification of small lakes using Landsat TM imagery	287

Page

8.6 Summary 290

Chapter 9 **THE USE OF GEOGRAPHICAL INFORMATION SYSTEMS** 295

9.1 Introduction 295

9.2 Hydrology and GIS 296

9.3 Creation of a Digital Elevation Model (DEM) 299

9.4 Soil and vegetation types 303

9.5 Satellite derived landcover classes 306

9.6 Summary 308

Chapter 10 **DISCUSSION, CONCLUSIONS AND RECOMMENDATIONS** 309

10.1 Discussion 309

10.2 Conclusions 313

10.3 Recommendations and future possibilities 316

REFERENCES 318

Appendix A Remote sensing parameter requirements for hydrology 337

Appendix B Sample Landsat Processing data 341

Appendix C Geocorrection Statistics 342

Appendix D Landsat TM and Landsat MSS data statistics 344

LIST OF FIGURES

		Page
Figure 2.1a	A conceptual overview of the hydrological cycle	37
Figure 2.1b	An engineering view of the hydrological cycle	38
Figure 2.2	Ordering systems	45
Figure 2.3	Variation of stream network depiction with Ordnance Survey map scale (Midford Brook, tributary of the Bristol Avon)	56
Figure 3.1	General location of the research area using a Landsat TM image	77
Figure 3.2	Extent of main research area with coordinates in British National Grid values	78
Figure 3.3	Physical features of the district around Harlech	82
Figure 3.4	Digital Elevation Model (DEM) of the research area with 2.7x vertical exaggeration, viewed from 195° with an elevation of 35°	83
Figure 3.5	Main types of drainage pattern	84
Figure 3.6	The major geological divisions of the research area, with an overlay showing the main structural features	87
Figure 3.7	Relationships of relief, hydrology and soils	92

		Page
Figure 3.8	Ground data location map	103
Figure 4.1	Comparison of wavelengths recorded by sensors	108
Figure 4.2	A passive remote sensing system	110
Figure 4.3	The electromagnetic spectrum and generalized atmospheric transmission	111
Figure 4.4	Idealized spectral reflectance curves for vigorous vegetation, soil and water	111
Figure 4.5	The angular difference between vertical, high oblique and low oblique aerial photographs	114
Figure 4.6	Illustration of aerial photographic coverage of an area	115
Figure 4.7	Photographic image displacement caused by relief variation	117
Figure 4.8	Landsat configuration (Landsats 1, 2 and 3)	118
Figure 4.9	Landsat orbital tracks for one day of coverage indicating variations in local time of data acquistion	119
Figure 4.10	Landsat MSS imaging configuration	120
Figure 4.11	Sampling pattern of the Landsat MSS	121
Figure 4.12	Configuration of Landsat's 4 and 5	123

		Page
Figure 4.13	Comparison of Landsat MSS and Landsat TM imagery for the same area; showing the effect of increased spatial resolution	126
Figure 4.14	Landsat ground receiving stations	129
Figure 5.1	Control point creation setup	140
Figure 5.2	Instantaneous field of view (IFOV) based on the amplitude of the Point Spread Function (PSF)	145
Figure 5.3	Zoomed and contrast stretched band 7,6,5 and band 7,5,4 Landsat MSS FCC's for part of the research area	147
Figure 5.4	Band histograms for the "raw" TM data	151
Figure 5.5	Graphical representation of contrast stretching for pixel values in a range 16-191. Values less than 16 are set to 0 and values greater than 191 are set to 255	153
Figure 5.6a	Landsat TM raw data and after stretching. Bands 1,2,3	154
Figure 5.6b	Landsat TM raw data and after stretching. Bands 4,5,7	155
Figure 5.7a	Landsat TM FCC's of band combinations 5,4,1 and 4,5,3 with contrast stretches applied	156
Figure 5.7b	Landsat TM FCC's of band combinations 5,4,3 and 4,3,2 with contrast stretches applied	157

Page

Figure 5.8	Density slices of TM band 4	159
Figure 5.9	Comparison of the 4/3 ratio with contrast stretched band 4	162
Figure 5.10	Perspective view of research area using TM bands 5,4,1 with 3.5x vertical exaggeration	168
Figure 5.11	Typical pattern of a narrow linear water body (stream) on Landsat TM imagery (e.g. band 4)	169
Figure 5.12	Directional gradient masks	171
Figure 5.13	The Laplacian filter	172
Figure 5.14	Image-minus-Laplacian filter	173
Figure 5.15	TM band 5,4,1 FCC without and with Laplacian filtering	174
Figure 6.1	Delineation of training areas on Landsat TM image	182
Figure 6.2	2-band scattergram of bands 4 and 1 of Landsat TM data, showing pixel intensities of the raw data	186
Figure 6.3	Histogram for band 4 of the moorland class training data set	187
Figure 6.4	Maximum likelihood classification using bands 3,4,5,7 with and without filtered training data	195

		Page
Figure 6.5	Graphical representation of statistics after classification using the maximum likelihood classifier	197
Figure 6.6	Pre and Post 3x3 modal filtering	199
Figure 6.7	Initial Landsat MSS supervised classification	203
Figure 6.8	Landsat MSS classification after modification of the water class training data	205
Figure 6.9	Landsat MSS classification after 3x3 modal filtering	206
Figure 6.10	Unsupervised classification for 10 initial classes and after merging to produce the desired output classes	210
Figure 7.1	The interpretoskop arrangement	215
Figure 7.2	Drainage network interpreted from 1:50000 panchromatic aerial photography	219
Figure 7.3	Delineated catchment boundaries	219
Figure 7.4	Landcover interpretation from the 1:50000 panchromatic aerial photographs	222
Figure 7.5	Lamprey box configuration	223
Figure 7.6	Drainage details interpreted from a Landsat MSS band 7,6,5 FCC transparency with 3x3 Laplacian filtering	225

Page

Figure 7.7	Drainage network delineated from Landsat TM transparency of a band 5,4,1 FCC with manual linear stretching and 3x3 Laplacian filtering	227
Figure 7.8	Landsat TM band 5,4,1 FCC with 3x3 Laplacian filtering, showing part of the research area with the drainage network highlighted	231
Figure 7.9	Drainage details interpreted from on screen interpretation of a Landsat TM band 5,4,1 FCC with manual linear stretching and 3x3 Laplacian filtering. Catchment boundary overlay	233
Figure 7.10	Illustration of the image addition principle, showing the moorland/lowland base layer and forestry.	235
Figure 7.11	Colour class map from screen delineation of landcover classes using Landsat TM band 5,4,1 FCC with manual linear contrast stretching	236
Figure 7.12	Drainage details from 1:50000 Ordnance Survey map, with catchment boundary overlay	238
Figure 7.13	Drainage details from 1:250000 Ordnance Survey map	239
Figure 8.1	Comparison of drainge lengths extracted from imagery types	245
Figure 8.2a	Stream interpretation discrepancies between aerial photography and 1:50000 OS map	246

Page

Figure 8.2b	Stream interpretation discrepancies between Landsat TM and 1:50000 OS map	247
Figure 8.3	Discrepancies between Landsat TM drainage network interpretations via Lamprey Box and On Screen methods	249
Figure 8.4	Stream width location map	250
Figure 8.5	Comparison of drainage delineation results from France and Vicary	252
Figure 8.6	Interpretation of drainage networks from Landsat TM colour transparencies and 1:50000 OS map	254
Figure 8.7a	Stream ordering for Landsat TM network derived via the Lamprey Box	256
Figure 8.7b	Stream ordering for aerial photographic derived network	256
Figure 8.7c	Stream ordering for 1:50000 map derived network	257
Figure 8.8	Stream ordering of imagery types using Strahler's ordering scheme	258
Figure 8.9	Bifurcation ratios derived from image interpretation of the drainage networks	259
Figure 8.10	Comparison of France and Vicary's network results	260

Page

Figure 8.11	Comparison of stream order interpretation from Landsat TM imagery	261
Figure 8.12	Comparison of stream order interpretation from 1:50000 OS map	261
Figure 8.13	Illustration of catchments used in analysis	263
Figure 8.14	Regression analysis: Landsat TM v 1:50000 OS map drainage length details for all seven catchments.	265
Figure 8.15	Regression analysis: Landsat TM v 1:50000 OS map drainage length details for all catchments except Mawddach	266
Figure 8.16	Regression analysis: Mainstream lengths of Aerial Photography v 1:50000 OS map details for 5 catchments	267
Figure 8.17	Regression analysis: Basin lengths of Landsat TM v 1:50000 OS map details for all catchments except Mawddach	268
Figure 8.18	Regression analysis: Basin lengths of Aerial Photography v 1:50000 OS map details for 5 catchments	268
Figure 8.19	Regression analysis: Landsat TM v 1:50000 OS map interpreted catchment areas for all 7 catchments	270

		Page
Figure 8.20	Regression analysis: Landsat TM v 1:50000 OS map interpreted catchment areas, excluding Mawddach	271
Figure 8.21	Regression analysis: Aerial photos v 1:50000 OS map interpreted areas for 5 catchments	272
Figure 8.22	Graph of landcover visual interpretation results	278
Figure 8.23	Graph of Landsat TM landcover results	280
Figure 8.24	Robertson's soil derived landcover classification	283
Figure 8.25	Broad landcover classification	284
Figure 8.26	Map of small open water bodies (lakes) for interpretation	288
Figure 9.1	Depiction of GIS as a series of layers	297
Figure 9.2	Contour and spot height information from the 1:50000 OS map	299
Figure 9.3	TIN structure derived for the research area	300
Figure 9.4	Surface interpolation using the TIN to form a DEM	301
Figure 9.5	Categorised slope map of the research area	302
Figure 9.6	Soil types for part of the research area	304

		Page
Figure 9.7	Vegetation classes derived from soil types, for part of the research area	305
Figure 9.8	Polygonised landcover classification	307

LIST OF TABLES

Page

Table 2.1a Spatial resolution requirements for hydrological and water management observations of geomorphic and landcover parameters using remotely sensed data 40

Table 2.1b Accuracy and frequency requirements for remote sensing observations of geomorphic and landcover parameters 41

Table 2.2 Morphometric variables commonly used by hydrologists 44

Table 3.1 Soil Wetness Classes 90

Table 3.2 Relationships of Wetness Class to Field Capacity Days and depth to Slowly Permeable Horizon 93

Table 3.3 Soil types to be found in the research area 94

Table 3.4 Stream width measurements 104

Table 4.1 The wavebands recorded by the Landsat Thematic Mapper on Landsats 4 and 5 125

Table 4.2 Summary of data types 131

Table 5.1a Landsat TM subscene image statistics 148

Table 5.1b Correlation Matrix for the six Landsat TM bands examined 149

		Page
Table 5.2	Image enhancements for visual interpretation	176
Table 6.1	Landsat TM - training data details	183
Table 6.2	Landsat TM research area subscene statistics	184
Table 6.3	Transformed divergence matrix for TM six-band combination	189
Table 6.4	Validation matrix for Bands 3,4,5,7 with a threshold value of 3.0	191
Table 6.5	Results of maximum likelihood classifiaction	193
Table 6.6	Results of maximum likelihood classification with "filtered" training data	197
Table 6.7	Classification statistics after one iteration of a 3x3 modal majority filter	200
Table 6.8	Pre and Post geometrical correction statisitics	201
Table 6.9	Landsat MSS - training data details	202
Table 6.10	Pre and Post 3x3 modal filtering statistics	204
Table 6.11	Results of unsupervised classification	211
Table 8.1	Drainage details extracted from the imagery types	244

		Page
Table 8.2	Stream interpretation discrepancies for Landsat TM imagery	248
Table 8.3	Stream width details of streams identified from Landsat TM imagery	251
Table 8.4	Comparison of drainage delineation results from France and Vicary	252
Table 8.5	Interpretation of drainage networks from Landsat TM colour transparencies and 1:50000 OS Map	253
Table 8.6	Streams orders interpreted from Landsat TM, aerial photos and 1:50000 map	257
Table 8.7	Stream lengths interpreted from Landsat TM, aerial photography and 1:50000 OS Map	264
Table 8.8	Comparison of cathcment areas from Landsat TM imagery and 1:50000 scale OS Map	269
Table 8.9	Drainage densities interpreted from Landsat TM, aerial photography and 1:50000 OS Map	273
Table 8.10	Stream frequencies expressed as segments and junctions interpreted from Landsat TM, aerial photography and 1:50000 OS Map	274
Table 8.11	R_c values derived from Landsat TM, aerial photography and 1:50000 OS Map	275

Page

Table 8.12	R_e values derived from Landsat TM, aerial photography and 1:50000 OS Map	276
Table 8.13	k values derived from Landsat TM, aerial photography and 1:50000 OS Map	276
Table 8.14	Landcover - visual interpretation results	277
Table 8.15	Comparison of Landsat TM landcover classifications	279
Table 8.16	Comparison of Landsat TM and Landsat MSS supervised classification results	281
Table 8.17	Vegetation classification from soil types	282
Table 8.18a	Confusion matrix for Landsat TM on screen classification v soil survey derived landcover classification	285
Table 8.18b	Confusion matrix for Landsat TM supervised classification v soil survey derived landcover classification	285
Table 8.18c	Confusion matrix for Landsat TM unsupervised classification v soil survey derived landcover classification	286

Page

Table 8.18d Confusion matrix for Landsat MSS supervised classification v soil survey derived landcover classification 286

Table 8.19 Identification of small lakes from Landsat TM imagery via Lamprey Box and on screen methods 289

Table 8.20 Identification of small lakes 290

Table 8.21 Summary of morphometric parameter correlations with 1:50000 OS map derived parameters 293

CHAPTER ONE: **INTRODUCTION**

In the field of hydrology, with increasing opportunities afforded by remote sensing for assessing and monitoring various components of the hydrological cycle, it is important to be aware of the current capabilities and appropriate applications of remotely sensed data. This research looks at three of the more widely available remotely sensed data types and examines their potential in assessing drainage basin characteristics.

As early as 1973, one year after the launch of the first earth resources satellite, the US Agency for International Development recognised the possibilities. In a report on Hydrological Potentials in Developing Countries (1973), it emphasised that, "Remote sensing offers a capability for approaching water resources development and management on a rational and integrated basis." With reference to hydrological modelling Ambaruch and Simmons (1973) state that "The models and procedures developed must be capable of predicting the hydrological performance of an ungauged catchment with parameters derived from space or aerial imagery, sparce ground samples, precipitation and evaporation data." More recently, Schultz (1989), writing in the Journal of Hydrology has stressed that the crucial problem in hydrology, in contrast to hydraulics, is that hydrologists almost always have insufficient data to adequately describe a hydrological process with sufficient accuracy. That to overcome this inadequacy hydrologists usually adopt one of the following remedies: a) collection of more, and more reliable conventional data; b) the application of more sophisticated mathematical techniques; and c) use of new acquisition techniques such as remote sensing. Schultz suggests that the last of these approaches shows far more promise than the first two approaches.

Wide-ranging reports covering many aspects of remote sensing in hydrology were produced by Blyth (1981) for the Institute of Hydrology and Farnsworth *et al.* (1984) for UNESCO. These reports provide the reader with a general overview of the possibilities and limitations of remote sensing applications in hydrology. Very recently, Engman and Gurney (1991) have published a book discussing state-of-the-art remote sensing applications in hydrology. Much of the research in hydrology/meteorology using remote sensing involves the assessment of rainfall using satellite and/or ground-based radar techniques. This area of research is not directly addressed in this thesis, though its importance in hydrological modelling must be recognised. Further information can be found in Engman and Gurney's chapter on precipitation.

All the above publications mention the opportunities afforded by remote sensing for assessing drainage basin characteristics. Once quantified to a suitable level of accuracy, these characteristics can provide water resource planners with the information they require on the extent of water bodies, catchment area, landcover and drainage details for the following purposes (Aston University, 1987):

a) recording of water bodies for statutory purposes;

b) estimating volumes of change in water stored in lakes, reservoirs and flood plains;

c) measurement of geomorphic parameters for the determination of flood flows;

d) measurement of geomorphic parameters for inclusion in rainfall-runoff models, in particular drainage details and landcover.

Early work by Rango *et al.* (1975) using satellite imagery from the Landsat MSS had provided good results in areas of high relief. With the improved spatial and spectral resolution offered by the second generation Landsat TM sensor it was thought profitable to investigate its potential for assessing drainage basin characteristics. Recently, Rango (1990) when discussing the measurement of physiographic and basin characteristics using remotely sensed data, remarked on the need for more research on the capabilities of high resolution data sources such as Landsat TM and SPOT. This work helps to address part of that need. Comparison with Landsat MSS imagery and aerial photographic imagery was necessary for the purpose of establishing their relative capabilities.

With these factors in mind a proposal was made, by the author, to the Hydrology and Water Management Working Group of the UK National Remote Sensing Centre, for funding to carry out this work. The proposal was accepted and funding was eventually forthcoming. The research was carried out, and preliminary findings together with work by research colleagues on similar topics were presented in a report by Aston University, Civil Engineering Department (1987), titled "An assessment of satellite and aerial imagery in evaluating water resources and land cover". Other information published in relation to this research can be found in France and Hedges (1986), France *et al.* (1986) and France and Hedges (1988).

This research was aimed at assessing some of the currently available remote sensing data sources and their usefulness for delineating, mapping and measuring:

i) open water bodies;

ii) drainage networks;

iii) catchment areas;

iv) landcover types.

The specific data types examined with these aims were:

i) Landsat Multispectral Scanner (MSS) satellite data;

ii) Landsat Thematic Mapper (TM) satellite data;

iii) panchromatic aerial photography at 1:50000 scale.

iv) drainage details from 1:50000 and 1:250000 scale Ordnance Survey maps (for use as reference data).

Comparative study of imagery types in an area of a developed country where much information on the area already exists in the form of accurate topographic, geological and soil maps, climatalogical data, and in this case some landcover data, allows the performance of accuracy checks on data from remote sensing using conventional data sources. In any given situation it is important to be aware of what data exists, how it can be accessed and its relative importance to the situation under consideration. The thesis also looks at how this data can be used in water resource assessment and hydrological modelling.

In Chapter 2 a review of relevant remote sensing developments and hydrological advances is presented. The chapter commences with an overview of the development of man's understanding hydrological processes. This is followed by a discussion of the requirements of remotely sensed data for the assessment of morphometric and landcover parameters. A review of morphometric parameters and their significance is then given in Section 2.2. Previous work using remotely sensed data to determine morphometric parameters, in particular Landsat MSS, is presented together with a discussion of the findings. The final part of the chapter discusses some of the ideas proposed for using data derived from remotely sensed imagery as inputs to existing and new hydrological models.

Chapter 3 examines the North Wales study area selected for this research. General physical characteristics of the area are outlined and features of an imaging or hydrological significance are highlighted. The chapter is divided into sections covering physiography, geology, soil types, landcover and climate. A final section on field survey discusses and presents details of field surveys carried out in the study area during this research.

The technical details of the imaging systems used in acquiring and storing Landsat MSS data, Landsat TM data and Panchromatic aerial photography are discussed in Chapter 4. This begins with a brief outline of the physical interactions involved in passive remote sensing of objects. A short history of remote sensing developments forms the next part of the chapter. The chapter includes a discussion of the imaging platforms, the imaged wavebands of the elecromagnetic spectrum, data collection, storage and dissemination. Comparsions are made between the imagery types, in particular the Landsat MSS and Landsat TM data.

A thorough examination of image processing and enhancement of the digital satellite data types follows in Chapter 5. This begins with image restoration techniques, including geometric correction. Image band selection criteria are then outlined, followed by sections discussing several enhancement techniques including filtering options. These techniques are all aimed at enhancing the imagery for visual interpretation purposes, in particular for delineating drainage networks and discriminating landcover types. The enhancement procedures concentrate in particular on Landsat TM imagery.

Chapter 6 contains a discussion of the automatic classification of digital satellite data. Again this concentrates on the Landsat TM imagery. Supervised and unsupervised classification theories are presented and the results obtained using these methods are presented.

The visual image interpretation and data extraction techniques used in this research are detailed in Chapter 7. Drainage details, catchment boundaries and landcover classes were delineated from each type of imagery. For the aerial photography, interpretations were carried out using stereoscopic photo-interpretation methods. For the satellite digital data, interpretations were from hard copy colour transparencies or on screen interpretation. Details were also extracted from the 1:50000 and 1:250000 scale Ordnance Survey maps of the area. A sub-section is included on the interpretation of small lakes in the area using Landsat TM imagery.

Quantitative results from the morphometric analysis of the different imagery types, and in some instances by different methodologies, are presented in Chapter 8. Comparisons of interpretation results of Landsat TM imagery by different workers are also made. Landcover classification results from visual and automatic classification are compared and contrasted. An assessment of landcover classification accuracy is also made. The final part of the chapter attempts to define the minimum area of open water consistently identifiable from Landsat TM imagery.

Possibilities for the integration of remotely sensed or remotely sensed derived data with other spatial data, such as a Digital Elevation Model (DEM), within Geographic Information Systems (GIS) are discussed in Chapter 9. The potential for hydrological modelling using these systems is also discussed.

The final chapter, Chapter 10, is a discussion of the results obtained, conclusions which can be drawn from these, a look at the future posibilities and recommendations for further investigation.

CHAPTER TWO: PREVIOUS RELATED WORK IN REMOTE SENSING AND HYDROLOGY

2.1 General Overview

Hydrology and Water Management are key areas of applied science in the current world economy. Remote sensing is a fairly new tool in the field of hydrology which will have a major role in future hydrologic applications (Engman, 1986). It is the bringing together of applied hydrology and remote sensing technology which forms the subject matter for the following discussion.

Hydrology's historical roots are based on ancient observations and man's attempts to manage water for survival. Chow (1964) has broken down the history of hydrology into eight epochs. This is in common with most other descriptions of man's increase in knowledge, typically an exponential curve. In the period of speculation (ancient-1400), Plato, Homer, and Aristotle in Greece; and Lucretius, Seneca, and Pliny in Rome; recognised some form of hydrological cycle. Although these early philosophers and scientists did not have a quantitative understanding of hydrology, a great number of practical hydraulic structures, such as aqueducts and irrigation systems, illustrated man's desire and need to control water resources as a prerequisite for civilisation as we know it.

During the Renaissance, in the Period of Observation (1400-1600), Palissy and Leonardo da Vinci described a hydrologic cycle in which water moved from the oceans to rain on the land and returned to the oceans. Quantitative hydrology probably began during the Period of Measurement (1600-1700) in which scientists such as Perrault, Mariotte, and Halley made measurements of different hydrologic components.

The Period of Experimentation (1700-1800) gave us a long list of familiar names that includes Pitot, Bernoulli, D'Alembert, and Chezy with discoveries that bear their names. According to Chow (1964), the nineteenth century, which he called the Period of Modernisation (1800-1900), saw the establishment of the science of hydrology as we know it. Many significant advances to hydrology were acomplished in that century, especially in the areas of groundwater and surface water. The foray into quantitative hydrology was extended in the Period of Empiricism (1900-1930). A lack of good scientific understanding of hydrology led to the development of a large number of empirical formulas for solving specific problems.

In the Period of Rationalisation (1930-1950) the true gurus of modern hydrology are to be found. People like Sherman, Horton, Theis, Gumbel, Hazen, Bernard and Einstein published their research and developed procedures that are still very much in use today. Horton's ideas on drainage networks and drainage density (Horton 1932, 1945), formed the basis for quantitative/morphometric analysis of drainage basins on which much of this research is founded. Chow's last epoch is the Period of Theorisation (1950 to date, i.e. 1964). Here hydrologists attempted to use theoretical approaches to solve hydrologic problems. This work has provided considerable insight into the complexities of hydrology.

Were this list to be updated to the present , several additional periods could be added, for instance, Engman (1986), has suggested the period of the computer, the period of multidisciplinary research, the period of systems analysis, the period of environmental quality, the period of modelling, the period of stochasticism versus determinism, and perhaps, the period of remote sensing applications. In the author's opinion the latter is as yet in an embryonic phase, apart from weather forecasting and rainfall monitoring.

The drainage basin (catchment), bounded by its drainage divide (watershed or catchment boundary) and subject to surface and sub-surface drainage under gravity forms the logical areal unit for hydrological studies (see Figure 2.1a). In the UK, for example, it was the river basin concept which formed the rationale behind the geographical extents of the Regional Water Authorities (now PLC's), which were set up during the mid 1970's. Each major river basin system can be divided into sub-catchments and these in turn into smaller sub-catchments and so on. Taken to its limit, each minor tributary of any river system has its own catchment area and constitutes a sub-catchment of downstream larger basins. The size of catchments studied will depend on the area and applications under consideration.

The catchment hydrological cycle can be viewed simply as inputs of precipitation being distributed through a series of transfers, leading to outputs of basin channel runoff, evapotranspiration, and deep outflow of groundwater (More, 1969). Figure

2.1a is a schematic representation of this cycle, itself forming part of larger regional and global hydrological cycles. An engineering view of the hydrological cycle is illustrated by Figure 2.1b. This includes the oceanic component for an overview of the complete cycle.

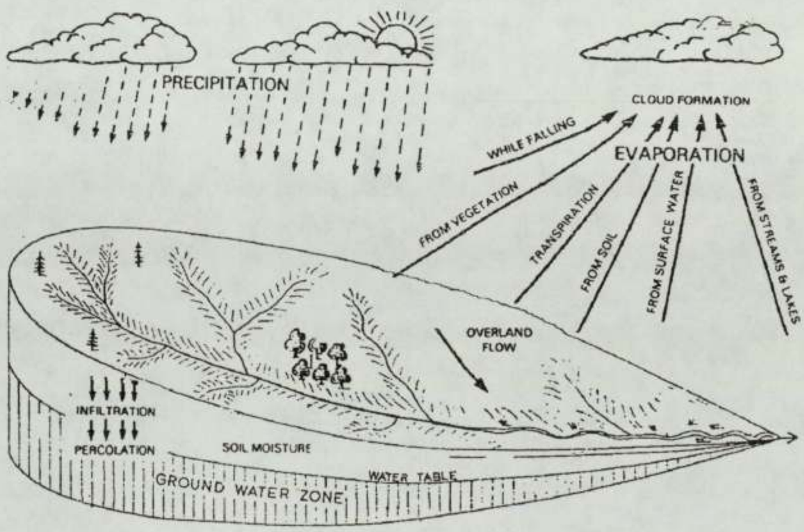

Figure 2.1a A conceptual overview of the hydrological cycle (adapted from More, 1969 and NASA, 1984).

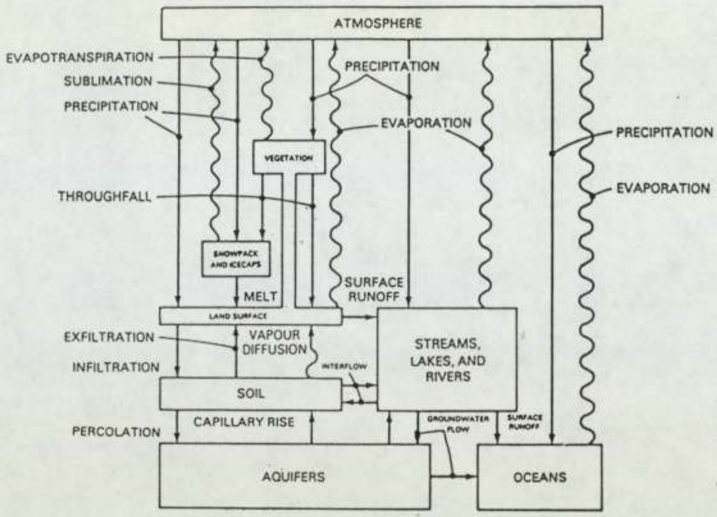

Figure 2.1b An engineering view of the hydrological cycle (after Eagleson, 1970).

The primary hydrological processes which are operationally measured are precipitation, runoff (stage and discharge), water storage, soil moisture and evaporation (Farnsworth *et al*., 1984). Of these processes, the main ones under examination in this research are runoff and water storage. An excellent review of remote sensing applied to the other processes can be found in Engman and Gurney (1991). In their book Engman and Gurney highlight the limitations of conventional hydrological instrumentation (i.e. rain gauges, weirs, etc.). These record point measurements that, in effect, sample a spatial phenomenom. Their usefulness is limited to some undefined area around the point, which may be valid for the particular basin, but in general is not transferable to other basins. Remotely sensed data with its inherent spatial nature lends itself to areal measurements, and the recording of spatial variability.

The estimation of runoff from catchments has been a topic of much research in the past few decades. The debates on runoff modelling practise have yet to be concluded and it is thought by many that remote sensing can provide some of the information required in this debate. Section 2.4, on remote sensing and hydrological modelling provides more discussion on this topic, and will be referred to later in this thesis.

Specific requirements of remote sensing for effectively assessing many hydrological variables have been discussed by, amongst others, Salomonson *et al.* (1975), Blyth (1981) and Barrett & Herschy (1985). Full details of their suggestions can be found in Appendix A. Tables 2.1a and 2.1b summarize their suggestions in relation to hydrological remote sensing of parameters of a geomorphic or landcover nature. Geomorphology was characterised by Brown (1970) as earth shape science. The quantification of these parameters is known as morphometry. Geomorphic observations such as basin area and shape, stream network organisation, drainage density and specific channel characteristics can enable an investigator to estimate the mean annual discharge and mean annual flood flows from a watershed, as well as the rapidity of watershed response to a particular rainfall event (Rango, 1975).

In Table 2.1a Salomonson *et al.* specify parameter requirements for a basin size of $40km^2$; Blyth, for three ranges of basin sizes; Barrett and Herschy specify the minimum, maximum and optimal requirements. It is evident that not all parameters are common to the three reports. All the authors provide figures for the measurement of surface areas of water bodies, though the resolution requirements of Salomonson *et al.* are significantly different from those of Blyth, and Barrett and Herschy.

Table 2.1a Spatial resolution requirements for hydrological and water management observations of geomorphic and landcover parameters using remotely sensed data (adapted from Salomonson *et al.*, 1975; Blyth, 1981; Barrett & Herschy, 1985).

Parameter	Salomonson *et al.*	Blyth			Barrett & Herschy		
	Basin area (km^2)						
	40	<100	100-1000	>1000	Min.	Max.	Opt.
	Spatial resolution (metres)						
Drainage area	-	30	30	100	100	10	20
Channel dimensions and patterns	-	30	30	100	-	-	-
Overland Flow Length	±10-20m	30	30	100	-	-	-
Surface slope	±3%	30	30	100	-	-	-
Areal extent of surface water	130-180	10	30	100	100	10	30
Land cover type	130-180 (see Table 2.1b)	100	100	100	-	-	-

Landcover requirements do not show such variation and can probably be justified to an extent by the difference between US and European land patterns, with generally larger homogenous units in the US.

Table 2.1b Accuracy and frequency requirements for remote sensing observations of geomorphic and landcover parameters.

Parameter	Accuracy					Frequency			
	Salomonson *et al.*	Blyth	Barrett & Herschy			Blyth	Barrett & Herschy		
			Mn	Mx	Op		Mn	Mx	Op
Drainage area	-	±1%	0.1 %	1.0 %	0.5 %	10y	10y	3y	5y
Channel dimensions and patterns	-	±5%	-	-	-	5y or after major flood	-	-	-
Overland flow length	±10-20m	±5%	-	-	-	5y	-	-	-
Surface slope	±3%	±5% horiz. ±5cm vert.	-	-	-	5y	-	-	-
Areal extent of surface water	±10%	5%	1%	5%	3%	daily (>1000km² - 4 days)	7d	12h	1d
Landcover	Impervious area ±10% Forested area ±4% Discrimination of grassland, moderate forest cover and heavy forest cover	±1% of water-shed area	-	-	-	1y	-	-	-

Notes: Mn - Minimum h - hour
Mx - Maximum d - day
Op - Optimal y - year

Generally, where common parameters are mentioned, there is a grouping of the requirements stated by Euro-based Blyth and Barrett & Herschy, when compared with those of American-based Salomonson *et al.*

The remainder of this chapter is devoted to more detailed discussions of:

i) those geomorphic (morphometric) parameters which require measurement;

ii) previous work in remote sensing and morphometry;

iii) the use of remote sensing in hydrological modelling.

2.2 Morphometry

Morphometric analysis, or morphometry, can be described as the measurement and mathematical analysis of the configuration of the earth's surface (Penning-Rowsell,1969). This discussion is concerned with morphometry as it relates to hydrological features such as streams, lakes and rivers i.e. hydromorphometry. The systematic description of the geometry of a drainage basin and its stream-channel system requires measurement of linear aspects of the drainage network, areal aspects of the drainage basin, and relief (gradient) aspects of channel networks and contributing ground slopes (Strahler, 1964).

A large number of morphometric variables have been developed. Strahler discusses many of them in a chapter of Ven Te Chow's book on Engineering Hydrology (Strahler, 1964). Newson (1975) provides a list of over 40 morphometric variables and explains which were selected for use in flood studies research. It is interesting to note that all these variables can be obtained from combinations of measurements of streams in a catchment, the catchment boundary and relief measurements. Morphometric variables have been grouped into three main types Strahler (1958):

i) properties measured solely from channel network and basin outline reduced to a horizontal plane;

ii) properties requiring areal mesurement (planimetry);

iii) properties involving elevation differences.

These parameters are used in some lumped parameter hydrological models which are discussed in more detail in Section 2.4.

Table 2.2 presents some of the more commonly used morphometric variables, which will be considered. These parameters are usually obtained by measurements from maps, though aerial photographs may be used with advantage to their determination (Verstappen, 1983). The use of satellite imagery in making these measurements is a major theme of this research. The following paragraphs give a brief description of each of the parameters mentioned in Table 2.2 and some indication of their purpose.

Table 2.2 Morphometric variables commonly used by hydrologists (adapted from Penning-Rowsell, 1969; and Newson, 1975).

A. Properties measured or counted solely from channel network and basin outline reduced horizontal plane		
Property	Symbol or Derivation	Where defined
Stream order	u	Horton, 1945, p.281-282
Number of streams or basins of order u	N_u	as above
Bifurcation ratio	$R_b = N_u/N_{u+1}$	Horton, 1945, p286
Stream length	L	Horton, 1945, p.283
Length of overland flow, or slope length	L_g	Horton, 1945, p.284
Basin length	L_b	Schumm, 1954
B. Properties requiring areal measurement (planimetry)		
Area of basin	A	Horton, 1945, p.283
Drainage density	$D = \Sigma L/A$	as above
Stream frequency	$F = N_u/A$	Horton, 1945, p.285
Basin circularity	$C = \frac{\text{area of basin}}{\text{area of circle}}$	Miller, 1953, p.8
Basin elongation ratio	$R_e = \frac{\text{diam. of circle}}{\text{basin length}}$	Schumm, 1956
Lemniscate k	$k = \frac{L_b{}^2\pi}{4A}$	Chorley *et al.*, 1957
C. Properties involving elevation differences (relief aspect)		
Stream channel slope	Θ_c	Horton, 1945, p.295
Overland slope	S	Nash, 1960
Relief ratio	$R_h = H/L_b$	Schumm, 1954
Ruggedness number	$R_g = H.D$	Strahler, 1958, p.289

Stream Order: Under the impetus supplied by Horton (1932, 1945) the description of drainage networks was transformed from a purely qualitative and deductive study to a rigorous quantitative science capable of providing hydrologists with numerical data of practical value (Strahler, 1964). The two concepts of drainage density and stream order introduced by Horton, laid the foundation for modern network analysis. His stream ordering system is a hierarchical one, in which stream segments are ordered according to their spatial location within the network. This ordering system was modified by Strahler (1952) and later by Scheidegger (1965) and Shreve (1967), with Strahler's system becoming the most widely used. These ordering systems are illustrated in Figure 2.2.

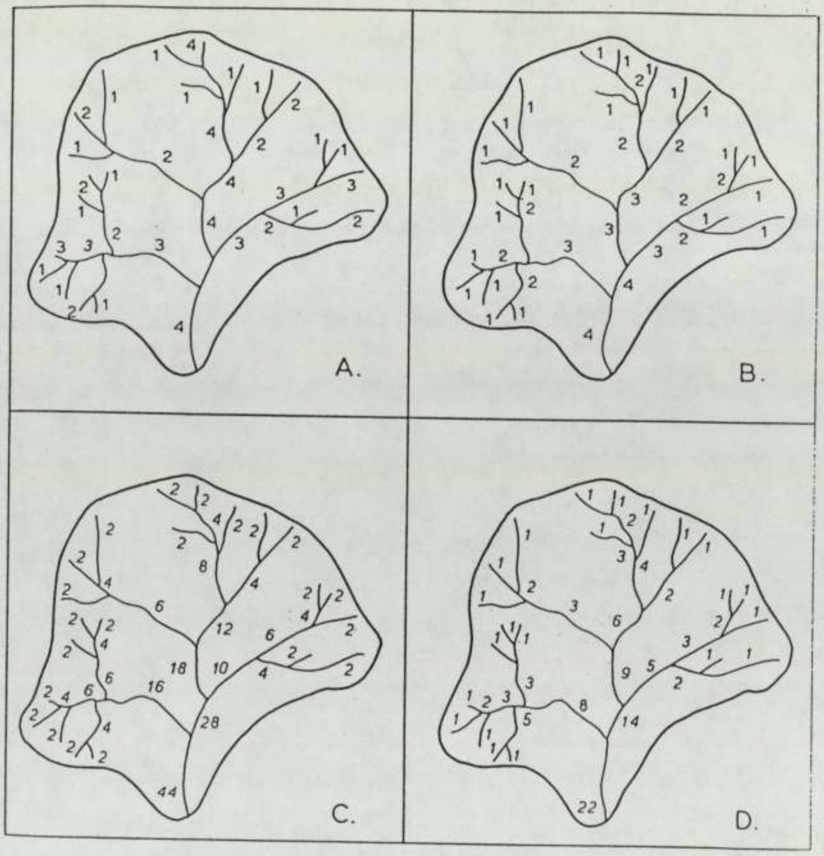

Stream labelling methods of

A. Horton (1945) B. Strahler (1952)

C. Scheidegger (1965) D. Shreve (1967)

Figure 2.2 Ordering systems (after Penning-Rowsell, 1969).

Strahler's system observes the following rules:

i) fingertip tributaries originating at a source are designated order 1;

ii) the junction of two streams of order u forms a downstream channel segment of order u+1;

iii) the junction of two streams of unequal order u and v, creates a downstream segment having an order equal to that of the higher order.

Usefulness of the stream-order system depends on the premise that, on average, if a sufficiently large sample is treated, order number is directly proportional to the size of the contributing watershed, to channel dimensions, and to stream discharge at that place in the system (Strahler, 1964). Because order number is dimensionless, two drainage networks differing greatly in linear scale can be compared with respect to corresponding points in their geometry through use of order number.

Bifurcation ratio: From his ordering system Horton formulated the Law of stream numbers. In this law, the number of streams of each order in a given basin form an inverse geometric series in which the first term is unity and the ratio is the bifurcation ratio R_b. The latter can be defined as the value with which the number of streams of a certain order has to be multiplied to obtain the number of streams of the order below. It can be expressed as:

$$R_b = \frac{N_u}{N_{(u+1)}}$$

This equation has been widely used in morphometric analysis. Although it will not be precisely the same from one order to the next, it tends to be constant throughout the series of orders in a particular network. When the logarithm of number of streams is plotted against stream order, most drainage networks show a linear relationship with little deviation from a straight line for each order plotted. Bifurcation ratios characteristically range between values of 3.0 and 5.0 for watersheds where the influence of the geological structure on the drainage network is negligible (Verstappen, 1983).

Abnormal bifuraction ratios usually have a marked effect on maximum flood discharges, for example, basins with a high R_b yield a low but extended peak flow. In areas of active gulleys and ravines, the bifurcation ratio between first and second order streams may be considerably higher than the R_b of higher order streams. This is indicative of a state of accelerated erosion (Verstappen, 1983). Basin shape also affects the bifurcation ratio with elongated basins tending to have high values.

Length of overland flow: The length of overland flow was considered by Horton (1945) to be "one of the most important independent variables affecting both the hydrologic and physiographic development of drainage basins." This is easily understood when one considers the speed of channel flow which is measured in terms of metres per second, compared to infiltration in units of centimetres per hour. The length of overland flow (L_g) is the mean horizontal length of the flow path from the divide to the stream in a first order basin. This parameter is a measure of stream spacing, or degree of dissection, and is approximately one half the reciprocal of the drainage density ($L_g \approx 1/2D$) (Chorley, 1969).

Basin length: There has been considerable debate by hydrologists over the definition of basin length, in fact Ongley (1968) has criticised the somewhat imprecise definitions in published work. Schumm (1954), defines basin length as the maximum length of the basin measured parallel to the main drainage line. Several common basin length parameters are discussed in Chorley (1969). Newson (1975) suggests the preferred definition of basin length as the radius of the circle centered on the mouth of the basin, whose circumference just touches the most distant part of the catchment.

Area of basin: The importance of this variable cannot be over-emphasised, as will be evidenced by the attention it receives in several parts of this thesis. Ward (1975) states, "the most important single catchment factor is the catchment area, other factors being equal, this determines the total amount of precipitation caught." Basin area can be defined as that area referred to the horizontal plane, which drains under gravity to the outfall of the catchment. The positioning of the catchment boundary is ideally delineated using relief information, though it is often possible to interpolate its approximate position between drainage networks.

Newson (1976) found a very strong correlation between mainstream length and basin area ($r = 0.95$) when examining 410 catchments in Great Britain. This relationship corresponds closely to those given in the literature by Hack (1957), Gray (1961) and summarised by Eagleson (1970). Variations are found with increasing catchment area

(Smart and Surkan, 1967) and catchments with chalk headwaters (Newson, 1976).

Drainage density: Horton's definition of the parameter drainage density was:

$$D = \Sigma L/A$$

where drainage density D equals the total length of stream channel (ΣL) divided by the drainage area A. The pattern and arrangement of the natural stream channels determine the efficiency of the drainage system (Newson, 1975). Other factors being constant, the time required for water to flow a given distance is directly proportional to length. Since a well-defined system reduces the distance water must move in overland flow, the corresponding reduction in time involved is reflected by an outflow hydrograph having a short, pronounced concentration of runoff. It is also known that the channel network is a useful index of the extent and contribution of the partial contributing area (Newson, 1975).

The drainage density is influenced by numerous factors, among which erosional resistance of the rocks, infiltration capacity of the land and climatic conditions are important (Verstappen, 1983). Low drainage densities and large basins with comparatively low-order main streams are common in resistant rocks, whereas high drainage densities and higher order basins are common in soft rocks such as shales. The infiltration capacity, as affected by permeability, slope and soil moisture conditions is another major factor as is the accompanying vegetation cover. Drainage density decreases in more arid and more humid areas because of reduced runoff potential and the impeding effects of vegetation respectively, although values may increase again in the seasonally humid and humid tropics where mean annual precipitation exceeds 1500mm (Abrahams, 1972). Areas of low relief and good infiltration capacity generally show lower drainage density values than zones of higher relief or lower permeability.

The effects of vegetation on drainage density are difficult to isolate because they are bound up with those of climate and soil cover (Knighton, 1984). Drainage density is highest in areas of sparse vegetation and also tends to decline as the extent of the vegetation cover increases (Melton, 1957). However, once a more or less complete cover exists, differences in vegetation density appear to have little further effect on drainage density, provided the infiltration capacity is high enough to preclude Horton overland flow (Dunne, 1980).

It is important to realise that present day drainage density may partly represent the long-term effects of changes in rainfall characteristics, climatic conditions or land management in the past (Verstappen, 1983). In Western Europe, for example, many current dry valleys were formed during the time of Pleistocene glacials. Overgrazing or deforestation may result in the formation of gullies, which persist as conspicuous channels for a long time. Melton (1958) suggests that drainage networks are capable of achieving an equilibrium form adjusted to prevailing environmental conditions of climate, vegetation, lithology and soils.

Stream frequency: Stream frequency (F) was defined by Horton (1945) as, the number of streams per unit area; or

$$F = \frac{\Sigma N_u}{A_k}$$

where ΣN_u is the total number of segments of all orders within the given basin of order k and A_k is the area of that basin. Stream frequency is often used as a substitute for drainage density due to its relative ease of measurement. The basis for this substitution is the strong correlation found between drainage density and stream frequency ($r = 0.94$) by Melton (1958) when examining 156 basins in the U.S. Newson (1975) also found high correlation, though not in all instances. The estimation of stream frequency merely involves counting stream links between junctions (or more simply junctions alone) and dividing by basin area. The practicalities of this are outlined in Newson (1975) and Drayton *et al*. (1980).

__Shape factors:__ Basin shape is instrumental in governing the rate at which water is supplied to the main stream as it proceeds to the outlet (Newson, 1975). It is, therefore a significant feature which influences the period of rise. The quantification of basin shape is a matter of continuing debate. Three common measures of shape are detailed below.

Basin circularity: Miller (1953), defined basin circularity as:

$$R_c = \frac{A_d}{A_c}$$

in which A_d is the basin area, and A_c is the surface of a circle, possessing the same in which A_d is the basin area, and A_c is the surface of a circle, possessing the same perimeter of the basin in question.

Basin elongation ratio:

$$R_e = \frac{D}{L}$$

in which D is the diameter of a circle having the same area as the basin and L represents the maximum length of the basin, measured parallel to the main drainage line (Schumm, 1956).

Lemniscate k: Chorley, Malm and Pogorzelski (1957) based their variable on a lemniscate loop. They defended their model as a more realistic measure than circular measures because "there seems to be no tendency in a dissected region of more or less uniform structure for the steady state basin shape to be in any way related to the circle." The lemniscate loop may be expressed as:

$$p = L_b \cos k \Theta$$

where p is the radius from the outlet to the rim, Θ the angle between the baseline and the radius under consideration and L_b is basin length measured from mouth to most distant point on the perimeter. k controls the shape of the loop and is unity when the loop is circular. The variable can also be expressed as:

$$k = \frac{L_b{}^2 \pi}{4A}$$

where A is catchment area.

<u>**Relief Factors:**</u> The general land slope has a complex relationship to the surface

phenomena because of its influence on infiltration, soil moisture content and vegetative growth (Newson, 1975). Steep slopes generally have high surface runoff values and low infiltration rates (Verstappen, 1983). Consequently they add to the steepness of the hydrograph and lead to relatively high peak discharges. On large watersheds, the time involved in overland flow is usually small in comparison with the time of flow in the stream channel. Conversely, on smaller areas, the overland flow regime may exert a dominating effect on the time relationship and the peak of the hydrograph.

Slope angle can be determined in the field, but contour maps or aerial photography are more commonly used. Because the measurements required are laborious, slope determinations are usually limited and grid sampling techniques are applied (Verstappen, 1983). This situation has now changed considerably and is discussed in Chapter 9. Benson (1949) has shown the close correlation of mainstream slope and tributary slopes, and Strahler (1950) has observed a correlation of channel slope and valleyside slope over a wide range of geographical regions. These findings, together with the difficulties of comprehensive slope measurements have led to the frequent use of mainstream slope as an indicator of overall basin slope.

Strahler (1956) developed a method for the preparation of slope maps by using good photogrammetrical maps at scales of 1:25000 or greater, depending on the relief and lengths of slopes. These measurements could however be taken directly from the aerial photographs. Verstappen (1983) describes a slope interpretation methodology using aerial photography.

Relief ratio: For small watersheds the average slope can be taken as the ratio of the difference in elevation between the watershed outlet and the most distant point on the drainage divide parallel to the principal drainage line (Schumm, 1956). The formula for the relief ratio then reads:

$$R_h = \frac{H_{max} - H_{min}}{L_b}$$

In the case of larger basins, more elaborate means of quantification are required.

Ruggedness number: The ruggedness number R_g is the product of the relief H and the drainage density D. This number implicitly suggests the steepness of slope. If the drainage density increases and the local relief remains the same, slope steepness will also increase. If the relief increases and the drainage density remains constant, then the slopes will be steeper and longer.

Drainage network variation: The extent of the drainage network itself can vary considerably according to seasonal and short-term precipitation patterns. Eight-fold variations in drainage density have been reported from a single catchment as the network expanded and contracted in response to short-term fluctuations in precipitation (Gregory and Walling, 1968). Blyth and Rodda (1973) monitored stream length on a weekly basis over a one year period for a small clay basin in a lowland area of southeast England. They found the main controls on total flow length to be the effective rainfall during the previous week and the length of stream flowing at the time of the previous week's observation. They also found that stream lengths of first-order streams showed most variation. Streams in drainage networks fall under three categories namely; perennial streams, which flow all year round; intermittent streams which flow for only part of the year (seasonal flows) and ephemeral streams which carry water only during, and immediately after, heavy rain (Zuidam, 1985).

Map data: Having decided on the presence of drainage bodies, according to the mapping criteria for the area under consideration these are then recorded on maps of the area by the relevant mapping agency, e.g. The Ordnance Survey. Problems then arise according to map scale. Effectively the smaller the map scale the less drainage details are likely to be present. Newson (1975) examined the effect of map scale on the drainage detail portrayed on maps of one small tributary catchment of the Bristol Avon, as illustrated in Figure 2.3.

Gardiner, (1982) examined Ordnance Survey maps of part of the area around Worcester, England, at scales ranging from 1:25000 to 1:625000. He found large variations in the number of links, sources and junctions mapped in the stream networks. He also found that the maps displayed decreasing apparent length of river reaches with decreasing map scale.

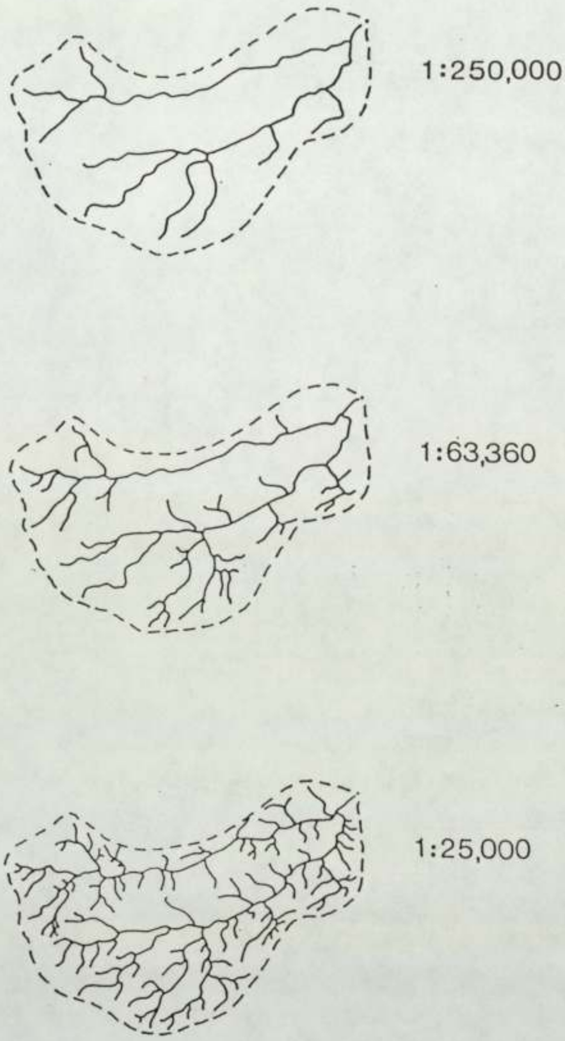

Figure 2.3 Variation of stream network depiction with Ordnance Survey map scale (Midford Brook, tributary of Bristol Avon) (after Newson, 1975).

The decision about which drainage details to keep and which to omit as map scale decreases is at the cartographers discretion. In this generalisation of the drainage details first-order streams tend to be eliminated first as scale becomes smaller. Unfortunately this elimination of first order streams is not totally consistent, and thus has inconsistent effects on the ordering of streams in a network.

Problems of drainage delineation from maps are further complicated by inconsistency of network delineation at the same scale. Wiltshire and Hewson (1983) found differences in drainage details when examining First and Second Series 1:25000 scale Ordnance Survey (OS) maps. It is important to know the data sources for these maps, which were detailed by Wiltshire and Hewson. The First Series 1:25000 scale OS maps are based on the nineteenth century 1:10560 scale County Series (revised in places according to more recent data). This Series is in turn based on various large scale surveys, typically at 1:2500 in rural areas, but 1:10560 in mountain and moorland areas. About 60% of the Second Series 1:25000 OS maps are based on 1:12500 and 1:2500 mapping in urban and rural areas, much of which is derived from post-war surveys, but some of which is based on revisions of the old 1:2500 series. The remaining 40% of the Second Series has been surveyed by aerial photography at a base scale of 1:10000. Witshire and Hewson compared 168 map sheets between series on a national basis and 50 on a regional basis. They concluded that "there are significantly more stream junctions on Second Series 1:25000 OS maps than those of the First Series." They proposed a general correction factor for stream junction estimation, such that:

First Series No. Junctions = 0.74 Second Series No. Junctions

the implication of this is 35% more junctions on the Second Series, this representing the mean correction and not extreme cases.

2.3 Previous work on Remote Sensing and Morphometry

This section details results obtained by various researchers when using remotely sensed imagery to estimate some of the morphometric parameters discussed above. The technical details of the sensors dicussed and the physical concepts involved are outlined in Chapter 4.

Aerial photography has been used on many occasions to assess hydrological parameters. Valleys, river and lake outlines, channel features, river bed material, current direction, relief (catchment boundaries), soils and vegetation can all be identified using aerial photography of appropriate type and scale (Kudritskii *et al.*, 1966). Thus, this section concentrates in particular on previous results obtained from spaceborne sensors.

Several workers have looked at satellite remotely sensed imagery for determining morphometric parameters. Cooper *et al.* (1975) suggest that the minimum possible width of a river that should theoretically always be detectable is equal to two pixel lengths or 374 feet (112 metres) crosstrack or 500 feet (158 metres) in-track . Crosstrack and in-track referring to the scanning mechanism of the Landsat MSS sensor (see Section 4.5). They also state the minimum possible areal size of a water body (pond) that would always be detectable is 4.3 acres (1.7 hectares). Bands 6 and 7, the near infrared bands of Landsat MSS are suggested for the interpretation of water features. In these bands surface waters usually appear uniformly dark due to their almost complete absorption of incoming radiation at these wavelengths.

Rango *et al.* (1975) examined a number of drainage basins in three physiographically disparate areas of the U.S.A. They used Landsat MSS imagery in single bands and colour composites, enlarged to 1:250000 or 1:100000 scale for the interpretation of basin area, shape and main channel sinuosity. The single band images used were the 0.6-0.7μm (band 5) and 0.8-1.1μm (band 7) images. The near infrared band (band 7) showed the most contrast between land and water features and was considered best suited for mapping large streams. The visible red band (band 5) showed good contrast between different land features and vegetated and non vegetated areas and was most useful for network delineation where streams were not large enough to be detected using Band 7 imagery. Summer band 5 imagery was used for mapping the drainage network in those cases where riparian vegetation highlighted the channels.

Results were compared with U.S topographic maps of 1:250000 scale. They found that catchment area was determinable to an accuracy of between 91 and 95 per cent, but that delineation of the drainage network was highly dependent on topographic relief. Low order streams were difficult to detect in heavily vegetated areas with little local relief, or in areas where stream channel development is limited. In areas of dissected topography their findings were that drainage networks delineated from the 1:100000 scale Landsat enlargements were commensurate with information on 1:62500 scale topographic maps. In winter imagery they found that snow cover enhances the drainage network and in summer imagery, along-stream vegetation aids interpretation. Thus, the interpretation and consequent drainage density interpretation values were image-date dependent. Interpretation of the imagery for land use information was considered possible for watersheds as small as $78km^2$ ($30mi^2$).

Blyth, (1981), refers to minor streams, only a few feet wide, being clearly inferred from Landsat MSS images as a result of topographic enhancement. He also states that "minor streams are often apparent due to vegetation changes, or human land use changes which can linearly enhance imagery, rather than from the water signal itself."

Much research on the use of satellite imagery for morphometric analysis has been carried out by Drayton and Chidley, and their colleagues. Drayton and Chidley (1985), examined 1:250000 scale photoprints for four dates of Band 7 Landsat MSS imagery, covering areas of South Wales, Somerset and North Devon, UK. The aim was to interpret key geomorphic parameters. They found that drainage density estimates from the satellite imagery were higher than those found on 1:250000 Ordnance Survey maps, and approached values estimated from 1:50000 maps. Examination of one-to-one correspondence of image interpreted streams and map streams generally showed poor correlation. Reasons for this may be the interpretation of roads and other dark lineaments as streams/rivers. The high degree of interpreter subjectivity was also recognised. It was thought that the use of multispectral colour composites might improve the interpretation. Reliability of stream frequency estimation was seen to improve significantly when using a compilation of details from several different image dates. Catchment area measurements, for 8 catchments, showed very good correlation with those obtained from 1:25000 scale maps, being at least 0.98 in each instance, though shape errors existed.

Further work was done on the same image set by Drayton *et al.* (1986a). A single observer interpreting different areas found that the efficiency of drainage mapping was likely to depend on land-use. Drainage details in areas of open moorland were more easily mapped than in areas of steeply incised landscape, with a close texture of field patterns. Unlike earlier research (Rango *et al.*, 1975) no correlation was found between drainage density and relief. Four observers were used to interpret drainage density, stream frequency and catchment areas. In contrast to their previous conclusions (Drayton and Chidley, 1985), estimates of individual catchment areas were seen to vary widely between different observers, with errors not confined to small catchments. Standard errors of estimate up to $57km^2$ were found for a sample of catchments from $62.2km^2$ to $455km^2$. It was also noted that even where catchment area was estimated well, the shape factor (Horton, 1932) could be up to 25% in error. Drainage density could not be estimated with any confidence for individual catchments. Profound differences existed in estimates made by different observers and from different image dates. Estimates over large areas (in excess of $1200km^2$) appeared better, as discussed in the previous, 1985, paper. They suggested objectivity in drainage mapping may be improved by the use of image enhancements, e.g. diagonal box filters, or from higher resolution satellites such as SPOT and Landsat TM.

Chidley and Drayton (1986a), reported on further work covering the same areas. They found a reasonable correlation (r^2=0.62) between stream frequency estimations from summer Landsat MSS imagery and 1:25000 map values. There was however, no correlation between the winter imagery and map values. This was thought to be due to the inconsistent enhancement of imagery by sun shading. They also noted the very poor correlation of stream frequency between different map scales (r^2=0.26 between 1:25000 and 1:50000; and r^2=0.11 between 1:25000 and 1:250000).

In a paper summarizing some of their findings, Drayton *et al.* (1986b) state that "at 1:250000 scale none but the largest rivers can positively be identified as open water. Thus mapping must be carried out through the interpretation of other features, principally topography and vegetation." They add the proviso that topography can only indicate the possible presence of a stream, and cannot help the interpreter in deciding whether or not streams are perennial. With regard to spectral bands, they found single band (near-infrared) images suitable for drainage mapping in most instances, with false colour composites proving more difficult to interpret and providing little additional information. However, for the examination of agricultural and forested areas in sub-tropical Africa using Landsat MSS imagery, the use of a false colour composite was found to be invaluable. Subjectivity of interpretation was thought to be avoidable by the restriction of catchment interpretations using Landsat MSS imagery to those greater than about 200km^2 in size.

Chidley and Drayton (1986b) reported on the use of SPOT-simulated imagery in hydrological mapping. They produced 1:50000 scale photoprints of simulated Panchromatic and Multispectral SPOT imagery for two test sites in Wales, U.K. Accuracies of 58-60% in drainage network delineation, were obtained using a combination of all photoprint types. Results were compared with details from 1:50000 scale Ordnance Survey maps of the areas. Errors occured in the delineation due to misinterpreting roads and woodland strips as part of the drainage network.

Comparison with map data on the basis of drainage network was found to be misleading. It was felt that the ground area of the images examined did not cover sufficient catchments for a complete assessment of the data type, though prospects for the measurement of catchment area were thought to be good. The SPOT imagery was seen to map drainage networks to an order of magnitude greater than 1:250000 scale Landsat MSS photoprints of the areas. The high spatial resolution of the SPOT data was seen to enable location and identification of open water bodies of less than 0.5 ha. This was achieved using density slicing of band 3 (near infrared) of the 20 metre resolution multispectral data.

Astaras *et al.* (1990), evaluated drainage system analysis using Landsat RBV, Landsat TM and SPOT Panchromatic (PA) imagery, and map data for three catchment areas (approx. 17, 43 and 134km^2 in extent) in Central Macedonia, Greece. Their interpretations were by visual analysis of photoprints, or stereo diapositives in the case of the SPOT imagery. They examined Landsat RBV at 1:125000, Landsat TM bands 3, 4, 5 and 7 at 1:125000, and SPOT PA at 1:200000. Landsat MSS imagery was available for examination, but was not used due to its coarser resolution and from previous experience (Astaras, 1985).

The Landsat TM image bands examined were: band 3 - September 1985; bands 4 and 5 - April 1985; band 7 - August 1984. The red band 3 showed better prospects for drainage line detection than bands 4 and 5. However band 7 was considered the most suitable of all. This superiority was due to spectral contrast between the black tones of the valley bottom and the lighter tones of the valley sides (covered by grasses or cultivated vegetation). The superiority of band 3 over bands 4 and 5 was thought to be due to its improved differentiation of riparian vegetation of evergreens, oaks and shrubs in contrast to the valley side vegetation, due to differences in absorption properties. Problems were encountered in discriminating streams from other linear features, such as roads or boundary shrubs, when examining gently sloping interfluve areas using the RBV or TM imagery. These problems were overcome by the use of the SPOT PA stereo pairs.

One of their main conclusions was that " the small superiority of the morphometric parameters drawn from the SPOT stereo-pair imageries over those drawn from TM images suggests that the greater spectral range of TM (0.45-12.5μm, compared with the 0.5-0.89μm range of SPOT stereo-pair images) vastly outweighs the advantages of SPOT's superior resolution, but not the superiority of the stereoscopic view." They also concluded that TM imagery can be used to map drainage networks to an order of magnitude more than the RBV imagery. In contrast to Chidley and Drayton (1986b) they consider that "the delineation of drainage systems and the measurement of catchment areas from hard copy satellite imageries is insensitive to quality of the imagery and degree of subjectivity."

Palero (1990) reports on on-going work examining morphological paramaters using

1:50000 scale aerial photographs, Landsat MSS imagery, Landsat TM imagery and topographic maps enlarged to 1:50000 scale. The study area included seven catchments in the piedmont of the Andes in the region of Mendoza, Argentina. The enhancement techniques applied were contrast stretching and bi-dimensional filtering to produce hard copy colour composites of the Landsat MSS and Landsat TM imagery at approximate scales of 1:112000 and 1:54000 respectively. She found that values of Horton's RA (Horton's law of stream areas, Horton, 1945) derived from the imagery showed dependence on scale, against the hypothesis. Values of RL (Horton's law of stream lengths; Horton, 1945) indicated that the enhancement techniques applied to the Landsat data enhanced other linear features, besides those of the natural drainage system. Values of the bifurcation ratio (R_b) indicated that this parameter is scale-independent and that Landsat MSS or TM can be substituted for aerial photography or topographic maps for its evaluation.

2.4 Previous work on Remote Sensing and Hydrological Modelling

The aim of most hydrological modelling is to provide a prognosis of the future performance of a hydrological system (Anderson & Burt, 1985). The three types of model that are classicallly identified are; black-box models, conceptual models and deterministic models.

Black-box models contain no physically based transfer function to relate input to output. They depend on establishing a statistical correspondence between input and output. Conceptual models occupy an intermediate position between the deterministic approach and empirical black-box analysis. These are quasi-physical in nature and use simple but plausible conceptual relationships to represent component processes (Wood & O'Connell, 1985). The Stanford Watershed Model (Crawford & Linsley, 1966) and Topmodel (Beven & Kirkby, 1979) are examples of this type of model. Deterministic models are based on complex physical theory. Such models make heavy demands on computational time, but offer the ability to predict catchment changes (Anderson & Burt, 1985). More detailed information on a wide range of hydrological models can be found in ASAE (1982) and Anderson & Burt (1985). The following paragraphs discuss the way remotely sensed information has been used in hydrological modelling.

Runoff is the one hydrologic variable that is most often used by hydrologists and water resource planners (Engman and Gurney, 1991). Accurate prediction of runoff rates and runoff volumes is used for water supply forecasting, flood predictions and warnings, navigation, water quality management, hydropower production and many other water resource applications. The objective most sought by hydrologists is the accurate and timely production of runoff at a given point in a drainage basin. Rodda (1969) puts it thus, "a precise method of predicting the size and shape of the flood hydrograph would be invaluable to the hydrologist, in place of the somewhat dubious means he is forced to employ at times."

Naef (1981), looked at the success of hydrologic models for reproducing measured discharge. He examined some of the many rainfall-runoff models developed over the previous two decades, and asked why new models continue to be developed if the results from older models were satisfactory, as their authors claimed. He also asked if complex models gave better results than simple ones. Conclusions were based on two projects: the World Meteorological Organisation Intercomparison of Conceptual Models (WMO, 1975), and on a study of rainfall-runoff models using data from small basins in Switzerland. Naef's study showed that simple models can give satisfactory results. Of those tested, however, neither the simpler nor the more complex were free from failure because none of them adequately described the rainfall-runoff process. In addition, it could not be proved that complex models gave better results than simpler ones.

Engman (1986) hyopthesises that the problems in hydrological modelling may, to a large extent, be due to a lack of the proper amounts and types of data. Remote sensing, he says, may be the only viable approach for handling the spatial variability of watershed properties because the basic data are spatial in nature.

Runoff cannot be directly measured by remote sensing. Its role is one of the provision of input data or as an aid for estimating equation coefficients and model parameters. Schultz (1988), discussing the use of remote sensing in hydrology makes the following remarks, "the hydrologist intending to build a mathematical model incorporating remotely sensed information has to find out first, which observed electromagentic signal (i.e. frequency or spectral band e.g. visible, IR,etc.) is relevant for which hydrological variable. This is a difficult task since the knowledge available in this field is not much advanced yet. Often one just assumes such relationships, builds a model accordingly and checks how well it functions."

There are two general areas where remote sensing has currently been used for computing runoff (Engman and Gurney, 1991). The first is based on producing data for a class of empirical flood peak, annual runoff, or low flow equations. These involve the estimation of morphometric parameters (as discussed in Sections 2.1 - 2.3). In the second approach, runoff models that are based on a land use component have been modified to use digital analysis or image interpretation of multispectral data to delineate land use classes. Other models have also been created which include aspects of both approaches . Engman and Gurney (1991) provide a good review of many of the models using remotely sensed data.

Empirical relationships

Many empirical formulae have been derived for estimating flood peaks, low flows etc. Map and photographically derived parameters have frequently been used in estimating the coefficients of these equations and later as data inputs (as discussed in Section 2.2). Data derived from satellite imagery, such as the morphometric parameters discussed in Section 2.3, can also be used in these equations, or for their improvement.

Work by Allord and Scarpace (1979) has shown how the use of Landsat MSS data can improve regression equations based on topographic maps alone. The addition of landcover determined from Landsat MSS for areas in Wisconsin, US, was found to reduce the standard estimate of error by 9% for 2 and 10 year 7-day low flow values, and by 14% for the 10, 50 and 100-year flood frequency estimates.

Drayton and Chidley (1985) refer to the usefulness of morphologically based catchment models in European sitautions, and their successful transfer to parts of the Third World where there is insufficient variation for landcover models to be effective. Chidley and Drayton (1986a) derived parameter estimates of catchment area and stream frequency from Landsat MSS imagery for seven basins in S.Wales, UK. They then implemented these in a regional flood estimator model from the UK Flood Studies Report (NERC, 1975) which includes catchment area, stream frequency, soil type, soil moisture, lake attenuation and slope factors. They found similar results using winter Landsat imagery and accepted values from the Flood Studies Report. Regressing catchment areas and stream frequencies alone they found a correlation coefficient of 0.82 for the seven catchments examined.

Runoff Models

Land use and runoff coefficients

Land use is an important characteristic in runoff modelling and will be discussed at several points in this research. Land use type affects infiltration, erosion and evapotranspiration. Early work by Salomonson *et al.* (1975) on parameter estimation, including landcover discrimination using satellite imagery, was mentioned in Section 2.1. Jackson *et al.* (1977) used satellite derived land use data for implementation in the STORM model (US Army Corps of Engineers, 1976). Much work has been done on using remotely sensed information in the Soil Conservation Service (SCS) runoff curve number (RCN) model (US Department of Agriculture, 1972). These models, based on land use and hydrologic soil types, are widely used and refined in the US, where their original application to agricultural regions has been broadened to include urban and suburban areas.

Engman and Gurney (1991) provide a review of results obtained by several workers using remotely sensed data from Landsat MSS in SCS models. These results show that remote sensing has been successfully used to derive landcover estimates for the SCS curve number models. Engman and Gurney emphasise the need for a general land use class table, which can be applied to specific watersheds. They also refer to the increased accuracy exepected using higher resolution data from Landsat TM and SPOT HRV. Mauser (1984) used satellite derived land use, soil and slope information for the reproduction of historical flooding scenarios, for a basin in Southern Germany. He also simulated the effects of land use change on hydrology. Zevenbergen *et al.* (1988) found significant correlations between five reflectance index models (RIM) and runoff curve numbers. They examined nine small watersheds using Landsat MSS data and nineteen derived RIM's. They state the need for further testing but conclude that "satellite data may eventually be employed to directly and efficiently estimate rangeland curve numbers."

Steube and Johnston (1990) applied the SCS runoff curve number model (USDA, SCS TR-55 Manual, 1986) to 6 small catchments in S. Dakota, using conventional (manual) and Geographic Information System (GIS) techniques. Digital elevation, soils and landcover data were employed in the latter method. The raster-based Geographical Resource Analysis Support System (GRASS) (U.S. Army, 1988) GIS was used for all phases of the modelling process, including watershed delineation and routing of runoff. Classified Landsat MSS data was used to provide the landcover data. Watershed delineation using a Digital Elevation Model (DEM) revealed areal discrepancies of between 0.4% and 37.6% with manual methods. The largest discrepancies occurred in areas of relatively flat terrain, and were attributed to orthophoto mapper signal noise.

Steube and Johnston concluded that GIS provide an acceptable alternative to conventional methods of SCS runoff modelling for watersheds lacking relatively flat terrain. Given this limitation, it was suggested that GIS methods may prove advantageous over manual methods when study areas are large or numerous, runoff is modelled repetitively, alternative landcover scenarios are explored, or a digital database already exists for the area.

New Models

The modification of existing hydrological models to receive remotely sensed data inputs has achieved varying degrees of success. Peck *et al.* (1981) wrote of the lack of existing models which had potential for the use of remotely sensed data. They state the need for the development of new models or subroutines for existing models which recognize the characteristics of remotely sensed data. Groves *et al.* (1983) describe the development and testing of a remotely sensing based hydrological model. Their model was based on the concepts of the Stanford Watershed Model, with restructuring of individual components to provide improved interfacing with remotely sensed quantities. They used a GIS as a spatially referenced data management system to define watershed segements with similar hydrological responses. The model was seen as a basis for improvements in operational streamflow prediction.

Drayton *et al.* (1986c) regressed a series of thematic classifications of Landsat MSS data against catchment rainfall and runoff values using a simple lumped model (Note: their thematic classifications were similar to the RIM's of Zevenbergen *et al.*). Unfortunately, for the catchments examined no significant correlations were found. Vieux *et al.* (1986) describe a hydrologic model using remote sensing, GIS and the finite element method. Remotely sensed data provides the land use information in the proposed scenario for incorporation with other data in a GIS, to create hydrologically homogenous subareas for modelling. Fortin *et al.* (1986) proposed a a system based on modules of square grid cells. The modules have variable-sized pixels to incorporate many types of remotely sensed data and to allow for variable basin size.

Abbott *et al.* (1986) in an introduction to the European SHE model (Systeme Hydrologique Europeen), remark on the inadequacy of lumped parameter hydrological models for many hydrological situations. The long meteorological and hydrological records required for calibration are not always available, and the curve fitting element makes any physical interpretation of fitted parameter values extremely difficult. The grid based SHE model was designed to incorporate more information on topography, soil and vegetation types. The potential for remotely sensed data in the model is specifically mentioned.

A new remote sensing based model is described by Allewijn (1990). This event-based rainfall-runoff model, denoted LACS (LAndsat-supported Conceptual Semi-distributed), uses Landsat TM for the delineation of vegetation and geomorphological units, from which the semi-distributed model is inferred. The LACS model was implemented and tested for a number of dolomite/limestone and marly tuff catchments (0.5 - 45km^2) in the N. Italian Alps. The model consists of two sub-models on water balance and time distribution. Using the water balance model Allewijn produced regional estimates with a mean difference between observed and simulated runoff of 21%.

Fett, Neumann and Schultz (1990), describe a distributed hydrological model based on the variable contributing area concept. They used Landsat TM imagery, a DEM , soil and geological maps to derive watershed characteristics. The drainage network and catchment boundaries were derived from the DEM. Land use data was derived from a multi-temporal maximum likelihood classification of the satellite data for a 94km^2 catchment. Accuracy tests showed an overall accuracy for land use classification of about 75% which the authors believe they can improve upon.

2.5 Summary

The first part of this chapter discussed the spatial, accuracy and frequency requirements for hydrological remote sensing suggested in three different works. These showed a fair degree of agreement, with some areas of disparity between the European and US requirements.

A review of numerous morphometric parameters developed for hydrological analysis was presented in Section 2.2. The derivation and significance of these parameters was highlighted. Many of the parameters can be measured using various types of remotely sensed imagery. The measurement and quantification of these parameters using the data types under comparison are discussed in Chapters 7 and 8. Relief factors were not measured in this research and the reasons for this significant omission are given in Chapter 7. The temporal variation of drainage networks was mentioned as was the variation in map delineation of drainage networks with scale and inconsistencies found between map series of the same scale.

In the discussions on previous use of remote sensing imagery in morphometry several researchers were seen to have used Landsat MSS to derive morphometric parameters. There was general agreement on certain matters. The near infrared band (Band 7) was considered the optimal band for the delineation of open water. The red band (Band 5) was recommended for vegetation/ non-vegetation contrast and, in particular, the discrimination of riparian vegetation.

Rango *et al.* suggested Landsat MSS as being appropriate for landcover interpretation from catchments greater than $78km^2$ in area, with drainage network detail commensurate with 1:62500 scale maps. Drayton and Chidley in their series of papers suggest a minimum catchment size of $200km^2$. They point to the degree of subjectivity in catchment boundary delineation, interpretation variations in summer and winter imagery due to differential shading effects, and the fact that only the largest UK rivers are seen as opposed to inferred from Landsat MSS imagery.

Drayton and Chidley suggested the examination of false colour composites and the application of box filters. Their examination of simulated SPOT imagery for drainage details revealed 58-60% agreement with 1:50000 maps, with a requirement for further investigation.

Comparisons of Landsat TM and stereo SPOT panchromatic imagery by Astaras *et al.* revealed that the Landsat TM has considerable spectral advantages over the SPOT imagery, but the stereoscopic possibilities of SPOT gives it overall preference. Landsat TM band 3 (red) was considered the most suitable band for network delineation, with discrimination of riparian and other vegetation types possible. Astaras *et al.*, in contrast to Chidley and Drayton are of the opinion that drainage network delineation does not involve a degree of subjectivity.

The final part of the chapter showed how remote sensing has been used in empirical hydrological models, land use runoff models and in new hydrological models. Chidley and Drayton showed the successful application of Landsat MSS derived parameters in a flood estimator model. However, most studies have concentrated on the use of Landsat MSS for landcover classification and its subsequent implementation in SCS runoff models. These applications have shown success and work by Steube and Johnston have taken this work further, with all modelling including a DEM within a GIS.

Landsat TM has been used with some success in a model developed by Allewijn and a model under development by Fett, Neumann and Schultz.

CHAPTER THREE : **THE STUDY AREA**

3.1 Introduction

This chapter describes the factors contained within the research area which are of importance from an imaging or hydrological point of view. The area selected for this research, some 235 km^2 in extent, was the Dolgellau and Coed-y-Brenin area of North Wales, UK, which forms part of the Snowdonia National Park (see Figs 3.1 and 3.2). This area was selected for the following reasons:

i) the availability of imagery: namely Landsat MSS, Landsat TM and aerial photography;

ii) relative accessibility of the area;

iii) the variety of landcover types.

The research area, illustrated in Figures 3.1 and 3.2, was covered by Landsat MSS imagery and Landsat TM imagery; aerial photography was available for almost the whole of this area. The limits of the main research area were defined by the extent of a 512x512 subscene of Landsat TM imagery (the reasons for this are outlined in Section 5.1.) For measurement on a catchment by catchment basis the area covered was extended beyond the main research area, as illustrated in Figure 3.2. The research area being in Southern Snowdonia was fairly easily accessible from the author's original research base of Birmingham, UK.

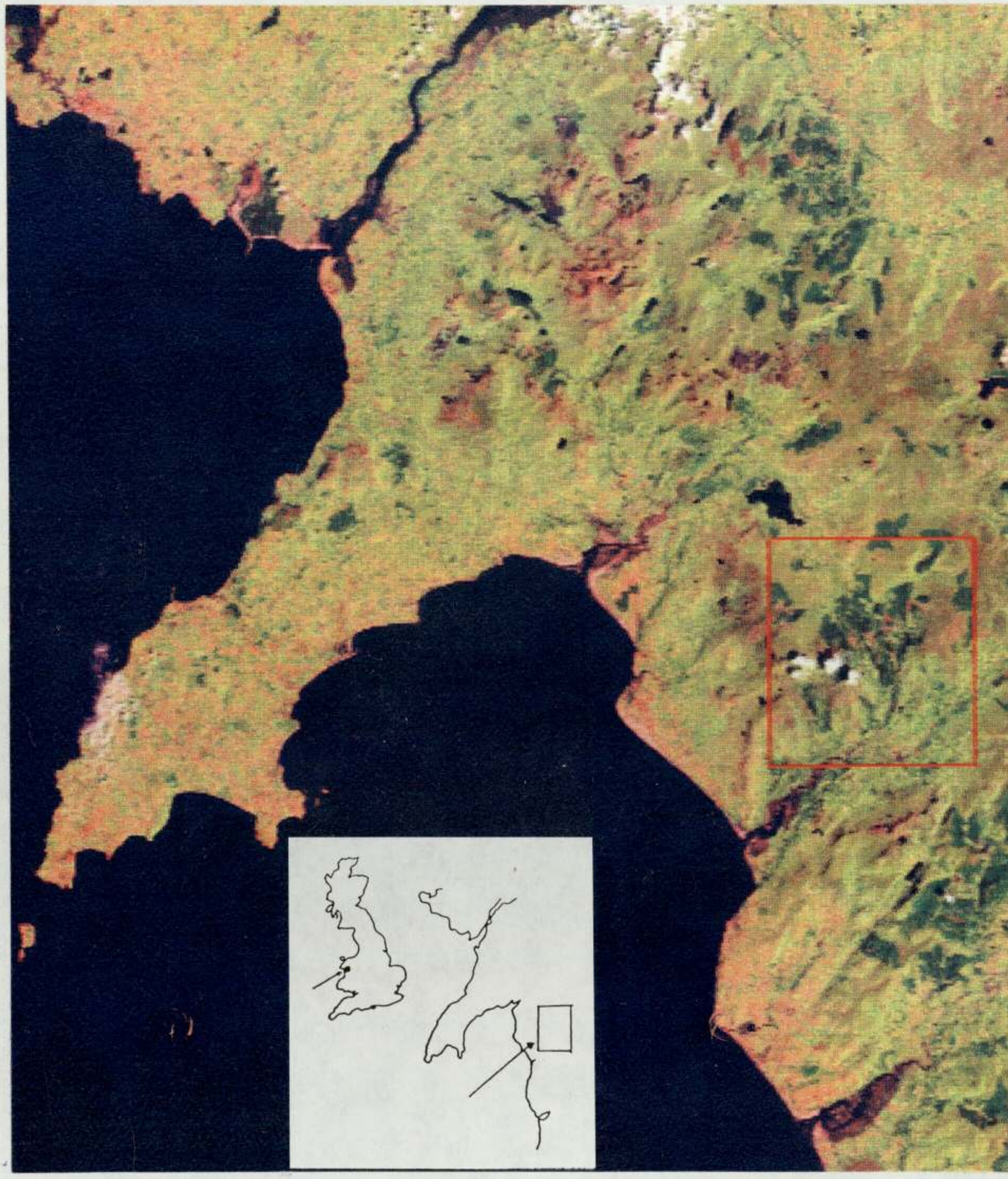

Figure 3.1 General location of the research area using a Landsat TM image.

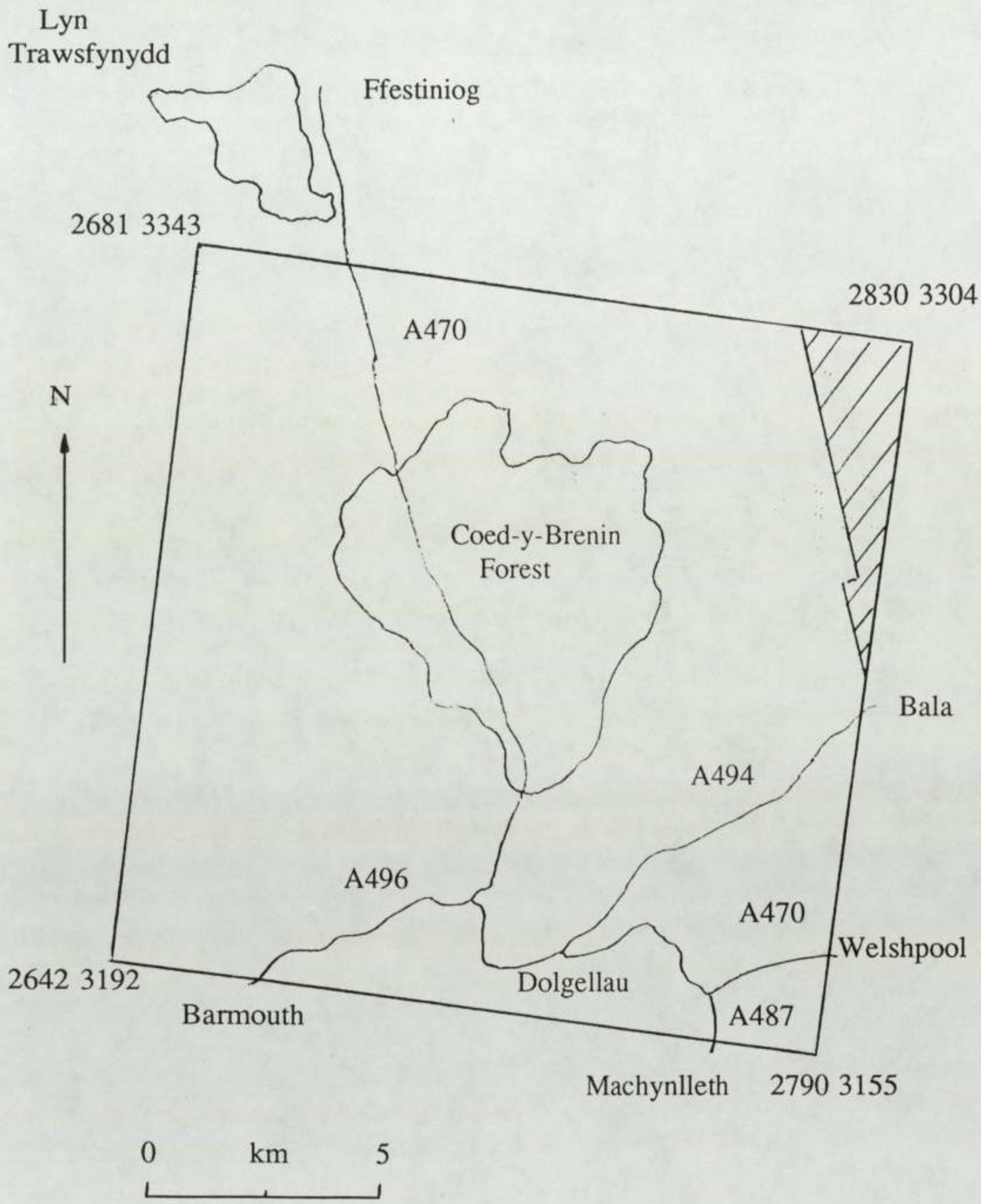

Figure 3.2 Extent of main research area with coordinates in British National Grid values (hatched area shows region not covered by the aerial photographs).

Streams and rivers in the area are bordered by various lowland and upland vegetation types and frequently pass through forests or woodland, giving rise to opportunities for the examination of several water/vegetation interfaces on the imagery.

In hydrological terms the physical characteristics of a catchment area profoundly affects the total amount of runoff, as mentioned in Chapter 2. Slope, soil and rock type and their complex interrelationships influence the total runoff from a catchment through their effects in delaying water movement after precipitation. In general, the highest annual runoff would be expected from steeply sloping areas having thin soils, impermeable rocks, and little vegetation cover (Ward, 1975). Average height of the catchment may also affect total runoff, through its direct orographic influence on precipitation amounts.

Meteorological factors affecting runoff can normally be measured with reasonable accuracy (assuming availability of appropriate equipment) thus facilitating their correlation with runoff characteristics. It is, however, much more difficult to apply such precise determinations to many catchment factors. Furthermore, some of these factors, such as shape, topography, and soil type, remain fairly constant over long time periods while others, such as those associated with land use, may change very rapidly (Ward, 1975). The determination of landcover types and the monitoring of any changes is one application which lends itself to the use of remotely sensed data.

The main problems of catchment modelling arise partly from the fact that the various components of runoff may be differently affected by each of the catchment factors, so that the net effect of any one catchment factor with time are difficult to establish. This is compounded by the fact that only limited, hydrologically responsive, areas of a catchment make a substantial contribution to quickflow (Ward, 1975). Thus, for applications such as peak flow modelling it is the influence of catchment factors in these limited areas, and not over the catchment as a whole, which is most important.

This chapter examines several different characteristics of the study area, the interactions of which affect the hydrological regime of the area. The physiographic nature, geology, soil types, landcover and climate are outlined and discussed with emphasis on the effect of their variable parameters on the hydrology. Each sub-section contains a general overview followed by specific deatails of the research area. Of these characteristics, the physiography and landcover are the most immediately relevant to the determination of stream networks and discrimination of landcover types using remotely sensed data, the main themes of this research. However, the influence of other factors must be recognised. The assessment of these may be undertaken using remotely sensed data or obtained from other sources for incorporation within a GIS or other modelling system. Section 3.7 describes the field data collected by the author on visits to the research area.

3.2 Physiography

The physiography of an area affects its hydrological response with, as previously mentioned, the catchment area having great importance. The catchment shape is known to influence runoff through its effects on the mean travel time to the catchment outfall. Generally speaking in catchments of a square or circular form, the tributaries often tend to come together and join the main stream in the centre of the area (Pardé, 1955). Consequently, the separate runoff peaks generated by a heavy rainfall are likely to reach the main stream in approximately the same locality at approximately the same time, thereby resulting in a large and rapid increase in the discharge of the main stream. If, on the other hand, the catchment area is long and narrow, the tributaries will tend to be relatively short, and are more likely to join the main stream at intervals along its length. This means that, after a heavy rainfall over the area, the runoff peaks of the lower tributaries will have left the catchment before those of the upstream tributaries have moved very far down the main stream. Elongated catchments are thus less subject to high runoff peaks. This situation is further complicated by the direction and speed of movement of storms.

A second pertinent topographical factor is the slope of the catchment area which may affect the relative importance of predominantly vertical movement of water by means of infiltration and the predominantly lateral movement of water by means of interflow and overland flow, the former tending to be more important in flat areas, the latter in steeply sloping areas. Furthermore, because the speed of water movement will tend to increase with slope, runoff in steeply sloping areas will reach stream channels quickly.

The shape of the runoff hydrograph depends not only on the speed with which water reaches the stream channel but also on the speed with which it moves down the channel to the outlet of the catchment. Channel slope may therefore be as important as catchment slope and has frequently yielded more significant correlations with runoff characteristics (Ward, 1975).

Turning to the effects of physiography on remotely sensed imagery, physiography can create significant relief distortions and shadow effects. These effects are dependent on factors such as sensor altitude and view angle, and the sun azimuth and elevation at the time of image acquisition. A more complete explanation of these effects is given in the technical imagery details presented in Chapter Four.

The particular study area under consideration is an upland one (in British terms) with a maximum elevation of 754 metres at the summit of Y Llethr (SH 661258 Ordnance Survey) which forms part of the Rhinog mountain range (see Figs. 3.3 & 3.4).

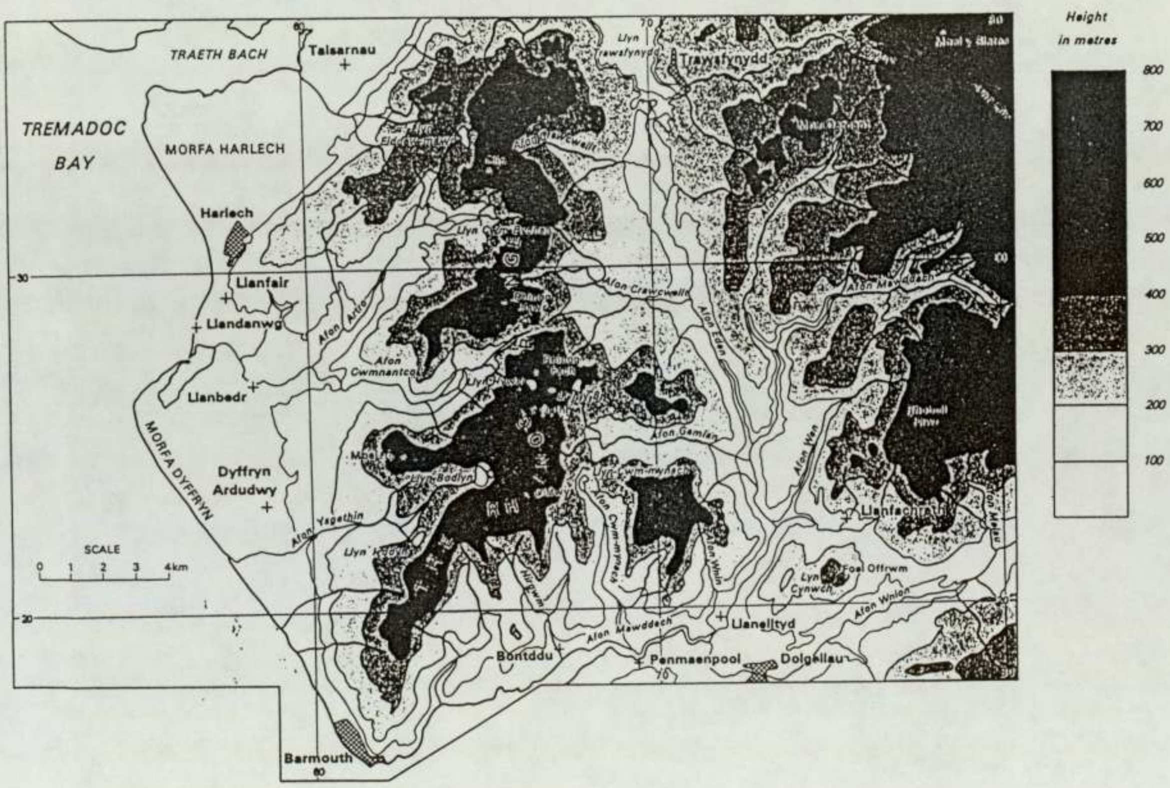

Figure 3.3 Physical features of the district around Harlech (after British Geological Survey (BGS), 1985).

This range runs in a roughly north-south direction along the western boundary of the area until brought to an abrupt halt at the southern end by the Afon (river) Mawddach floodplain and estuary. The land to the east of the Rhinog mountains drops moderately steeply over several kilometres before falling steeply into the valley of the Afon Eden, or more southerly the Afon Mawddach. These two river valley systems together with the smaller river Afon Wen effectively dissect the area in a north-south direction.

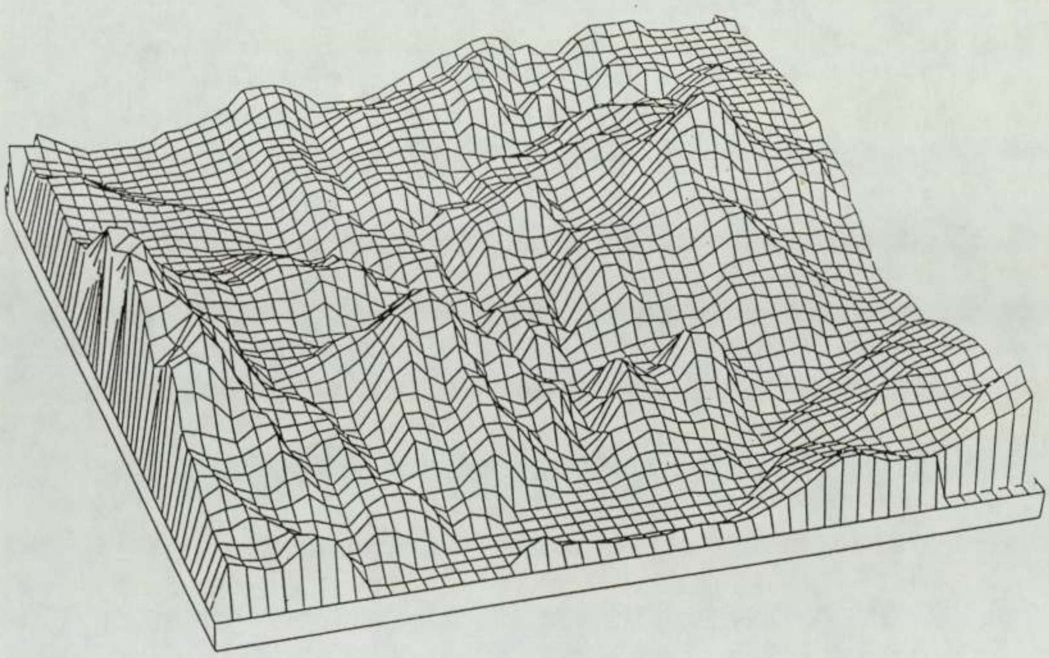

Figure 3.4 Digital Elevation Model (DEM) of the research area with 2.7x vertical exaggeration, viewed from 195° with an elevation of 35° (see also Chapter 9).

The topography of the eastern part of the area is largely dominated by the extinct volcano Rhobell Fawr. Travelling in a southerly direction from its summit the slopes after a steep initial section descend moderately steeply into the valley of Afon Wnion. This valley runs east north east / west south west having a floodplain width of around 1 kilometre, and after joining with the Afon Mawddach continues in a similar direction and forms the beginings of the Mawddach estuary.

The extreme southern part of the area consists of moderate slopes rising southwards and forming the footslopes of the mountain Cader Idris. Drainage patterns over the area as a whole tend to be dendritic, sub-dendritic or in some instances sub-parallel (see Fig. 3.5). Dendritic patterns indicate homogenous rock and soil material with little or no structural control from the geology (White, 1977). Sub-parallel streams may indicate a fault or fracture line.

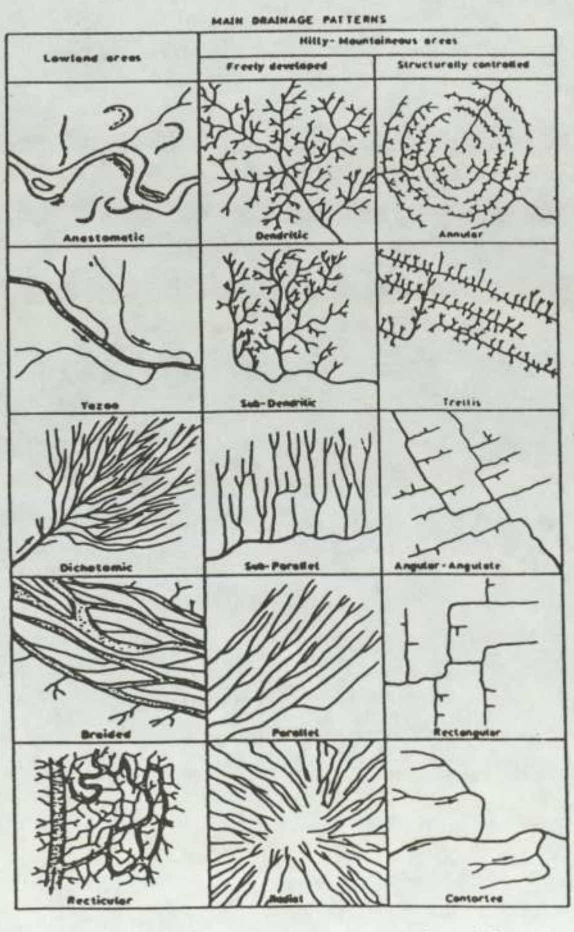

Figure 3.5 Main types of drainage pattern (after Verstappen, 1972).

3.3 Geology

The geology of the area must be examined in terms of the way in which it affects surface and groundwater flow. This can be expressed in terms of the porosity and permeability of the various rock strata. A knowledge of the stratigraphic succession, rock type and main structural features is required to determine the likely areal extent and occurence of the various strata: e.g. sedimentary rocks, volcanic dykes etc. This information can be determined through the examination of geological maps or from remotely sensed data. Aerial photography, and more recently satellite data have been used in much exploratory geological interpretation. This aspect of remote sensing is not investigated in the current research and the reader can find more detailed information in Sabins,1987 and Drury, 1987 amongst others.

The amount of groundwater stored in saturated material depends upon its porosity, however, by no means all of this water will be available for movement in the context of the hydrological cycle. For instance, clay which so often forms an aquiclude, has a very high porosity, while good aquifers, like sandstone and limestone have only low to medium porosities. The proportion of groundwater which is potentially "mobile" will depend partly on how many of the interstices contributing to the overall porosity are interconnected, including joints, bedding planes and fractures. Water locked up in enclosed interstices however large, may be almost permanently out of circulation.

The influence of rock type on runoff may be seen in the close relationships which often exist between geology and the pattern of the drainage. In a catchment where subsurface storage and hydraulic conductivity are low the ground surface will be prone to saturation resulting both from the downslope movement of the interflow and the increase in elevation of shallow water tables during and immediately after precipitation (Ward, 1975). In this situation the channel network will expand rapidly during precipitation.

Geological structure is largely important as a factor guiding the movement of groundwater to the streams. It is probable that the time lag between precipitation and the groundwater flow peak will be smaller in the case of the synclinal catchment than in the case of the horizontally bedded catchment, even when the rock types are similar in both cases. Structure can also produce an occasional lack of correlation between the topographical and hydrological divides of adjacent catchments.

This particular research area is dominated by rocks of Cambrian age forming part of the Harlech Dome structure (see Fig. 3.6). The Cambrian succession consists of clastic sedimentary and volcanic rocks, divisible into three major groups. In ascending order they are the Harlech Grits Group, the Mawddach Group and the Rhobell Volcanic Group. The Harlech Grits Group consists mainly of coarse-grained greywacke interbedded with siltstone and mudstone. The Mawddach group consists of the Clogau formation of 90-105m of dark grey or black banded carbonaceous mudstones followed by 2.5km of turbidites, siltstones and mudstones (BGS, 1985). These two rock groupings form the upper geological member for the eastern and central part of the area.

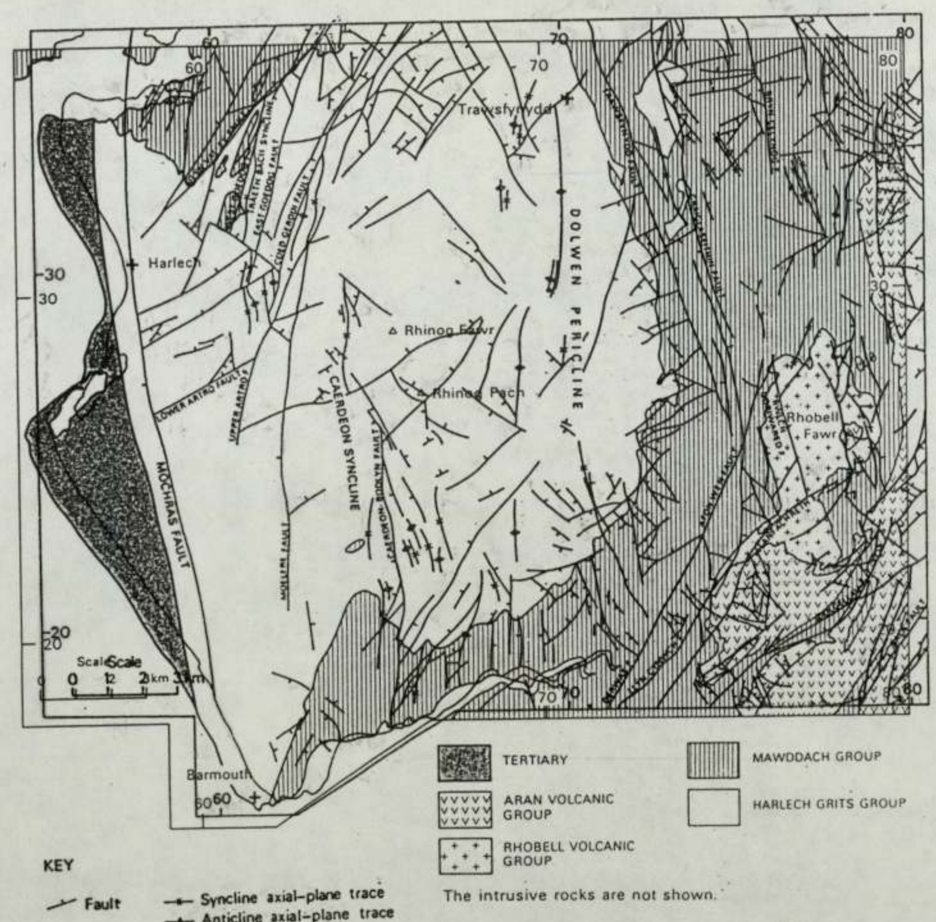

Figure 3.6 The major geological divisions of the research area, with an overlay showing the main structural features (after BGS, 1985).

On Rhobell Fawr (787 257) the outcrop is of volacanics known as the Rhobell Volcanic Group. These extrusives which lie unconformably above sedimentary rocks of the Mawddach Group are basaltic in composition, and Kokelaar (1979) estimated that a thickness of 3.9km of lavas had been erupted, but there are a number of outliers to the north, east and south. Together they comprise the southern part of a single volcano.

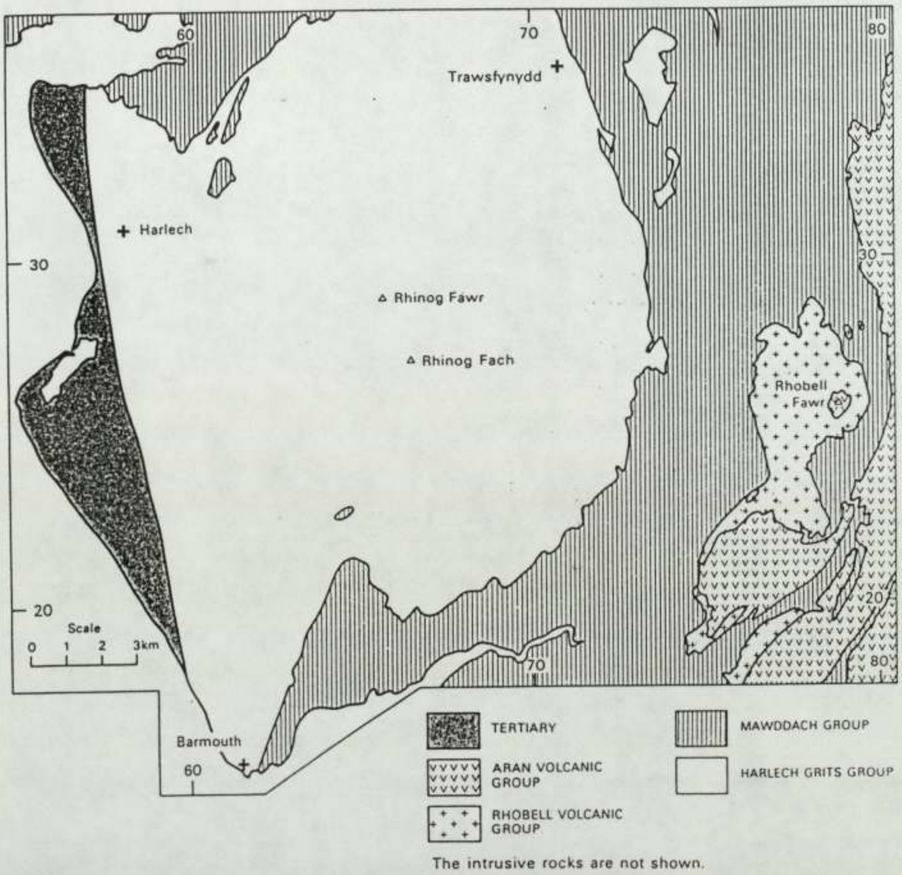

Figure 3.6 The major geological divisions of the research area, with an overlay showing the main structural features (after BGS, 1985).

On Rhobell Fawr (787 257) the outcrop is of volacanics known as the Rhobell Volcanic Group. These extrusives which lie unconformably above sedimentary rocks of the Mawddach Group are basaltic in composition, and Kokelaar (1979) estimated that a thickness of 3.9km of lavas had been erupted, but there are a number of outliers to the north, east and south. Together they comprise the southern part of a single volcano.

Throughout the Cambrian period, sediment accumulated in a submarine trough on the north-east margin of the European continental plate. In structural terms, late Tremadoc folding and faulting resulted in a regional uplift which was greatest in the west. The Rhobell Volcanic Group was erupted subaerially onto an irregular topography (Kokelaar, 1979). A renewed period of folding was followed by further erosion reducing the Rhobell Volcanic Group and hinterland of folded Cambrian sediments to a peneplain.

The Ordovician rocks of the Aran Volcanic Group lie unconformably above Cambrian rocks and consist of a mixed suite of basalts, rhyolites, volcaniclastic and sedimentary rocks. These rocks form the most recent solid geological deposits in this area and were subjected together with previous rocks to folding and regional metamorphism during the Caledonian orogeny. The current structure is shown on the overlay of Figure 3.6. Drift deposits of Quaternary times consist of areas of boulder clay and undifferentiated drift over most of the area except on Rhobell Fawr. Peat occurs sporadically on the Rhinog Mountains as does the occasional head deposit. This information together with maps of the area could be used in hydrogeological model possibly using a GIS, together with information derived from the remotely sensed imagery. Such a scenario is discussed in Chapter 9.

3.4 Soil Types

The influence of soil type on infiltration characteristics, and its consequent effect upon the dispostion of rainfall as either overland flow, interflow or groundwater flow involves many factors (Ward, 1975). This sub-section gives information on relevant soil hydrology followed by detailed descriptions of the soils to be found in this area. The soil types of this area were not determined using remotely sensed imagery, though soil type can be inferred from vegetation type (Mulders, 1987). In this instance soil data was available from the Soil Survey of England and Wales (SSEW, 1984). Boorman and Hollis (1990) stress the major influence which soil type has on the hydrological processes and overall response of a catchment. They describe a hydrologically-based soil classification for England and Wales (HOST). This classification has developed from experience with the WRAP soil classification (NERC, 1975). Extended soils details are presented due to the importance of hydrological soil type in hydrological modelling.

Soil profile characteristics are important in relation to their effects upon infiltration and the generation of interflow. In particular, marked reductions in the hydraulic conductivity with depth, especially in the upper horizons, facilitate the formation of interflow and, during prolonged rainfall, the saturation of the soil surface and the generation of overland flow. On the other hand, deep uniformly permeable soils tend to encourage continued vertical infiltration and the dominance of baseflow over quickflow (Ward, 1975).

Hydrologists have for a long time recognised the relationship between the amount of runoff (especially quickflow) produced by a given rainfall and the moisture content of the soil, expressed either as a direct measurement or indirectly as an antecedent precipitation index. In general the source areas (contributing areas) within a catchment will tend to expand as the catchment becomes wetter and the precipitation continues.

The "soil water regime" (SSEW, 1984) is the cyclical seasonal variation of wet, moist or dry soil states, and can be very important in determining the effect of precipitation at various times of the year. The duration and degree of waterlogging can be described by a system of wetness classes (see Table 3.1), grading from Wetness Class I, well drained, to Wetness Class VI, almost permanently waterlogged within 40cm depth (Hodgson 1976). The incidence of waterlogging depends on soil and site properties, underdrainage and climate.

Table 3.1 Soil Wetness Classes (after SSEW, 1984).

Soil Wetness Classes

Wetness class	Duration of waterlogging
I	The soil profile is not waterlogged within 70 cm depth for more than 30 days[1] in most years[2].
II	The soil profile is waterlogged within 70 cm depth for 30-90 days in most years.
III	The soil profile is waterlogged within 70 cm depth for 90-180 days in most years.
IV	The soil profile is waterlogged within 70 cm depth for more than 180 days, but not waterlogged within 40 cm depth for more than 180 days in most years.
V	The soil profile is waterlogged within 40 cm depth for 180-335 days, and is usually waterlogged within 70 cm for more than 335 days in most years.
VI	The soil profile is waterlogged within 40 cm depth for more than 335 days in most years.

[1] The number of days specified is not necessarily a continuous period.
[2] *In most years* is defined as more than 10 out of 20 years.

The main property affecting the soil's natural water regime and its response to drainage measures is its permeability. Field assessments of permeability are made from estimates of soil texture, structure and packing density, which are refined using laboratory measurements of macroporosity (Hall *et al.* 1977) and the limited data available on hydraulic conductivity. Dense clayey, fine loamy or fine silty subsoil horizons with a saturated hydraulic conductivity (Thomasson 1975) of less than 0.1m per day are classified as slowly permeable. These are effectively impermeable in terms of their contribution to the movement of water to field drains (Luthin 1957). In soils with a thick slowly permeable substratum, movement of excess water in the upper horizons is mainly lateral. The term permeable (SSEW, 1984) is used for sandy, loamy or well structured clayey and peaty soils that are assumed from available data to have a horizontal saturated hydraulic conductivity of greater than about 0.6m per day. The term moderately permeable is restricted to soils which lack clear evidence to place them in either the permeable or slowly permeable categories or in which hydraulic conductivity is variable. Fine-textured alluvial soils are often placed in this category, as are some clayey soils.

Gley morphology is an essential part of soil classification and usually indicates some degree of waterlogging (SSEW, 1984). Soils lacking either gley features or slowly permeable horizons within 70cm depth are usually considered to be well drained (Wetness Class I). Soils with gley features and a slowly permeable horizon are almost certainly waterlogged for some time in most years, though the duration and severity of waterlogging depend on the efficiency of any drainage measures and on the local climate.

Relief and slope shape also influence hydrology and soil water regime (Rudeforth, 1967 & 1970). On undulating ground with slowly permeable parent materials, surface waterlogging causes gleying on flat ground, but soils on the slopes are drier as most rainwater moves to lower ground producing the pattern of soil distribution illustrated in Figure 3.7. In sands and other permeable materials water penetrates to the subsoil, leaving relatively high ground well drained, but soils on lower land are affected to some degree by groundwater. On slopes, water moving through permeable material

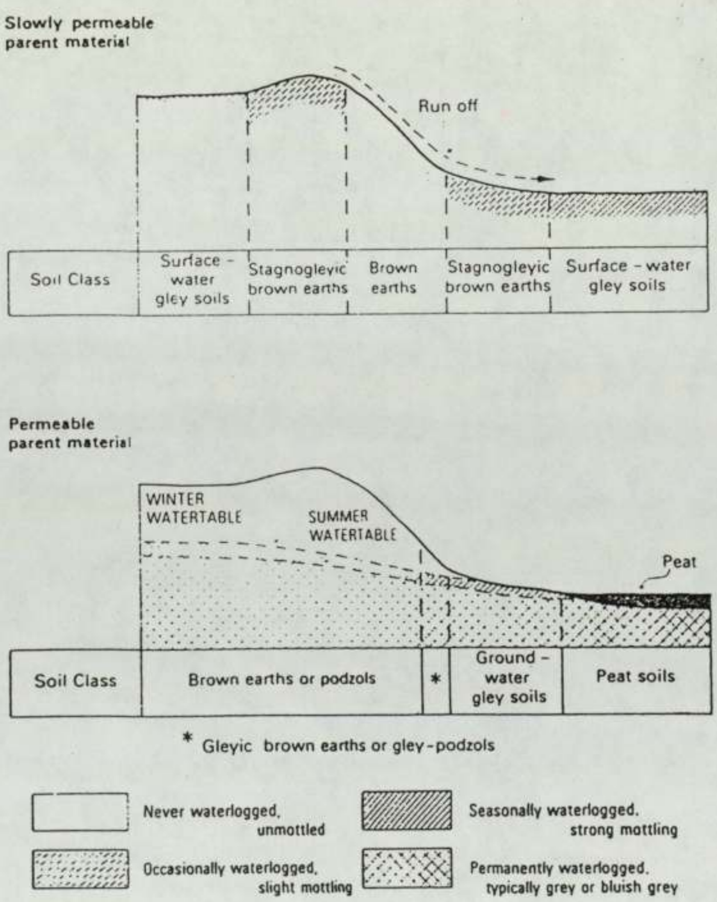

Figure 3.7 Relationships of relief, hydrology and soils (after SSEW, 1984).

often reappears as springs at the junction with less permeable strata. Soils affected by groundwater and those affected by surface water are not always as distinct from one another as Figure 3.7 suggests, since permeability of the parent material can change with slope and many soils possess features of both (SSEW, 1984).

The meteorological field capacity (SSEW, 1984) measured in days, is a valuable indicator of the climatic influences affecting a piece of land, but to predict the duration and severity of waterlogging (Wetness Class) it must be considered together with soil and site properties. Table 3.2 illustrates the features used to describe the wetness classes of soils described below.

Table 3.2 Relationships of Wetness Class to Field Capacity Days and Depth to Slowly Permeable Horizon (after SSEW, 1984).

Average Field Capacity Days	Gleyed within 70 cm depth				Ungleyed within 70 cm depth
	Depth to slowly permeable horizon				
	<40 cm	40-80 cm	>80 cm		>80 cm
			Drainage outfalls limiting	Drainage outfalls not limiting	
<100	(x)	II	II-VI	I	I
100-125	(x)	II-III'	III-VI	I	I
125-150	(x)	II-III'	III-VI	I	I
150-175	(x)	III-IV'	III-VI	I	I
175-200	IV	III-IV'	IV-VI	I	I
200-225	V	III-IV'	V-VI	I-II	I
225-250	V	IV-V'	V-VI	II	I
250-300	V-VI	V	V-VI	III	I
>300	VI	VI	VI	IV	I

' The drier of the two wetness classes indicated is likely to occur either on slopes or in soils where the slowly permeable horizon is between 60 and 80 cm depth. Soils in these circumstances are normally not gleyed within 40 cm depth.

(x) In climates with less than 175 F.C. days subsoiling or other soil loosening techniques are usually effective to 40 cm depth. In this Table it is assumed that permeability has been improved to at least that depth.

The remainder of this section outlines the soil types found within the study area and gives a review of the hydrological significance of these soil types. Table 3.3 gives details of the approximate extent of coverage for each soil type in the area and Figure 3.8 illustrates the spatial distribution pattern for most of the area (see also Chapter 9).

Table 3.3 Soil Types to be found in the Research Area

Soil No.	Soil Series	% Cover Research Area (Approx.)
611	Manod/Malvern	35
311	Revidge	25
1013	Crowdy 2	11
713	Brickfield 1	10
721	Wilcocks 2	10
654	Hafren	5
651	Hexworthy	4
811	Conway	4
612	Moorgate	2

Descriptions of the various soil types were obtained from SSEW (1984).

Manod Series: permeable well drained soils (Wetness Class I) but as the climate over much of the season is wet, most of the soils remain wet throughout most years. The soils readily absorb excess winter rainwater except on steep land or where bedrock is near the surface.

Malvern Series: generally occurs on steep bouldery slopes, the principal soils are brown podsols formed in shallow drift over igneous rocks of varying acidity. They are well drained and readily absorb winter rainfall except on the steepest slopes. The shallower soils are liable to drought.

Crowdy 2 Series: raw acid peat soils with peat thicker than 40cm, they are more or less permenantly wet (Wetness Class VI). The available water capacity of peat soils is about twice that of mineral soils (Rudeforth and Thomasson 1970) and the peats store large amounts of water which is released slowly, thus sustaining flow in dry periods. During protracted dry spells the peat contracts so that heavy subsequent rains pass rapidly through cracks to the streams and rivers and locally form dendritic erosion channels in the peat itself. In winter when the peat has swollen and the cracks have closed, excess rainfall flows rapidly from the saturated surface.

Revidge Series: shallow peaty soils on gritstone and sandstone interspersed with deeper soils of the Crowdy and Winter Hill series. Very acid, often wet with high rainfall and low summer temperatures. Terrain is rough and mountainous with heather moor and extensive bare rock and scree.

Brickfield Series: fine textured wet soils developed on gentle slopes, the soils are slowly permeable and waterlogged for long periods in winter, and, where the topsoil is humose or peaty, well into the growing season. They are cambic stagnogley soils with a stony clay loam and a Wetness Class of IV or V (or III-IV with drainage). There is usually a break of slope to steeper ground where the soils meet the drier Manod Association, and in places this is marked by spring-lines with wet peaty flushes.

Wilcocks 2: wet, loamy soils with peaty tops. Usually occupies drift-covered gentle slopes, where natural drainage is impeded. These stagnohumic gley soils lie wet for long periods or are permenantly waterlogged (Wetness Classes V or VI). During winter excess rainwater moves rapidly from the saturated soil to streams.

Hafren Series: develop in rock debris from Palaeozoic mudstones, shales, siltstones and occasionally slates. The water regime is complicated by the presence of contrasting horizons. Water is held in the surface horizons of Hafren soils, the peat acting as a sponge so that they are seasonally waterlogged even though the subsoils drain freely (Wetness Class III or IV).

Hexworthy: iron stagnopodzols, with seasonally waterlogged peaty surface horizon. Loamy very acid permeable upland soils.

Conway Series: deep stoneless fine silty soils dominate this series, which is found on the floodplains of rivers and streams. Excess winter rain is absorbed fairly slowly on level ground, but it reaches rivers relatively quickly because they are close by. High groundwater and the slow infiltration of Conway soils makes them seasonally or severely waterlogged (Wetness Class IV or V).

Moorgate: well drained coarse loamy humic brown podzolic soils (Clayden and Hollis, 1984) with a dark humose topsoil overlying a finely structured permeable brown or brightly coloured subsoil of gritty sandy silt loam or gritty sandy loam.

The spatial distribution pattern for soils in much of this area can be seen in Figure 9.6 of Chapter 9. Both satellite imagery and aerial photography can be used in the interpretation of soil types, where the surface cover is natural or semi-natural vegetation, or bare soil. The methods used are described in detail in Mulders book on remote sensing in soil science (Mulders, 1987).

3.5 Landcover

Determining the landcover types of an area is an important element in predicting the hydrological response and also in assessing the capabilities afforded by remote sensing technology. The possibility of obtaining information on the spatial distribution pattern of various landcover types, in an easy and relatively cheap manner, for incorporation in hydrological models is something which has hitherto been unavailable. Even in developed countries such as the U.K., there is no systematic large scale landcover mapping, those areas which are covered often having information which is now dated. In Chapter 2, reference was made to the use of landcover classes derived from Landsat MSS data as inputs to SCS models. The need for detailed information on the capabilities of higher resolution satellites, such as Landsat TM was also highlighted.

The amount of precipitation actually reaching the ground is largely dependent upon the nature and the density of the vegetation cover, or upon the existence of an artificial cover in urban areas. The three main components are interception loss: i.e., water which is retained by plant surfaces and which is later evaporated away or absorbed by the plant; throughfall, i.e., water which either falls through spaces in the vegetation canopy or which drips from leaves, twigs, and stems to the ground surface; and, stemflow, i.e., water which trickles along twigs and branches and finally down the main trunk to the ground surface (Ward 1975). Only in the case of interception loss is the water prevented from reaching the ground surface and so taking part in the land-bound part of the hydrological cycle.

The fact that following a dry spell interception loss is usually greatest at the begining of a storm and reduces with time, reflects the interaction of the main factors which affect it. Of these, undoubtedly the most important is the interception capacity of the vegetation cover (Ward 1975), i.e., the ability of the vegetation surfaces to collect and retain falling precipitation. At first, when all the leaves and twigs or stems are dry, this is high, and a very large percentage of precipitation is prevented from reaching the ground. As the leaves become wetter, the weight of water on them eventually overcomes the surface tension by which it is held and, thereafter, further additions from rainfall are almost entirely offset by the water droplets falling from the lower edges of the leaves. Even during rainfall, however, a considerable amount of water may be lost by evaporation from the leaf surface, so that even when the initial interception capacity has been filled, there is some further fairly constant retention of water to make good this evaporation loss. Other conditions remaining constant, evaporation tends to increase with increasing windspeed, so that during prolonged periods of rainfall the interception loss is greater in windy than in calm conditions. Penman (1948) devised a formula to estimate potential evapotranspiration which combines turbulent transfer and energy balance theories.

Considerable attention has been paid in studies to the interception loss from woodland, in particular the examination of possible differences in the magnitude of loss from coniferous and deciduous forests. Despite the fact that, in most cases, the leaf density is greater in deciduous than in coniferous forest, the bulk of experimental evidence shows that interception losses are greater from the latter. Reviewing a broad range of Russian, European, and American data, Rakhmanov (1966) suggested that coniferous forests, together with sparse woods and inhibited stands on peat bogs and other marshy terrain, intercept an average of 25-35 per cent of the annual precipitation compared with 15-25 per cent by broad-leaved forests.

A thorough discussion of the classification and interpretation of the landcover classes discernable from the remotely sensed imagery is given in Chapters 5, 6 and 7, and thus will not be dwelt on here. Hydrologically speaking landcover is important from an interception and evapotranspiration point of view, and also in how it affects the relative proportions of runoff and infiltration.

This area lies in a relatively remote part of the U.K. and is, in the main, one of semi-natural vegetation, with some areas influenced by man, others completely unaffected. The climate and frequency of steep slopes is not conducive to arable agriculture, though some exists in the valley of Afon Wnion. Pasture for sheep grazing and some dairying predominate the local agriculture. The other major economic landuse is forestry, the large Coed-y-Brenin forest and other smaller forested areas are mainly coniferous. Deciduous woodland occurs sporadically, in small irregularly-shaped blocks, particularly in the Wnion valley. Permanent and ley grassland covers the floodplain of the Mawddach valley. Unforested valley sides tend to be covered with numerous mountain grasses (*Nardus* sp., *Agrostis* sp., *Molinia* sp.) (Baker *et al.*, 1991), which are sometimes bracken-encroached and give way at higher altitudes to heather (*Calluna-Vaccinium* sp.) moorland. Wetland and bog areas of rushes (*Juncus* sp.), moss (*Sphagnum* sp.) and cotton-grass (*Eriphorum* sp.) occur intermittently on the moorland area. Surface water occurs as numerous tiny lakes/ponds and the slightly larger Lyn Cynwch (British National Grid Reference:2737 3207), together with many streams the study of which form a major part of this research.

Dolgellau, a small town (2730 3177), forms the only urban area of any significance, scattered farmhouses existing elsewhere in the area. Major roads of the area tend to follow the lower valley sides, close to the floodplain eg. A496 (2700 3195). Minor roads occur on valley sides in the Wnion valley primarily for access to farms. Forest roads, many unsurfaced, occur throughout the major forest blocks.

From this information, together with field investigations and knowledge of previous work (as discussed in Chapter 2) it was decided to concentrate on five major classes, these being:

- Forest/Woodland;
- Moorland (including mountain grasses, heather, bog, bracken);

- Lowland Agriculture (including pasture and the few arable areas);
- Water;
- Urban.

These are the classes which were for use in visual and automatic classification of landcover, which are detailed in Chapters 6,7 and 8.

3.6 Climate

The most obvious, and probably the most effective influence on the total volume of runoff is the long-term balance between the amount of water gained by a catchment area in the form of precipitation, and the amount of water lost from that catchment area in the form of evapotranspiration (Ward, 1975). In this sense, the climate of the catchment area sets the broad upper limits to the total volume of streamflow leaving the area, but this relationship between annual totals and means of rainfall and evapotranspiration may be modified by short-term factors, such as the manner in which precipitation occurs, and sudden changes in vegetation cover.

This area lying on the western fringe of Great Britain is one of the first parts encountered by the moist air masses associated with frontal systems advancing eastwards from the Atlantic. Local differences in climate within the area relate mainly to altitude varaitions. With increasing height above sea level, average temperatures fall and precipitation increases - the mountains here tend to be cloudy, cold and exposed, with high rainfall. Meteorological office records for the 30 year period 1941-1970 show an average annual rainfall of around 2000mm (Meteorological

Office, 1967).

In soil moisture terms, transpiration usually first exceeds rainfall during April in an average year. Soil moisture deficits then accumulate, usually reaching a maximum in June or July in the study area. Thereafter rainfall is normally greater than potential transpiration and soil reserves are replenished during Autumn. The mean P.S.M.D. (Potential Soil Moisture Deficit) in the growing season for this area is 40mm or less, most of the area being 25mm or less. Soil wetness is a more common problem in Wales than droughtiness. The times of image acquisition in this research were June 1975 for Landsat MSS, June 1981 for the aerial photography and July 1984 for the Landsat TM imagery.

In June 1975 the area was under drought conditions, the rainfall over the February to June period being less than half the normal amount. The rainfall in June 1981 was around 112mm which is slightly above the average of 105mm (figures from 1962-1980; NERC, 1985). The rainfall figure for May 1981 was also above average. In July 1984 the area was under severe drought conditions with only 64mm rainfall compared to the average July figure of 106mm (figures from 1962-1983). During the period April to August 1984 the rainfall was only 30-40% of the average (figures from 1941-1970; NERC, 1986). These figures indicate that channel flow in the drainage networks of the area would be low in June 1975 and July 1984, but about normal for the time of year in June 1981. It is possible that some of the more minor streams were dry during the image acquisition of the Landsat MSS and Landsat TM imagery.

3.7 Field Survey

Ideally a field survey should be carried out simultaneously with image acquisition; this, however was not possible in this case, the Landsat MSS imagery coming from June 1975, the Landsat TM imagery from July 1984 and the Panchromatic Aerial Photos from 1981. Ground truth data is required for supervised automatic landcover classification and verification of manual interpretation results, or accuracy checks. An initial field survey of the area was carried out over the weekend of 9-11th March, 1985. This survey concentrated on taking stream width measurements and a first look at general landcover types. Readings of stream width were taken at the locations indicated on Figure 3.8. The stream width values can be seen in Table 3.4.

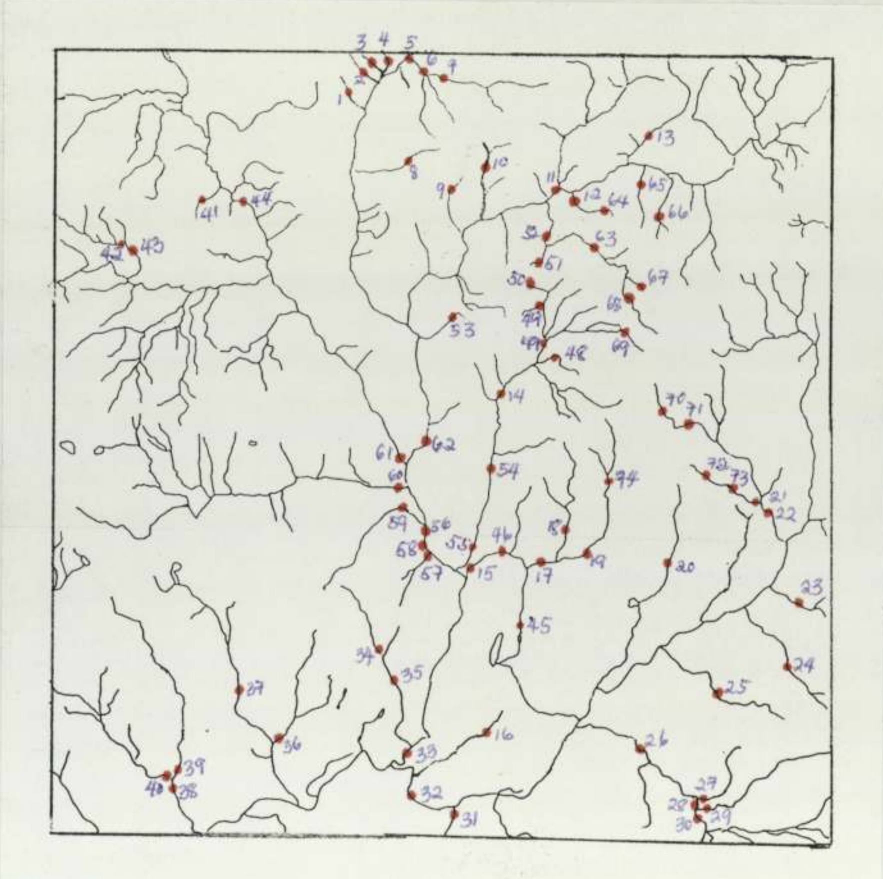

Figure 3.8 Ground data location map. Numbers indicate the stream width measurement locations (see Table 3.4).

The stream width measurement was taken as the water surface width. Some landcover details were recorded and photographs were taken of several parts of the area. The measurements were recorded as "Ground truth" data for comparison with features which can be interpreted from each type of imagery, for a quantitative assessment of image capabilities. A further field survey was undertaken from 24-26th June, 1985, to coincide with the season of image acquisition.

Table 3.4 Stream width measurements. Note: all full grid references are preceded by 2 and 3, i.e. full reference for point 1 is 2735 3317.

Point No.	Stream Width (metres)	Grid Ref.	Point No.	Stream Width (metres)	Grid Ref.	Point No.	Stream Width (metres)	Grid Ref.
1	1	735 317	16	1.25	734 192	31	4	721 178
2	2	739 322	17	6	748 223	32	18	714 184
3	0.5	741 323	18	3	756 227	33	31	718 193
4	0.5	744 324	19	3	760 223	34	2	714 214
5	12.5	743 323	20	2	774 217	35	3.5	718 204
6	4	743 323	21	4	795 224	36	2.5	691 200
7	3.5	759 319	22	7	797 223	37	9	685 210
8	1.5	745 305	23	5	796 204	38	8	668 199
9	1.5	755 305	24	4	789 198	39	4	670 200
10	2	750 300	25	1	777 190	40	4.5	669 199
11	11	764 294	26	8	761 179	41	0.5	703 308
12	0.5	779 289	27	2	771 169	42	1.5	684 303
13	3	790 299	28	10	748 178	43	2.5	685 302
14	5.5	756 257	29	7	770 167	44	11	709 305
15	4.5	735 224	30	5	768 167	45	1.5	744 213

Table 3.4 continued

Point No.	Stream Width (metres)	Grid Ref.	Point No.	Stream Width (metres)	Grid Ref.
46	6.5	744 226	61	19	728 248
47	2	760 263	62	10	734 252
48	1.5	761 261	63	2.5	774 281
49	1	763 272	64	1	777 287
50	0.5	761 276	65	0.5	786 286
51	1	763 280	66	0.5	787 280
52	2	766 284	67	0.5	783 271
53	1	745 273	68	1	780 268
54	9	746 244	69	1	777 263
55	9	737 228	70	0.5	782 244
56	19	730 234	71	1.5	783 242
57	0.5	729 229	72	1	784 233
58	1	278 233	73	1.5	789 228
59	2.5	722 238	74	2	767 234
60	8	726 244			

3.8 Summary

The chapter commenced with a discussion of the reasons for selecting the research area, namely; the availability of imagery, relative accessibility and the variety of landcover types in the area. A discussion of the physiography highlighted the importance of elevation and slope on drainage network development and surface runoff. Relief distortions and shadowing effects in remotely sensed imagery due to physiographic factors were also mentioned.

The influence of the underlying geology on hydrology was discussed in Section 3.3, and the incorporation of geological details in a GIS is considered in Chapter 9. Considerable attention was paid to the discussion of soil type variation and their hydrological significance. Landcover in the area was broken down in to five broad groups for discrimination by remotely sensed imagery. The climate of the area was discussed, with particular attention given to precipitation details prior to image acquisition.

The field survey was used to obtain stream width measurements for quantitative assessment of image capabilities in drainage network delineation. Some landcover details were also recorded with a view to the provision of training data for supervised classification as described in Chapter 6.

CHAPTER FOUR: **DETAILS OF IMAGERY**

4.1 Introduction

The following chapter gives a description of each of the types of imagery (data) used in this research. Two types of digital satellite imagery, namely Landsat MSS and Landsat TM data, and one form of analogue panchromatic aerial imagery were examined. The spectral ranges of these imagery types are shown in Figure 4.1. The chapter commences with brief sections on the importance of historical remote sensing and the physical basis of remote sensing.

4.2 The significance of historical remote sensing

The history of remote sensing may seem at first sight to be of minimal interest to the rest of this research. However, it is important to understand the way remote sensing has developed, and the way it is likely to develop in the future. This could have very serious implications for its application to the assessment of various hydrological parameters. Some of the most important questions one should ask are:

i) what are the past and present remotely sensed data types?

ii) what are the application potentials of these data types?

iii) what is the likelihood of their continued availability?

iv) what new remotely sensed data types are planned, or likely in the future?

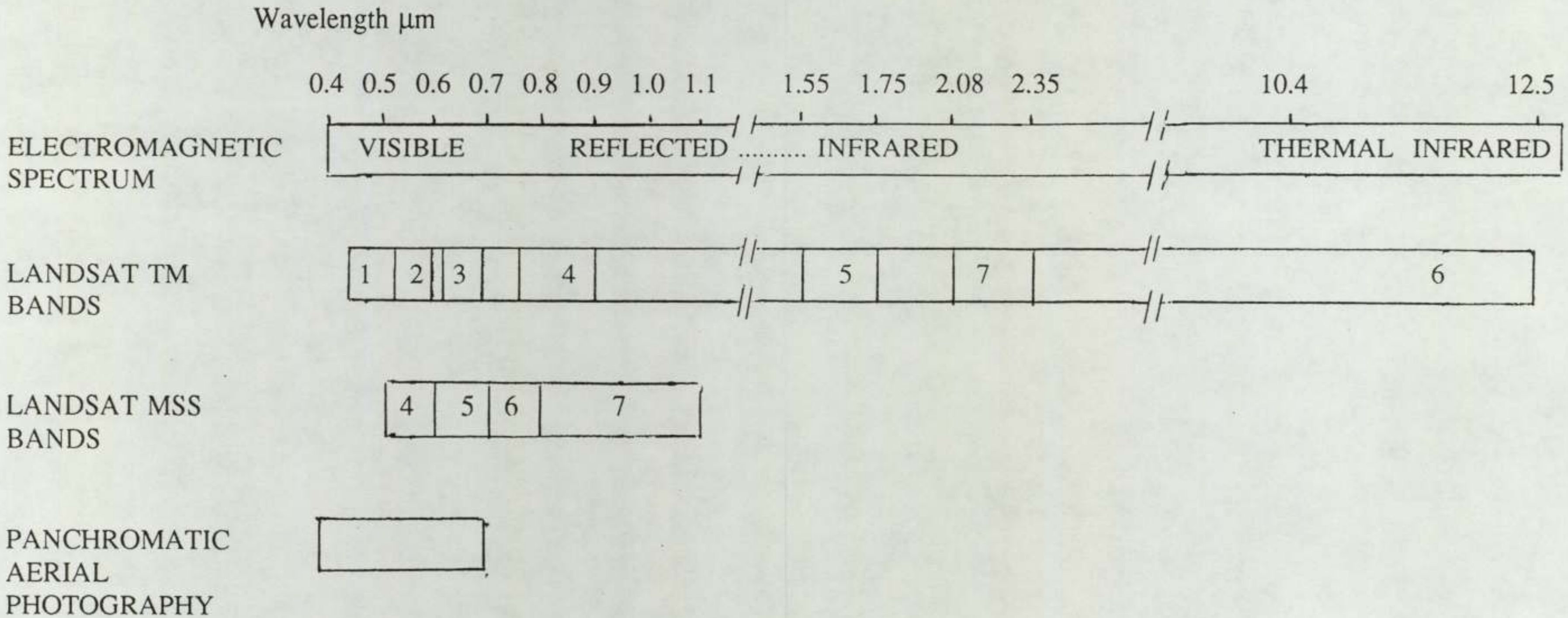

Figure 4.1 Comparison of wavelengths recorded by sensors.

v) what are the costs of the various remotely sensed data types now and likely costs in the future?

vi) how do these remotely sensed data costs compare with each other and other possible data sources?

From these questions, the importance of the development of remote sensing can clearly be seen. It is not proposed to give a detailed account here of all the remote sensing sensor devices and platforms. An account of many remote sensing systems is given in the Manual of Remote Sensing (1983). More recent details can be found amongst others in Mather (1987), Szekielda (1988) and Engman and Gurney (1991). Details specific to the imagery types used in this research are given in the following sections.

4.3 The Physical Basis Of Remote Sensing

To interpret fully a remotely sensed image it is necessary to understand the way in which electromagnetic radiation interacts with the earth's surface. A comprehensive review of all the physical processes involved would require a lengthy exposition. The following paragraphs provide a brief account of the major processes, further more detailed explanations can be found in Curran (1985), Mather (1987), Szekielda (1988).

In this research the sensors studied are passive sensors recording existing radiation, as opposed to active sensors such as radar. Figure 4.2 illustrates the main elements of a passive remote sensing system. The sensor can be seen to record reflected electromagnetic radiation which emanates from the sun and is recorded after interaction with the earth's surface and atmosphere. No thermal imagery was used in this research.

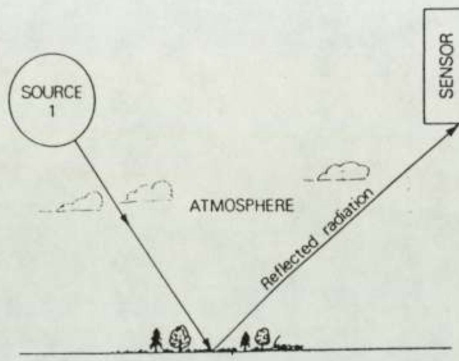

Figure 4.2 A passive remote sensing system (adapted from Curran, 1985).

Only certain wavelengths of the electromagnetic energy which emanates from the sun pass through the earth's atmosphere without significant attenuation. It is these wavelengths or "windows" which are used in remote sensing. Figure 4.3 illustrates the windows where atmospheric transmission is high. Comparison of figures 4.1 and 4.3 show the use of atmospheric windows for recording the remotely sensed imagery used by the sensors in this research.

The reflectance properties of materials varies according to the wavelength of radiation. It is a knowledge of these variations which is used to select the wavelengths imaged

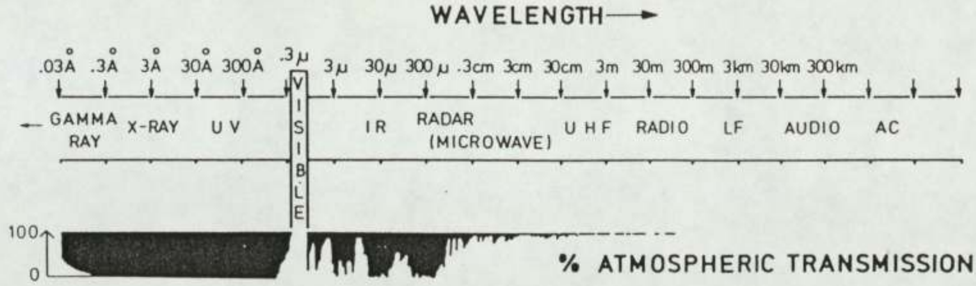

Figure 4.3 The electromagnetic spectrum and generalized atmospheric transmission (after Szekielda, 1988).

by a sensor. Idealized spectral reflectance curves for vegetation, soil and water are presented in Figure 4.4. It was this type of information which was used to define the ranges of wavelengths to be included in the bands recorded by the Landsat MSS and Landsat TM sensors as shown in Figure 4.1.

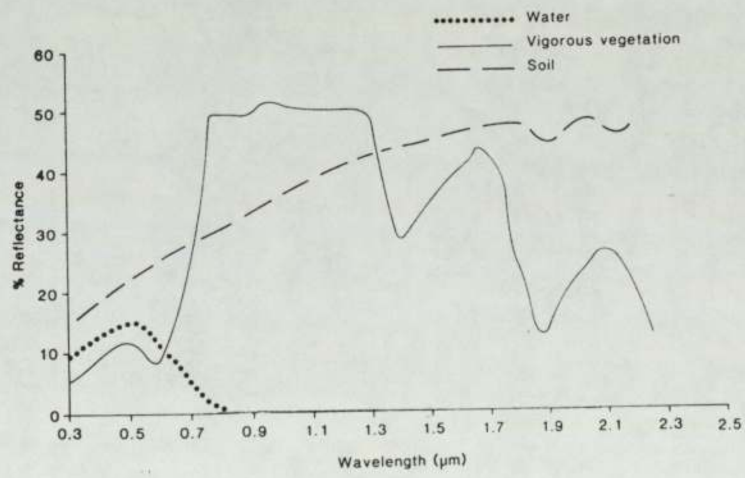

Figure 4.4 Idealized spectral reflectance curves for vigorous vegetation, soil and water (after Mather, 1987).

The reflectance values recorded by the sensor can be used to discriminate different earth surface cover types. Attempts have been made to define "spectral signatures" for various surface materials. These attempts have met with only limited success due to the numerous factors which affect the signal recorded by the sensor. Perhaps the most difficult effects to allow for are the atmospheric conditions at the time of image acquisition. Sensor viewing angle, solar elevation, earth surface topography, material status (e.g. varying vegetation growth state), spatial variation frequency relative to sensor sensitivity are many of the other factors which influence the interpretation and classification of remotely sensed imagery. Many of these factors are discussed at various points throughout this research.

4.4 Panchromatic Aerial Photography

Aerial photography was the first method of obtaining remotely sensed data, and is currently the most widely used type of remotely sensed data. Aerial photographic images are recorded by a camera mounted in the base of an aircraft. Many archives of air photos exist, and these are frequently used to monitor environmental changes over time. However, the temporal frequency of these coverages can vary widely and may or may not be of great value. The six characteristics of aerial photography which make its use so common are:- its availability, economy, synoptic view point, time freezing ability, spectral and spatial resolution, and three dimensional perspective.

i) Availability: aerial photographs are readily available from appropriate libraries at a range of scales for much of the world. However there are access retrictions in many countries of the world for security reasons.

ii) Economy: aerial photographs are less expensive than field surveys, and are often cheaper and more accurate than maps for many countries of the world.

iii) Synoptic Viewpoint: aerial photographs enable the detection of small scale features and spatial relationships that would not be evident on the ground.

iv) Time freezing ability: an aerial photograph is a record of the Earth's surface at one point in time and can therefore be used as a historical record or even legal evidence.

v) Spectral and spatial resolution: aerial photographs are sensitive to electromagnetic radiation in wavelengths that are outside the spectral sensitivity range of the human eye, these include both ultra-violet (0.3-0.4μm) and near infrared (0.7-0.9μm) radiation. They can also be sensitive to objects outside the spatial resolving power of the human eye.

vi) Three dimensional perspective: a stereoscopic view of the Earth's surface can be created which enables both horizontal and vertical measurements to be made. This is a characteristic which is lacking for the majority of remotely sensed satellite images.

Several film types are available for aerial photography, namely: black and white panchromatic; black and white infrared; colour and colour infra-red. This research is limited to the examination of black and white/panchromatic film which is capable of recording, in tone variations, most colours of the visible spectrum. Details of other photographic types can be found in White (1977), The Manual of Remote Sensing

(1983), Curran (1985), Mulders (1987), amongst many others. Owing to the precise requirements of aerial photography, for subsequent map-making, the film has a polyester base which provides greater dimensional stability (i.e. minimal stretch and shrinkage).

The angle at which an aerial photograph is taken is used to classify the photograph into one of three types: vertical; high oblique or low oblique (see Fig. 4.5). Vertical photography is taken with the camera axis (focal plane) pointing vertically downwards and oblique photography is recorded with the the camera axis pointing at an oblique angle to the observed surface. Low oblique photography incorporates the horizon into the photograph while high oblique does not.

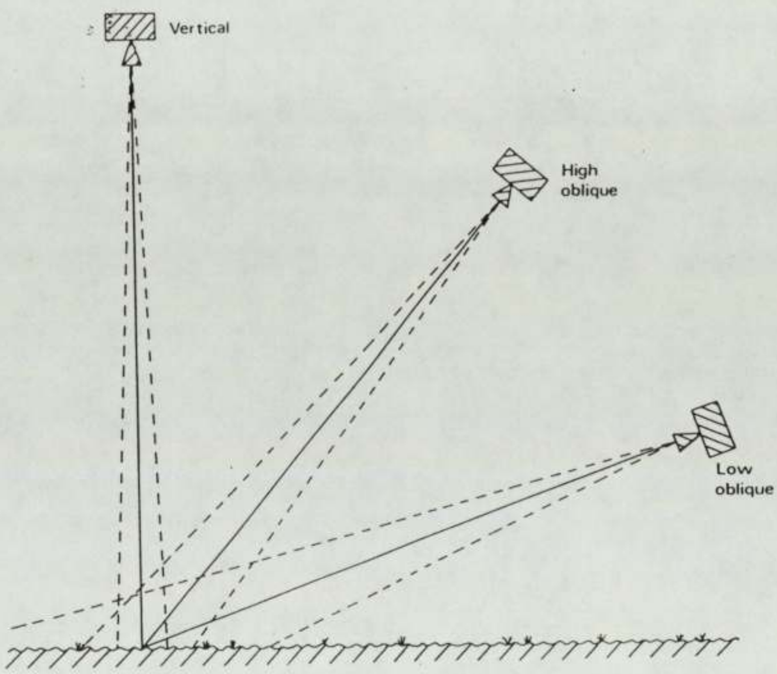

Figure 4.5 The angular difference between vertical, high oblique and low oblique aerial photographs (after Curran, 1985).

Vertical aerial photographs, as employed in this research are the most widely used form as they have properties that are similar to those of a map. They possess an approximately constant scale over the whole photograph and as a result can readily be used for mapping and measurement (Curran, 1985). These photographs are usually taken in sequences along the aircraft's line of flight (Fig. 4.6) in such a way that overlap (called forward lap) is of the order of 60%. This is to facilitate the stereoscopic viewing of adjacent prints. To ensure that all of an area is covered the aerial photographs also overlap sideways (called sidelap) by around 30%. This means that each point on the ground appears at least twice in an aerial photographic coverage.

Flying pattern used to obtain stereoscopic aerial photography. There is 60% overlap between aerial photographs in a run and 30% overlap between aerial photographs in adjacent runs. Circles mark the photocentres which are located directly beneath the aircraft.

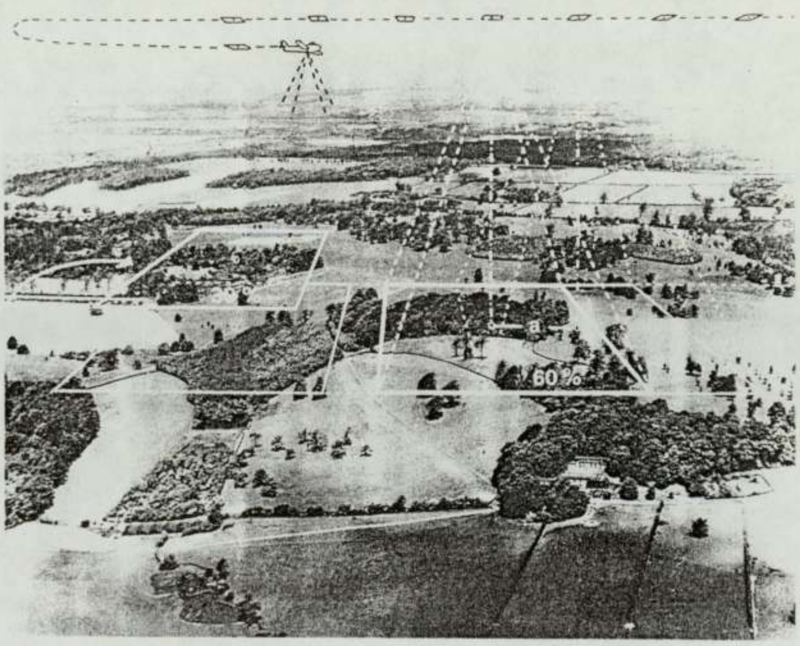

Figure 4.6 Illustration of aerial photographic coverage of an area (after Curran, 1985).

The scale of an aerial photograph, together with its type, determine its value for particular applications. In this study the photographs have scale of 1:50000 which is a relatively small scale in aerial photographic terms; scales of 1:5000 and 1:10000 are common in aerial survey. The scale was determined from the focal length of the camera used and the vertical height of the lens above the ground (see Fig. 4.7). The scale of an aerial photograph is determined by the focal length of the camera and the flying height of the aircraft (Fuller, 1981). If a feature is higher or lower than the datum set for determining flying height, then it will be at a larger or smaller scale than the surrounding land (see Figure 4.7). The scale of a vertical photograph is given by :

$$S=f/(H-h)$$

where S is the scale, f is the focal length, H the flying height and h the height of an object above datum.

An object above the datum will also appear to be displaced from the centre of the photograph. The amount of displacement is given by :

$$d_e = rh/H \quad \text{(for a vertical photograph)}$$

where d_e is the displacement and r the distance from the nadir point.

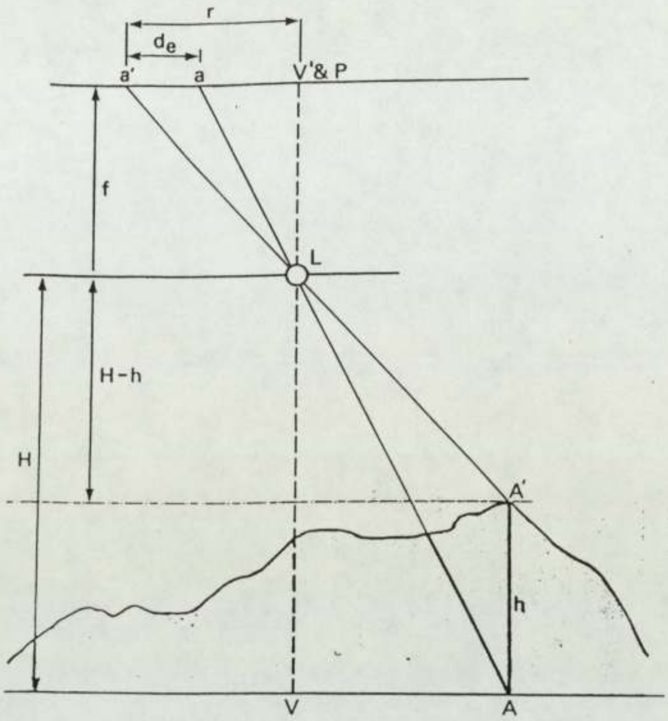

f - *focal length of camera*

H - *flying height*

h - *height of A' above datum*

A - *vertical projection of 'A' onto the datum plane*

L - *camera lens*

P - *principal point*

V - *nadir point*

V' - *image of V on negative*

d_e - *displacement of a' (image of A') from a (its planimetrically correct position)*

Figure 4.7 Photographic image displacement caused by relief variation (after Fuller, 1981).

Timing of the image acquisition can also be of importance, with varying drainage network extents, and also differing shadow effects according to time of day/year. This imagery was recorded in June 1981, as part of a coverage of Wales flown by the Royal Air Force on behalf of the Welsh Office.

4.5 Landsat Multispectral Scanner (MSS) Imagery

The Landsat Multispectral Scanner (MSS) imagery examined in this research was from the Landsat 2 satellite (see Fig. 4.8) which was operated by NASA (National Aeronautic and Space Administration) from January 1975 to February 1982. Landsat 2 was one of the series of Landsat satellites forming a continuous imaging succession from July 1972 to the present date. This type of imagery has similar general characteristics to those mentioned for aerial photography, however, it has no inherent three dimensional perspective.

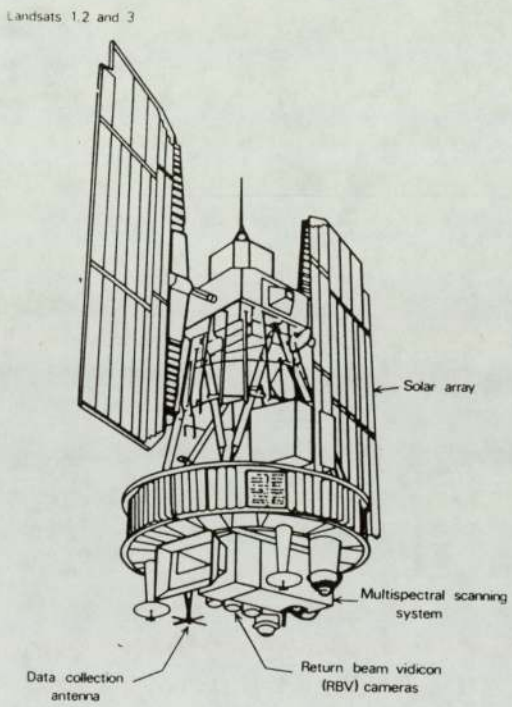

Figure 4.8 Landsat configuration (Landsat's 1, 2 and 3)(after NASA, 1976).

When in operation, this satellite had a near polar sun-synchronous orbit at a nominal altitude of 919Km and covered the earth from 82° degrees N to 82° degrees S. The orbital period was 103 minutes, with the imaging orbit crossing the equator at 9.30

hours local time, as illustrated in Figure 4.9.

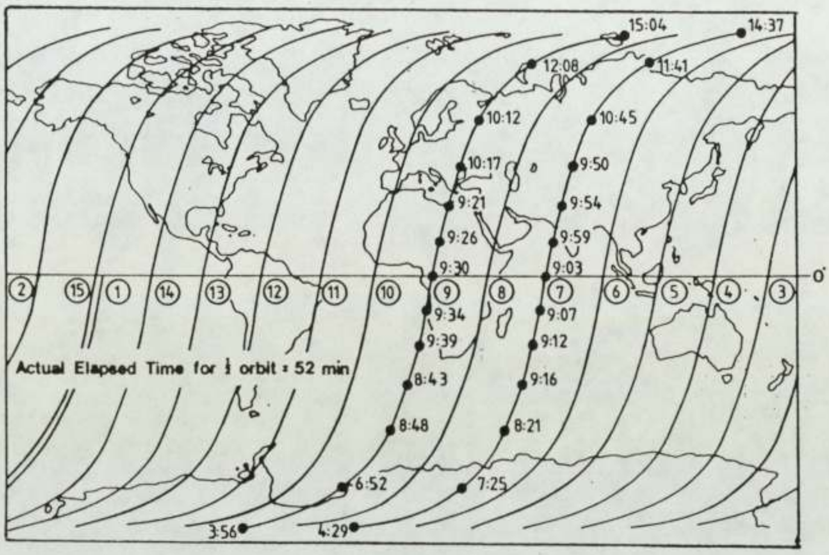

Figure 4.9 Landsat orbital tracks for one day of coverage indicating variations in local time of data acquisition (NRSC, 1986).

This orbital pattern resulted in a repeat cycle of 18 days. The current Landsat 4 and Landsat 5 satellites have slightly different orbital parameters (see Section 4.6) and they also carry MSS sensors. The Landsat Multispectral Scanning System (MSS) records four images of a scene, each covering a ground area of 185Km by 185Km at a nominal ground resolution of 79m (see Fig. 4.10). These images fall within the green, red, near infrared wavebands (see Figure 4.1) and are identified by the channels they occupied in the satellite telemetry system which were 4,5,6 and 7 respectively on Landsat 2.

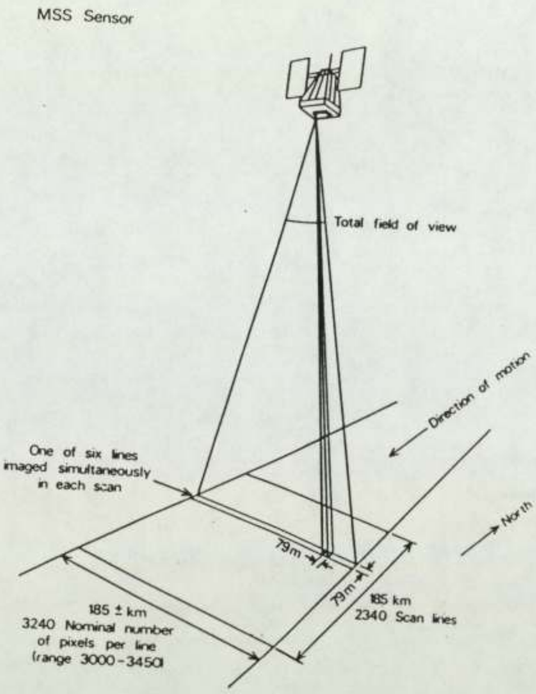

Figure 4.10 Landsat MSS imaging configuration (after Curran, 1985; NASA, 1976).

The MSS images are produced by directing the radiance, recorded from 79m wide scan lines on the Earth's surface, to detectors on board the satellite (Fig. 4.7). To measure the radiance for a particular area, the scan line is divided into units by the Instantaneous Field Of View (IFOV) of the sensor. The IFOV is a geometric measure of spatial resolution and as such can be thought of as representing the original "pixel size" (Townshend *et al.*, 1988). The formula for calculation is:

$$IFOV = \frac{HD}{f}$$

where H is the height of the satellite above the ground, D is the detector size and f the focal length of the scanner. Substituting the appropriate values for the MSS yields a value of 79m for the MSS. The sampling procedure used for MSS data is not the same as the scanning rate. As a result the pixels correspond to a ground area of 56x79m. This rectangular as opposed to square shape for pixels has considerable distortional effects on the imagery, making geocorrection essential (see Section 5.2.2). The sampling pattern is illustrated in Figure 4.11.

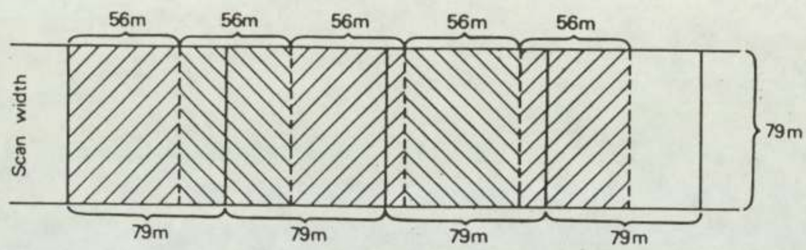

Figure 4.11 Sampling pattern of the Landsat MSS (after Curran, 1985; NASA 1976).

As the satellite moves forward at a high speed it is pragmatic to record 6 across track scan lines simultaneously, necessitating the use of 24 detectors, 6 in each of the 4 wavebands viewed. Each one of these detectors converts the recorded radiance into a continuous electrical signal which is then sampled at fixed time intervals and converted to a 6 bit number (0-64). Each number is then either recorded onto a magnetic tape or transmitted directly to earth where it is rescaled to a 7 bit number (0-128) for 3 of the bands (4,5 and 6) with its fourth (band 7) unaltered. The Landsat receiving stations covering the U.K. and Europe are at Fucino in Italy and Kiruna in Sweden, both are part of the Earthnet data network programme, which can

Landsat receiving stations covering the U.K. and Europe are at Fucino in Italy and Kiruna in Sweden, both are part of the Earthnet data network programme, which can provide data on scene availability, cloud cover details etc by accessing the LEDA database at Frascati, Italy (Hyatt *et al.*, 1988).

A complete channel of Landsat MSS imagery comprises 2,340 scan lines and 3,240 pixels per line, a total of around 7.5 million pixels per channel and 30 million pixels per scene of 4 channels (bands). This large amount of data is collected in 25 seconds and fills one computer compatible tape (CCT) at 1600 bpi (bits per inch). It is impractical to record every possible scene of Landsat data as this would generate 30 million CCT's each year.

For the study, four suitable Landsat MSS scenes were available. Of these, a scene from June 1975 and one from May 1977 proved to be the best images. The scene from June 1975 had no cloud cover, but some striping was visible in Band 4. The May 1977 scene had some slight cloud cover and striping in Bands 4 and 5.

4.6 Landsat Thematic Mapper (TM) Imagery

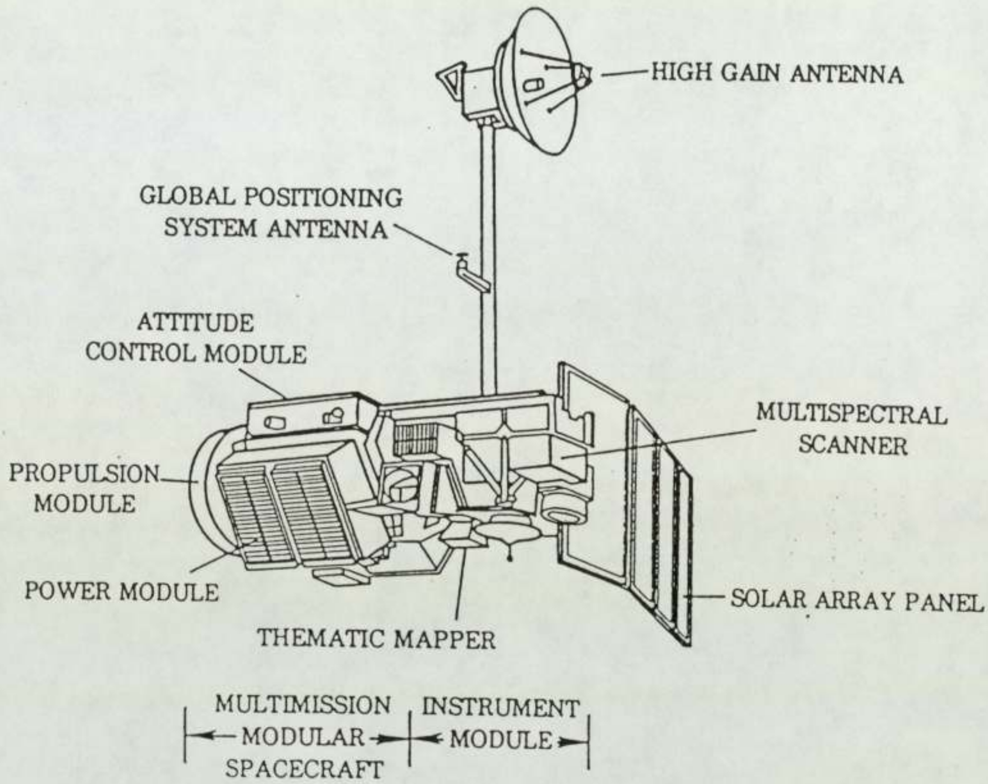

Figure 4.12 Configuration of Landsat's 4 and 5 (after NRSC, 1986).

The second generation of NASA's Landsat series was initiated in July 1982, with the launch of Landsat 4 and subsequent launch of Landsat 5 in March 1984. The Thematic Mapper 1/4 Scene used in this research was recorded by Landsat 5 on 22 July 1984. Several major differences exist between the basic design of the Multispectral Scanner and the Thematic Mapper (TM). First, the TM acquired images during both the forward (west-to-east) and reverse (east-to-west) sweeps of its scan mirror. This bidirectional approach was adopted to reduce the rate of oscillation of the scan mirror and increase the dwell time of individual detectors upon the earth's surface.

the earth's surface.

The TM does not rely on fibre optics as does the MSS, to direct incoming electromagnetic energy onto photosensitive detectors. Fibre optics are incapable of transmitting 100 per cent of the incident energy from the focal plane to the sensor's detectors. Instead the TM focuses incident radiation directly onto detectors within a prime focal plane assembly. This assembly contains four sets of 16 detectors for four spectral bands in the visible and near infra-red portions of the spectrum. A cooled focal plane assembly contains two arrays of 16 indium antimonide (InSb) photodiodes for two middle infra-red spectral bands and four mercury cadmium telluride (HgCdTe) detectors for a thermal band (Jensen, 1986).

The use of multiple detectors for each spectral band results in the generation of 16 scan lines of data for the six reflective bands and four lines of data for the thermal band during each sweep of the scan mirror. At any one instant, surface radiance is sensed by a total of 100 TM detectors. The Thematic Mapper records 256 radiance levels (8-bit data) in 7 wavebands (see Table 4.1) with a spatial resolution (IFOV) of around 30m in Bands 1,2,3,4,5 and 7; and 120m in Band 6 the thermal infrared band. The effect of increased spatial resolution of Landsat TM imagery with respect to Landsat MSS imagery is illustrated in Figure 4.13.

Table 4.1 The Wavebands recorded by the Landsat Thematic Mapper on Landsats 4 and 5.

Band number	Band name	Band width(μm)	Remarks
1	Blue/Green	0.45-0.52	Good water penetration, strong vegetation absorbance
2	Green	0.52-0.60	Strong vegetation reflectance.
3	Red	0.63-0.69	Very strong vegetation absorbance.
4	Near infrared	0.76-0.90	High land/water contrasts, very strong vegetation reflectance.
5	Near-middle infrared	1.55-1.75	Very moisture sensitive.
6	Thermal infrared	10.4-12.5	Very sensitive to soil moisture and vegetation.
7	Middle infrared	2.08-2.35	Good geological discrimination.

Sources : NASA 1982a, 1982b

The orbit of Landsat 5 is sun-synchronous with an altitude of 705km, and a global coverage from 81° N to 81° S. The orbital period of 99 minutes, crossing the equator at 9.45 hours local time, results in a repeat cycle of 16 days. Data for each scene is acquired during a 25.87 second increment corresponding to approximately 5700 scan lines of image data. Both the MSS data and the TM data cover a surface area of approximately 170km along-track by 185km across-track.

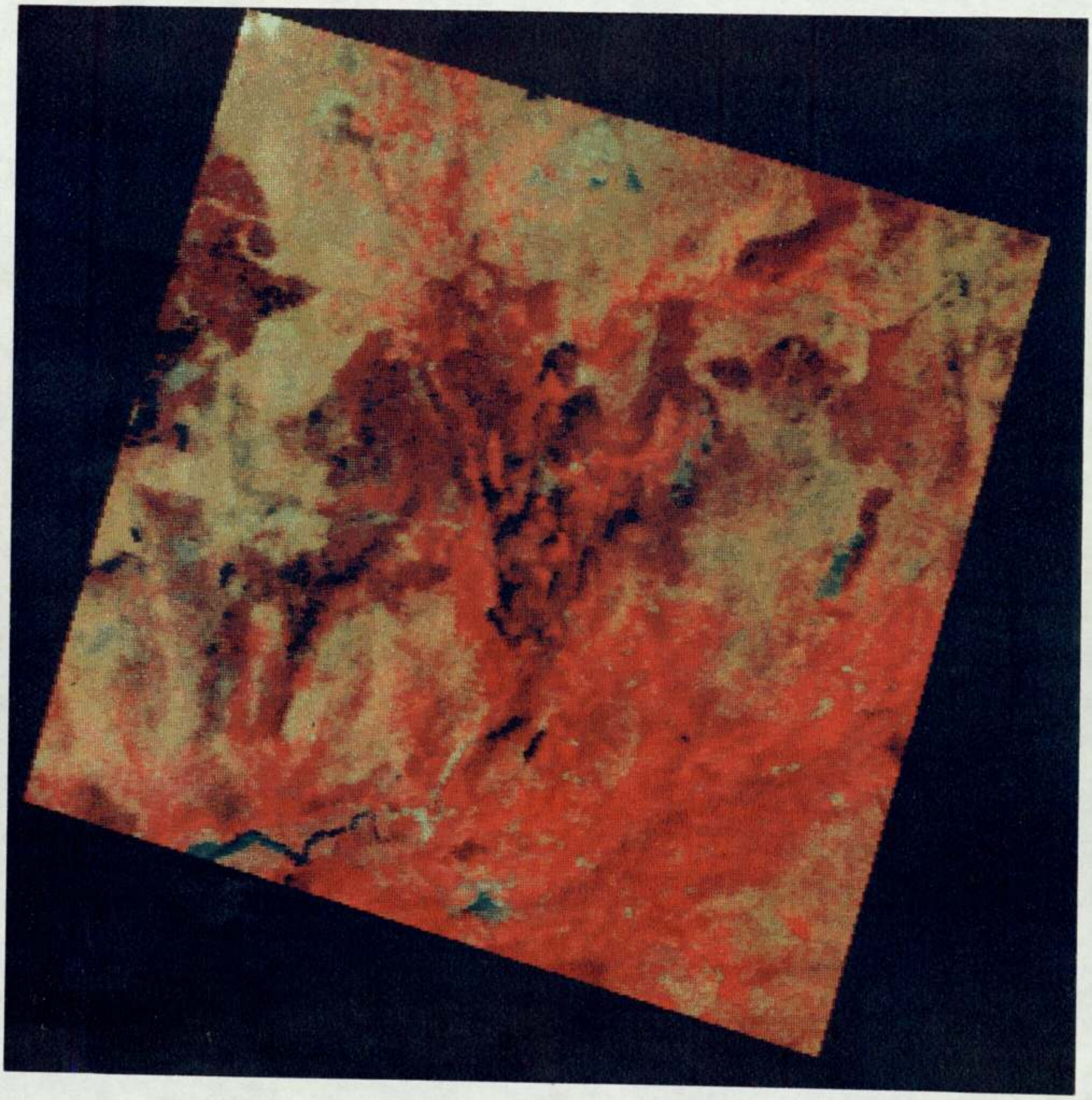

Figure 4.13 Comparison of Landsat MSS imagery (a) and Landsat TM imagery (b) (overleaf) for the same area; showing the effect of increased spatial resolution.

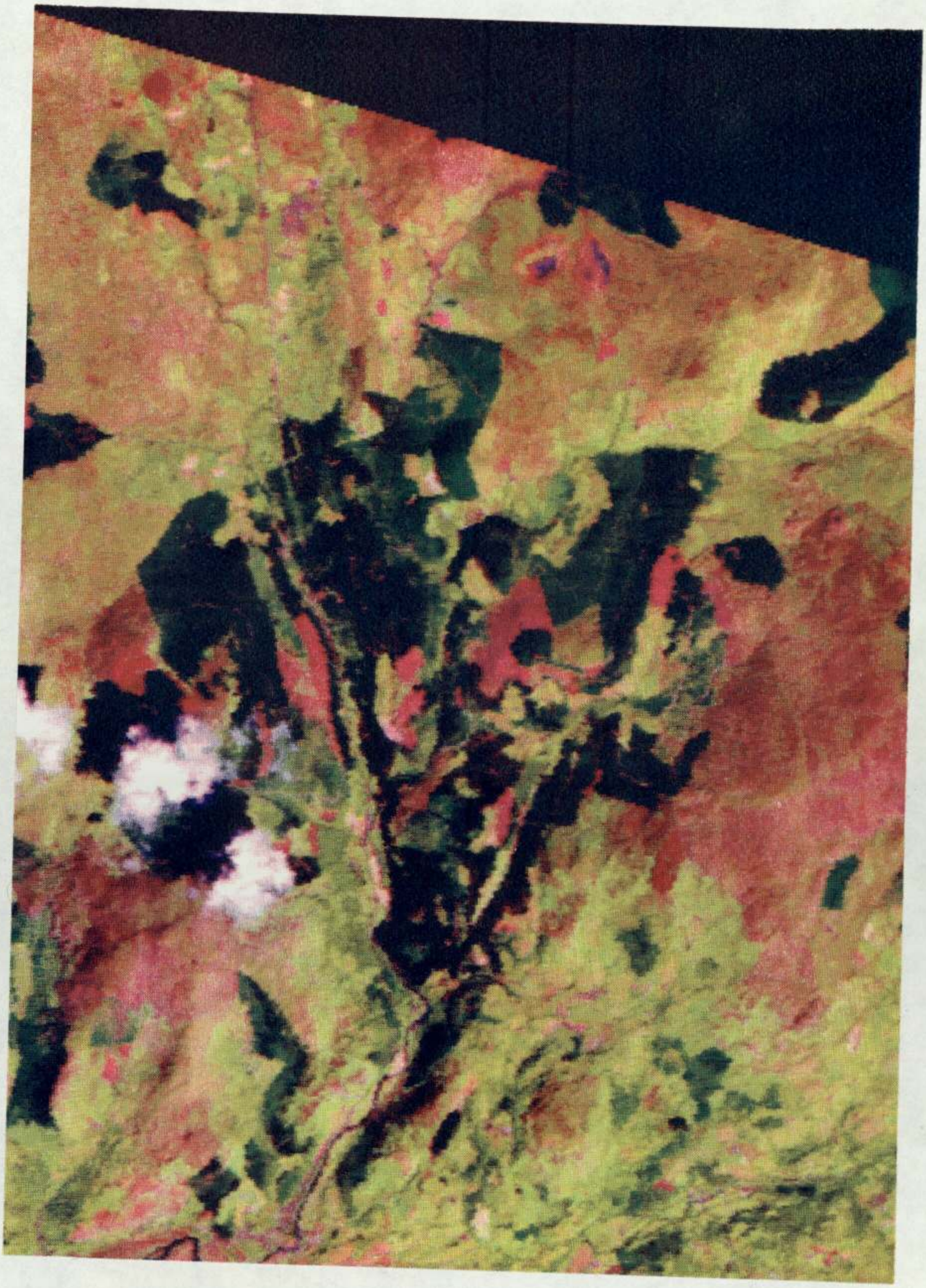

Landsat TM data has a high internal geometric consistency (Colvocoresses, 1986). It is possible to use publish TM multicoloured image maps of 1:100000 scale with suitable geometric fidelity and information content. The geometric characteristics of Thematic Mapper data are substantially superior to those of the Multispectral scanner system, as a consequence of superior ancillary data on the pointing of the sensor, and its finer spatial resolution (Townshend *et al.*, 1988). This means that TM images require less geometric correction and are capable of utilization for mapping at much finer scales than MSS data.

With regard to off-nadir viewing, Mogorovich (1989) discusses errors pertaining to TM data. Each land point of height h, viewed from angle the satellite at angle a with respect to nadir, is recorded in a position which is displaced towards the exterior of the path by a value dX, where

$$dX = h.\sin(a)$$

When the value of dX is small with respect to the dimensions of the pixel, the deformation is negligible. Spatial resolutions such as that of the TM can, however, cause macroscopic errors. For example, a point at 60km from the path of the satellite will be displaced towards the exterior by 85m for every 1000m of altitude, which is approximately equivalent to a 3-pixel shift. Similar calculations can be made for MSS data with a different spatial resolution, and possibly a different altitude, depending on the recording satellite.

Landsat 5 uses a new communications system, called Tracking and Data relay Satellite System (TDRSS) which eliminates the need for onboard recorders. TDRSS will eventually consist of two satellites (plus an in-orbit space) in geosynchronous orbits and a centralised ground receiving station located at White Sands, New Mexico. TDRSS-East is currently in geosynchronous orbit over the equator at 41 (degrees) west longitude at an altitude of 35,890 Km. The second TDRSS satellite was lost on board the Challenger Shuttle disaster in January 1986. In theory Thematic Mapper data should have been obtainable from almost any location in the world via TDRSS (Townshend *et al.*, 1988). In practise many fewer data have been collected than anticipated via this system, due in part to the disaster, and much more reliance has been placed on the ground receiving stations. The locations of stations currently receiving Thematic Mapper data is shown in Figure 4.14. The lower orbit of Landsats 4 and 5 means that the area of coverage of these ground receiving stations is somewhat smaller than that for Landsats 1,2 and 3.

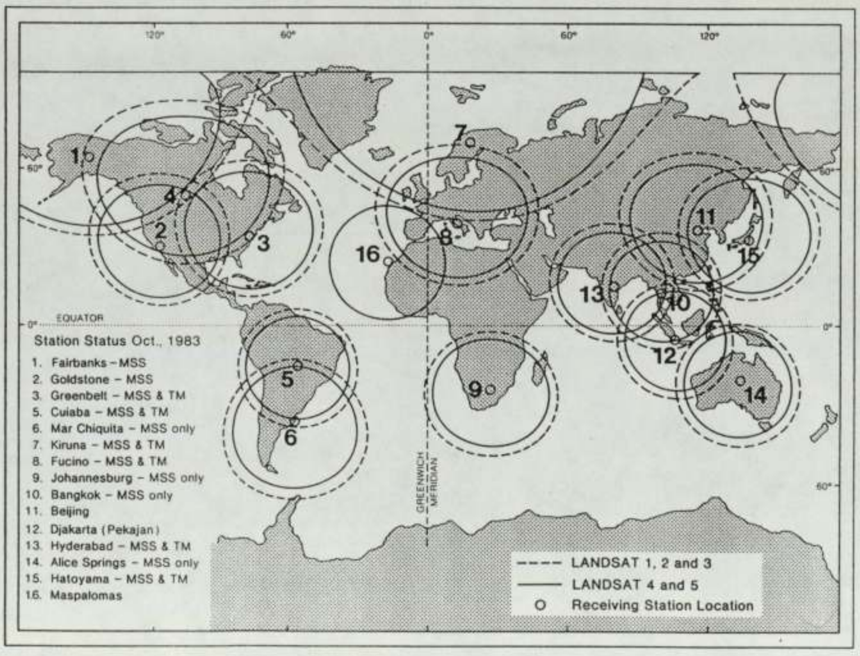

Figure 4.14 Landsat ground receiving stations (after Townshend *et al.*, 1988).

When this research was initiated only one suitable Landsat TM scene was available for the research area. This was from 22 July 1984, and though it has some slight cloud cover, the overall image quality is very good. The sun elevation at time of image acquisition was 51.7° and its azimuth 139.6° . More recently the author has had access to a further Landsat TM scene of the area from 27 September 1985.

4.7 Summary of Data Types

The importance of technological developments and their affect on the type and continued availability of specific remotely sensed data types was mentioned at the begining of this chapter. The basic physical principles involved in imaging remain constant, but the imaged portions of the electromagnetic spectrum will vary according to sensor. Spectral response variations according to wavelength must be understood when analysing remotely sensed imagery.

This chapter has shown the considerable differences between the analogue photographic media and the digital data types of Landsat MSS and Landsat TM. The major difference between the latter two is the increased spatial and spectral resolution of Landsat TM data with respect to Landsat MSS data. Quantitatively the spatial difference is a factor of 7:1 (TM:MSS) based on 79m resolution for MSS and 30m for

TM. However, the real difference in pattern recognition by the interpreter is more difficult to determine (see Figure 4.13). The effects of these differences in data type will become increasingly evident in later chapters. Table 4.2 gives a summary of the data types used in this research.

Table 4.2 Summary of Data Types

	Panchromatic Aerial Photos	Landsat MSS	Landsat TM
Acquisition Date	June 1981	15 June 1975	22 July 1984
No. of Scenes Required	16 photos	1	1
No. of Bands	1	4	7
Spatial Resolution	1:50000 (very high)	80m	30m
Data Type	Analogue	Digital	Digital

Note: for spectral resolution ranges refer to Figure 4.1

CHAPTER FIVE: **IMAGE PROCESSING AND ENHANCEMENT**

5.1 Introduction

This part of the research forms a vital element in the whole data analysis procedure and is concerned with the digital data types, namely Landsat MSS and, in particular, Landsat TM. The image processing techniques or more correctly the image enhancement techniques are aimed, as the name would suggest, at enhancing the imagery to aid interpretability of the features under consideration. This chapter discusses the ways in which these techniques were applied to produce imagery ready for on screen interpretation or hard copy production and subsequent data extraction, which are described in Chapter 7.

A thorough examination of the data was enabled over a period of time, though not at Aston University due to a lack of image processing facilities. Image enhancement was carried out at the National Remote Sensing Centre, R.A.E., Farnborough; Silsoe College, Bedford; The Natural Environment Research Council (NERC), Swindon; Telespazio, Rome and latterly at NERC Computer Services, Wallingford. The first two of these locations use GEMS image processing systems and the latter three use International Imaging Systems (I^2S) Model 75 image processing systems. The capabilities of the GEMS system (at the time of use by the author) were not as extensive as those of the I^2S system, in particular, with regard to geometric correction possibilities. This lead to different enhancement possibilities at various stages during the course of the research, the affects of which will be addressed.

The questions to be addressed when examining remotely sensed digital data types include the following:

i) data availability (see also chapter 4);

ii) standard hardcopy product v specialised enhancement cost;

iii) which enhancements to apply;

iv) hardcopy output form.

Some sixteen years after the first Landsat MSS imagery became available image enhancement of satellite data is often a complex issue. This is due, in no small part, to the preponderence of new satellites in recent years such as Landsat-4,1982; Landsat-5,1984; SPOT-1, 1986; SPOT-2, 1990;MOS-1, 1987; IRS-1,(imminent); ERS-1 (due 1991), J-ERS-1 (due 1992) each with increased spatial and spectral resolutions over the Landsat MSS data. This increased resolution has greatly increased the number of possible data applications, and also the complexities of possible data combinations and manipulations, together with increased textural and contextual possibilities.

Image enhancement is in the main a series of software questions, but hardware limitations can have a profound effect on the possible enhancements, processing time and the output products. Some hardware points which should be borne in mind are as follows:

i) Display screens normally have a 512 x 512 pixel resolution (occasionally 1024 x 1024). This can lead to many problems in data processing as images/areas of interest are usually larger than this, and will require processing by the CPU as opposed to dedicated hardware, which can add substantial difficulties, time and money to the image enhancement programme. Recent developments with fast processors such as RISC chips e.g. on SUN, DEC, IBM RS6000 or Silicon Graphics workstations, or parallel processing systems will lead to the resolution of these problems. It is this current 512x512 limitation that was the deciding factor in determining the limits of the main research area. As many different enhancement and processing techniques were to be applied it was thought wise to concentrate on a 512x512 window, with extension to the surrounding areas for interpretations on a catchment basis once enhancement procedures had been determined. Since Landsat TM data has a higher spatial resolution than Landsat MSS data it was the Landsat TM data which defined the research area as a 15km x 15km (512 x 30m) area, giving a total area of 235km^2.

ii) The selection and cost of the various hardcopy possibilities must be considered during the enhancement phase. A combination of hardcopy outputs is often preferable, though it is vital that the operator fully understands the output that will result from certain enhancement procedures. One must be aware of the effects of illumination in the image processing area and resulting visual appearance of the image; hardware recording settings; film production limitations etc. This is discussed further in Section 5.5.

As previously mentioned, Landsat TM being a more recent data type has had less investigation than Landsat MSS. Thus, it was decided to concentrate most of the enhancement techniques on the TM data, but with comparison to MSS data.

The following sections describe various methods of image enhancement for the discrimination of streams, rivers and landcover classes. The first group of techniques examined are preprocessing techniques designed to remove data deficiencies. This includes geocorrection of the imagery for registration with other data types. Geocorrection is particularly important for the Landsat MSS digital data, due to its rectangular pixels (56m x 79m) which produce relative scale distortions in the raw data.

Several image enhancement techniques are then outlined. These include band selection criteria; contrast stretching; ratioing; vegetation indices; image transforms; colour representations; 3-dimensional observation and spatial filtering techniques.

5.2 Image Preprocessing

5.2.1 Introduction

Satellite data in its raw form, as received from satellites, may contain flaws or deficiences of one type or another. The correction of these deficiencies and flaws is known as preprocessing since it is carried out prior to the main use of the data for the desired purpose. Moik (1980) refers to the processes as image restoration, since the intention is to restore the image as far as is possible, both geometrically and radiometrically, to the radiant energy characteristics of the original scene. Some corrections are carried out at the satellite ground receiving station and the user should be aware of what preprocessing has been performed. This can include such things as radiometric calibration, geometric corrections for scanner mechanisms and orbital perturbations (a sample report is given in Appendix B). Once aware of these processes the user must decide what further processing is still required for the application in hand. It is important to understand what is necessary for the particular application under consideration, since not all possible preprocessing possibilities are appropriate or even desirable in each case. In fact to carry out certain preproccessing processes may actually decrease the usefulness of the data and cause the creation of errors not present in the raw data.

To correct the image data internal and external errors must be determined (Jensen, 1986). Internal errors are created by the sensor itself. They are generally systematic (predictable) and stationary (constant), and may be determined from pre-launch or in-flight calibration measurements. External errors are due to platform perturbations and the modulation of scene characteristics, which are variable in nature. Such unsystematic errors may be determined by relating points on the ground (ie. ground control points) to sensor measurements. Radiometric and geometric errors are the most common type of error encountered in remotely sensed imagery.

The Landsat MSS and Landsat TM imagery used in this research had no "dropped lines" (missing scan lines), which are normally seen as black or white eg. 0 or 255, and striping effects due to sensor bias was only observable when the three "visible" bands (bands 1,2 and 3) of TM imagery were viewed simultaneously as a simulated "true colour" image. Since this band combination was not used to any major extent in the research it was not considered necessary to use destriping methods such as the linear or histogram matching methods (Jensen, 1986). It is worth noting though that difficulties can occur in applying these correction algorithms since the ground receiving stations do sometimes add interpolated lines, thus destroying the regular 6 or 16 scan-line patterns of Landsat MSS and Landsat TM.

5.2.2 Geometric Correction

Many actual and potential uses of remotely sensed data require that data be expressed in terms of a map projection so that information on image and map can be correlated (Mather, 1987). The images themselves are not maps having been recorded in the manner described in Chapter 4 and have thus been affected by orbital patterns and the earth's rotation, together with topographic effects. The procedures developed to correct for these effects are commonly known as geocorrection, since they adjust the image data in such a way as to render the output spatially correct in a geographical sense. To enable these corrections, reference points from the desired map projection are required. This of course assumes map availability at an appropriate scale, accuracy (and possibly a particular time), which for many areas of the world is not possible.

The application of orbital geometry models based on knowledge of satellite orbital patterns can be used to correct imagery for across-scan scale changes, skew effects related to orbital inclination and latitude and earth rotational effects. These type of corrections are however only accurate to 1-2% but can be used in the cases where suitable maps are unavailable (Landegrebe *et al.*, 1975). Image to image registration for multitemporal analysis uses similar methods to geocorrection techniques and involves choosing reference points from an image selected as the reference image, to which the other images are referenced. This methodology does not require maps, as for geocorrection, though in most cases geocorrection is desirable, if possible.

It is not proposed to give here an exhaustive discussion of all the factors involved in geometric correction though the following section outlines some of the main principles of the operation. Further information can be found in Drury, 1987; Jensen,1986; Mather 1987.

The initial requirement is an image processing system which enables geocorrection. At the start of this research the author had no access to systems with geometric correction capabilities. In an intermediate phase only correction of 512 x 512 extracts was possible using the GEMS system, the resultant image also being restricted to the same dimensions, thus resulting in the loss of part of the image data during the warping procedure. A preferable situation is one such as offered by the I^2S system which permits an overview of large images e.g a whole TM scene size (approx. 144 times larger). This image can then be roamed over at full resolution, viewing three bands simultaneously with a stash file applied to contrast stretch the imagery (see Section 5.3.2) for ease of ground control point location and selection.

The ground control points are those points which can be precisely identified on both imagery and map to use as "control points" for the subsequent warping procedure. The control points could be, for example, road/rail intersections, but should not include geographically unstable features such as meandering rivers etc. The number of control points needed will depend on the size of imagery one is trying to correct, the topography of the area, the number of suitable control point sites and the interpolation one desires to apply to the image during the warping phase. A relatively even spread of control points over the whole area is highly desirable, though a concentration of points is required for areas of high topographic variability. In this case, the area was relatively small (512 x 512 pixels) though topography varied somewhat by U.K. standards (0 - 754 metres). The image used was a band 5,4,1 FCC with linear contrast stretching (as discussed in Sections 5.3.1 & 5.3.2). Seven control points were selected when the image was geocorrected at Telespazio, using an I^2S. Points were input using a digitiser on which a 1:50000 scale O.S map of the area was mounted and points selected from the image displayed on the graphics monitor were related to map coordinates by a mouse input. Figure 5.1 illustrates the control point extraction set-up.

Once the relationship between image and map projection has been established by the creation of a control point file this should be examined to check for errors which can be remedied by deletion or reselection of the control point(s) concerned. The next decision to be made is which interpolation method to use in geocorrecting the imagery. Three main interpolation possibilities exist these being nearest neighbour; bilinear; or cubic convolution.

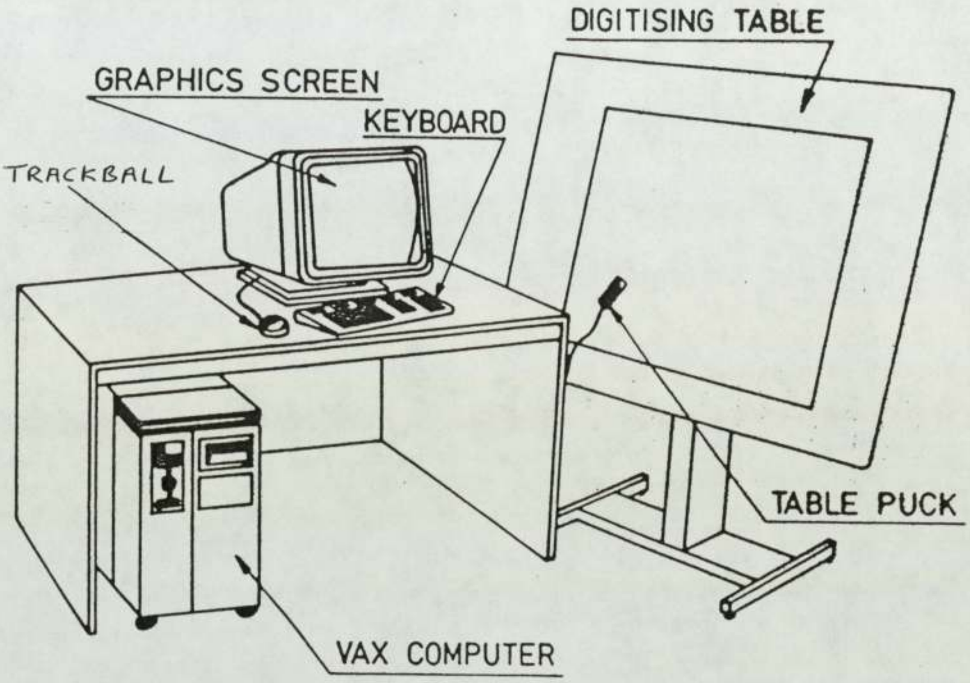

Figure 5.1 Control point creation setup.

The nearest neighbour algorithm applies the grey level of the nearest pixel in the original image as interpolated value. This method leaves the original values unchanged though geometrical errors of up to two IFOV's can be introduced (Atkinson, 1988). This results in the warped image having a "blocky" appearance rather than smooth boundaries and the effects of which are particularly detrimental to the interpolation of narrow linear features, such as streams and rivers.

In bilinear interpolation the new grey level is computed as the proximity weighted mean of the grey level values of the four nearest pixels. Cubic convolution is the least computationally efficient, using an approximation of two cubic functions. The new grey level is calculated using 16 input pixels. The weights assigned to the input pixels are dependent on the distance of the output pixel from the input pixels in both the along-scan and along-track directions. A full description of these interpolation methods can be found in Mather (1987).

It was decided to use the cubic convolution method in this case as the nearest neighbour created problems for drainage network delineation due to the reasons outlined above. Although the cubic convolution method results in some change in grey levels the contrast in water and vegetation grey levels is still maintained and the geometric properties are an advantage.

The control points selected were then use to warp the image to a British National Grid map projection, with a 30m spatial resolution using a least squares best fit bivariate Legendre polynomial (I^2S, 1989), to transform the pixel locations and a cubic convolution algorithm to determine the pixel intensity values. In this case the R.M.S. pixel location error was 0.638 pixels i.e. sub-pixel, with a maximum error of 0.995 pixels. Full details of the geometric rectification parameters are given in Appendix C.

A similar methodology was adopted for the Landsat MSS imagery. Control points were selected from a band 7,5,4 FCC with linear contrast stretching. Five points were selected and used to warp the image, with resampling to 50x50 metre resolution from the 56x79m original data, again using a bivariate polynomial with cubic convolution interpolation. The R.M.S. locational error was 0.207 pixels with a maximum of 0.257 pixels.

5.2.3 Atmospheric Correction

Atmospheric scattering and absorption effects decrease the ability to extract useful information from remotely sensed images. These effects vary with climatic status and according to the wavelengths of radiation being recorded. Atmospheric scattering in the visible range of the spectrum adds to the pixel intensity values (PI) and histogram adjustment techniques can be applied to "correct" for this. The effect of this scattering is particularly noticeable in Band 1 of TM imagery, which corresponds to the blue range of the visible spectrum (see Fig. 4.1). In this case the minimum pixel intensity (brightness value) was 55 compared to an average minimum value of 8 for the other 5 bands examined.

The atmospheric correction algorithm effectively shifts the histogram of pixel intensities, for a particular band, so that the minimum pixel intensity values are 0. The algorithm can be defined as:

$$\text{Output PI}_{i,j,k} = \text{Input PI}_{i,j,k} - \text{Bias} \qquad (5\text{-}1)$$

where input $PI_{i,j,k}$ is the input pixel value at line i, column j of band k; and output

$PI_{i,j,k}$ is the corrected pixel value at the same location (after Jensen,1986).

This correction was applied to the imagery during the stretching procedure described in section 5.3.2, especially since band 1 of the TM imagery was used extensively in this research.

Adjustments for atmospheric absorption, which affects radiation of wavelengths greater than 0.8 μm (i.e. the near infrared) is difficult to determine because it is largely a function of the amount of water vapour in the atmosphere at the time of image acquisition. The requisite in situ recordings were not available for the digital data used, and thus atmospheric absorption corrections were not possible in this instance.

5.3 Image Enhancement

5.3.1 Band Selection

Band selection is a fundamental decision in obtaining the optimal information from the available imagery, and can be very application dependent. As outlined in Chapter 4 the Landsat MSS sensor records images in four spectral bands and the Landsat TM sensor in seven. A knowledge of the physical interaction of electromagnetic radiation with different ground surface types is a prerequisite for deciding the appropriate band selection for the application under consideration.

With discrimination of linear features such as streams and rivers from surrounding vegetation being a major topic of this research, a band showing high spectral contrast between water and the adjacent vegetation is required. In the near infrared region of the spectrum vegetation shows a high spectral response (see Fig. 4.4)(typical values are pixel intensities in the range 63 to 165 - Landsat TM band 4 unstretched/raw data) and low spectral response is shown by water bodies (typical pixel intensity values 8 to 40 - Landsat TM band 4 unstretched/raw data) in the imagery used. This contrast is particularly important in detecting small streams of narrow widths. The spectral contrast between water and vegetation can so affect the overall pixel intensity value of a TM pixel with a theoretical 30 x 30 metre Instantaneous Field Of View (IFOV), that streams much narrower than 30 metres width can be identified.

The Point Spread Function (PSF) has been used to explain these spectral contrast effects (Moik, 1980; Slater, 1980; Billingsley,1983). If one examines how the radiance from a point source is expressed on the resultant image, one can observe that a highly-reflective point source on the ground does not produce a single bright point on the recorded image. Due to the optical imaging system the point source is instead seen as a diffuse circular region due to the properties of the optics involved in imaging. A cross-section of the recorded intensity distribution from a single point source is illustrated in Figure 5.2, and can be seen to have a Gaussian-type distribution. The distribution shape will depend on the imaging system involved and the relative brightness of the source (Mather, 1987).

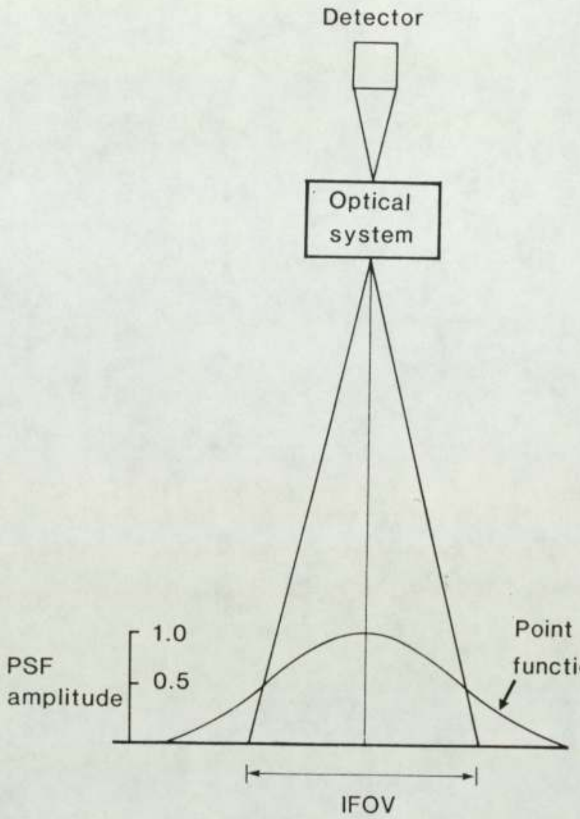

Figure 5.2 Instantaneous field of view (IFOV) based on the amplitude of the Point Spread Funcion (PSF) (after Mather, 1987).

The presence of relatively bright or dark features within the IFOV of the sensor will increase or decrease the amplitude of the PSF so as to make the observed radiance either higher or lower than that of the surrounding areas. In this research the contrast of water bodies, in particular the linear water bodies, with their surroundings (usually vegetation) in the near-infrared bands reduces the radiance value of the pixel element containing the water so that it is easily discriminated from adjacent high radiance vegetation pixels. Thus it was important to consider MSS band 7 and TM bands 4 and/or 5 for enhancement, especially in view of previous work using MSS Band 7 (see Section 2.3). The spectral response variations in the near infrared bands also aids in the other main topic of interest in this work , that of discriminating between certain landcover classes.

The initial decision in band selection is whether to use:

a) individual image bands giving a grey-level image;

b) a three band combination with each band assigned to one of the three colour guns on a high resolution colour monitor, to produce a false colour composite (FCC);

c) some other transformation (see Sections 5.3.3 - 5.3.8).

In the case of Landsat MSS examination of the individual bands revealed band 7 from the near infrared region of the spectrum to be the most informative for the applications under consideration, with high spectral contrast between the low pixel values for water bodies and high values for vegetated areas. This is what would be expected for a band in this region of the electromagnetic spectrum, as outlined in Sections 2.3 and 4.3. It should be noted that linear stretching (as outlined in Section 5.3.2) was applied to make band comparisons since the raw data is of low intensity relative to the possible display range and thus appears as a fairly dark image on the monitor prior to contrast stretching.

Although the drainage network could be observed on band 7 imagery, easier discrimination was found using either a band 7,6,5 (see Fig. 5.3) or band 7,6,4 combination, since colour differentiation is much easier for the eye than grey-level discrimination. For both of these 3-band combinations the bands were assigned respectively to the red,green and blue colour channels on the monitor to produce what is known as a False Colour Composite (FCC). For the visual dicrimination of landcover classes a standard 7,5,4 band combination was found to be most appropriate. This combination was less suitable for drainage delineation due to the preponderance of bright red colouration of the healthy lowland vegetation, as illustrated in Figure 5.3.

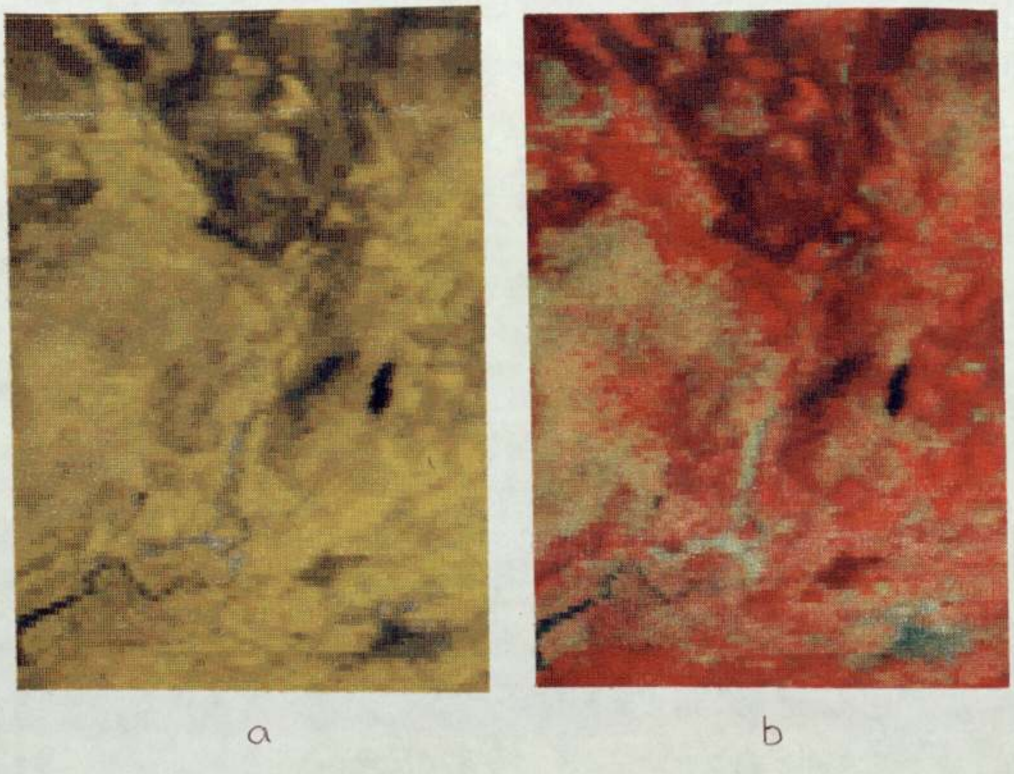

Figure 5.3 Zoomed and contrast stretched band 7,6,5 (a) and band 7,5,4 (b) Landsat MSS FCC's for part of the research area.

With Landsat TM data one has seven possible bands to choose from, though the thermal infrared band (band 6) with its 120 metre spatial resolution was not studied in this research as its resolution was considered too coarse for detailed delineation of narrow linear water bodies. Examination of individual bands (with a linear stretch applied) revealed bands 4 and 5 to be the most suitable individual bands for this application. These bands lie in the near infrared region of the spectrum and are useful for discriminating water and vegetation in a similar manner to Landsat MSS band 7. Details of the statistics for all six TM bands calculated from the 512x512 subscene covering the study area are given in Table 5.1a. This shows the great spectral range and high standard deviations exhibited by bands 4 and 5 relative to the other bands. The ranges of pixel intensity values for the visible bands 1,2,3 are distorted by the presence of clouds, as can be seen in the histograms of the Landsat TM bands are shown in Figure 5.4 (in Section 5.3.2). A correlation matrix was created using the image statistics and is presented in Table 5.1b. This shows low correlations between bands 4 & 3, and bands 4 & 1. High correlations are exhibited between the visible bands (1,2 & 3).

Table 5.1a Landsat TM Subscene Image Statistics

Statistics	Band 1	Band 2	Band 3	Band4	Band 5	Band 7
Minimum	55	17	12	8	5	0
Maximum	254	218	251	217	254	172
Mean	69.4	29.3	25.9	88.2	72.3	25.1
Standard Deviation	16.2	9.5	11.8	21.6	24.0	11.4

Table 5.1b Correlation Matrix for the six Landsat TM bands examined.

Band	Band 1	Band 2	Band 3	Band 4	Band 5	Band 7
1	1.000					
2	0.961	1.000				
3	0.957	0.979	1.000			
4	0.252	0.357	0.234	1.000		
5	0.595	0.679	0.686	0.537	1.000	
7	0.768	0.821	0.857	0.307	0.914	1.000

From the figures in Tables 5.1a&b it seemed reasonable to include at least one of bands 4 and 5 in any colour composite combination. In fact it was decided after examination of several possible combinations to concentrate on the use of bands 4 and 5 together with band 1 in the order 5,4,1, assigned respectively to the red, green and blue channels of the graphics monitor. The combinations 5,4,2 and 5,4,3 produced similar visual results and the final choice was based purely on the author's personal preference. The visual appearance of band combinations 5,4,1; 5,4,3; 4,5,3 and the frequently used 4,3,2 are illustrated after contrast stretching in Figure 5.7.

A statistical band selection method based on the total amount of variance and band correlation within and between bands was developed by Chavez *et al*. (1982, 1984). This is known as the Optimum Index Factor and is described in Jensen (1986). It is interesting to note that Jensen's application of this index to his Landsat TM scene gave 5,4,1; 5,4,2 and 5,4,3 as the three best 3-band combinations of bands out of 20 combinations examined.

5.3.2 Contrast Enhancement (Stretching)

This type of enhancement is particularly important in the enhancement of imagery for visual interpretation, and is intimately linked with the band selection choices just outlined. One is almost invariably required to enhance the spectral values obtained in the raw data for any visual work. The reason for this is that the MSS and TM sensor systems are designed to record spectral responses from all kinds of terrain, including those of a highly reflective nature such as ice and snow. Thus in imaging, the usual range of values recorded is found within only part of the total possible range.

Table 5.1a in Section 5.3.1 gives the initial ranges for each of the TM bands imaged. The resultant effect when viewing these bands individually on the screen is to see grey-level images of little variation in visual terms (bands 4 and 5 apart). To increase contrast, and so improve visual discrimination "stretching" is applied. The principle behind stretching is to use the full range of values possible on the display device i.e. 0 - 255 (8 bits/channel). There are various stretching techniques, such as linear, non-linear, histogram equalisation, gaussian, which should be used according to histogram shape. Manual interaction capabilities allow even greater possibilities, though exact repetition of a complex manual stretch may prove difficult. The histograms of the raw TM data are given in Figure 5.4.

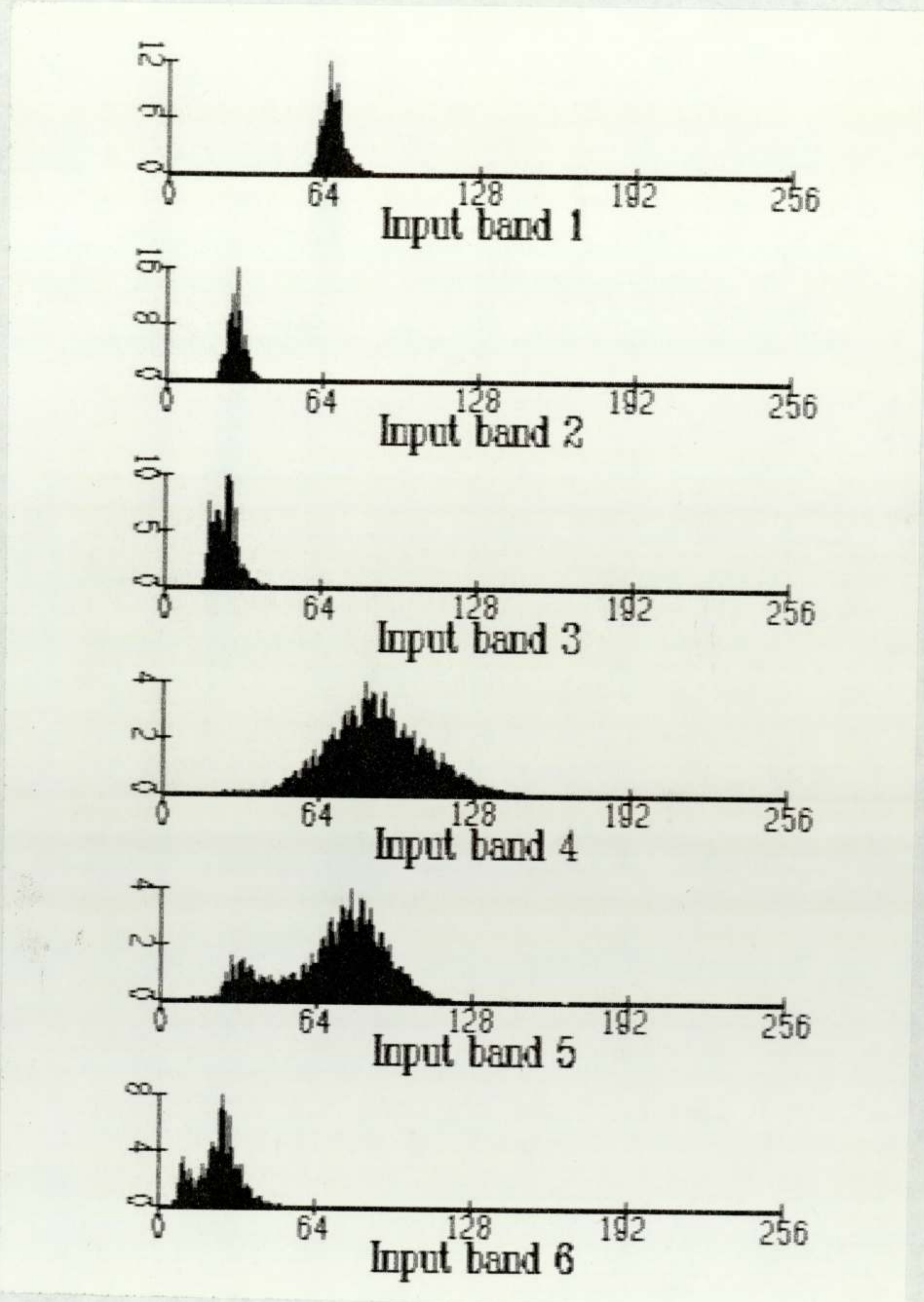

Figure 5.4 Band histograms for the "raw" TM data (note: input band 6 is Landsat TM band 7).

Linear contrast enhancement is best applied to remotely sensed images with Gaussian or near-Gaussian histograms, that is, where all the brightness values fall generally within a single, relatively narrow range of the histogram and only one mode is apparent. To perform a linear contrast enhancement, the analyst examines the image histogram and determines the minimum and maximum pixel intensities in the image, PI_{min} and PI_{max}, respectively. The output brightness value PI_{out}, is computed according to the equation:

$$PI_{out} = \frac{PI_{in} - PI_{\min}}{PI_{\max} - PI_{\min}} \; x \; PI_r \quad (5\text{-}2)$$

where PI_{in} is the original input brightness value and PI_r is the range of the brightness values that can be displayed on the CRT (e.g. 256). It can be seen from the band histograms of Fig. 5.3 that for the TM imagery bands 1,2,3 and 4 conform to this criteria whereas bands 5 and 7 reveal bimodal distribution patterns. Linear contrast stretches were thus applied to all bands other than bands 5 and 7, to which two part linear stretches were applied. Figure 5.5 shows the effect of a typical manual linear stretch stretch on the pixel intensity values. The visual effects of the stretches applied are illustrated in Figure 5.6a & b.

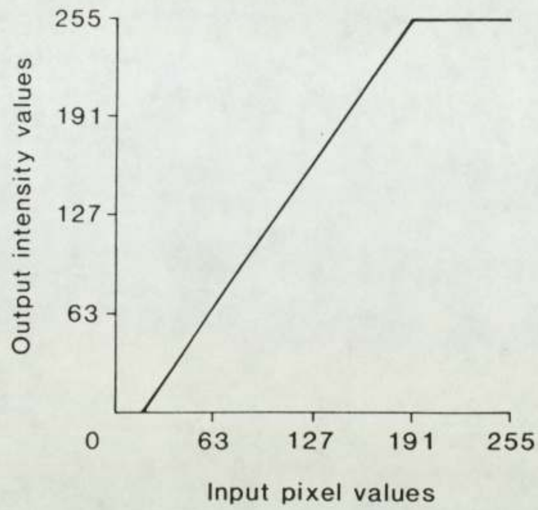

Figure 5.5 Graphical representation of contrast stretching for pixel values in a range 16-191. Values less than 16 are set to 0, and values greater than 191 are set to 255 (after Mather, 1987).

As stated in Section 5.3.1 the bands selected for three-band combination were bands 5,4 and 1 although the 5,4,3; 4,5,3 and 4,3,2 combinations were also examined, as illustrated Figure 5.7.

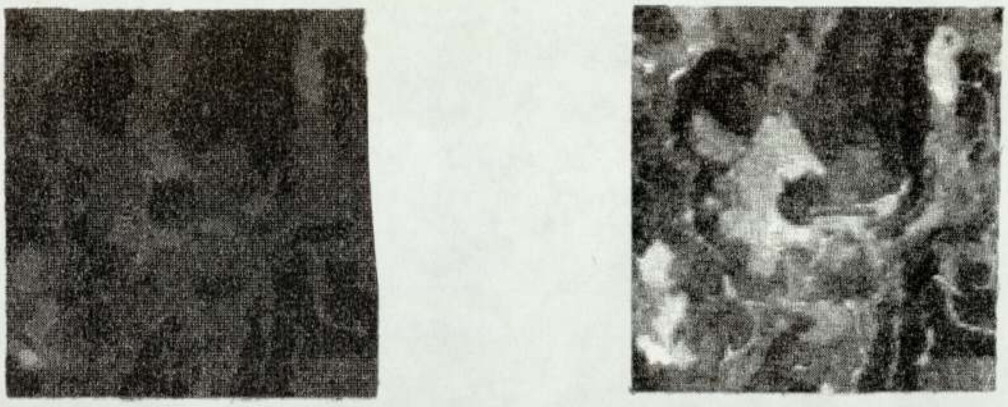

Band 1

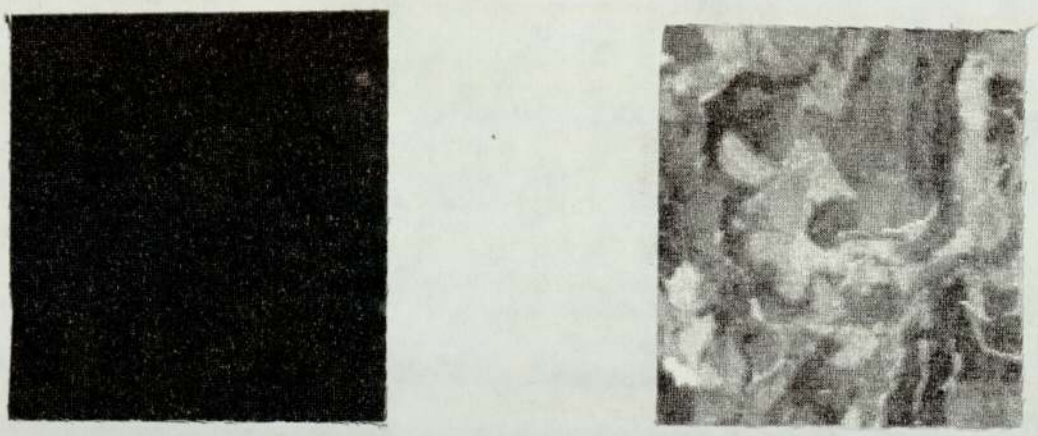

Band 2

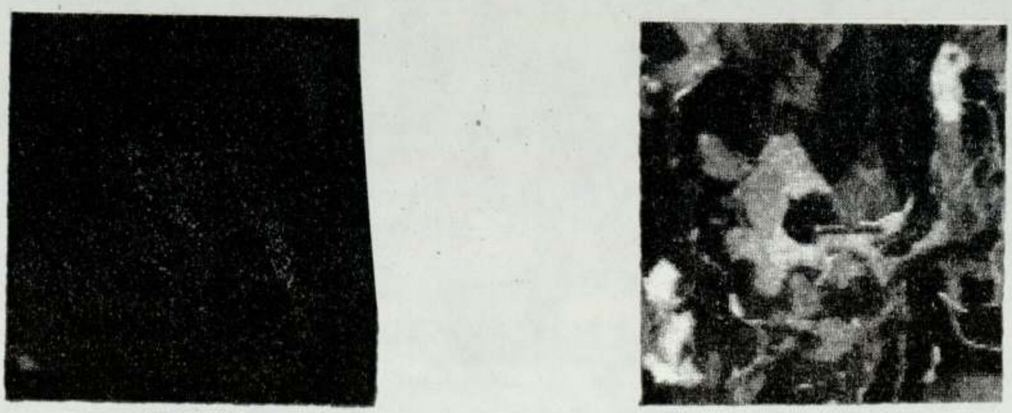

Band 3

Figure 5.6a Landsat TM raw data (left side) and after stretching (right side). Bands 1,2,3.


Band 4


Band 5

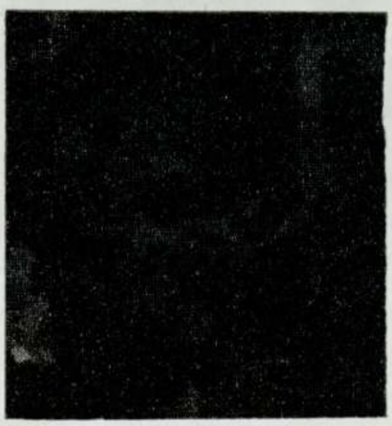


Band 7

Figure 5.6b Landsat TM raw data (left side) and after stretching (right side). Bands 4,5,7.

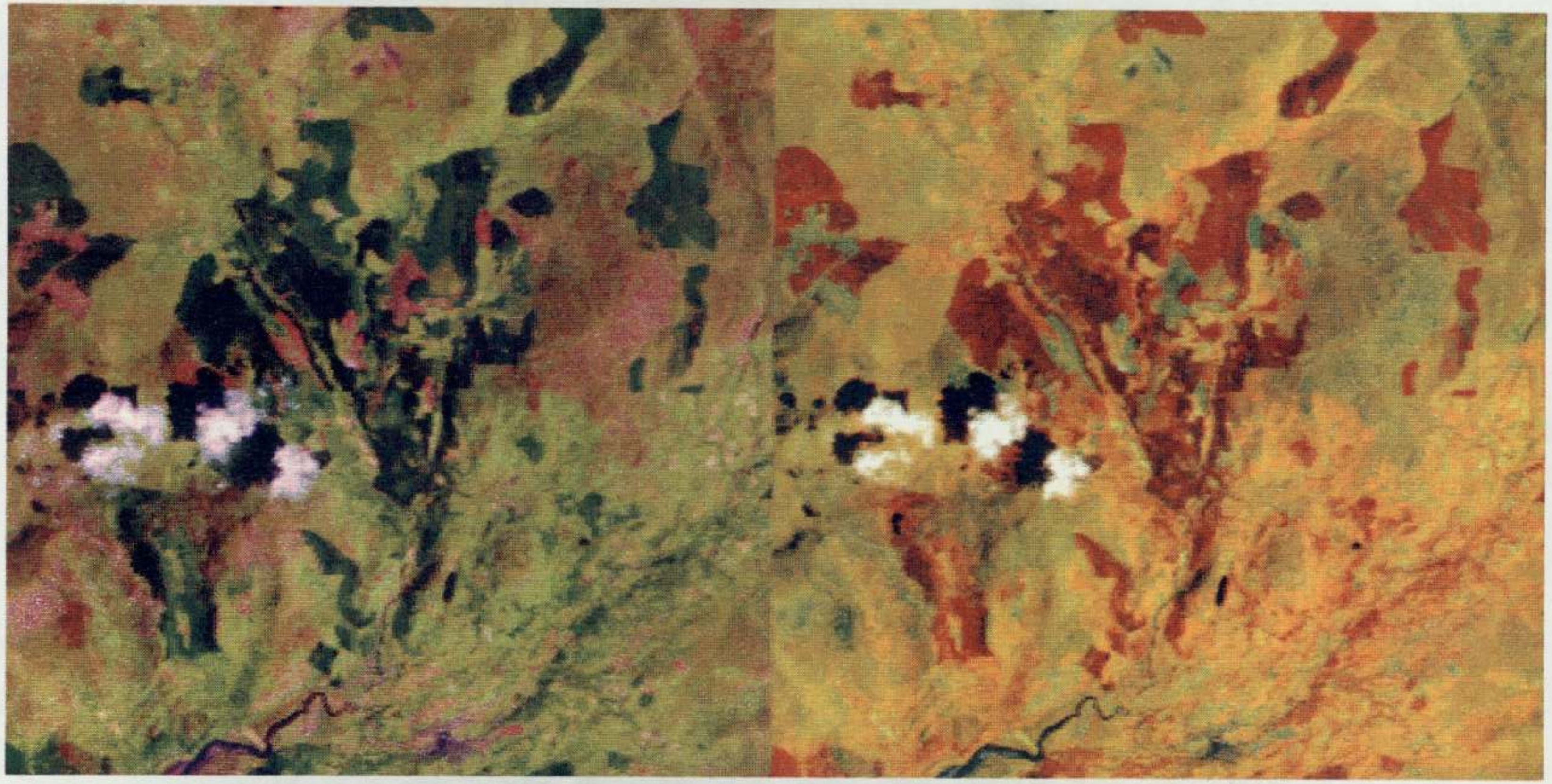

a b

Figure 5.7a Landsat TM FCC's of band combinations 5,4,1 (a); 4,5,3 (b); with contrast stretches applied.

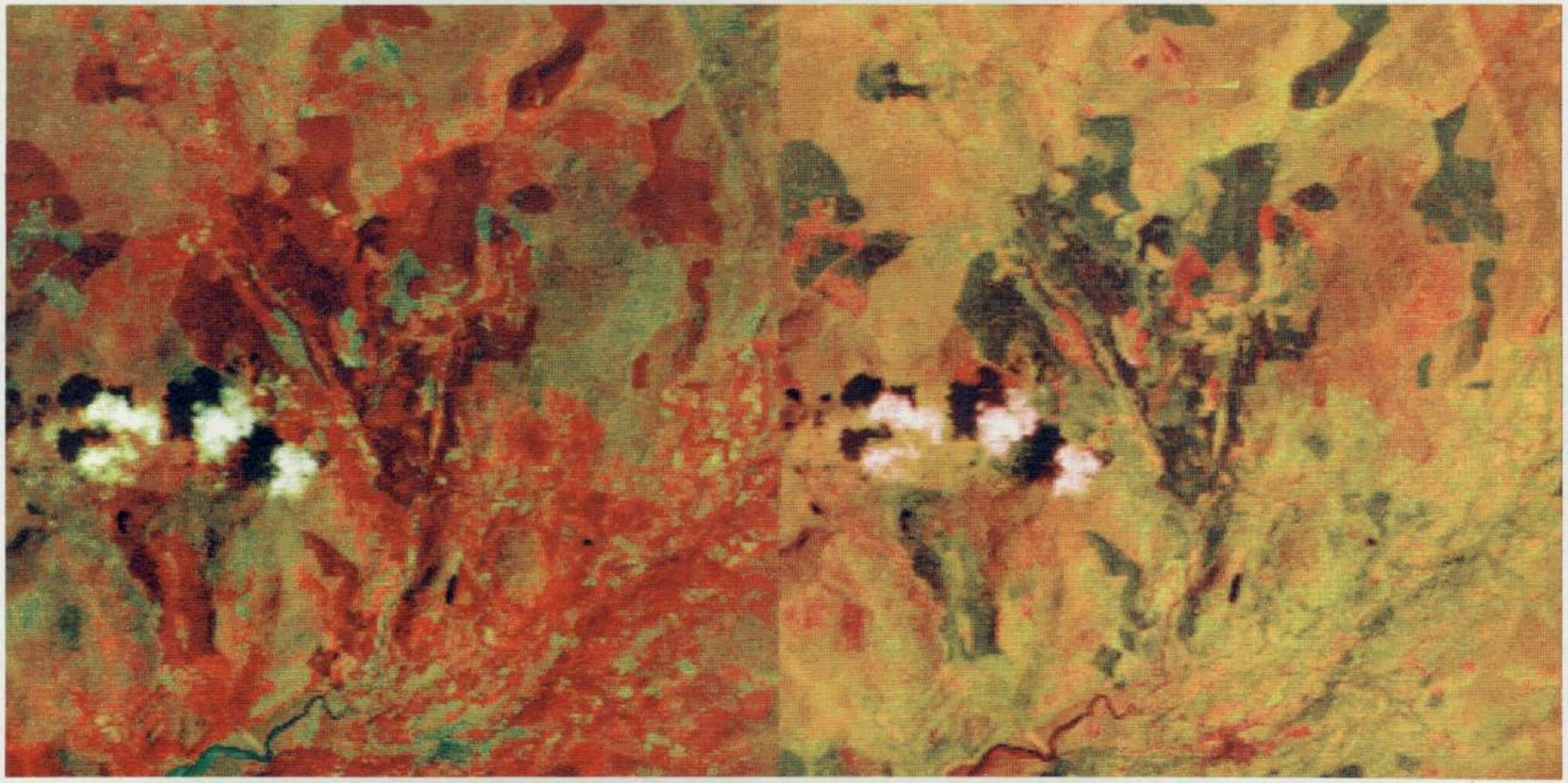

c d

Figure 5.7b Landsat TM FCC's of band combinations 5,4,3 (c); 4,3,2 (d); with contrast stretches applied.

For the MSS data, after the examination of several stretch types a Gaussian stretch or the manual linear contrast stretch were deemed the most useful. The gaussian stretch is so-called because it involves the fitting of the observed histogram to a normal or gaussian histogram which can be defined by:

$$f(x) = Ce^{-ax^2} \quad (5\text{-}3)$$

where $a=h^2$ and h is known as the precision constant, $C = (a/\pi)^{0.5}$ (Kennedy & Neville, 1976). The standard deviation, σ, is defined as the range of the variable x for which the function f(x) drops by a factor of $e^{-0.5}$ or 0.607 of its maximum value, and is equal to $1/(2a)^{0.5}$. Thus, 60.7% of the values of a normally-distributed variable lie within one standard deviation of the mean (Mather, 1987).

5.3.3 Density Slicing

Density slicing is a process used to depict a range or ranges of pixel intensities using a single band of imagery. The concept is that the interpreter uses their knowledge of reflectance properties at various wavelengths, together with scene-specific spatial knowledge to define image classes. The density slicing is carried out interactively using a trackball (or mouse) with a graphics colour representing the areas of pixels within the specified range(s). In this research the low reflectance of water bodies in the near-infrared was utilised to define water areas on TM band 4 as illustrated in Figure 5.8 (band 5 showed similar effects).

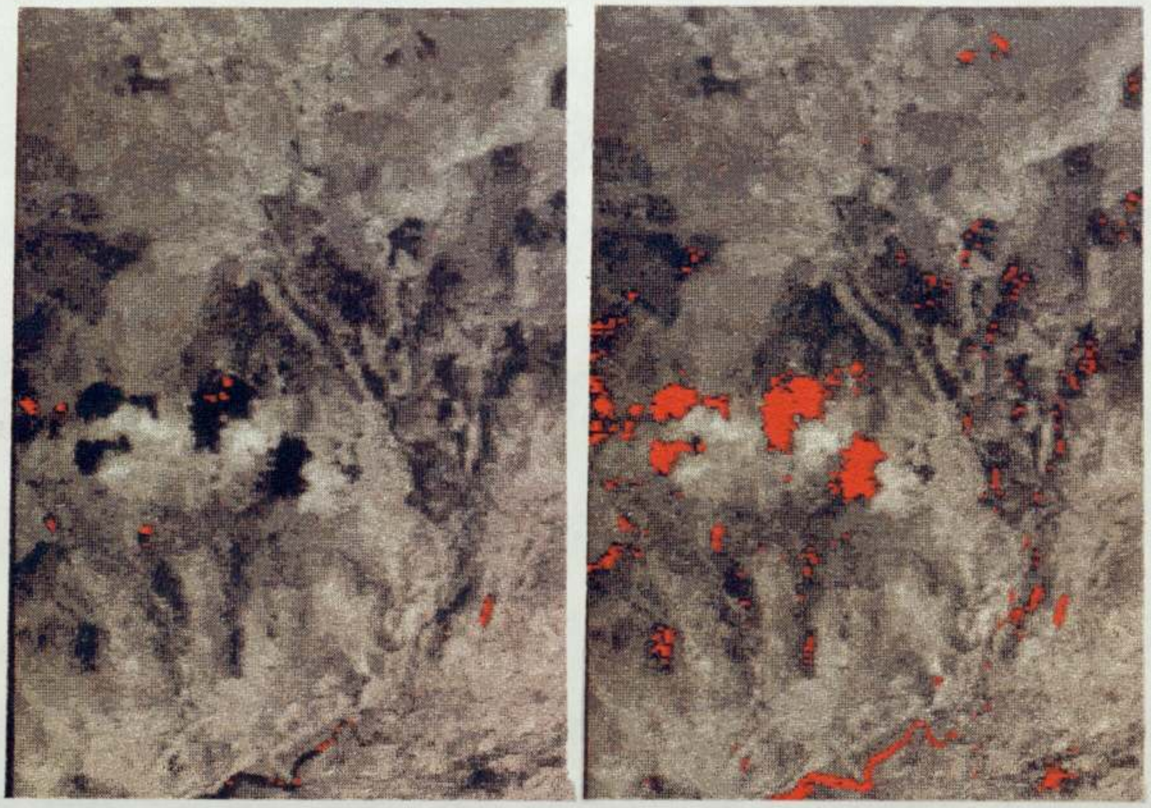

a b

Figure 5.8 Density slices of TM band 4. Range 0-17 (a); 0-45 (b).

If each class under consideration exhibited spectrally disparate properties in any of the individual imaged bands, then image classification would be simply a matter of defining the pixel intensity ranges demarking these classes. Unfortunately this is not the case. Figure 5.8 shows the major water bodies delineated in the pixel range 0-17, but further increases (range 0-45) highlight cloud shadow, forest shadow and urban areas, rather than finer linear water bodies.

5.3.4 Band Ratios

Sometimes the differences in pixel intensities from similar surface materials are caused by topographic conditions, shadows, or seasonal changes in sunlight illumination angle and intensity (Jensen, 1986). These conditions may hamper the ability of an interpreter or classification algorithm to correctly identify surface materials or landcover in a remotely sensed image. Ratio transformations of the remotely sensed data can, in certain circumstances, be applied to reduce the effects of such environmental conditions (Friedman, 1980), and thus enhance interpretation possibilities.

One method of performing a ratio transformation is by a two-pass solution. In the first passage the ratio values for the entire image are calculated and the maximum and minimum values determined, then on the second pass the ratios are calculated again and scaled to a 0 - 255 range (or appropriate display device dynamic range) using the formula:

$$R'(x,y) = \frac{R(x,y) - R_{min}}{R_{max} - R_{min}} \; x \; 255 \quad (5\text{-}4)$$

In this relationship R'(x,y) is the ratio between two wavebands at pixel (x,y) after scaling, R(x,y) is the corresponding raw ratio value and R_{max} and R_{min} are the maximum and minimum raw ratio value for the whole image. It is possible to increase the computational efficiency of this procedure by sub-sampling. Alternative methods of ratioing can also be applied (Mather, 1987).

Ratioing was only applied in this instance to the Landsat TM imagery. With six bands to choose from several ratioing possibilities exist. Previous observers (Jensen, 1986) suggest that, in general, the lower the correlation between the bands, the greater the information content of the band-ratioed image. The band combinations examined for their visual discrimination capabilites were selected using their correlation coefficients (see Table 5.1) and suggestions from previous work (Jensen, 1986).

Calculation of the correlation coefficients (see Table 5.1b) showed the combinations 4/3, 4/1, 4/2, 7/4 to have little correlation. Examination of the images produce using formula (5-4) showed very good delineation of linear features in the combinations 4/2 and 4/3 (see Fig. 5.8), showing an improvement in delineation of water bodies over the stretched Band 4 data. This was particularly apparent in the forested areas, however the forest tracks appeared very similar to the water bodies and were difficult to discriminate other than by logical exclusion due to their patterns, this was not always possible though.

The combinations 4/1 and 7/4 were not so useful, as was the recommended 2/5 combination (Jensen, 1986) which gives the water pixels high values with respect to vegetation, but fails to improve discrimination capabilities. The band ratios 4/3 and

4/2 were merged with band 4 of the TM data in the order 4/2; 4; 4/3 (blue, green, red) to give a FCC which was manually stretched. This proved successful in revealing linear water bodies, with a colour variation for vegetational discrimination.

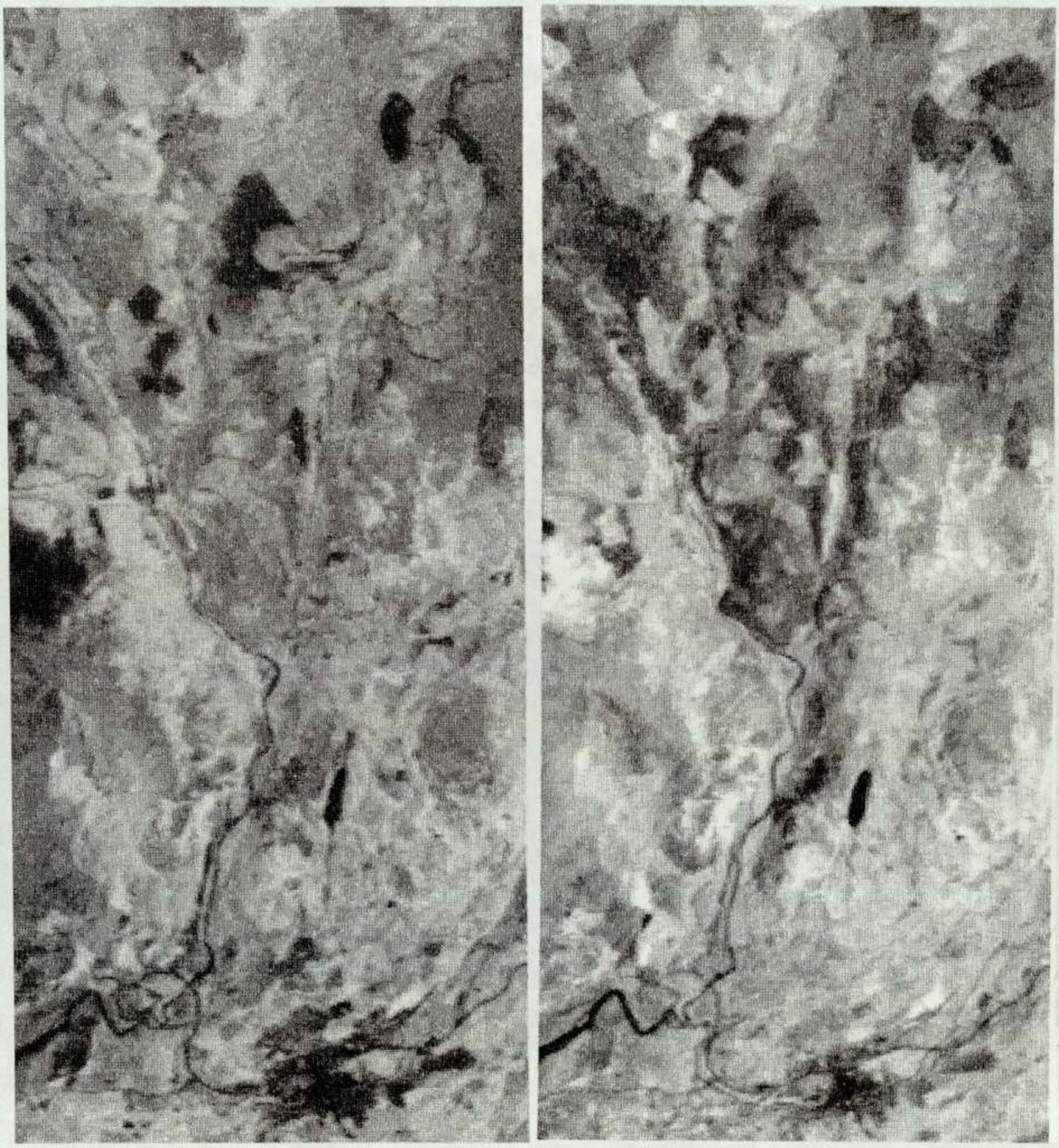

Figure 5.9 Comparison of the 4/3 ratio (left) with contrast stretched band 4 (right).

5.3.5 Vegetation Indices

Vegetation indices are a special case of ratioing and make use of the different response of various vegetation types at different wavelengths (as discussed in Section 4.3). These differing responses are reflected in the pixel intensities for selected bands. Many indices exist (Rouse et al. 1973,1974; Richardson and Wiegen, 1977; Curran 1984) several of which are detailed in the Manual of Remote Sensing (2nd edn., 1982). In this case only the so-called Normalized Difference Vegetation Index (NDVI) was examined (Tucker, 1979). This is defined as:

$$NDVI = \frac{NIR - RED}{NIR + RED} \quad (5\text{-}5)$$

where NIR and RED are image bands recorded in the Near Infrared and red regions of the spectrum. This can be defined for Landsat TM imagery as:

$$NDVI = \frac{TM4 - TM3}{TM4 + TM3} \quad (5\text{-}6)$$

where TM4 and TM3 are bands 4 and 3 respectively.

Application of this formula to the TM data produced an image in which water bodies had a high intensity compared to vegetation. For linear water body delineation the index was of little use, as only the major rivers were easily identified. However, for vegetation discrimination it was possible to distinguish several vegetation types, even though the image is monochromatic. Combination with stretched bands of TM data in the three-band combination TM5, TM4, NDVI gave an image where water bodies appear bright blue and there is good vegetation discrimination, however the image clarity was not as good as the stretched 5,4,1 combination (see section 5.3.2). The NDVI maybe more successful in an automatic classification implementation.

5.3.6 Kauth Thomas or Tasselled Cap Transformation

Experience with Landsat MSS data for agricultural regions and difficulties using simple ratios and principal component analysis (section 5.3.7), led to the development of image transforms. These are based on the observations that: i) clustering of the MSS data in agricultural areas occupied a defineable region in 4-dimensional feature space; and, ii) within this feature space the region occupied by "soil" pixels was a narrow elongated ellipsoid. Kauth and Thomas (1976) proposed a transformation which would by rotating and scaling the data within the feature space would give a clearer view of the data structure. This was later modified for TM data by Crist and Cicone (1984a, 1984b) to produce "brightness", "greeness" and "wetness" functions. The brightness function is a weighted average of each of the six TM bands (the thermal infrared band is excluded), the greeness is a visible/near infrared contrast, with little contribution from bands 5 and 7. Wetness is a contrast between bands 5 and 7 and the bands 3 and 4.

Application of this transform to the test area produced a three band image in which most of the information was contained in the first two bands. The first band appeared similar to band 4 of the TM data, the second band revealed more information on linear features but not as much as either the band ratio 4/3 or simple band 4 data. The third band was of little use with the forested areas having very low pixel values. A manually stretched image using the bands in order 2, 1, 3 (RGB) revealed good discrimination of lowland vegetation types with field boundaries often clearly defined, but there was not as much moorland information as in the 5, 4, 1 TM band combination. Again this transform could be used in an automatic classification procedure.

5.3.7 Principal Component Analysis (PCA)

Principal component analysis is a technique which seeks to replace the original data wavebands which describe the data with new orthogonal axes defined by lines of maximum variance within the data. This effectively compresses the information component of several images into two or three transformed principal component images. It is not proposed to give a full description here of the processing involved since the results in this application were of little advantage. Jensen (1986) and

Mather (1987) provide detailed accounts of the computations involved.

Transformation of the test TM image into three principal components revealed band 1 to be of little informational value in terms of linear features. Band 2 showed more linear information but less than band 4 of TM, and the third component showed only large agricultural blocks. A stretched colour composite of the three components exhibited bright colours but was of little use for drainage network or visual agricultural discrimination.

5.3.8 HSI Colour Space

The most precise representation of human vision is through the three parameters, hue, saturation and intensity (the HSI system). The hue of an object is the average wavelength of light which it emits. Saturation expresses the range of wavelengths around the average wavelength in which most energy is carried. A high value of saturation results from a spectrally pure colour - a single wavelength. A low value expresses increasing mixture of wavelengths, and produces pastel shades. Intensity is a measure of the total energy involved in all wavelengths, and is akin to albedo. A detailed explanation of this colour space can be found in Drury, 1987.

The HSI system was applied to the band combinations 5,4,1; 5,4,3 and 7,5,4 of the TM data. The most useful of these was the 5,4,3 combination which revealed linear detail but the boundaries of forest blocks were not so clearly defined. The other two combinations produced interestingly coloured images, however they were not as useful as the standard 5,4,1 FCC band combination.

5.3.9 Perspective View

Perspective view is an image processing facility which enables a two-dimensional image to be combined with elevation data in raster format to produce 3-dimensional perspective views. It is possible to alter the input parameters to look at a surface from a variety of azimuths, elevations and effective distances. Experimentation is required to find good viewing distances which are neither too distant nor so close that individual pixels become too evident. The image to be viewed in perspective can be an FCC, a classification or some other raster data set (see Fig. 5.10). Care should be taken when calculating the vertical exaggeration of the perspective view to allow correct appreciation of the topographic effects of the data under examination. This facility allows a user to visualize in high detail a landform and its surface detail particularly with a FCC overlay. For data calculations such as slope, aspect etc. which are of great importance in hydrological work it is preferable to transfer the image data to a GIS such as ARC/INFO (see Chapter 9).

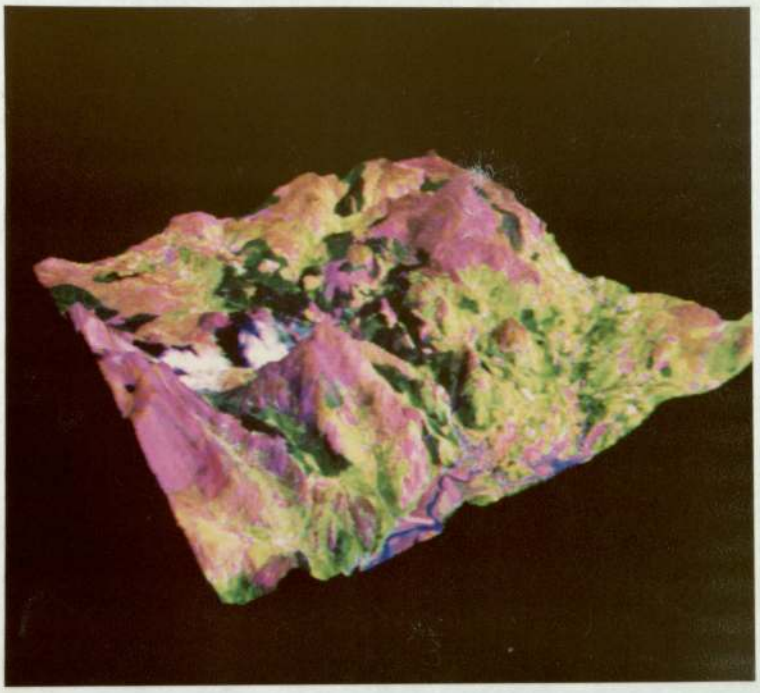

Figure 5.10 Perspective view of the research area using TM bands 5,4,1 with 3.5x vertical exaggeration.

5.3.10 Spatial Filtering

A major part of this research is concerned with enhancing digital data to improve delineation of the drainage network. Previous sections, 5.3.2 - 5.3.8, have described ways of achieving this using the spectral properties of individual pixels in different bands. Another possibility is to use these spectral properties combined with a spatial analysis of the "local region", i.e. the pixels surrounding the each individual pixel. The parameter known as spatial frequency can be defined as the number of changes in pixel intensity per unit distance for any particular part of an image (mod. from Jensen, 1986). If there are very few changes in intensity value over a given area, this is referred to as being a "low-frequency" area. Conversely, if the pixel intensities change dramatically over very short distances, this is an area of "high-frequency" detail.

In this work the main concern was with high frequency areas where a narrow water body can be considered as a line of pixels (see Fig. 5.11). In those bands recorded in the near infrared regions of the spectrum these pixels have a high contrast with the surrounding vegetation (see Section 5.3.1), and are thus high frequency areas.

The technique used to analyse the various spatial frequency components of an image is called Fourier analysis. A simplified explanation of this technique is that after analysing the various spatial components found in an image it is possible to emphasize some features at the expense of others. The algorithms used to perform these processes are known as filters; the two main types being high-pass filters, since they emphasize high frequency components, and low pass filters which suppress the high-frequency components while emphasizing areas of gradual change.

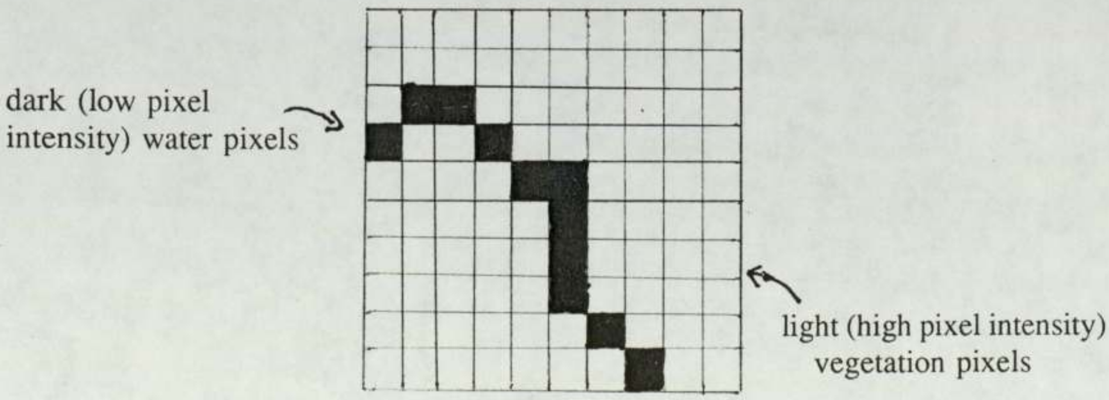

Figure 5.11 Typical pattern of a narrow linear water body (stream) on Landsat TM imagery (e.g. band 4).

Although the operation of spatial filters is conveniently described through the concept of Fourier analysis, the implementation does not have to be through the Fourier transform. Linear spatial filters can be used to analyse images, e.g. for a pixel at location i, j with intensity $PI_{i,j}$ the output pixel in the resulting image will be a function of some weighted average of the pixel intensities in a particular spatial pattern around the pixel location in the input image. This process is known as two-dimensional convolution (Rosenfeld and Kak, 1986).

A first derivative compass gradient mask can be used to perform two dimensional discrete differentiation enhancement (Robinson, 1977). Gradient masks are used to emphasize linear features in certain directions (see Fig. 5.12). However, in this instance the drainage networks being dendritic or sub-dendritic in nature (see Chapter 3) have no preferred directional orientation and therefore to use directional filtering would emphasize some stream orientations and surpress others. In theory, it would be possible to produce gradient masks for instance of compass directions every 45°, giving eight masks which could be combined to produce a line enhanced image, however this would be computationally inefficient. Directional filtering could be applied in an area where drainage was parallel or sub-parallel. Although compass gradient masks are generally used for detecting linear features, a Laplacian filter (normally used for edge and boundary detection) could be used. Laplacian filters are non-directional because they enhance linear features in almost any orientation in an image. The exception being those feature oriented parallel with the direction of filter movement; these features are not enhanced. The Laplacian edge enhancement emphasizes maximum values, or peaks within the image. In human

$$\text{mask F} = \text{north} = \begin{array}{rrr} 1 & 1 & 1 \\ 1 & -2 & 1 \\ -1 & -1 & -1 \end{array}$$

$$\text{mask G} = \text{northeast} = \begin{array}{rrr} 1 & 1 & 1 \\ -1 & -2 & 1 \\ -1 & -1 & 1 \end{array}$$

$$\text{mask H} = \text{east} = \begin{array}{rrr} -1 & 1 & 1 \\ -1 & -2 & 1 \\ -1 & 1 & 1 \end{array}$$

$$\text{mask I} = \text{southeast} = \begin{array}{rrr} -1 & -1 & 1 \\ -1 & -2 & 1 \\ 1 & 1 & 1 \end{array}$$

$$\text{mask J} = \text{south} = \begin{array}{rrr} -1 & -1 & -1 \\ 1 & -2 & 1 \\ 1 & 1 & 1 \end{array}$$

$$\text{mask K} = \text{southwest} = \begin{array}{rrr} 1 & -1 & -1 \\ 1 & -2 & -1 \\ 1 & 1 & 1 \end{array}$$

$$\text{mask L} = \text{west} = \begin{array}{rrr} 1 & 1 & -1 \\ 1 & -2 & -1 \\ 1 & 1 & -1 \end{array}$$

$$\text{mask M} = \text{northwest} = \begin{array}{rrr} 1 & 1 & 1 \\ 1 & -2 & -1 \\ 1 & -1 & -1 \end{array}$$

Figure 5.12 Directional gradient masks (after Jensen, 1986)

vision physiological research suggests that we see objects in much the same way. Hence the use of this operation produces a more "natural look" than that of the other edge-enhanced images.

The blurring effects of the imaging system's PSF (as outlined in section 5.3.1), in which high frequencies are supressed relative to low frequencies, can be attenuated using high-pass convolution filtering. Rosenfeld and Kak (1982) show that the Laplacian operator approximates in mathematical terms to Fick's law, which describes two-dimensional diffusion. Thus subtracting the Laplacian operator is equivalent to removing the diffused element of the signal from a given point. Diffuse reflection from the earth's surface in all probability contributes increased radiance to the imaged pixel from its neighbouring pixels. The Laplacian operator effectively subtracts this contribution.

The weight matrix to be passed across the image to compute the Laplacian can be defined by :

0	1	0
1	−4	1
0	1	0

Figure 5.13 The Laplacian filter

while the image-minus-Laplacian operation can be performed directly using the following mask (Bernstein, 1983):

0	−1	0
−1	5	−1
0	−1	0

Figure 5.14 Image-minus-Laplacian filter

A high-pass spatial filter normally enhances features which are less than half the dimensions of the convolution matrix used, in this instance the narrow water bodies are frequently represented by only one pixel width. The application of the Laplacian filter was performed using bands 1, 4, 5 and 7 of the TM data. Band 1 results showed some improvement over the stretched "raw" data and band 7 showed a distinct clarification of the detail. Applications of the filter to the near infrared bands (bands 4 and 5) showed great improvement in clarity of the image in general and a highlighting of the fine details of linear features such as the water drainage network. Comparison with the 5,4,1 band combination shows this improvement, as illustrated in Figure 5.15.

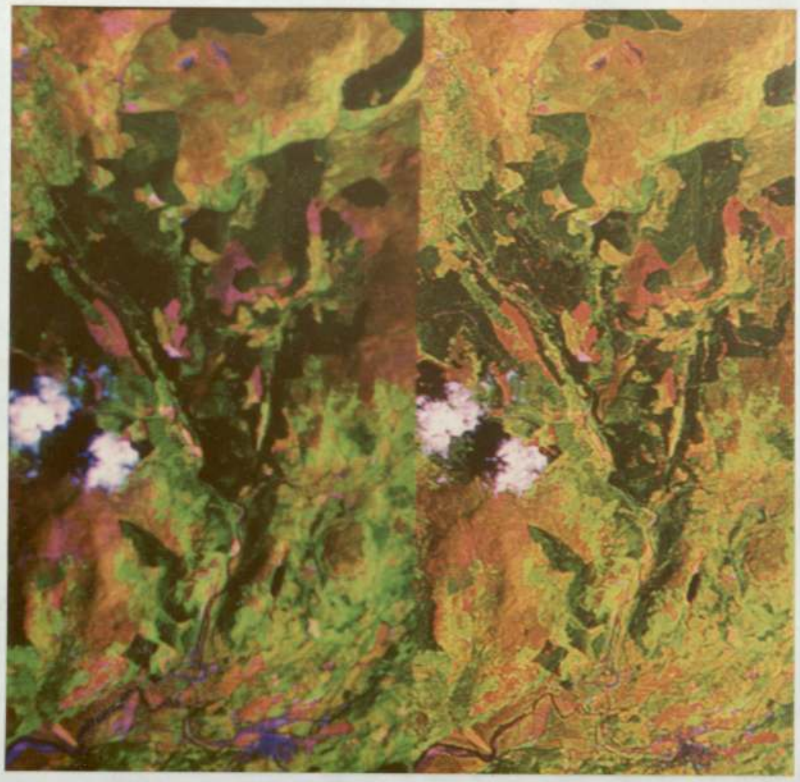

Figure 5.15 TM band 5,4,1 FCC without (left), and with (right) Laplacian 3x3 filtering.

5.4 Summary

Many image enhancement techniques were examined and applied to both the Landsat TM and Landsat MSS imagery for the highlighting of linear water bodies and for visual discrimination of the landcover classes. It was found that False Colour Composites (FCC's) were advantageous both for drainage network delineation and for landcover discrimination. Manual linear contrast stretching was sufficient for enhancement of all the combinations, though Gaussian was used for the MSS 7,5,4 combination.

For the Landsat TM, combinations 5,4,1; 4,5,3; 5,4,3,; 4,3,2 could be used for either network delineation or landcover discrimination. The first of these combinations was selected by personal preference. In the case of Landsat MSS imagery FCC's of bands 7,6,5 or 7,6,4 were most suitable for drainage network delineation, with the standard 7,5,4 FCC selected for landcover discrimination.

Density slicing could be used for highlighting the major rivers and some lakes, but not for smaller rivers and streams. Band ratioing and use of the HSI colour space showed no advantages over the simpler FCC's of this area. The NDVI, Tasselled cap transformation and principal components proved not to be useful for the applications under consideration in this area.

The perspective view was helpful for visual appreciation of the terrain, however this data can be used more effectively in a GIS, as will be considered in Chapter 9. Spatial filtering using a 3x3 Laplacian filter was found to be of considerable assistance in drainage network delineation for both Landsat MSS and Landsat TM imagery. Table 5.2 gives details of the imagery which was produced for visual interpretation by "on screen" methods or lamprey box colour transparency interpretation. These techniques are described in Chapter 7.

Table 5.2 Image enhancements for visual interpretation.

Imagery Type	Interpretation purpose	Bands Used (RGB)	Contrast Stretching	Filtering
Landsat TM	Drainage network delineation	5,4,1	Manual linear	3x3 laplacian
	Landcover discrimination	5,4,1	Manual linear	-
Landsat MSS	Drainage network delineation	7,6,5	Manual linear	3x3 laplacian
	Landcover discrimination	7,5,4	Gaussian	-

5.5 Problems of Image Hardcopy Consistency

It is perhaps pertinent at this point to mention the differences encountered during this research when producing similar hardcopy types, from different source locations. These differences were important in this research where visual interpretaion was often based on very subtle colour and intensity variations in the hardcopy output in the form of colour transparencies.

The aim in image processing with regard to hardcopy output is to obtain an output product of a similar appearance to that observed on the monitor. A broader aim is to achieve similar results from similar processing procedures carried out at whatever establishment.

It was soon noticed by the author that the hardcopy output in the form of colour transparencies from NERC, Swindon produced using the Matrix camera and the hardcopy output from Silsoe College also produced using a Matrix camera had distinctly different appearances. The images from Silsoe were much brighter (of higher intensity) than those from NERC and proved significantly better for discriminating linear water bodies. Particular difficulty arose in interpretation from the NERC images when examining the visually darker landcover types such as the forested areas. Images from NRSC Farnborough were similar to those from Silsoe, though not exactly the same.

These differences could be due to one or more of several causes, such as: hardcopy device type; level of illumination in the processing area; monitor settings; settings of the hardcopy device (Matrix camera); state of the film emulsion; processing of the recorded film (film types were similar).

The level of illumination in the processing area is an important determinant in the stretching processes involved here for subsequent visual interpretation and affects this in that a light working area renders the screen image relatively darker and vice versa. The operator may adjust stretches accordingly to give a similar visual appearance on the screen but resulting in differing hardcopy output appearances. This is closely linked to screen setting determinants such as brightness and contrast which if varied can affect the decision the processor makes in determining the optimal stretch for the later visual interpretation (unless standard linear stretching is applied). Settings on the hardcopy device are normally set by a technician and the relationship between these and the screen image should be known by the image processor.

The films used were all within their expiry dates, so emulsion problems should not arise. The films were not processed at the same laboratory, though standard processing procedures should produce fairly similar results. However, other work using colour transparencies has revealed considerable brightness differencies in films developed by the same laboratory with only a 24 hour time difference.

In the final analysis the question arises " How does one optimise the stretching of an image if the resulting hardcopy output for interpretation work, is significantly different in appearance from that of the screen image during the processing and enhancement phase?". It would seem appropriate to do some further research on this aspect of remote sensing which can create problems in optimal data usage. As far as the author is aware this aspect of remote sensing is given scant attention in remote sensing literature.

CHAPTER SIX: AUTOMATIC CLASSIFICATION

6.1 Introduction

The automatic classification procedures described in this chapter use the same image processing equipment as that used for image enhancement in Chapter 5. In this case the processing capabilities are used to classify the digital data into landcover classes. As the name would suggest these are classification procedures which contain some inherent degree of automation. Since an image processing system is required to carry out the following procedures, the costs of this should be borne in mind when considering the classification methodology to be adopted - the alternative being manual classification by visual interpretation, as described in Chapter 7. Two main types of automatic classifiers exist for analysing digital remotely sensed data, these being so-called "supervised" and "unsupervised" classifiers. These classifiers rely on discriminating different classes using purely spectral information recorded by the various sensors (see Chapter 4) and have no spatial analysis component, other than that implied by the spatial resolution of the sensor. They are commonly referred to as per-pixel classifiers. Algorithms for textural and contextual analysis are being developed but are uncommon on most image processing systems at present, though it could be beneficial to incorporate these at a future date if they prove advantageous for the applications under consideration.

Unsupervised classifiers examine the data statistics such as minimum, maximum, mean, standard deviation, covariance and eigen values, obtained from the pixels of the imaged bands to define separable classes. These derived parameters are then used to assign image pixels to particular classes. Interaction by the analyst is usually required to group the output classes from the classification according to the classification scheme adopted. Supervised classifiers use supervision in the form of known ground data to provide training areas for specific classes. These areas are interactively related to their corresponding image pixels by the image analyst and used to define the classification parameters for assignment of all other image pixels.

In this research the aim was to separate those classes with divergent hydrological properties, since those with similar properties can be grouped for hydrological analysis and modelling purposes. As previously discussed in Section 3.5, of Chapter 3, the classes selected for this area were forest/woodland, moorland, lowland agriculture, water, urban. A class of cloud/cloud shadow was included in an attempt to separate such areas from other unclassified areas. These classes are all areal/polygonal data types. No attempt was made to automatically classify narrow linear water features such as streams or rivers since these techniques are not suitable for such an application. Both supervised and unsupervised classification techniques were used in analysing the data and these are reported in Sections 6.2 and 6.3.

The choice of images and bands for the classification is dependent on the available imagery and the the classes one is trying to discriminate between. The pixel intensities recorded for different classes at various wavelengths (bands) provide the discriminating factor. It is also possible to use band ratios, vegetation indices or other image transforms in automatic classification, however these procedures were not investigated in this research. The results of other workers on Landsat TM classification (Townshend (1984); Belward *et al.* (1990); Khorram & Brockhaus (1991)) were considered in applying the classifications. The description of the supervised method for classification uses the Landsat TM as an example; with results for the Landsat MSS supervised classification presented in Section 6.2.5.

6.2 Supervised Classification

6.2.1 Training Data

Supervision of the classifier using known ground data taken from the area at (or for) the time of image acquisition should include sufficient representation of each class intended for classification, both for training data for the classifier and also for later evaluation of the classification accuracy. Literature suggests (Jensen,1986) that at least 10n pixels of training data are required for each class, where n is the number of spectral bands to be used in the classification. Details of the field surveys undertaken are given in Section 3.7. These were made some time after the image acquisition, although the second survey was undertaken to coincide with the season of acquisition in order to facilitate closer comparison with the imagery. This situation was not ideal but as the landcover patterns in this upland area show only small changes (certain forested areas apart), this was not an insurmountable problem. Stream measurements were the main aim of the surveys and the recording of landcover information was afforded only a secondary priority, given the time available. The field work resulted in the recording of sufficient data for training the classifier but precludes accuracy assessment, which was attempted using data from other sources, and is discussed in Section 8.4.

The training areas were defined interactively on the I^2S image processing system using a Landsat TM band 5,4,1 FCC with a contrast stretch applied to increase visual contrast for easier location of the training areas. This procedure and the classification was carried out prior to geocorrection of the imagery since delineation of the training areas is more difficult after geocorrection due to the "blocky" appearance of the imagery (see also Section 5.2.2). Figure 6.1 illustrates delineation of the training areas on the stretched 3-band FCC.

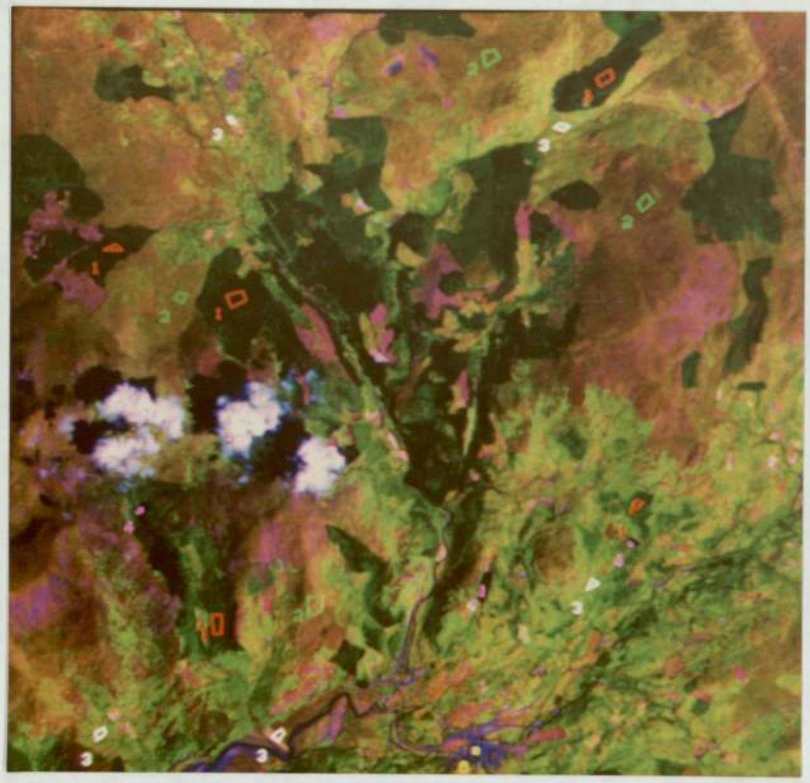

Figure 6.1 Delineation of training areas on Landsat TM image (Band 5,4,1 FCC).

Individual training areas were fairly easily identified on the image, using field data recorded on the 1:50000 map or from field photos of the area. The easiest training areas to identify were those for classes possessing high spectral contrast with their surroundings. Problems were only encountered when the fields were small in size (field size < 2ha). Landcover information recorded on the ground survey maps was used to identify the training sites for each class except cloud, which of course was image specific. Only small lakes and one small town occur in the area, thus the training areas for these classes were restricted. Details of the training data extracted are given in Table 6.1.

Table 6.1 Landsat TM - training data details.

Class	No. of Training Areas	No. of pixels of Training Data
Forest/Woodland	5	309
Moorland	4	301
Lowland Agriculture	5	156
Water	3	37
Urban	2	47
Cloud	1	16

Once defined as a vertices file the training areas can be extracted for any combination of bands from the 6 bands of Landsat TM imagery. The statistics of these combinations were then examined to decide on the most useful band combinations prior to applying a classifier to the whole image area. Values of mean, minimum and maximum pixel values, standard deviation, covariance and correlation matrices are calculated for each class and band combination. Examples of these are given in Table 6.2, and a more complete example in Appendix D.

Table 6.2 Landsat TM research area subscene statistics.

Class	Statistic	Band					
		1	2	3	4	5	7
Forest/ Woodland	Min.	58	20	15	38	56	6
	Max.	67	27	21	100	50	15
	Mean	61.5	23.2	17.8	64.6	30.6	9.4
	Std. Dev.	1.7	1.5	1.0	12.1	5.4	1.8
Moorland	Min.	60	25	21	61	60	22
	Max.	80	37	39	116	126	46
	Mean	68.6	29.7	27.6	86.0	84.5	29.2
	Std. Dev.	3.9	3.3	4.0	12.8	16.9	6.0
Lowland Agriculture	Min.	61	24	18	63	63	18
	Max.	86	40	37	165	134	54
	Mean	68.6	29.6	24.1	115.1	84.7	26.2
	Std. Dev.	5.1	3.1	4.3	23.4	16.6	8.4
Water	Min.	58	17	13	10	5	2
	Max.	63	23	21	41	52	16
	Mean	60.5	19.6	14.8	16.8	12.9	5.2
	Std. Dev.	1.6	1.6	2.2	9.0	9.6	3.0
Urban	Min.	78	31	30	27	34	21
	Max.	88	37	38	40	53	32
	Mean	83.4	33.3	33.7	31.3	41.8	25.1
	Std. Dev.	3.5	1.6	2.1	3.3	5.0	2.6
Cloud	Min.	222	102	118	140	186	92
	Max.	254	218	251	215	254	164
	Mean	252.3	163.6	190.1	181.5	236.7	130.1
	Std. Dev.	6.7	28.3	33.0	15.5	18.0	15.7

The statistics in Table 6.2 are the spectrally derived statisitics which will be used by any decision rules of the classifier implemented, to allocate each image pixel to a particular class. The differences in ranges and mean pixel intensities between the bands and classes can be seen to vary considerably. For example the forest/woodland class shows a range of 62 (38-100) in band 4, but only 9 (6-15) in band 7, whereas the lowland agriculture class exhibits ranges of 98 and 36 for the same bands. The standard deviations also show large variations, from 1.0 for band 3 of the forest/woodland class to 33.0 for the same band of the cloud class.

Returning to the question of band selection, the classes for discrimination in this research were mostly vegetative in nature and thus show greatest spectral response variation in the near infrared region of the electromagnetic spectrum (see also Section 4.3). This is represented in Landsat TM imagery by bands 4 and 5, which have spectral ranges of 0.76-0.90μm and 1.55-1.75μm respectively. Water has a low spectral response at these wavelengths and can thus be easily discriminated from the vegetation. Plotting scattergrams of 2 bands of spectral information is useful in determining spectral separability by visual analysis (see Figure 6.2). 3 band separability can also be visualised but computer processing is required for the analysis of several information channels (bands) such as exist here.

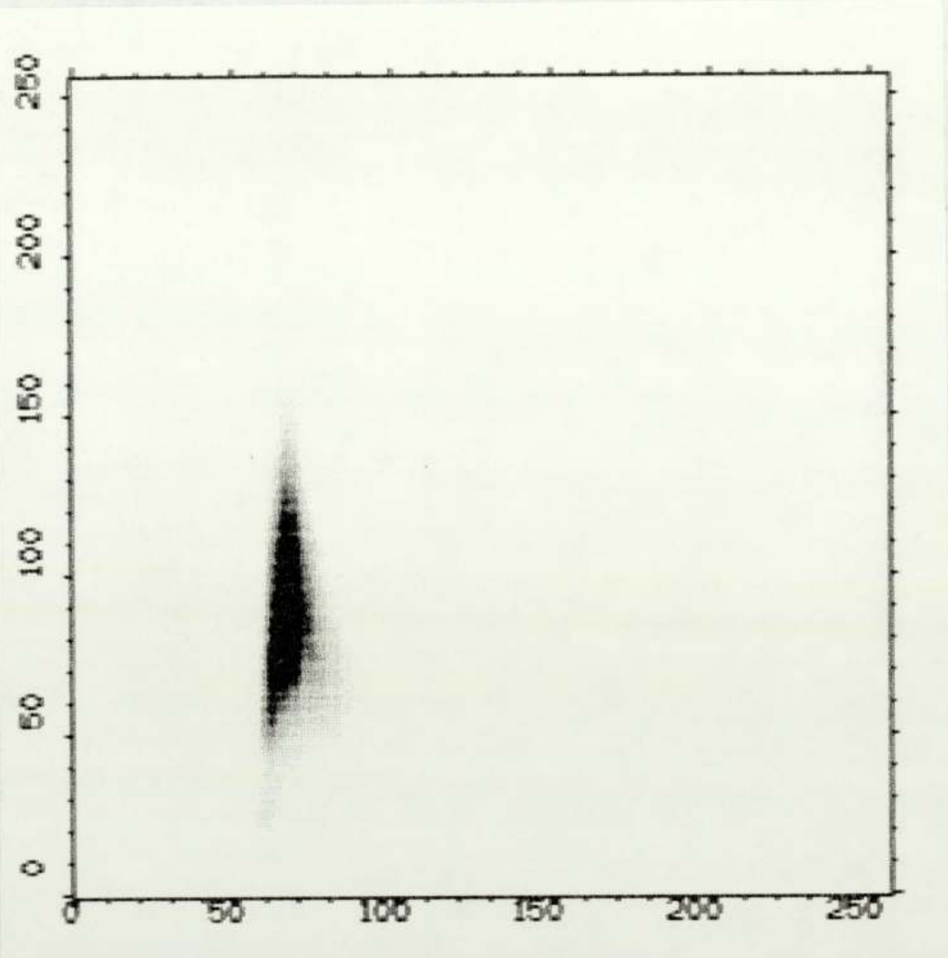

Figure 6.2 2-band Scattergram of bands 4 (y-axis) and 1 of Landsat TM data, showing pixel intensities of the raw data.

The previous paragraphs have dealt with band selection for landcover discrimination on a physical basis. The following paragraphs examine statistical methods for determining optimal band combinations. The commonly used divergence measure is discussed as is a validation procedure which performs a minimum distance to means classification on the training data.

A method which is often used in determining the optimum band combination for classification is known as the divergence measure. The technique requires that measurements on the members of the training classes are distributed in a multivariate-normal form (Jensen, 1986). The effect of departures from this assumption is not known, but one can be certain that the results of the analysis would be less reliable as the departures from normality increased. Examination of the class histograms, for the training data revealed non-gaussian distributions for bands 4 and 5 in the moorland and lowland agriculture classes. Figure 6.3 illustrates the distribution of pixel intensities for band 4 of the moorland training data set.

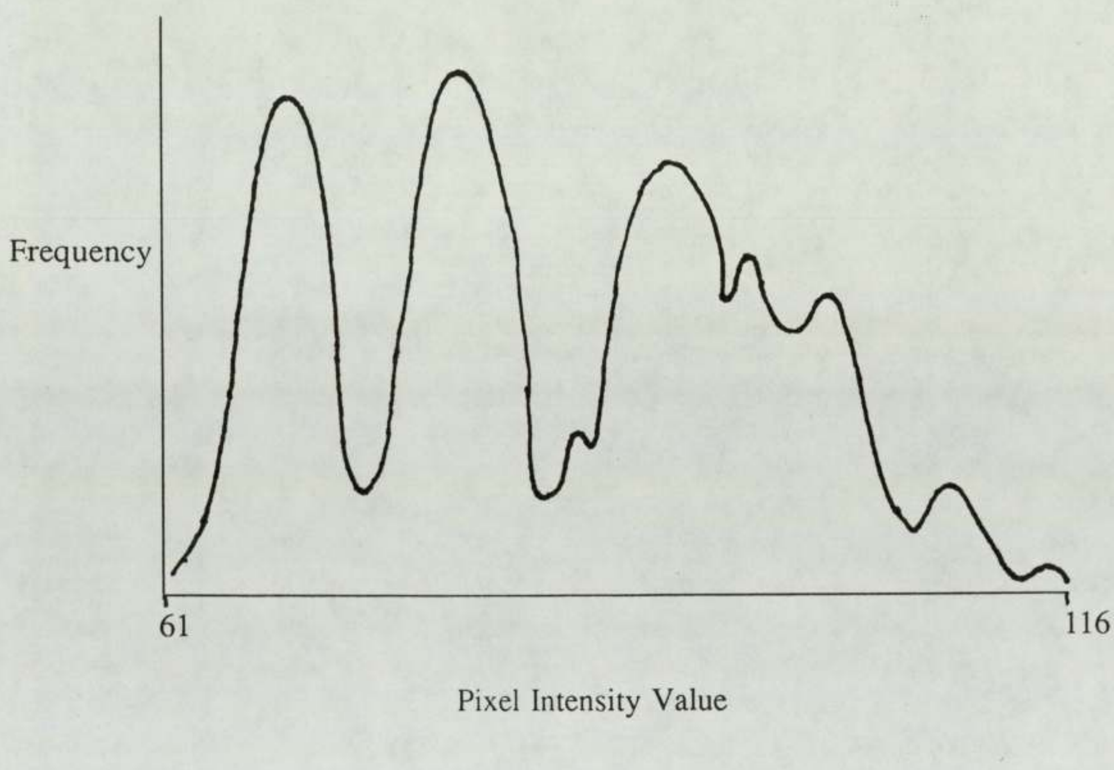

Figure 6.3 Histogram for band 4 of the moorland class training data set.

Divergence measures how separable two classes are, given their covariance matrices and mean vectors. If we presume that the statistics file derived from the training class data defines NC classes from an NB image feature space (no. of bands), where NC and NB represent the number of classes and image bands respectively, then divergence is expressed as (Jensen, 1986):

$$D_{ij} = \frac{tr((C_i - C_j)(C_j^{-1} - C_j^{-1})) + tr((C_i^{-1} - C_j^{-1})(M_i - M_j)(M_i - M_j)^T)}{2} \quad (6-1)$$

where: C_i and C_j = the NB by NB covariance matrices of the i^{th} and j^{th} classes,

M_i and M_j = the NB mean vectors of the ith and jth classes,

i and j = 1 to NC

$i \neq j$

This equation is evaluated for each class pair. The distribution of divergence is not well known so a measure called the transformed divergence is used instead. This has the effect of reducing the divergence statistic, the effect increasing with the magnitude of divergence. Thus, when averages are taken, the influence of one or more pairs of widely-seperated classes will be reduced. The divergence values undergo a transformation giving them a saturating behaviour:

$$D_{ij} = 100*(1.0- exp(-D_{ij}*0.125) \quad (6-2)$$

It can be seen that a maximum value of 100 is possible, but values of 80 or more indicate good separability of the two classes concerned. The transformed divergence values are averaged for all possible mutually-exclusive pairs of classes and the average (the average pairwise divergence) is calculated. Transformed divergence values for the six-band TM combination are given in Table 6.3.

Table 6.3 Transformed Divergence Matrix for TM six-band Combination

Class No.	Class Name	Class Number					
		1	2	3	4	5	6
1	Forest/ Woodland	0.0	100.0	100.0	100.0	100.0	100.0
2	Moorland	100.0	0.0	97.4	99.9	100.0	100.0
3	Lowland Agriculture	100.0	97.4	0.0	100.0	100.0	100.0
4	Water	100.0	99.9	100.0	0.0	100.0	100.0
5	Urban	100.0	100.0	100.0	100.0	0.0	100.0
6	Cloud	100.0	100.0	100.0	100.0	100.0	0.0

From these figures the average transformed divergence values can be calculated, that is the overall value for the 36 (6x6) possible permutations. This combination of six TM bands gives an averaged transformed divergence of 99.82, which is good when compared to that for bands 1 2 3 of 95.02. Values for increasing number of bands, when including the near-infrared bands, showed improvements to a maximum of

99.91 using all six bands. These values are all high when compared to values obtained by Boarelli and France (1989) when examining more extensive training data for agricultural classification of an area in Northern Italy.

The second method of statistical evaluation examined was validation. The validation procedure available on the I^2S system is used to analyse the training data for its consistency and determine if certain pixels are sufficiently different to the general training class statistics that they warrant exclusion from the classification procedure. The method applies a minimum distance to means classifier to the training classes in the bands selected (Curran, 1985). This is a classifier which calculates the mean position in feature space for each training class and assigns pixels to the nearest mean class position in feature space terms. Pixels which lie beyond a certain distance form any class mean, e.g. 3 standard deviations (or whatever threshold is desired), are assigned to the reject class. Table 6.4 shows the example for bands 3,4,5,7 with a threshold level of 3.0.

Validation, like the divergence measure gives an indication of the best band combinations for class separation. It is useful to examine not only the correctly classified figures in the confusion matrix, but also the number of training pixels rejected. The band 3,4,5,7 combination produces good results in this examination, improved in correct classification terms by combinations including more bands as for divergence. However, this increase in correct classification is accompanied by a worrying increase in the number of pixels rejected. This is discussed further in the

Table 6.4 Validation Matrix for Bands 3,4,5,7 with a threshold value of 3.0

Class No.	Trained as:	Classified as:						
		1	2	3	4	5	6	Reject
1	Forest/ Woodland	278	0	0	0	0	0	31
2	Moorland	0	229	43	0	0	0	29
3	Lowland Agriculture	0	27	115	0	0	0	14
4	Water	3	0	0	32	0	0	2
5	Urban	0	0	0	0	15	0	1
6	Cloud	0	0	0	0	0	43	4

next section (Section 6.2.2). Decreasing the threshold value improves separability but also increases the rejection level. It is possible to create new "filtered" extract files of thresholded data for subsequent preparation of statistics and implementation in classification. This was carried out and is discussed in Section 6.2.2.

6.2.2 Classification Methods

After examination of the band combinations using divergence and validation procedures together with knowledge of the physical responses of the landcover types and experience with agricultural crop classification using Landsat TM imagery of Northern Italy (Boarelli and France, 1989), it was decided to use the following band combinations : 3 4 5 7; 4 5 7 and all six bands; for the classification. A maximum likelihood classifier with a 90% confidence level was applied to the selected band combinations for classification. The maximum likelihood classifier is a commonly used classifier (Mather, 1987) which assumes that the training statistics for each class in each band are normally distributed (i.e. Gaussian in nature). This classifier calculates the mean position in feature space of each class of training data and assigns pixels to the nearest mean class position in the feature space. The classifier determines the probability of all points in the feature space belonging to a particular class, so that each point has a probability of belonging to each of the classes identified. The class to which it is assigned is the class for which it has the highest probability, that is the maximum likelihood of belonging to that class.

If the mean measurement vector, M_c, for each class and the covariance matrix of class c for bands k through l, V_c; then the decision rule applied to the unknown measurement vector, X, is (Anuta, 1977): Decide X is in class c if, and only if,

$$p_c \geq p_i, \text{ where } i = 1, 2, 3, .., m \text{ possible classes}$$

and

$$p_c = [-0.5\log_e(\det(V_c))] - [0.5(X - M_c)^T(V_c)^{-1}(X - M_c)] \quad (6\text{-}3)$$

where X $= [PI_{i,j,1}, PI_{i,j,2}, PI_{i,j,3}, PI_{i,j,4}, PI_{i,j,5}, PI_{i,j,6}]$

i.e. the pixel intensities for a pixel at location i,j in the imaged bands (1 - 6) and det (V_c) is the determinant of the covariance matrix V_c. Therefore, to classify the measurement vector X of an unknown pixel into a class, the maximum likelihood decision rule computes the value p_c for each class. Then it assigns the pixel to the class that has the largest value. With a 90% confidence level implemented, any pixel with less than a 90% probability of belonging to one of the defined classes is designated unclassified. Table 6.5 gives results of the classification performed using the different band combinations.

Table 6.5 Results of Maximum Likelihood Classification

Class	Bands 4 5 7	Bands 3 4 5 7	All Six Bands
	%	%	%
Forest/Woodland	9.8	14.4	15.4
Moorland	34.8	8.9	17.2
Lowland Agriculture	22.3	73.0	52.6
Water	0.1	0.2	0.4
Urban	0.1	0.1	0.1
Cloud	0.1	0.1	0.1
Unclassified	31.7	3.5	14.4

These results showed as expected a dominance of moorland and lowland agriculture in the area with some forested areas. High rejection levels are observed using just bands 4, 5 and 7 (NIR, NIR, MIR) and fairly high rejection level is also seen in the six band combination. The band 3, 4, 5, 7 combination gives a very high percentage of lowland agriculture, more than it is reasonable to expect after general field survey of the area. It is possible to view the classifications by assigning colours to the classes (see Figure 6.4a). This revealed large misclassification of the moorland areas by lowland agriculture in the 3,4,5,7 classification. A similar occurence was apparent in the six band combination though not to the same extent. It can also be seen that some cloud shadow areas are misclassified as water and some of the wide river Afon Mawddach (675 186) and its floodplain are misclassified as urban areas, which is probably due to similar spectral responses from the urban area and these areas of sand/mud/alluvium.

As mentioned in Section 6.2.1, examination of the class histograms revealed bimodal distributions for bands 4 and 5 in the moorland and lowland classes. The large variety of vegetation types covered by these two very general classes (see Section 3.5) would help to explain this, and perhaps further class distinction is necessary to alleviate this problem.

Another way of approaching this problem is to use the "filtered" training data set provided by the validation procedure as previously described. Using a threshold value of 3 standard deviations on the training data the results shown in Table 6.6. and Figures 6.4b & 6.5 were obtained. Figure 6.4b reveals large changes in the distribution of the moorland and lowland agriculture classes when compared with Figure 6.4a.

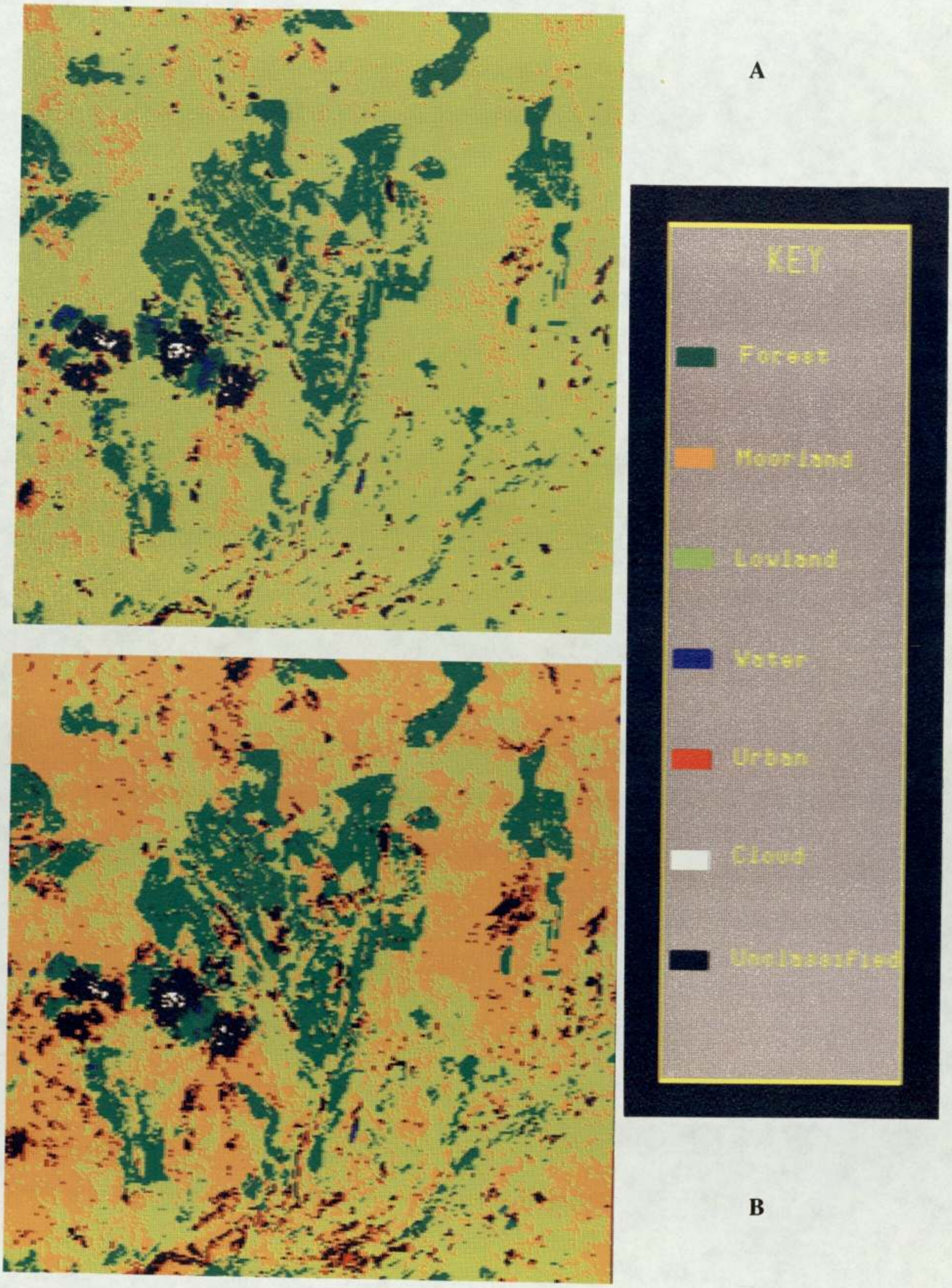

Figure 6.4 Maximum likelihood classification using bands 3,4,5 and 7 (**A**), and with filtered training data (**B**).

These classifications with filtered training data show classification figures which are closer to what would be expected in the area, after general survey, apart from the band 4,5,7 combination which gives an unacceptably high rejection class. The band 3,4,5,7 combination still has a fairly low rejection level. The six band classification shows a very high rejection level which reduces its usefulness. From examination of Fig. 6.4b and comparison with an FCC (see Figure 5.7), it is clear that the majority of unclassified areas correspond to areas of cloud coverage or cloud shadow. Examination of Table 6.2 reveals large standard deviations in the training data for clouds which explains this high rejection level (unclassified area).

Other unclassified areas occur in the small "urban" area of Dolgellau, where there his a high degree of pixel intensity variance, and also in parts of the moorland class. Parts of the floodplain of the Afon Mawddach have been miclassified as moorland and parts of the the estuary itself have been misclassified as urban. The estuarine misclassification is probably due to exposed or shallow water mud flats with similar reflectance properties to the slate roofs of the urban area.

Table 6.6 Results of Maximum Likelihood Classification with "filtered" training data - 3.0 Standard Deviation Limit.

Class	Bands 4 5 7	Bands 3 4 5 7	All Six Bands
	%	%	%
1 Forest/Woodland	8.7	15.9	11.5
2 Moorland	45.4	43.8	33.5
3 Lowland Agriculture	13.2	32.5	27.5
4 Water	0.6	0.1	0.1
5 Urban	0.2	0.1	0.0
6 Cloud	0.3	0.1	0.0
7 Unclassified	31.6	7.5	27.4

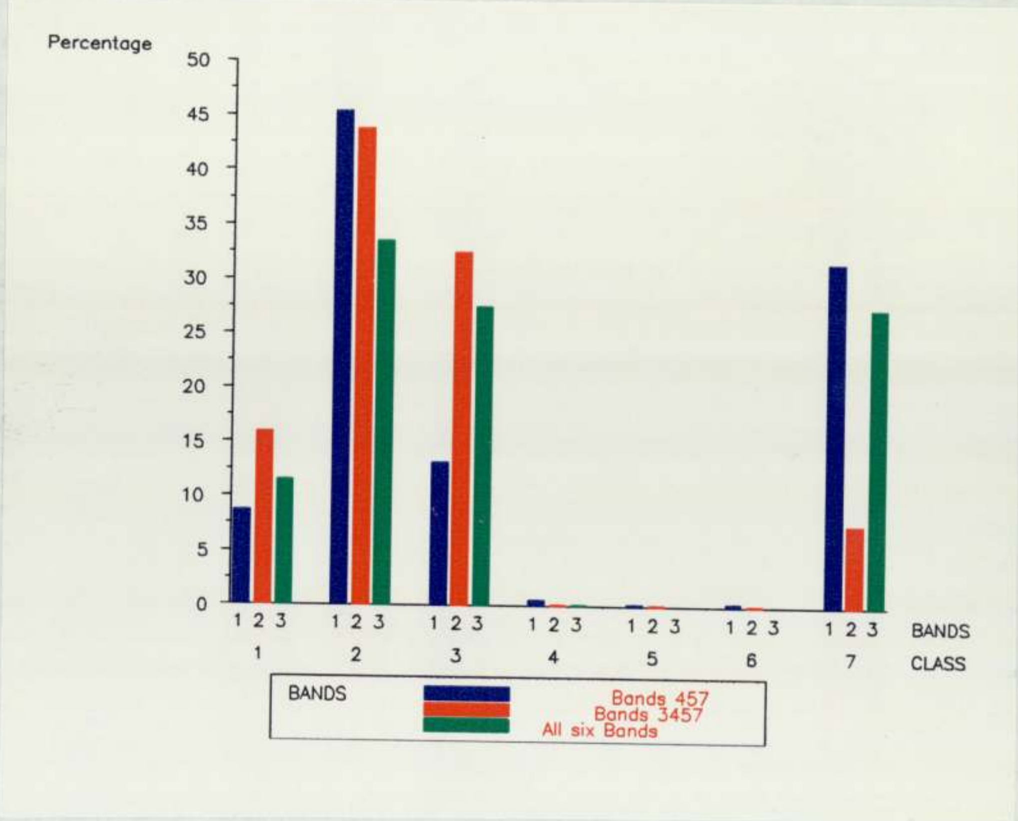

Figure 6.5 Graphical representation of statistics after classification using the maximum likelihood classifier (for class nos. refer to Table 6.6).

6.2.3 Smoothing

It can be seen (Figure 6.4) that while the classification follows the general pattern that would be expected, there are many instances of single or small numbers of pixels at variance with homogenous surrounding areas. These are errors of classification and can be improved by the application of a low pass "smoothing" filter. The filter used was an equally weighted modal filter, with a 3 x 3 kernel size and a majority modifier. This is a 9 pixel filter which as it passes over the image assigns to the central pixel of the kernel the modal value of pixels within the kernel, providing the majority of pixel values in the kernel are of the modal value. Otherwise the pixel values are left unaltered. This filter results in a classification image exhibiting a much greater degree of homogeneity, as shown in Figure 6.6. It does however result in the loss of some fine linear detail such as rivers and in this area some small clumps of trees.

Table 6.7 shows the classification statistics after one iteration of the modal filter, using the band 3,4,5,7 classification with filtered (validated) training data. Attempts to smooth the classification using a median filter proved less successful, with much important information lost in the process. Comparison with figures for the classification prior to smoothing, as given in Table 6.6, reveal only small changes in the overall class percentages for the same band combination.

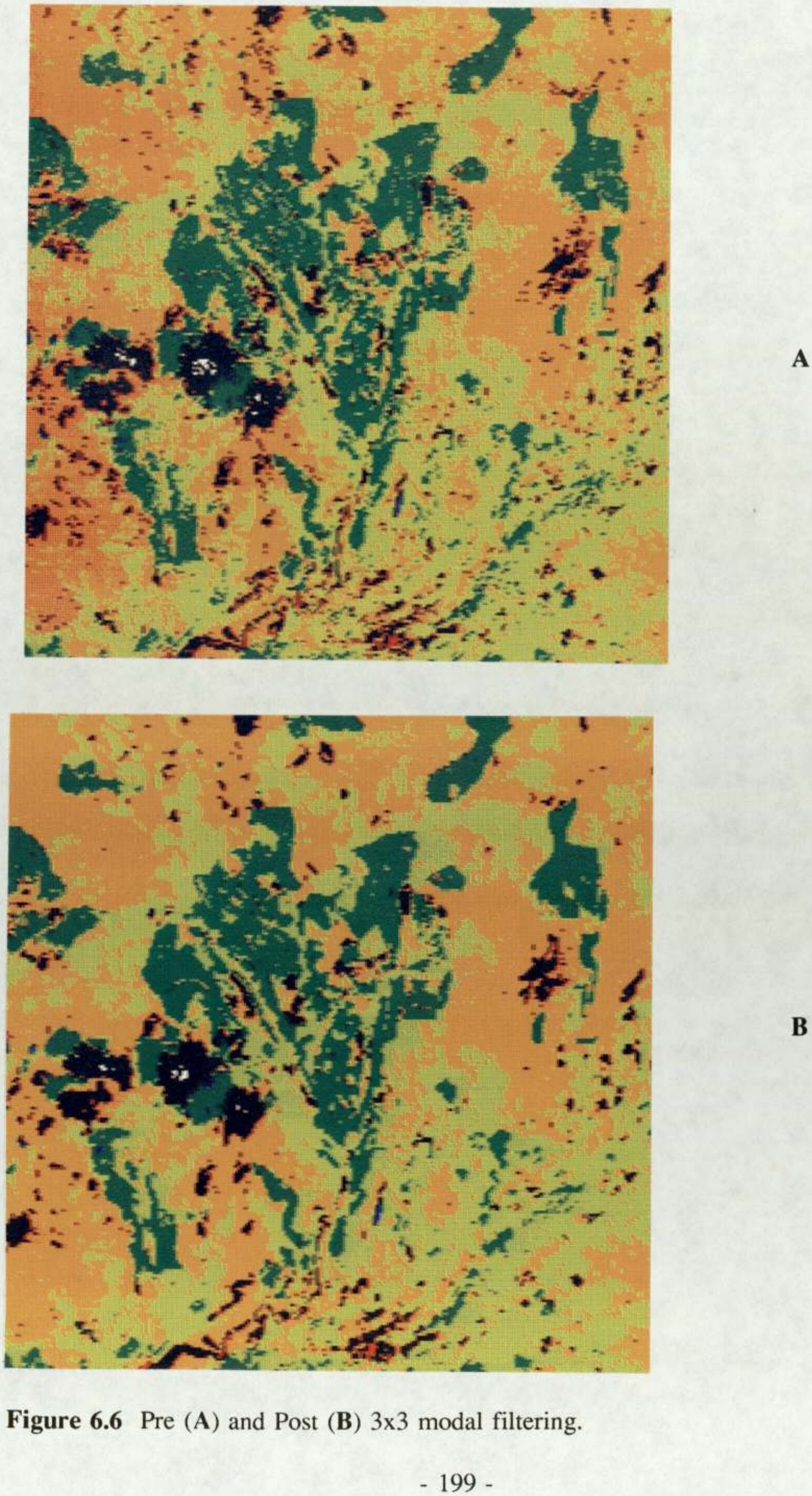

Figure 6.6 Pre (A) and Post (B) 3x3 modal filtering.

Table 6.7 Classification Statistics after one iteration of a 3x3 modal majority filter

Class	No. of Pixels	%
Forest/Woodland	42312	16.1
Moorland	117446	44.8
Lowland Agriculture	84850	32.4
Water	212	0.1
Urban	93	0.04
Cloud	117	0.05
Unclassified	17094	6.5

6.2.4 Geometric Correction

The classification was carried out as described in section 5.2.1, however it is not possible to accurately relate the results to the other geographical data, such as in a GIS (see Chapter 9), or use a multitemporal approach, until geometric correction has been applied to the imagery. To execute a geometric correction, control points were extracted as outlined in section 5.2.1. The extracted control points were then used to warp the classified image (rather than the raw image data) with a nearest neighbour interpolation algorithm. As mentioned previously, the nearest neighbour algorithm has the least effect on pixel intensity of the common pixel value interpolation methods, leaving the resulting warped image with similar pixel intensity values to the original image. Thus in this instance the nearest neighbour algorithm is preferable to the cubic convolution algorithm, since intensity rather than locational accuracy was the priority. The use of a cubic convolution interpolation algorithm would cause alteration of some of the pixel values, which in this instance represent classes. This alteration would distort the class statistics. Table 6.8 gives a comparison of statistics for the modal filtered band 3,4,5,7 classification before and after geometric rectification using a nearest neighbour interpolation algorithm.

It can be seen from Table 6.8 that changes in the classification statistics due to geometric correction are minimal being a maximum absolute value of 333 pixels total difference for Lowland Agriculture. This represents an area of 30 hectares, compared to a total area of 23593 ha for the class (i.e. less than 0.1%).

Table 6.8 Pre and Post Geometrical Correction Statistics

Class	No. of Pixels		%	
	Pre	Post	Pre	Post
Forest/Woodland	42312	42425	16.1	16.1
Moorland	117446	117707	44.8	44.8
Lowland Agriculture	84850	85183	32.4	32.4
Water	212	209	0.1	0.1
Urban	93	89	0.04	0.04
Cloud	117	119	0.05	0.05
Unclassified	17094	17126	6.5	6.5

6.2.5 Supervised Classification of Landsat MSS data

Training areas were selected from a stretched false colour composite (bands 7,5,4) of the June 1975 Landsat MSS image. The regions selected are presented in Table 6.9.

Table 6.9 Landsat MSS - training data details.

Class	No. of Training Areas	No. of pixels of Training Data
Forest/Woodland	4	67
Moorland	4	118
Lowland Agriculture	5	40
Water	1	12
Urban	1	14

Statistics were extracted for all four bands and can be found in Appendix D. The classification was executed with a classification limit of 5.0 standard deviations. Problems were encountered with large areas classified as water. Figure 6.7 illustrates the spatial distribution pattern of the classes. It can be seen that areas of forest have been misclassified as water, along with some other areas which were known not to be water. Examination of the class statistics revealed standard deviations of 12.3 and 7.2 for bands 6 and 7 of the water training data set. Redefining of the water training class was not possible using the small water bodies in the research area, since insufficient "pure" water pixels were found at this spatial resolution. Training pixels for the water class were drawn from a larger water body outside the research area. Standard deviations for the water class in bands were then found to be 2.2 and 1.4 respectively. Classification using the new water training statistics produced improved results.

Geometric correction of the classification was carried out using the procedure described in Section 5.2.2, with nearest neighbour interpolation in this instance, to produce a square-pixel output with 50m spatial resolution. The research area was then extracted from the classification using a defined region of interest. The results are presented in Table 6.10, together with results after the application of a 3x3 modal filter for smoothing.

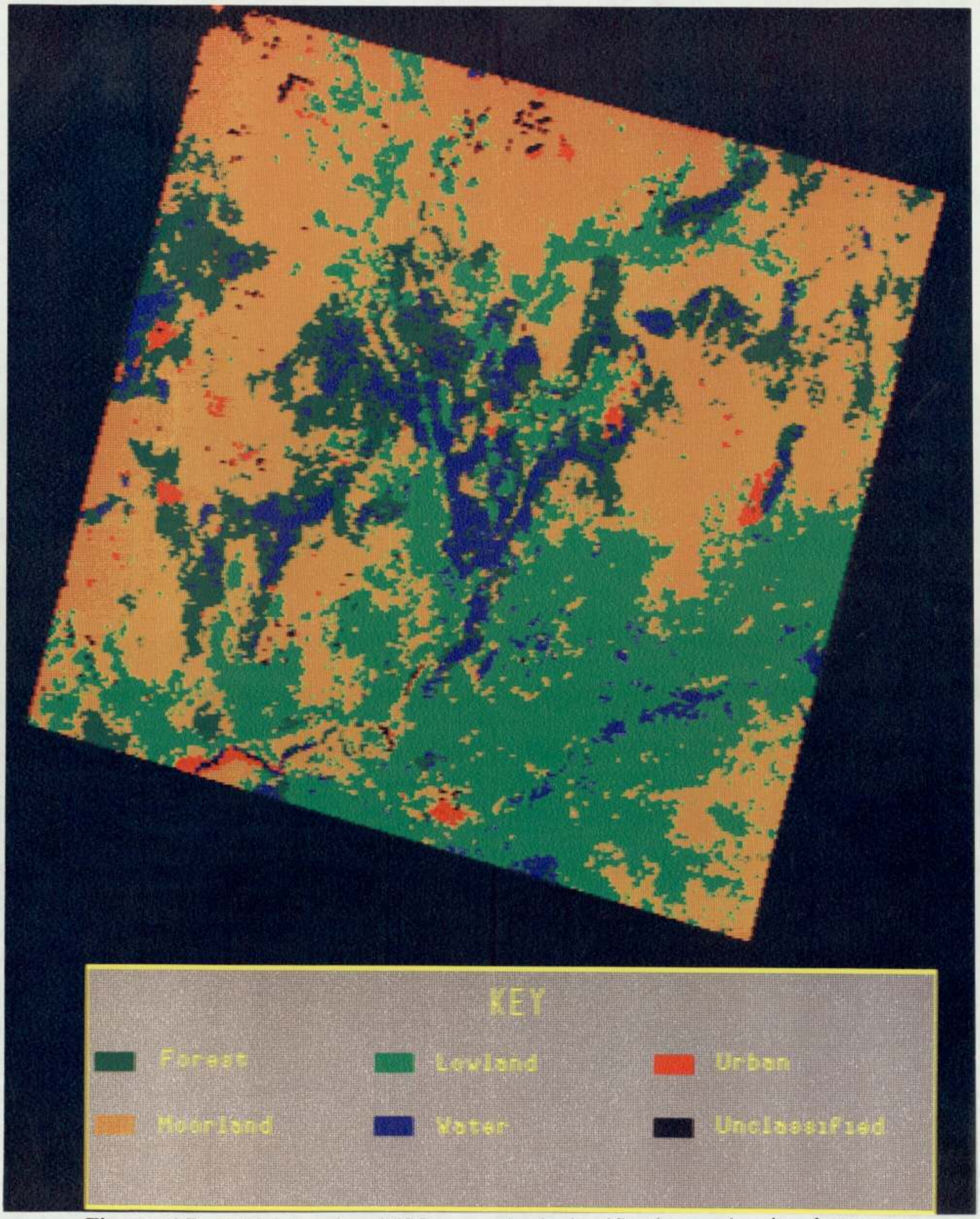

Figure 6.7 Initial Landsat MSS supervised classification - showing large areas misclassified as water.

Table 6.10 Pre and Post 3x3 Modal Filtering Statistics

Class	No. of Pixels		%	
	Pre	Post	Pre	Post
Forest/Woodland	18702	18697	19.3	19.3
Moorland	46171	46475	47.5	47.9
Lowland Agriculture	30586	30702	31.5	31.6
Water	47	41	0.05	0.04
Urban	773	635	0.77	0.65
Unclassified	831	560	0.86	0.58

It can be seen in Figures 6.8 and 6.9 that several areas are misclassified as urban. Most of these areas are in moorland or in the Mawddach estuary. A visual comparison of Figures 6.4b, the Landsat TM classification, and Figure 6.9 from Landsat MSS shows general agreement, but with some areas of discrepancy.

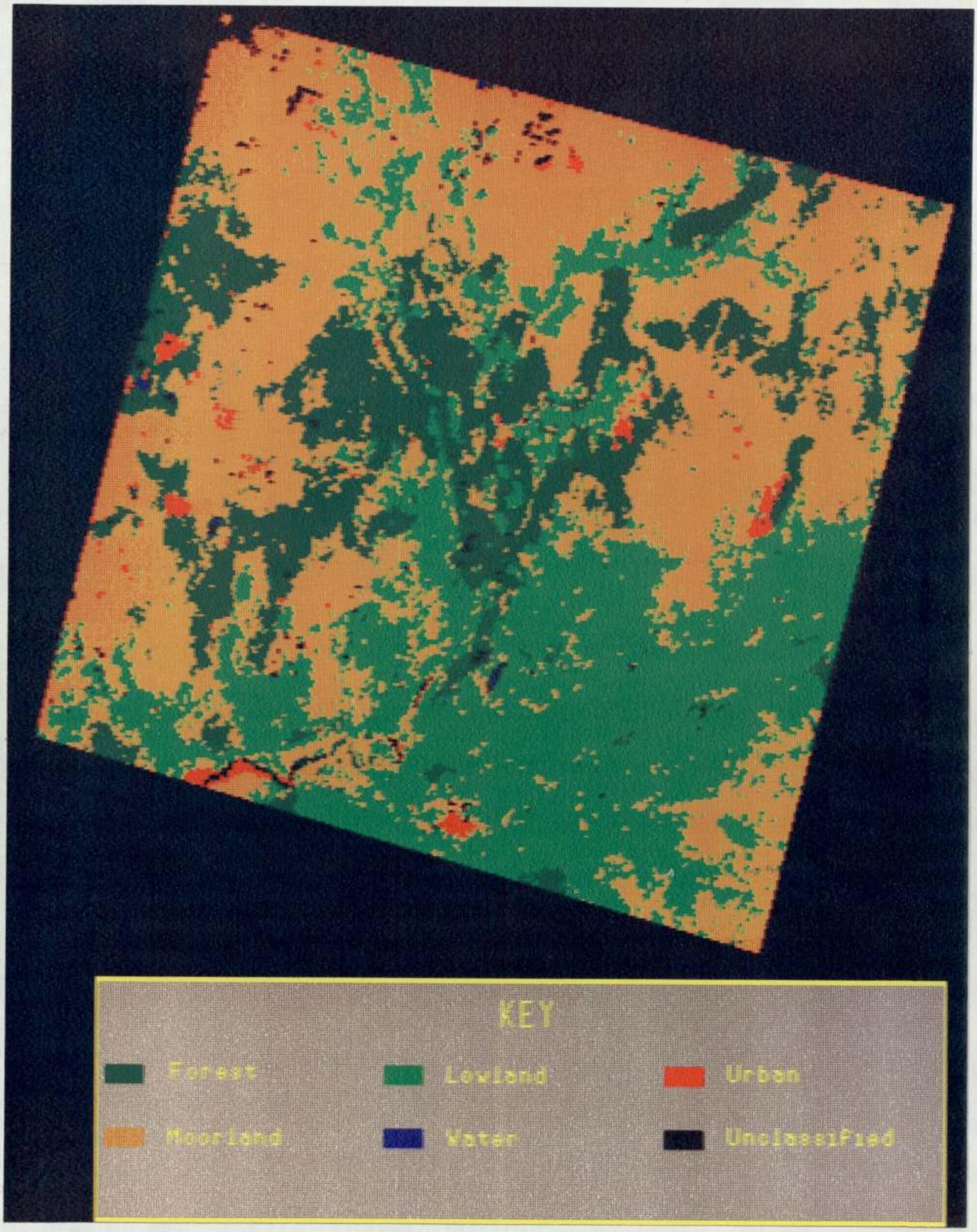

Figure 6.8 Landsat MSS classification after modification of the water class training data.

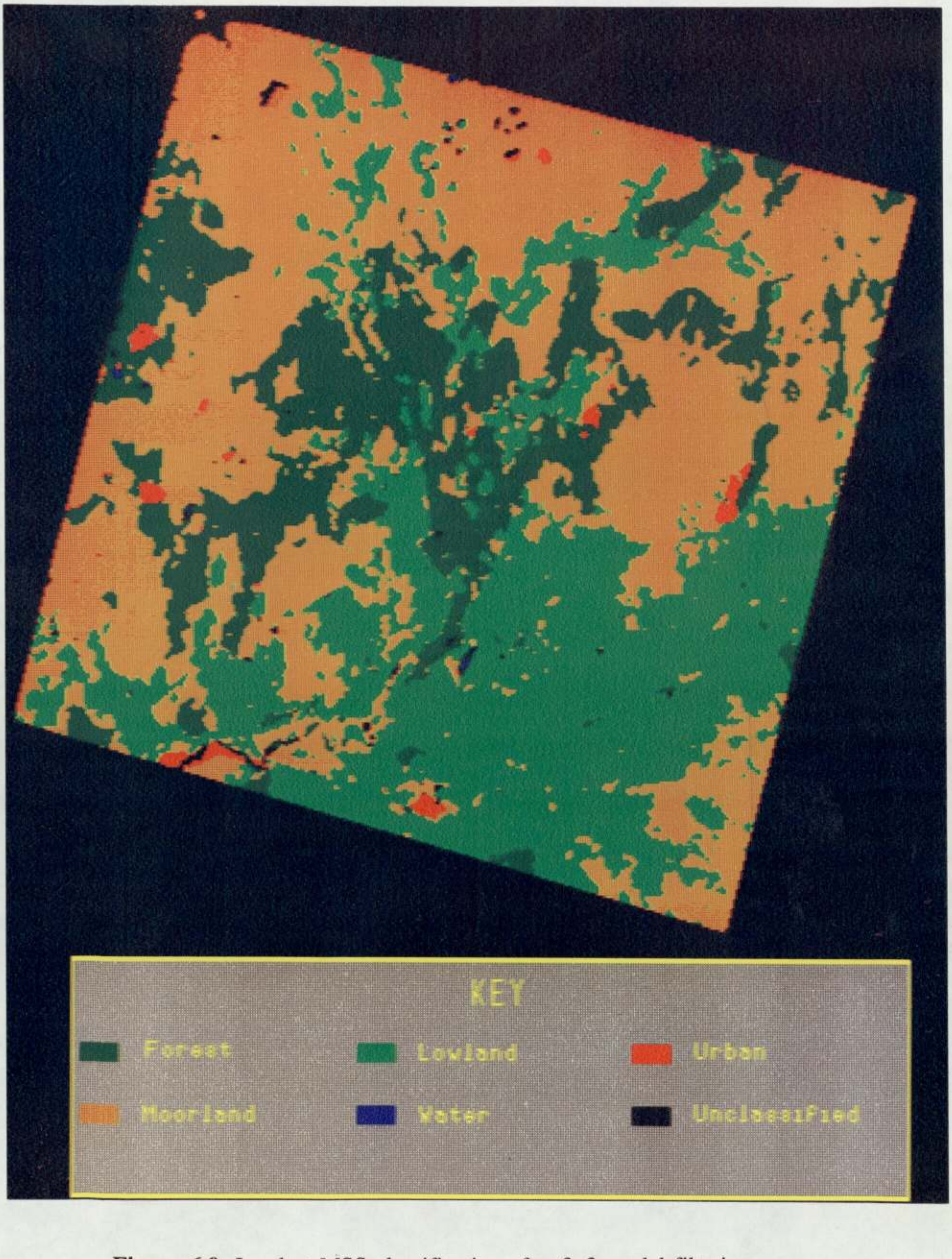

Figure 6.9 Landsat MSS classification after 3x3 modal filtering.

6.3 Unsupervised Classification

In contrast to supervised classification, unsupervised classification requires only a minimal amount of initial input from the analyst. This type of classification is a process whereby the spectral properties of the imaged pixels are used to define "natural" groupings. Clustering algorithms used for the unsupervised classification of remotely sensed data generally vary according to the efficiency with which the clustering takes place. Different efficiency criteria lead to different approaches (Duda and Hart, 1973; Goldberg and Shlien, 1976; Haralick and Fu, 1983). Schowengerdt (1983) suggests that virtually all of the commonly used clustering algorithms use iterative calculations to find an optimum set of decision boundaries for the data set under examination.

The I^2S computer program used in this instance begins by making an estimate of "seed" locations in the feature space based on the number of initial classes requested by the operator. It divides these classes among the feature space according to the total variance in each feature (each band) and then by equal area under the histogram of each feature. The actual seed location is at the centre of each equal area portion of the histogram.

The process of classification is performed in iterations in the following manner:

i) the data is classified;

ii) the results are examined;

iii) the seed location is modified and the process repeated.

This process continues for the number of iterations defined by the operator, unless an improvement threshold is reached prior to completion of the full number of iterations. As the results of the iterative process converge, a stable classification emerges. This classification divides the feature space into a set of clear classes.

Several important options are available for controlling the classification and monitoring the statistical output. These include:

- the number of initial classes;
- the number of iterations;
- a stability threshold for determining when to end the classification prior to the number of iterations specified. The threshold is in terms of average change in mean vector location from the last iteration, measured in feature space units;
- Maximum or minimum numbers of pixels contained in any one class;
- A merging distance for merging classes that are very close together in the feature space;
- An option to include seed location at the extreme values in each band. This is to include very bright or dark pixels, that might otherwise be ignored.

It is important to think carefully through these parameters before initiating the classification procedure.

Once completed the classified image should be coloured as described in section 6.2.2. The colours can be used to examine which classes should be merged together by the analyst to produce a classification containing the classes desired for discrmination.

This make use of the analyst's general knowledge of the area. The image can then be coloured again assigning the same colour to those classes from the same desired class groupings.

These procedures were performed on the Landsat TM data for the test area. Initial class numbers of 10 and 16 were used with an extreme option used in addition to the standard classification. Using 10 or 16 initial classes made little difference in the final outcome other than having to assign more classes to the moorland and lowland agriculture general classes. The water, urban and cloud classes were not represented by the final clusterings and thus could not be discriminated. It can be seen in Fig. 6.10 that the 10 class classifier resulted in some urban areas being misclassified as moorland and the rest unclassified, together with water and cloud areas.

For the 16 class classification more urban was misclassified as moorland and again water and cloud areas were unclassified. Also in this classification, some forest areas were misclassified as lowland which would be expected for little used forest tracks with vegetative cover. However, this does not account for all the misclassified areas of this type.

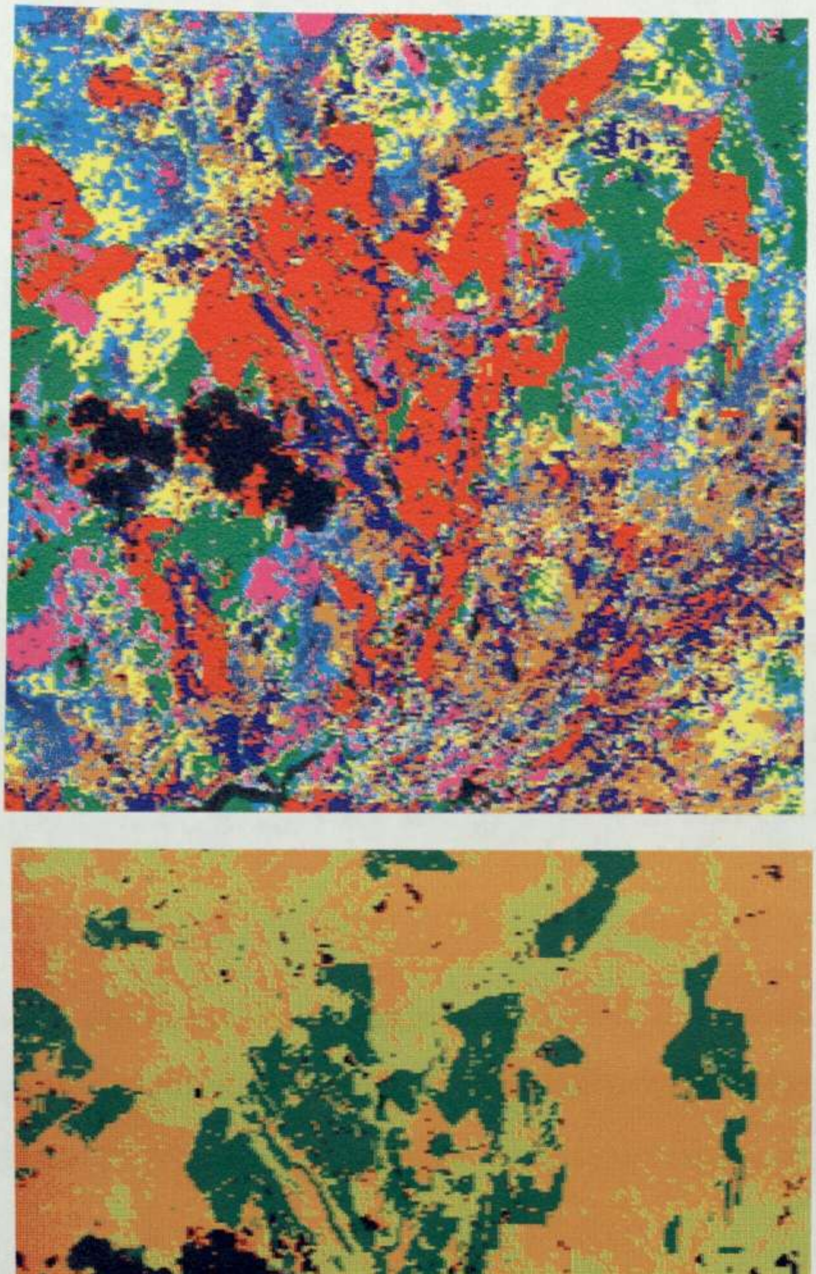

A

B

Figure 6.10 Unsupervised classification for 10 initial classes (**A**), and (**B**) after merging of classes to produce the desired output classes (see Fig. 6.4 for output class types).

The results after merging of the similar classes are presented in Table 6.11. It can be seen that the use of the extreme seeding location modifier made no difference to the outcome and thus did nothing to reveal the water, urban and cloud classes.

Table 6.11 Results of Unsupervised Classification

Class	No. of Initial Classes			
	10	10 (with extreme option)	16	16 (with extreme option)
	%	%	%	%
Forest/Woodland	16.0	16.0	12.8	12.8
Moorland	43.7	43.7	45.2	45.2
Lowland Agriculture	34.9	34.9	34.9	34.9
Water	0.0	0.0	0.0	0.0
Urban	0.0	0.0	0.0	0.0
Cloud	0.0	0.0	0.0	0.0
Unclassified	4.5	4.5	3.4	3.4

6.5 Summary

In both supervised and unsupervised classification procedures the operator is required to make important decisions with regard to training area selection, band selection, confidence limits, or the merging of output classes. These decisions can have significant effects on the final classification statistics. It is therefore vital that the operator understands, as fully as possible the consequences of these decisions.

Supervised classification of the Landsat TM imagery proved easier than for Landsat MSS at the training stage. This was due to the easier recognition of training areas on Landsat TM imagery. Classification was most successful using the band 3,4,5,7 combination, which includes visible, near infrared and mid infrared bands. This proved advantageous over the band 4,5,7 or six band combinations, though a full quantitative comparison was not possible. Post classification smoothing removed "noise", with very little impact on overall class statistics.

Training for the Landsat MSS imagery required larger minimum areas, with additional problems of either rectangular pixels pre geocorrection, or a blockier image for post geocorrection training. Training and classification was done pre geocorrection. After initial problems with the water class a satisfactory classification was achieved using all four image bands.

Unsupervised classification of the Landsat TM imagery showed little difference in using 10 or 16 classes. Problems were encountered with small areas of water, urban and cloud, which remained unclassified.

Many permutations of possible options existed during these automatic classifications. The options employed were used due to knowledge gained from literature and past experience. Some of these classification results are compared with results obtained from visual interpretation in Section 8.3. An accuracy assessment is also presented in Section 8.4.

CHAPTER SEVEN: **IMAGE INTERPRETATION AND DATA EXTRACTION**

7.1 Introduction

This chapter describes the methods which were used in visual interpretation and data extraction of the morphometric and landcover details for the study area. Interpretation was carried out using the following data types:

i) 1:50000 scale panchromatic aerial photography;

ii) colour transparencies from image enhancement of the Landsat MSS and Landsat TM (as described in Chapter 5);

iii) on screen interpretation of enhanced Landsat TM imagery,

iv) 1:50000 and 1:250000 scale Ordnance Survey maps of the area.

The chapter commences with an examination of the extraction techniques for aerial photography. This involves using stereoscopic photo-interpretation, mosaicing of the output data, scaling and the subsequent digitisation and quantification of results. It then goes on to discuss interpretation of the hardcopy output from digital data; in this case the colour transparencies produced from enhanced Landsat MSS and TM data. The projection of these transparencies onto transparent overlays is outlined, followed by scaling and the final digitisation and quantification of results.

A method of "on screen" interpretation using direct interaction with the image processing system is then presented. This involves displaying the image for interpretation on the monitor of the image processing system, with delineation of the linear features and areal boundaries on a graphics overlay plane by manual interaction with a trackball. Only the Landsat TM imagery was examined using this technique for purposes of comparison with results obtained using other TM interpretation methods. The final part of the chapter outlines the data extraction methodology employed for extracting the 1:50000 and 1:250000 Ordnance Survey map data. Interpretation of areas outside the main study area was also included in some instances to delineate details from catchments extending beyond the main research area, for catchment analysis.

The subjective elements of this work, as highlighted by Chidley and Drayton (1986) were recognised at the outset of this research. This, together with the overall impression of the area gained by the author during field work, led to a need for data interpretation by other interpreters. Three Civil Engineering students undertook data interpretation as part of their final year projects, two during 1986 and one in 1987. These students had some rudimentary training in photo-interpretation techniques but had no detailed knowledge of the study area.

The quantitative results obtained by implementing the methodologies described below are reported on and analysed in Chapter 8.

7.2 Aerial Photography

The panchromatic aerial photography of nominal scale 1:50000, acquired as described in Chapter 4, was examined using either a Carl Zeiss Jena Interpetoskop or a Wild ST4 stereoscope with an 8x magnification factor in the viewing lens. Each of the 16 photographs measuring 230 x 230 mm was viewed in sequence with its adjacent photograph so forming stereo pairs for the stereoscope. With the 60% overlap only alternate photos required acetate overlays, thus creating stereo triplets. Figure 7.1 illustrates the Interpretoskop arrangement.

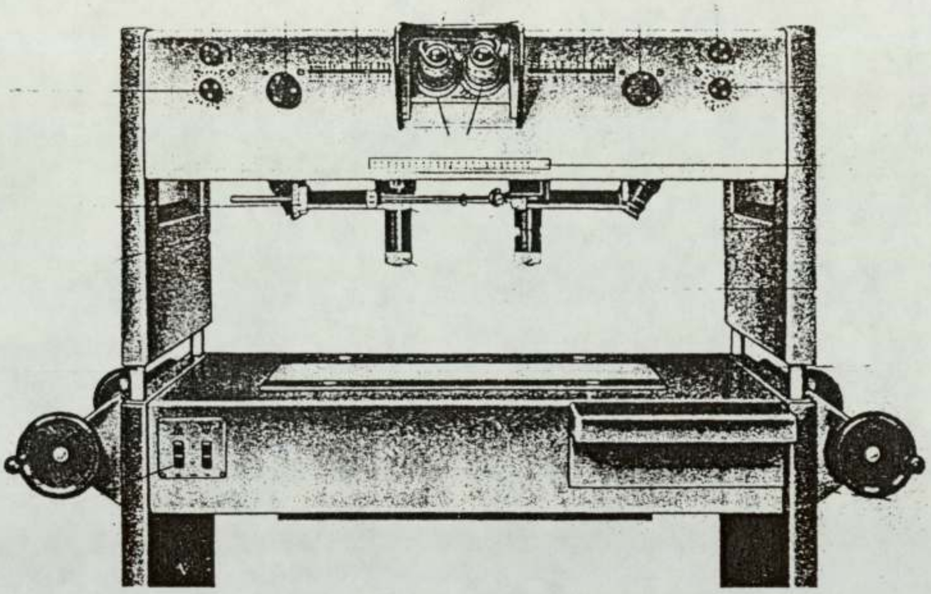

Figure 7.1 The interpretoskop arrangement (after CZJ, 1967).

Drainage patterns, catchment boundaries and landcover details were recorded on transparent acetate overlays using a fine drawing pen and annotating areas as required. Three separate coverages were made, one for drainage network features, a second delineating the catchment boundaries and the third for general land use classes. This was done to avoid confusion of linear and areal features, though coloured annotation could have overcome this. In such a case, one would need to use more than one pen and possible mistakes of colour change can occur. In addition, it is easier to look for one feature type at a time. The mosaicing procedure may also be complicated by delineating two feature types simultaneously, with possible confusions arising over the interpretation of linear features and areal boundaries.

The following paragraphs describe the interpretation of the morphometric details as discussed in Chapter 2. Relief parameters were not estimated due to the limitation of the data types considered. Landsat MSS and Landsat TM are only useful for interpreting general topography. Precise elevation information can be extracted from stereo aerial photography though a stereo/contour plotter is required for this procedure.

The methods and knowledge used in interpretion of the landcover classes is also detailed. Some general comments which can be made are that:

i) constant adjustment for stereo viewing was required due to relief displacement;

ii) the photographs were dark at the edges and corners when compared to larger scale photographs. This made interpretation more difficult;

iii) identification and discrimination was on a basis of tone rather than colour.

Drainage network details: Streams and small rivers generally appear as dark lines on the photographs with tone variation seen in the wider rivers, such as Afon Mawddach (Grid Ref. 2680 3186) according to sediment load and water depth. The vertical exaggeration afforded by the stereoscopic viewing of these images is a great aid in interpretation, as water courses lie in depressions of varying degrees. Drainage details were drawn in using the larger stream first and then the minor ones for each stereo triplet.

The vegetation types adjacent streams can aid or hinder its interpretation according to tonal contrast. In forest or woodland areas the stream itself may be obscured by tree canopies e.g. Afon Crawcwellt (2675 3295) . In such instances the network can be interpolated between the existing network sections according to topographic observations.

Once interpretation of the area was complete (and after interpretation of the catchment boundaries), the acetate overlays of drainage details were transferred to a single transparent overlay using a Bausch and Lomb stereo zoom transferscope, with the 1:50000 map as a geometric reference. Details from the resulting overlay were digitised using a Hewlett Packard digitiser coupled to an "Acorn" BBC microcomputer. A series of software programs was then applied to calculate stream lengths.

The digitiser used had a high spatial sensitivity, and recording of parameters can be specified in distance or time limitations of cursor movement e.g. 0.5 mm or 5 seconds, the former being of greater importance in this work. Hence a spatial sampling limit of every 0.5mm and a 20 second time limit were specified. Stream segments were marked in pencil on the map once digitised to ensure digitisation of each segment in the research area.

Unfortunately, the original overlays were destroyed in fire related damage at Aston University. From these overlays some quantitative information on drainage lengths and network ordering remains but not the spatial arrangement.

Interpretation was therefore repeated and the resulting acetate overlays were mosaiced together to produce a single complete coverage. Unfortunately, the author no longer had access to a zoom transferscope for scale correction, so mosaicing was carried out on a best-fit basis by visual examination using the slight overlap from acetate to acetate. The resulting drainage network is presented in Figure 7.2.

Catchment boundaries: Once the drainage network had been defined, acetate sheets were overlain on the network acetate sheets and a different ink colour used to delineate the catchment boundary. This method of delineation made catchment boundary delineation easier due to the highlighted drainage network. In this work the relief perspective with the 3x (approx.) vertical exaggeration was vital in precise positioning of the boundaries. Most boundaries were easily defined in this area with a 750m relief range. Problems occurred in exact positioning of the boundaries on wide craggy ridges and also on flat valley sides. Using the photographic coverage it was possible to delineate five catchment areas, as illustrated in Figure 7.3.

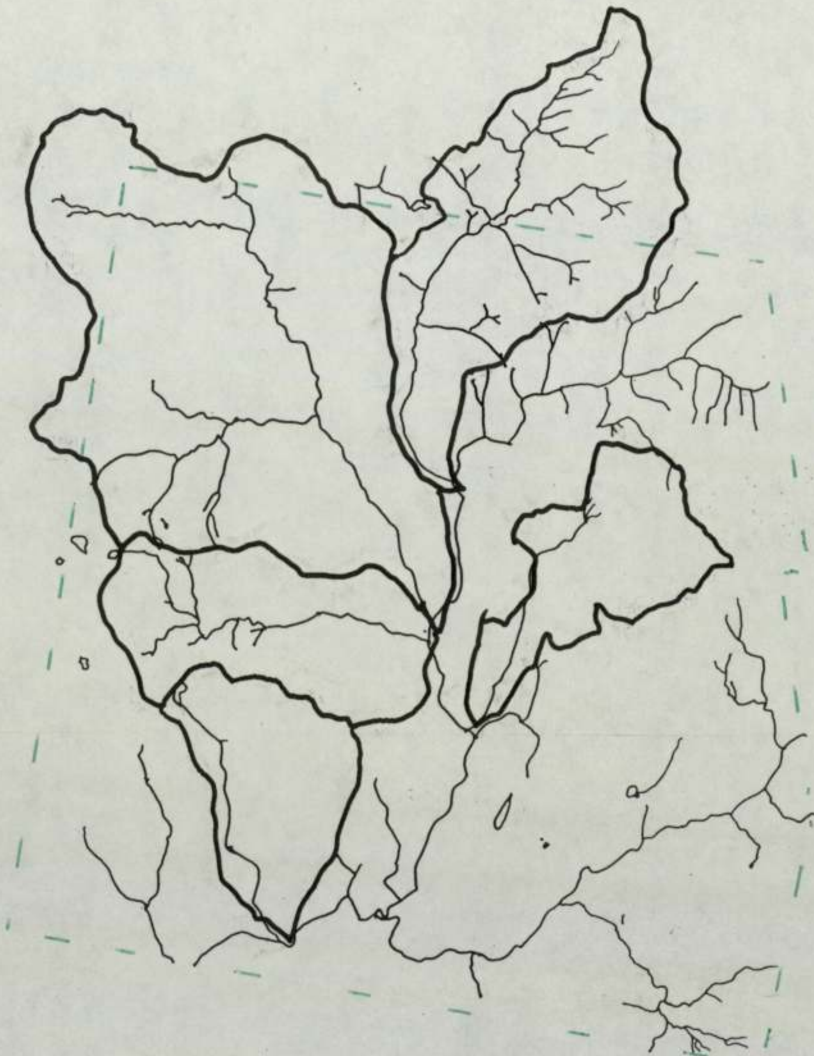

Figure 7.2 Drainage network intepreted from 1:50000 panchromatic aerial photography.- - = limit of research area covered by aerial photography. **Figure 7.3** (overlay) Delineated catchment boundaries. Note: scale reduced to 1:150000.

Landcover classes: As discussed in Section 3.5 the landcover classes for discrimination were forest/woodland, moorland, lowland agriculture, water and urban.

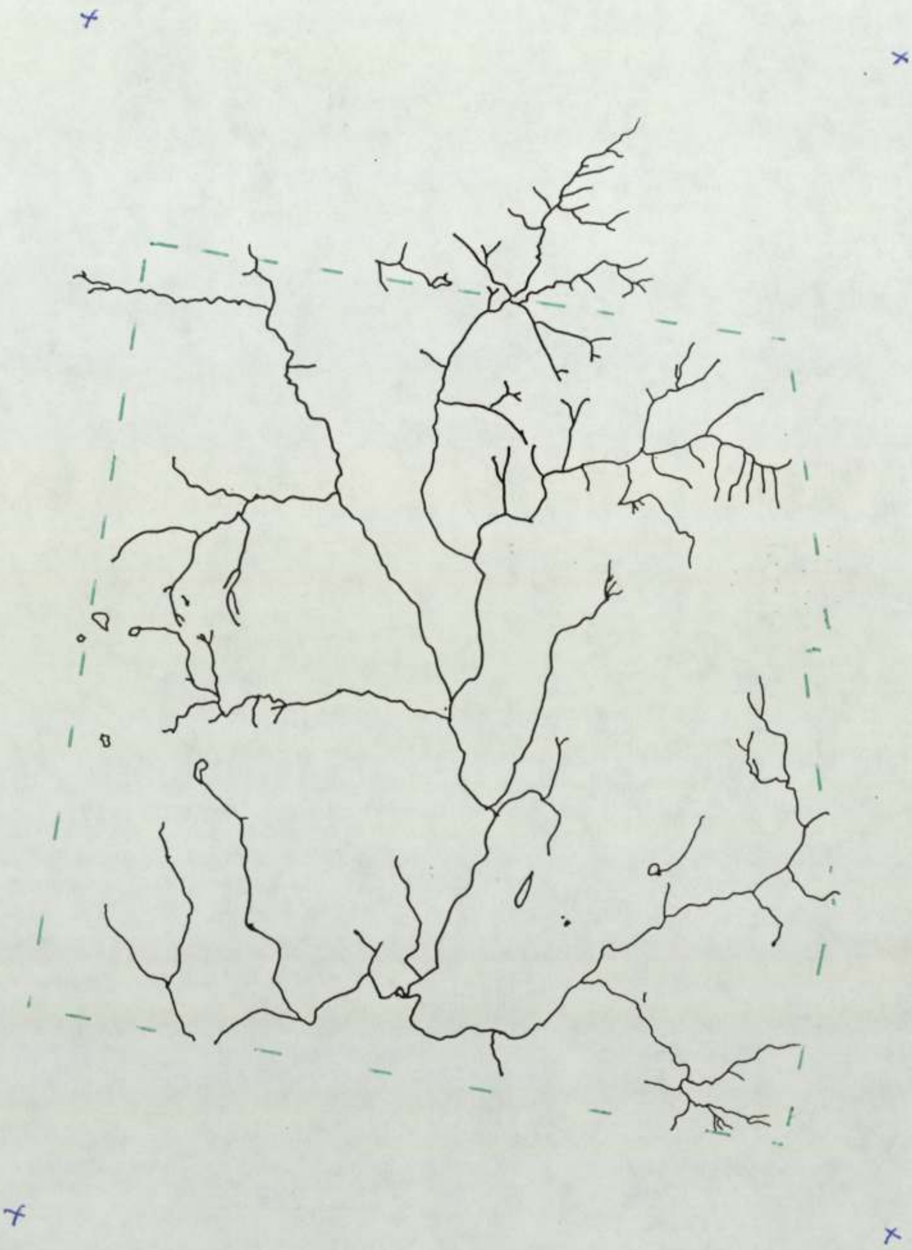

Figure 7.2 Drainage network intepreted from 1:50000 panchromatic aerial photography.- - = limit of research area covered by aerial photography. **Figure 7.3** (overlay) Delineated catchment boundaries. Note: scale reduced to 1:150000.

Landcover classes: As discussed in Section 3.5 the landcover classes for discrimination were forest/woodland, moorland, lowland agriculture, water and urban.

There were only small clouds in parts of the research area at the time of photography, so it was possible to interpolate obscured regions during the interpretation process. Much of this work was carried out by Martin Smith of the Remote Sensing Unit, Aston University, with checking by the author. The following sentences provide a description of the factors used in identifying the various landcover classes on the aerial photos.

Forest/Woodland: large forest blocks are easily discerned as dark blocks with their elevation above the surrounding landcover evident at the boundaries. Forest tracks are clearly seen, and individual trees can be seen when in isolation. Deciduous crowns are distinguishable, for example in the Wnion valley (2770 3200).

Moorland: the raised elevation of these areas is readily observable. Slopes are often steep and their is high frequency tonal variation producing a heterogenous pattern of landcover. Rocky areas can be distinguished from vegetated areas at this photographic scale.

Lowland Agriculture: these lowland areas of valley floor, lower valley slopes and flood plain are readily discriminated. Their relative elevation, with little or no slope and field patterns of a generally homogenous within-field nature combine to aid interpretation.

Water : The features of interest here were open water bodies i.e. lakes, tarns etc. of any size as far as these are discernable on the imagery. Open water bodies appear as very dark homogenous areas their interpretation being aided by the 3-D capability of the stereoscopic viewing due to water bodies always resting in "depressions" of one kind or another. The largest lake in the research area, Lyn Cynwch (2737 3206) exhibits very bright "sun glint" reflection. In one image of the relevant stereo pair the lakes have a white appearance, and in the second the second shows variable tone from light to dark for the lake and the third photo of the triplet exhibits the more usual dark appearance. The flight line was southwards in this instance, with the first photo showing "sun glint" effects the lakes being in the forward look part of the photo i.e. a south facing view angle. The third photo, with a northward view angle for the lake exhibited no "sun glint" effects. None of these effects were seen in the adjacent (sidelap) stereo triplet with a northward flightline. The magnification factor (8x) allows good examination of detail and shows the shape of lake boundaries very clearly.

Urban: there is only one urban area of significance within the study area, this being the town of Dolgellau (2730 3175). Street patterns and housing blocks are easily distinguished.

In this instance the resulting acetates were used to produce a 1:50000 scale output via the stereo zoom transferscope, in a similar manner to that for the original drainage network. Scale correction is even more important for areal features than for linear features due to the increased error possibilities. The resulting output is given in Figure 7.4.

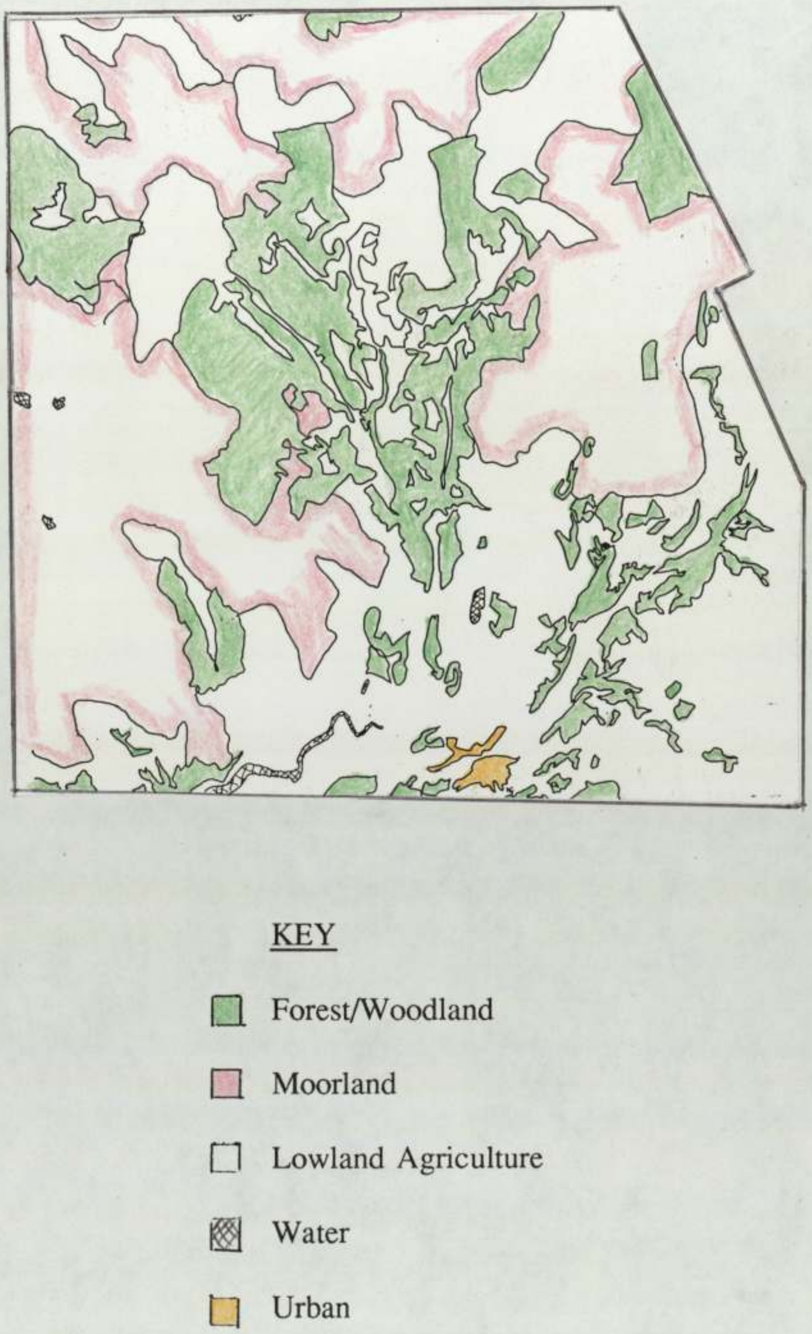

Figure 7.4 Landcover interpretation from the 1:50000 panchromatic aerial photographs. Scale = 1:150000.

7.3 Colour Transparencies of Landsat MSS and Landsat TM Imagery

The 35mm colour transparencies of the Landsat MSS and Landsat TM imagery produced by image enhancement techniques, as outlined in Chapter 5, were projected individually onto transparent overlays using a "Lamprey Box" configuration. This system, as illustrated in Figure 7.5, uses a 45° mirror to project slides from a normal slide projector onto a horizontal glass sheet. The glass sheet is overlain with a transparent overlay. The procedure should be carried out in a room with dimmed lighting to enable good distinction of the image features (total darkness creates a strain on the eyes). Care must be taken to keep the line of projection horizontal so as to minimise distortional errors in this optical system. The surface of the glass sheet should also be at a convenient working height for the interpreter.

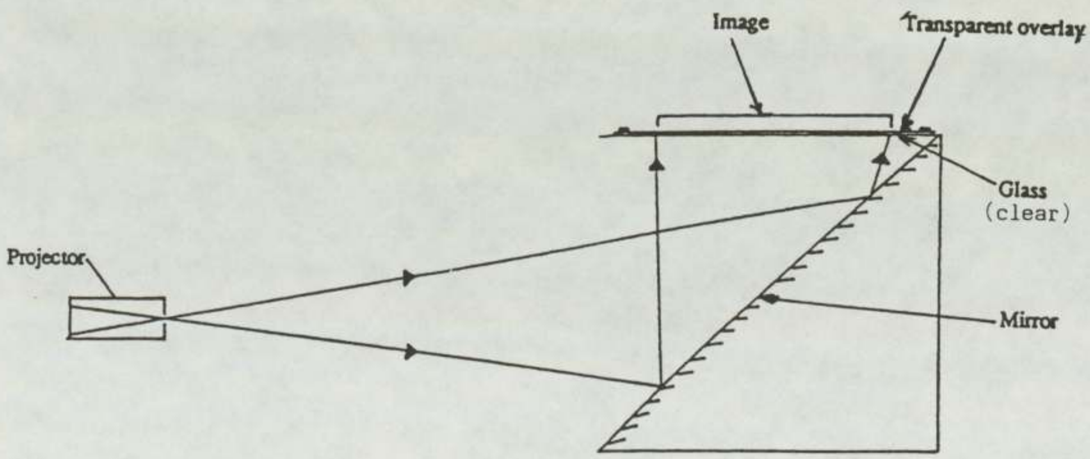

Figure 7.5 Lamprey box configuration.

7.3.1 Landsat MSS Imagery

For the Landsat MSS imagery two different transparencies were used for interpretation. These were the band 7,6,5 FCC with manual linear stretching and 3x3 laplacian filtering, and a band 7,5,4 FCC with manual linear stretching. These were used respectively for drainage network delineation and landcover interpretation. The reasons for their initial selection are outlined in Section 5.3.1.

Drainage details: These transparencies were projected at a scale of 1:44000 on to the transparent overlay via the Lamprey Box. The scale was the result of a 35x35 cm display of the MSS transparency. Drainage details were recorded using a drawing pen and the limits of the area defined as accurately as possible. The scale of the imagery after projection through the Lamprey box system was 1:44000 . The dark lines of pixels defining the drainage details were followed up the main observeable river channels until further delineation of network detail was not possible. Interpretation of network structure was minimal due to large breaks in the interpretation, as shown in Figure 7.6. The results were input to the digitiser for quantification of the drainage lengths.

With a lack of drainage detail it was not possible to delineate catchment boundaries in the area using the Landsat MSS imagery.

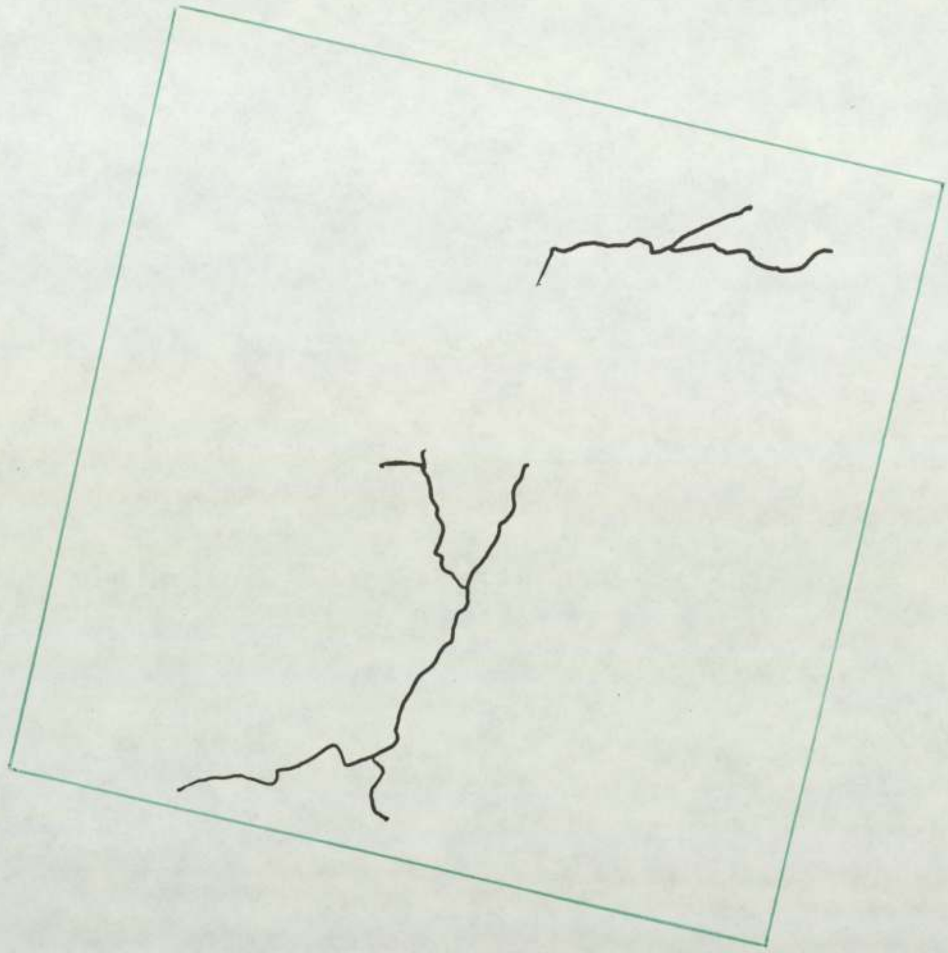

Figure 7.6 Drainage details interpreted from a Landsat MSS band 7,6,5 FCC with 3x3 Laplacian filtering. = extent of main research area. Scale = 1:150000.

Landcover classes: Landcover discrimination was carried out using a transparency of bands 7,5,4 (FCC) with Gaussian contrast stretching. The scale of the imagery after projection through the Lamprey Box system was again 1:44000. Each area was coded according to landcover type. Discrimination was based on interpretation using the following factors:

Moorland: Moorland areas appear on this imagery as a greyish-green or brown colour.

Lowland Agriculture: This class is readily distinguished as bright red coloured areas, with some variation in shade giving a heterogenous texture.

Water: Water areas are depicted by very low pixel intensities producing dark areas, almost black in appearance.

Urban: The only significant urban zone in this area is depicted as dark grey and is easily discriminated from the surrounding bright red areas of lowland agriculture.

Once all landcover classes had been delineated on the overlay, class areas were calculated using millimetre graph paper as an underlay.

7.3.2 Landsat TM Imagery

For the interpretation of the Landsat TM imagery the transparencies used were FCC's of bands 5,4,1, with high frequency (3x3) laplacian spatial filtering for the drainage interpretation. Four transparencies were used for the interpretation of the drainage network each with a 2x zoom applied in order to aid intepretation of the fine detail of the linear water bodies. The scale of the image displayed through the Lamprey Box setup was 1:21950.

Drainage details: The drainage details appear as dark blue/black linear features which in most instances are easily differentiated from roads, which appear as pink, redish or purple linear features. Any small gaps in the network, such as in forested areas where the forest/water contrast is small, were interpolated.

The resulting four overlays were then taken and used as input to the digitiser. The method of digitisation was similar to that described for the aerial photographic interpretation in Section 7.2.1. Figure 7.7 illustrates the drainage network delineated.

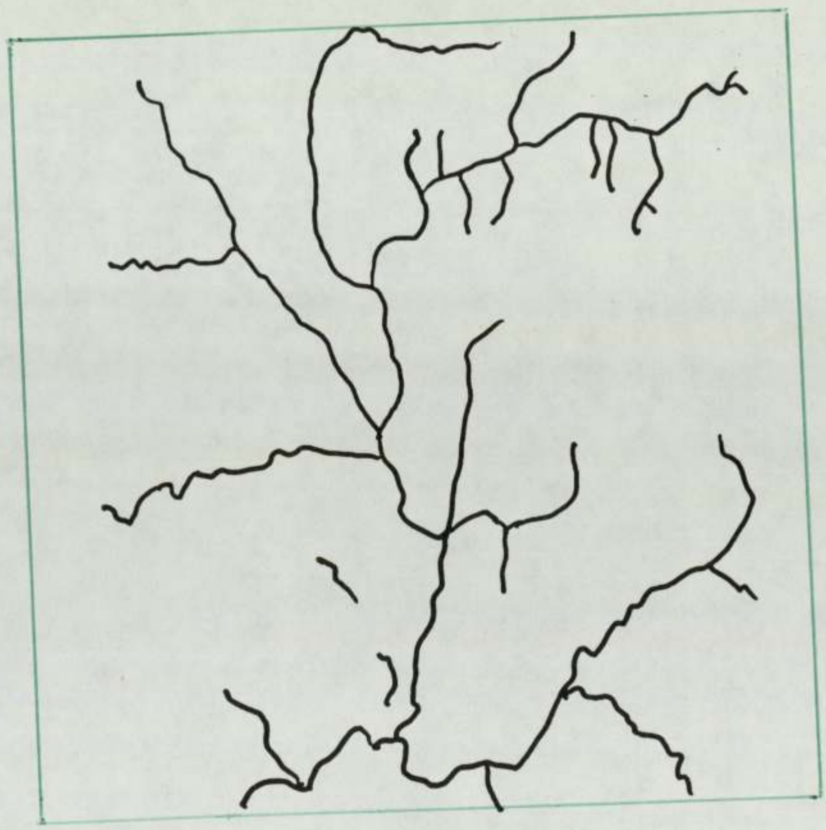

Figure 7.7 Drainage network delineated from Landsat TM transparency of a band 5,4,1 FCC with manual linear stretching and 3x3 Laplacian filtering. = extent of main research area. Scale = 1:150000.

Landcover classes: For the discrimination of landcover classes a single transparency of band 5,4,1 FCC was used, since areal feature identification rather than fine linear detail was the aim. In this instance a non-filtered image was interpreted. The landcover classes were discriminated using the following interpretation factors:

Forest/Woodland: Forest blocks are easily discriminated as dark green homogenous areas. Smaller wooded areas tend to be lighter green, including some known to be deciduous . Clear felled areas are revealed as deep pink areas.

Moorland: The moorland areas appear as mottled pink and tan/brown coloured areas, with some relief indication given by small intensity variations. The moorland/lowland agriculture boundary was frequently gradual causing some difficulty in precise positioning.

Lowland Agriculture: The heterogenous pattern of fields with a mixture of light green, yellow and pale orange colouration defines most of this class. The flood plain area of Afon Mawddach (2690, 3185) appears brownish with the major river meandering.

Water: Open water bodies such as lakes appear as very dark blue/black areas which are easily discriminated in all areas, apart from the forest blocks where discrimination is more difficult due to less spectral contrast e.g. the small lake at (2679, 3238).

Urban: The urban area appears as a dark central area with pink, purple and smaller dark areas surrounding. The major roads can also be seen emanating from the area.

Clouds: The cloudy areas appear as white areas on the imagery with corresponding dark shadow areas.

The landcover areas delineated in pencil on the overlays were numerically coded according to landcover class. As for the Landsat MSS, interpreted areas were calculated using millimetre graph paper as an underlay. An appreciation of the spatial distribution pattern can be gained from Figure 7.11 in the following section.

Interpretation of small lakes

Thirty four small lakes in the research area and adjacent area to the west were used to obtain an idea of the minimum lake size visible on TM imagery. The sizes and grid references of the lakes are given in Section 8.5. All lakes visible using the TM lamprey box method were marked on a transparent overlay for comparison with 1:50000 OS map details.

7.4 "On Screen" Image Interpretation

This method of image interpretation involves the interactive use of an image processing system. Firstly, the image for interpretation is displayed on the monitor of the image processing system. A trackball, can then be used to delineate the linear features or areal boundaries on the display screen. Delineated pixels appear as a coloured graphics overlay on the original display image as the interpretation progresses. The pixels delineated for any particular feature type can then be stored as a disk image file. Interactive use of the zoom facility of the image processing system enables the interpreter to look at the display image with the desired zoom level for delineation.

Drainage details: The image used was that for interpretation by the Lamprey box method, i.e. a band 5,4,1 FCC with linear contrast stretching and laplacian filtering. The author found that zooms of 4x and 8x of the 512x512 Landsat TM extract on a high resolution graphics monitor were particularly useful in delineating linear features, such as streams and rivers. Interpretation techniques were similar to those for the colour transparencies, though the zoom flexibility afforded by this interactive method proved a considerable aid in interpretation. Figure 7.8 shows part of the interpreted network. Details for the Gamlan catchment were interpreted from a September 1985 image due to cloud cover in the catchment on the July 1984 image.

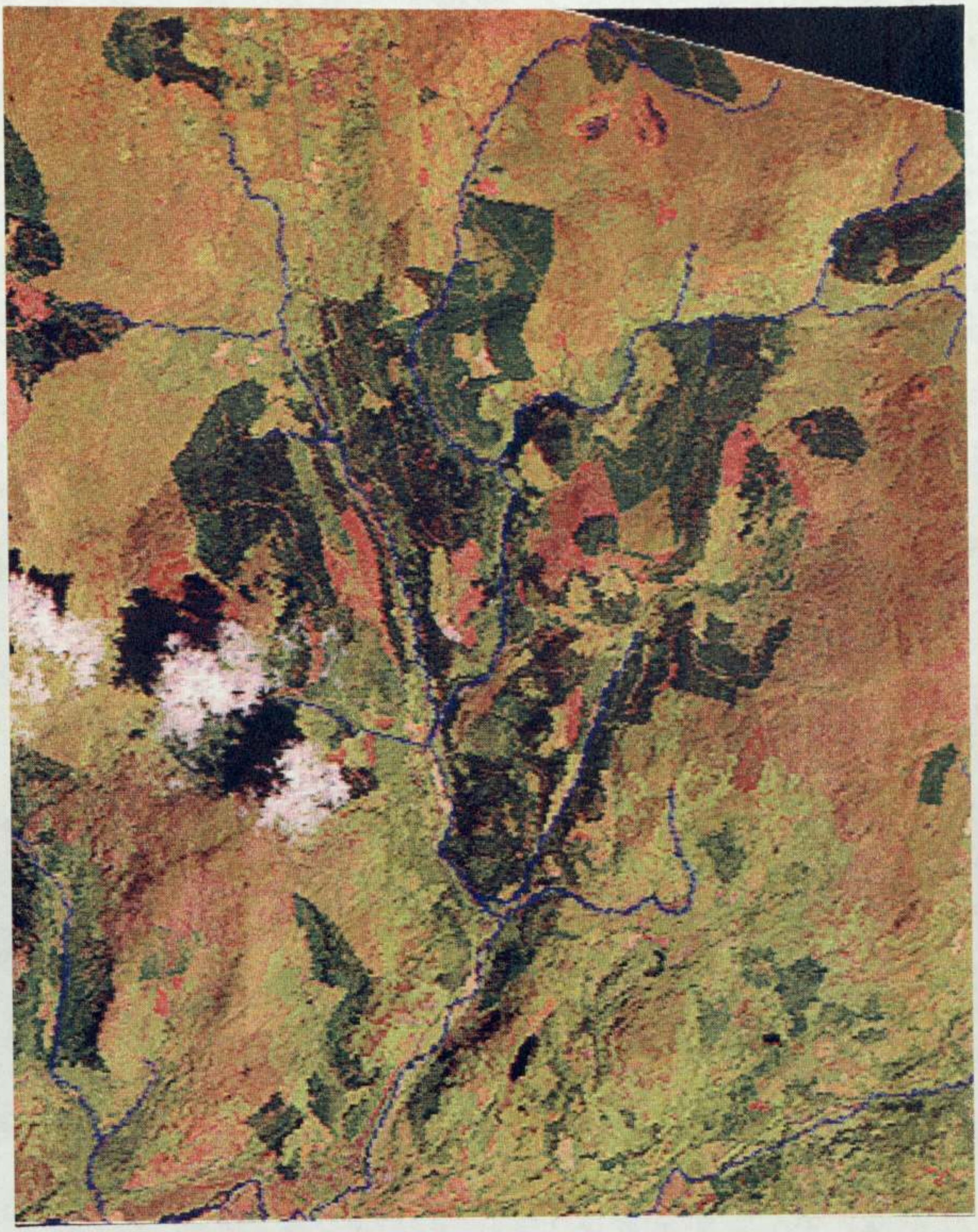

Figure 7.8 Landsat TM band 5,4,1 FCC with 3x3 Laplacian filtering, showing part of the research area. Delineated drainage network is shown as a blue graphics overlay.

Once delineated, a hardcopy of the drainage network was created using a D-Scan thermal transfer plotter. Channel lengths were then measured from this hardcopy using dividers and scaled appropriately to produce channel length details. Drainage details from outside the main 512x512 research area were interpreted for the parameterisation of catchment factors. Catchment boundaries were also interpreted using a different graphics overlay plane. The boundaries were interpreted using the delineated drainage network and the general relief indications in the imagery. The confidence of boundary positioning was greater in some areas than in others. Difficulties were encountered when catchment boundaries extended beyond the 512x512 window of the research area. This entailed careful matching of boundary delinations from the research area and surrounding areas. The spatial distribution pattern of the derived network and catchment boundaries are illustrated in Figure 7.9.

Recent observation of a November 1985 Landsat TM image of the area revealed the effects of a low, winter sun elevation angle. In this topographically variant area the catchment boundaries formed by mountain ridges were highlighted. However, shadow effects cause problems in the imagery if landcover interpretation is the aim of analysis.

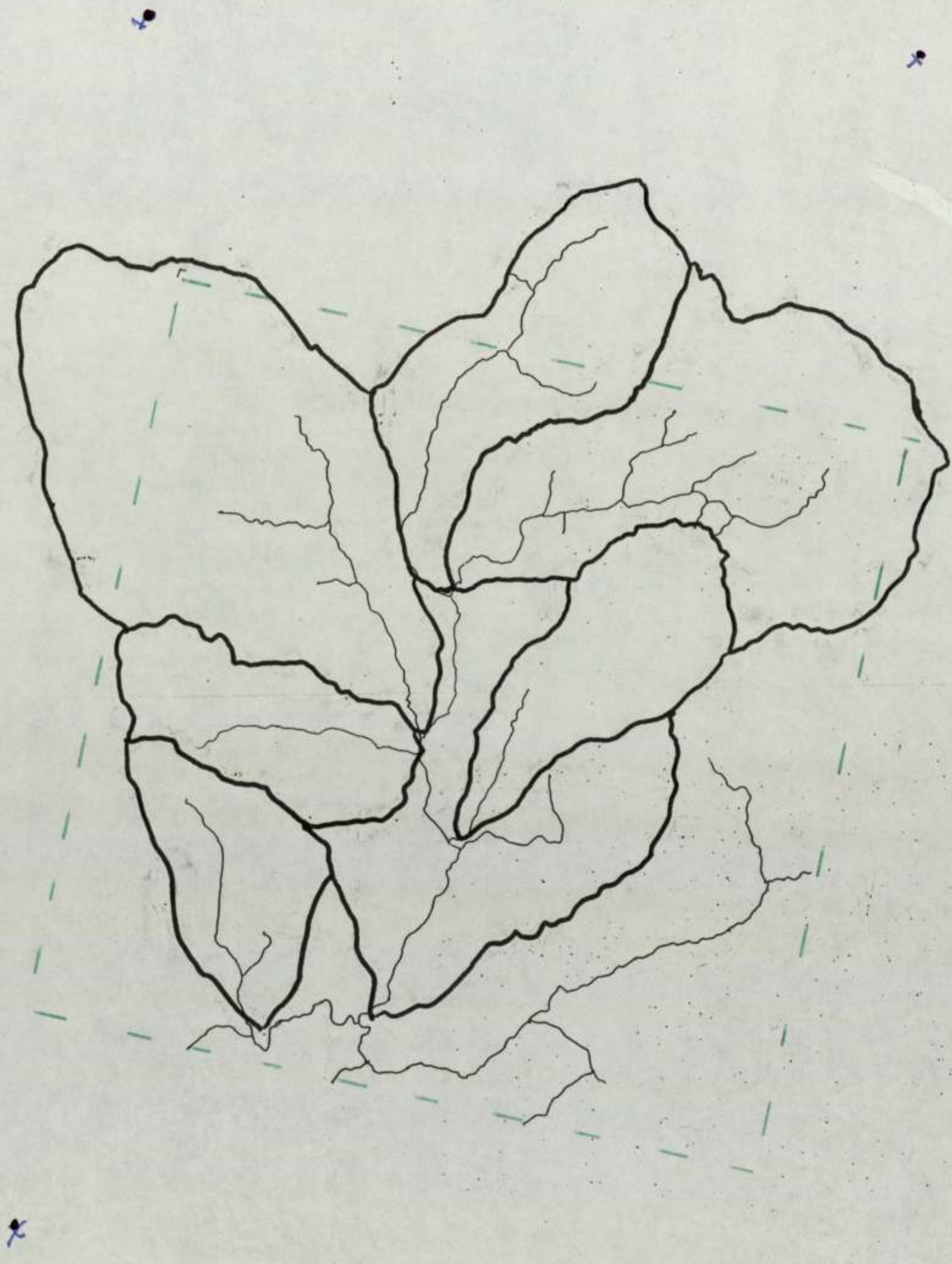

Figure 7.9 Drainage details interpreted from on screen interpretation of a Landsat TM bands 5,4,1 FCC with manual linear stretching and 3x3 Laplacian filtering. Overlay - Catchment boundaries interpreted from the same imagery. – –= extent of main research area.

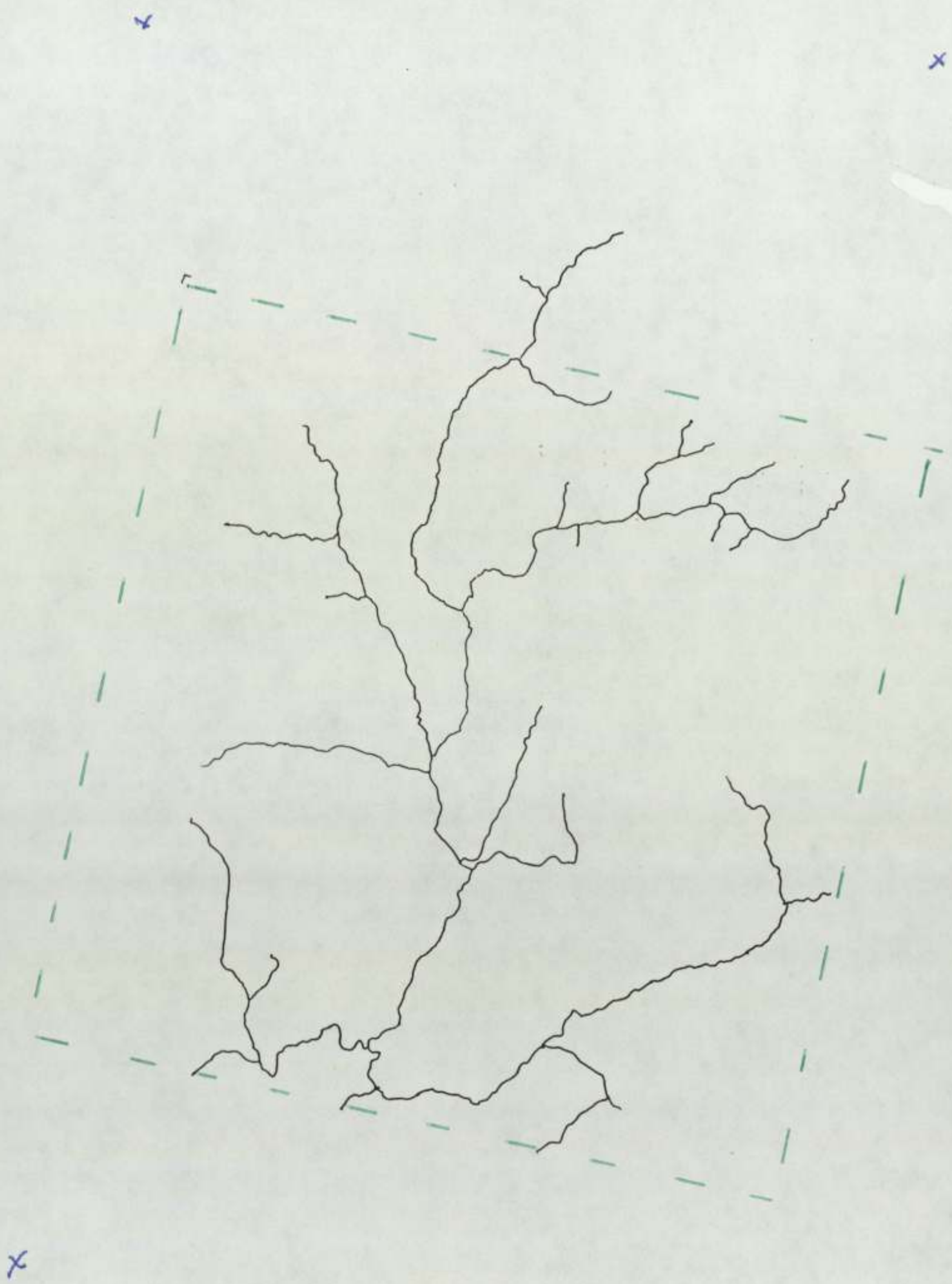

Figure 7.9 Drainage details interpreted from on screen interpretation of a Landsat TM bands 5,4,1 FCC with manual linear stretching and 3x3 Laplacian filtering. Overlay - Catchment boundaries interpreted from the same imagery. — — = extent of main research area.

Landcover classes: The image used for delineating landcover classes was, as for the colour transparency interpretation a band 5,4,1 FCC with manual linear contrast stretching, though without filtering. A zoom of 4x , displaying 128x128 pixels was used for delineating areal boundaries. For areal features, such as the landcover classes, it was necessary to delineate each class on a separate graphics overlay plane, except for the mooorland/lowland agriculture division. These two most extensive classes, moorland and lowland agriculture, which spatially encompassed all other classes were initially separated on an either/or basis. For the other classes, e.g. forest/woodland, the polygon boundaries for each individual area of the class were delineated. This procedure proved to be very time consuming, particularly for defining small areas with relatively complex boundaries. Once all areas of a particular class had been defined, the overlay plane was saved as a disk file.

For the moorland/lowland agriculture file stretching of the pixel values to produce different values for the two classes was possible using the graphics overlay plane to define regions of interest. The next step in the procedure was to take each of the other files of delineated boundaries and fill the areas using a connected component algorithmin these files were then filled using a connected component algorithm (Rosenfeld and Kak, 1976). This algorithm which was implemented on the I^2S by Hopper (pers. comm.) was used to identify and label all polygons in the files. Resulting polygons were given the same value for each class e.g. 6 for forest polygons, non-forest areas having a null value.

Finally the output files were added to produce a single file/image with pixel values representing one of the six landcover classes. Figure 7.10 illustrates the summation principle with moorland and lowland agriculture having their original pixel value. The other classes being 2 or 6 greater in value than their initial value. With only six classes, final class attribution was a fairly simple task. Once completed the area of each class could be calculated. A coloured image of the class map is given in Figure 7.11.

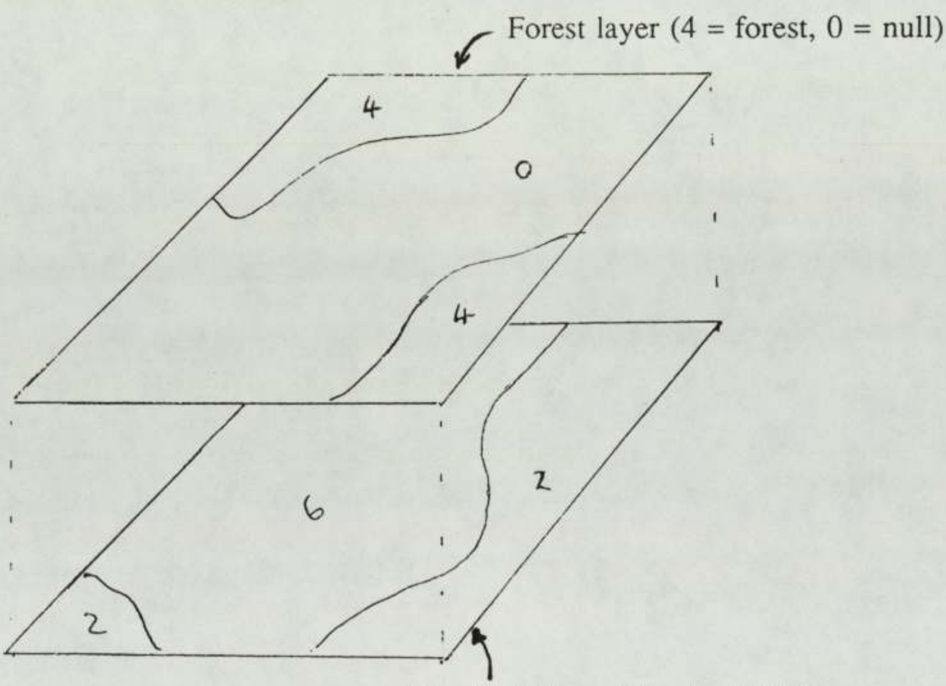

Figure 7.10 Illustration of the image addition principle, showing the moorland/lowland base layer and forestry.

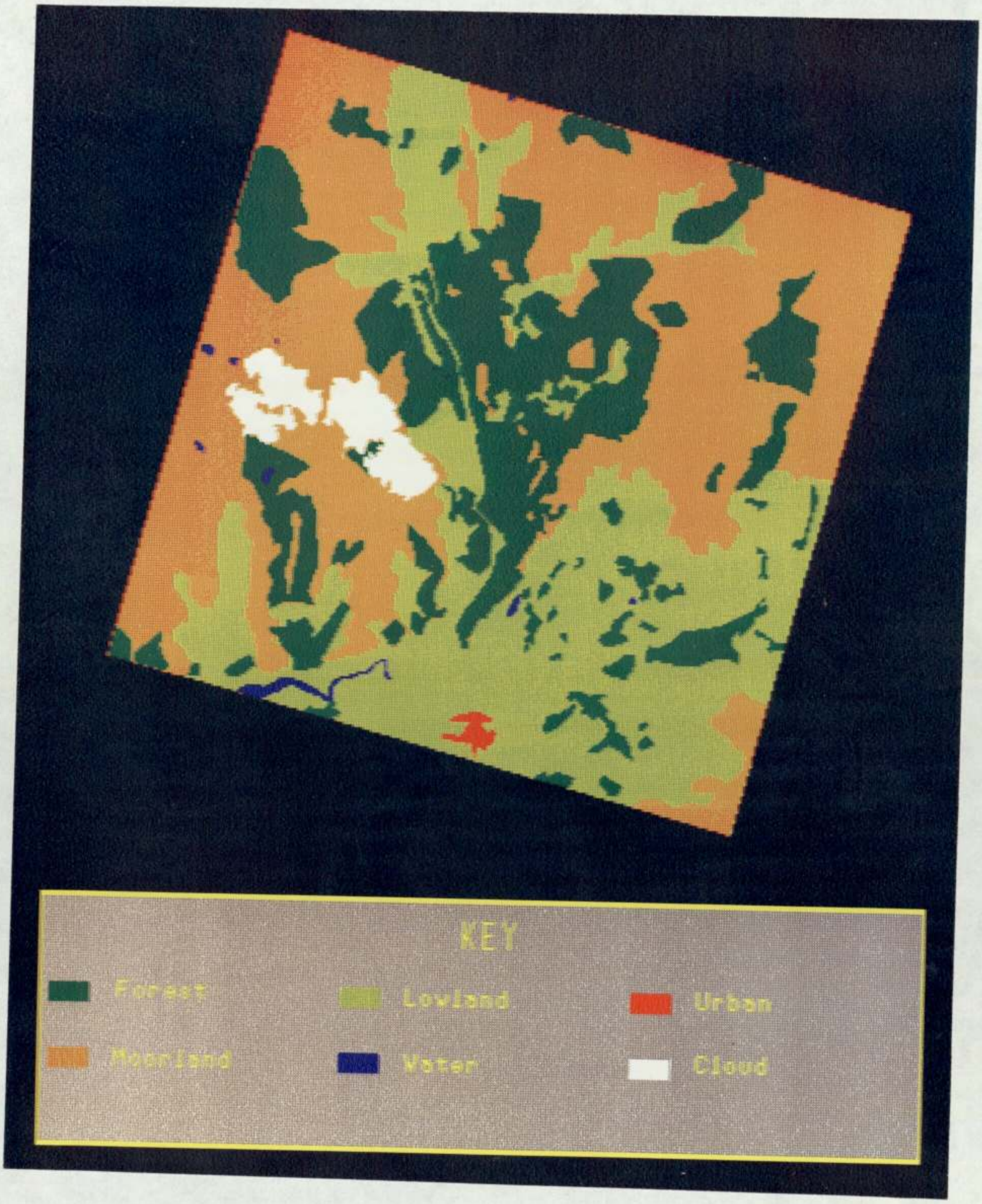

Figure 7.11 Colour class map from screen delineation of landcover classes using a Landsat TM band 5,4,1 FCC with manual linear contrast stretching.

__Identification of small lakes__

The on screen method was used with TM imagery in an attempt to identify the 34 small lakes in the area and adjacent region, for comparison with the lamprey box method. Again results are in Section 8.5.

7.5 1:50000 & 1:250000 Ordnance Survey Sheets

The boundary of the study area was delineated on a 1:50 000 scale Ordnance Survey Sheet for the area, sheet No. 124, last revised in 1982. Drainage details for use as "ground truth" were then extracted from the map. This included all mapped water bodies for the area. It should not be noted that drainage details printed on 1:50000 scale Ordnance Survey maps are extracted from the 1:10000 sheets and generalised at the cartographers discretion, as discussed in Section 2.2. However, the only watercourses found to be absent from the 1:50000 map during the course of field survey were a few streams of one metre or less in width. A similar procedure was used for the drainage network on the 1:250000 scale map (Ordnance Survey, 1986).

Details of the drainage features on the map were input directly from the map into a BBC micro using the digitiser. The setup used was similar to that used for aerial photography, as described in section 7.2.1. Landcover areas were not input though forest blocks, lakes and urban areas are marked on the map. The drainage details recorded from the 1:50000 map are shown in Figure 7.12. Catchment boundary details were interpreted by the author using contour information at 10 metre intervals on the map. This proved to be very easy along the obvious ridges and high points in ths area, but difficult to position precisely on some of the flatter valley sides. The drainage details from the 1:250000 scale map are portrayed in Figure 7.13.

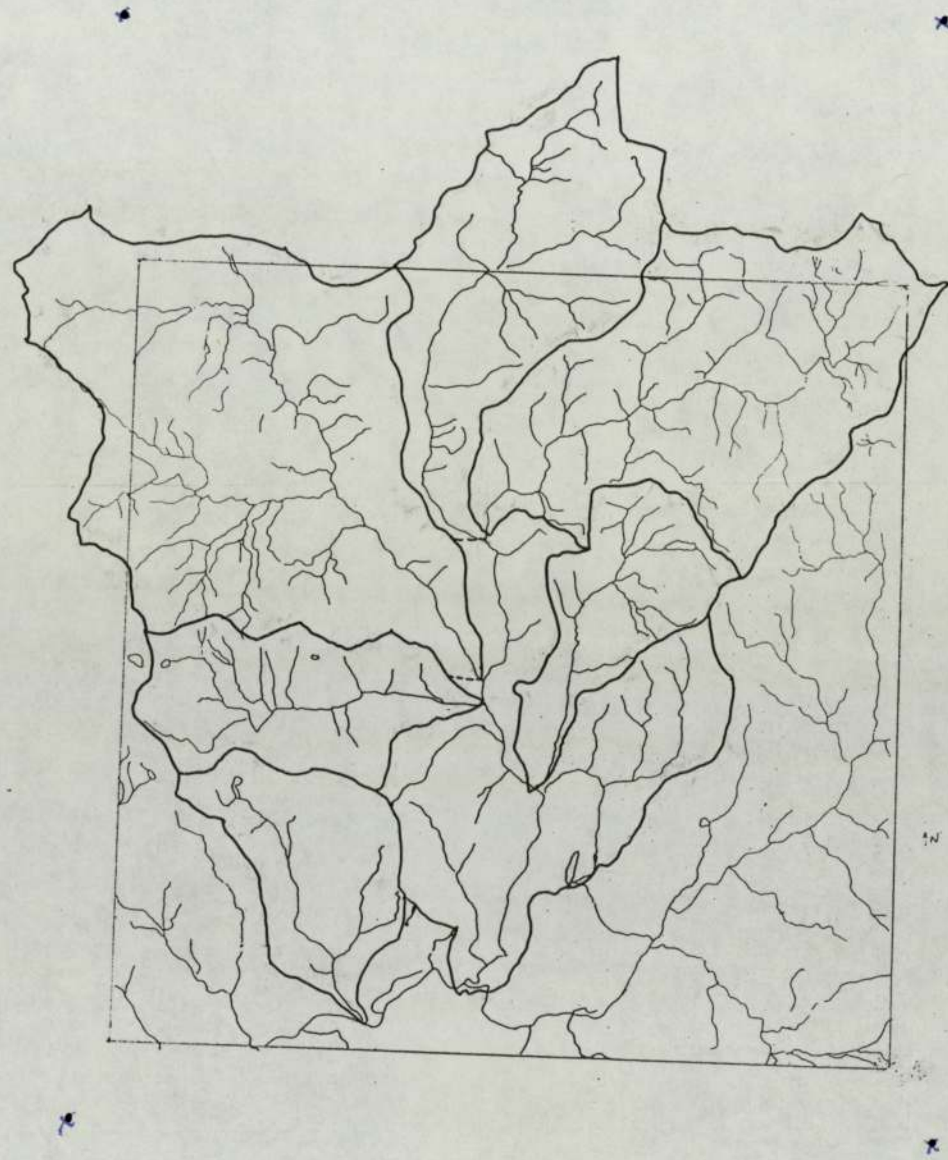

Figure 7.12 Drainage details from 1:50000 Ordnance Survey map. Overlay - Catchment boundary details. — = extent of main research area. Scale reduced to 1:150000 .

recorded from the 1:50000 map are shown in Figure 7.12. Catchment boundary details were interpreted by the author using contour information at 10 metre intervals on the map. This proved to be very easy along the obvious ridges and high points in ths area, but difficult to position precisely on some of the flatter valley sides. The drainage details from the 1:250000 scale map are portrayed in Figure 7.13.

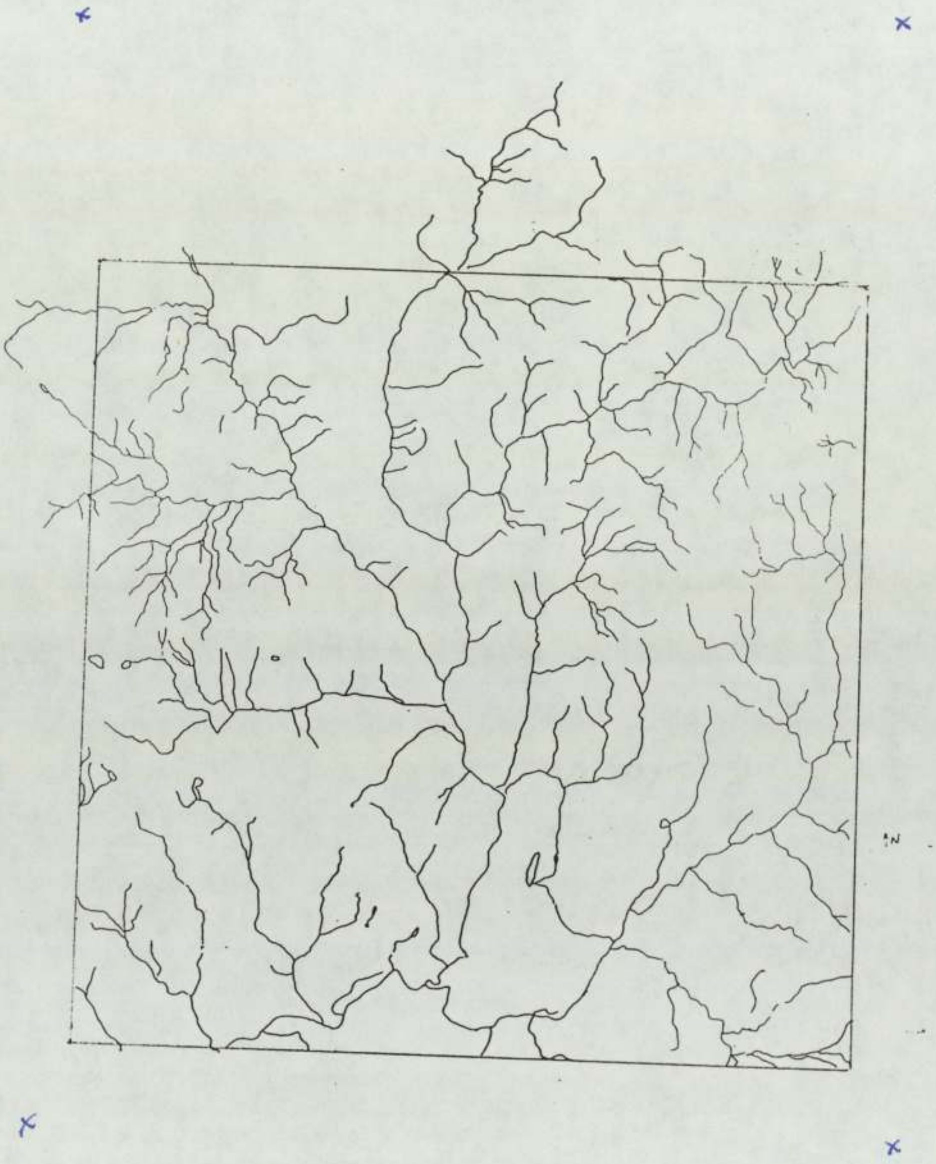

Figure 7.12 Drainage details from 1:50000 Ordnance Survey map. Overlay - Catchment boundary details. — = extent of main research area. Scale reduced to 1:150000 .

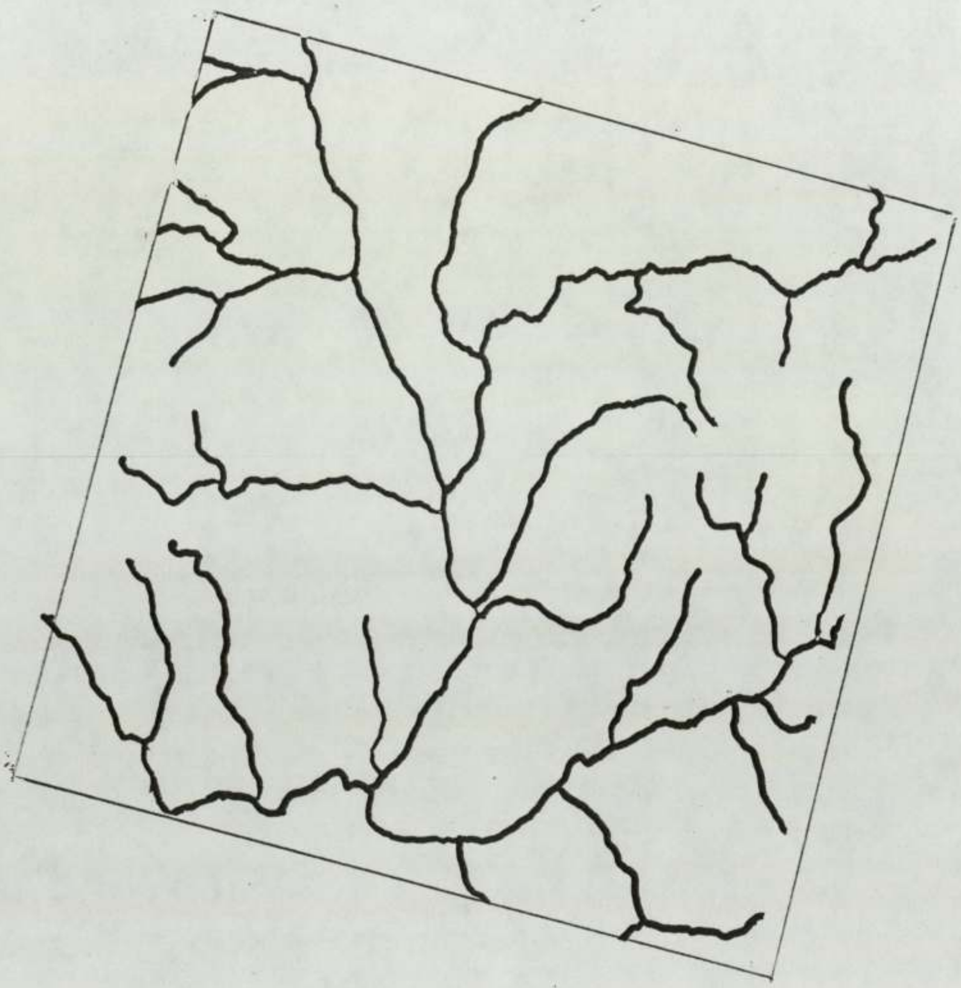

Figure 7.13 Drainage details from 1:250000 Ordnance Survey map. Scale increased to 1:150000 for comparison with other interpretations.

7.6 Summary

From each type of imagery the drainage networks, catchment boundaries and landcover classes were delineated. Drainage details and catchment boundaries were also delineated from the 1:50000 OS map and drainage details from the 1:250000 OS map. Small lakes in the region were also interpreted from Landsat TM imagery.

Using the 1:50000 scale aerial photography the 3-dimensional stereoscopic effect was very helpful. Drainage networks were easily delineated even at this relatively small photographic scale. Catchment boundaries were positioned using the vertical exaggeration afforded. The major inconvenience was discontinuity of imagery with several photos and the mosaicing required. Landcover discrimination was possible using for the classes selected, with stereoscopy aiding the moorland/lowland division. Colour or colour infrared photography would improve the ease of landcover discrimination.

Interpretation of Landsat MSS imagery using colour transparencies via the Lamprey Box method enabled the identification of only a few rivers in this area. This lack of drainage information, together with only general relief trends interpretable from the imagery, rendered catchment boundary delineation impractical for this area.

Drainage network interpretation from the Landsat TM imagery via the Lamprey Box provided a substantial network. Other linear features such as roads were discriminated from rivers on a colour basis. Catchment boundary delineation was possible using the drainage network delineated together with the general relief information visible in the imagery. Landcover interpretation was easier than on the Landsat MSS imagery due to an increased level of recognisability resulting from the increased spatial and spectral resolution.

The on screen method of interpretation used for the Landsat TM imagery proved successful for the delineation of drainage networks, though a hard copy output device was necessary. On screen delineation of landcover classes was possible. However this method of interpretation proved to be very time consuming.

The interpretation of small lakes from Landsat TM imagery was possible using either Lamprey Box or on screen methods. Quantitative results for this and the other parameters measured or derived are presented in Chapter 8.

CHAPTER EIGHT: QUANTITATIVE RESULTS AND ANALYSIS

8.1 Introduction

This chapter presents the quantitative results obtained by the author using the methods outlined in Chapters 6 and 7, and also results obtained by other interpreters for the same research area. The chapter is divided into two major sections, the first discussing drainage analysis and the derivation of morphometric parameters, which were defined in Chapter 2, and the second examining the general landcover results obtained.

The drainage analysis section commences with interpreted linear features such as streams and rivers, followed by network analysis. These results are from the main research area for comparison with results obtained by other interpreters. Sections 8.2.3 and 8.2.4 present results obtained by the author on a catchment by catchment basis, with the parameterisation of several catchment factors. Analysis was carried out by comparing results derived from the Landsat TM, Landsat MSS and aerial photography with details from the 1:50000 Ordnance Survey map.

Landcover results are discussed in Section 8.3, with a comparison of automatic classification results obtained using the methods outlined in Chapter 6, and those results obtained using the visual interpretation techniques described in Chapter 7. Part of the area was subjected to accuracy assessment, as described in Section 8.4. A sub-section is also included on the discrimination of small lakes using Landsat TM imagery.

8.2 Morphometric Details of the Hydrological Features

8.2.1 Drainage network details for the main research area

Having extracted the drainage details using visual interpretation via the Lamprey box or on screen methodologies outlined in Chapter 7, a quantitative comparison is possible. Table 8.1 gives details of total channel lengths interpreted by the author from all three types of imagery, using the different methodologies. These are presented together with details extracted from the 1:50000 and 1:250000 scale Ordnance Survey maps, for purposes of comparison.

The values of drainage density for each data type are also presented. Drainage density values were calculated by dividing total channel length by the image area, which was 235km^2, except for the aerial photographs where the area was 224.3km^2. Stream frequency comparisons are also presented, the stream frequency being the number of stream segments per unit area.

It is clear from the figures presented in Table 8.1 that the amount of drainage detail that can be interpreted from the different types of imagery varies considerably. Landsat MSS imagery with its relatively low spatial resolution of 79m was only useful for delineating 25km of channel in this area, which represents less than 10% of the drainage detail delineated on the 1:50000 OS map. Landsat TM imagery enabled interpretation of around a third of the Ordnance Survey detail and the aerial photography was slightly better. The 1:250000 scale map showed almost 50% of

Table 8.1 Drainage details extracted from the Imagery types.

Imagery Type	Landsat MSS	Landsat TM		Air Photos	1:250000 OS Map	1:50000 OS Map
Methodology	Lamprey Box	Lamprey Box	On Screen	Stereoscopy	Direct Digiti-sation	Direct Digiti-sation
Total Channel Length (km)	25.21	88.75	85.58	121.50	136.05	272.40
Channel Length as % of 1:50000 OS Map Value	9.3	32.6	31.4	44.6	49.9	100
Drainage Density (km/km^2)	0.11	0.38	0.43	0.54	0.58	1.53
Stream Frequency (streams $/km^2$)	0.04	0.18	0.20	0.42	0.24	0.89

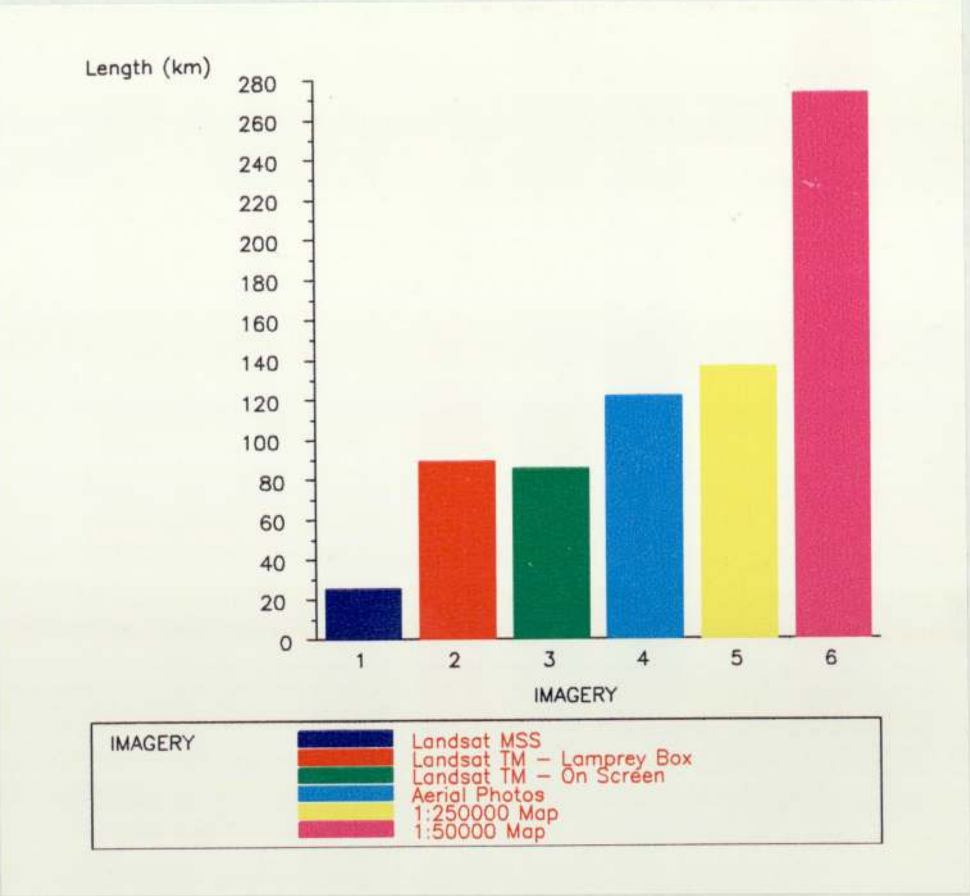

Figure 8.1 Comparison of drainage lengths extracted from imagery types.

drainage detail on the larger scale 1:50000 map. Figure 8.1 provides a graphical illustration of the differences. The catchment parameters of drainage density and stream frequency reflect these low interpretation values for satellite and aerial imagery when compared to the 1:50000 map details.

A comparison was carried out to ascertain the amount of interpreted drainage network details which did not agree with those on the 1:50000 OS map. Figures 8.2a and 8.2b illustrate the discrepancies from interpretation of aerial photography and the on screen Landsat TM imagery. There were no discrepancies on the Landsat MSS imagery.

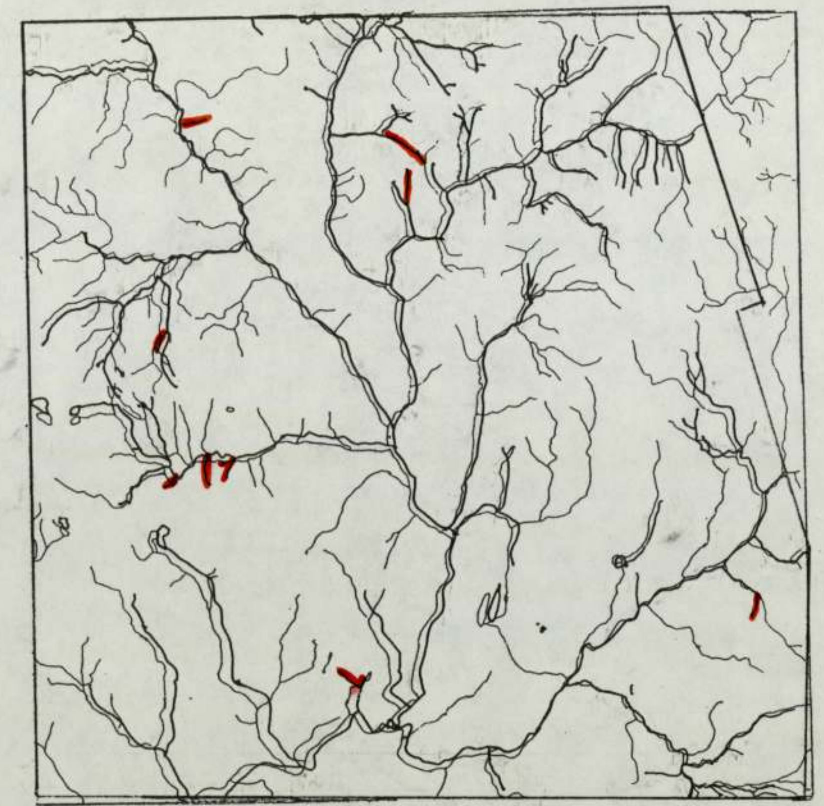

Figure 8.2a Overlay highlights in red those streams interpreted from the aerial photography which did not coincide with streams on the 1:50000 OS map.

From Figure 8.2a it can be seen that there are several places where first order streams were interpreted, from the aerial photography by the author, where none are denoted on the 1:50000 OS map. Which data is correct is not easy to decide, since as mentioned in Chapter 2, the 1:50000 OS drainage details are generalised from 1:10000 maps which for this area were probably interpreted from 1:10000 scale aerial photography. A total length of 9.36km was interpreted in this way, representing 7.7% of the total network interpreted. For the on screen Landsat TM interpretation, as

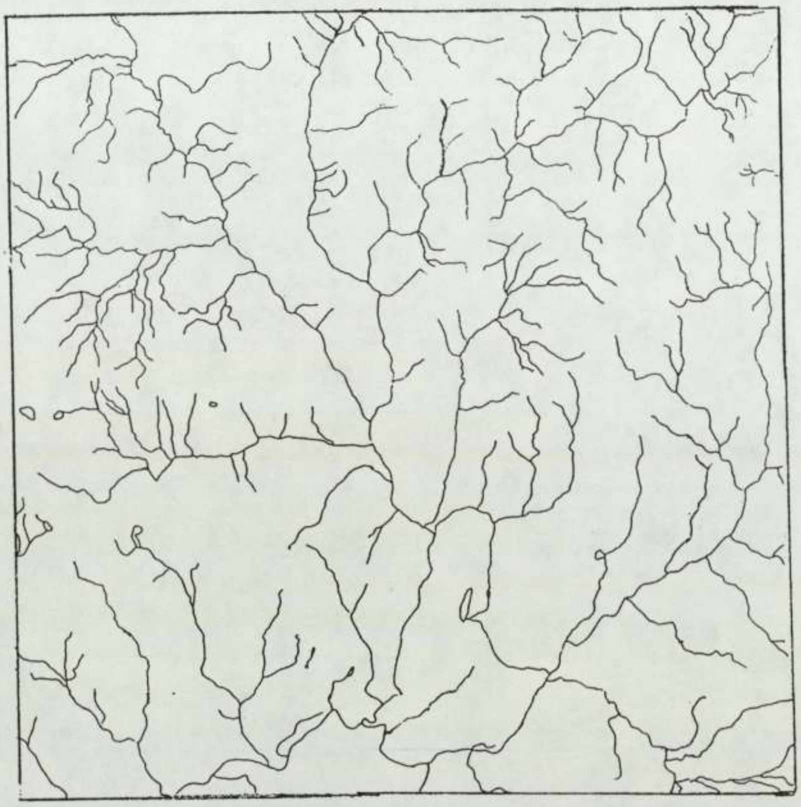

Figure 8.2a Overlay highlights in red those streams interpreted from the aerial photography which did not coincide with streams on the 1:50000 OS map.

From Figure 8.2a it can be seen that there are several places where first order streams were interpreted, from the aerial photography by the author, where none are denoted on the 1:50000 OS map. Which data is correct is not easy to decide, since as mentioned in Chapter 2, the 1:50000 OS drainage details are generalised from 1:10000 maps which for this area were probably interpreted from 1:10000 scale aerial photography. A total length of 9.36km was interpreted in this way, representing 7.7% of the total network interpreted. For the on screen Landsat TM interpretation, as

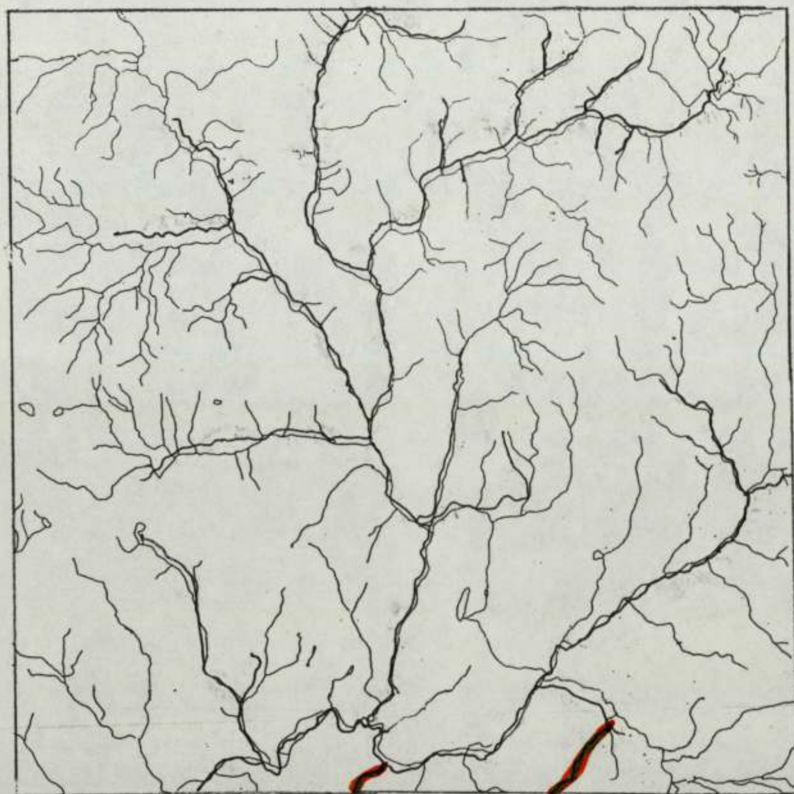

Figure 8.2b Overlay highlights in red those streams interpreted from on screen Landsat TM imagery which did not coincide with streams on the 1:50000 OS map.

shown in Figure 8.2b, 3.3km of network was delineated which does not correspond to drainage details depicted on the 1:50000 OS map. This represents 3.8% of the network delineated from the Landsat TM imagery. Comparison of drainage network interpreted from TM imagery via the Lamprey Box v 1:50000 map details showed a 1.2km discrepancy (1.4%). Field checks would help to resolve the discrepancies one way or another, though errors are minimal.

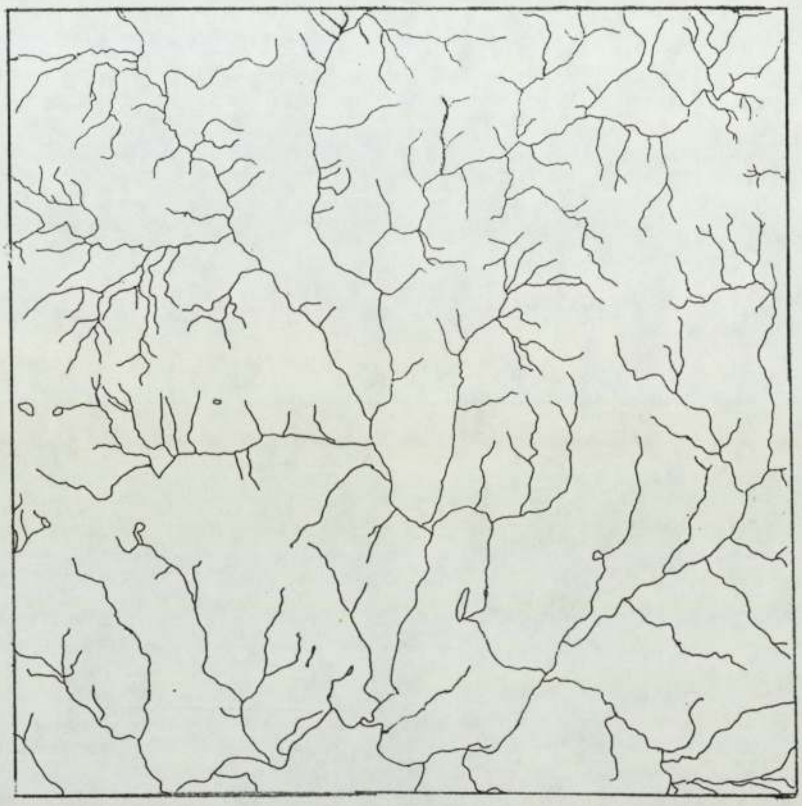

Figure 8.2b Overlay highlights in red those streams interpreted from on screen Landsat TM imagery which did not coincide with streams on the 1:50000 OS map.

shown in Figure 8.2b, 3.3km of network was delineated which does not correspond to drainage details depicted on the 1:50000 OS map. This represents 3.8% of the network delineated from the Landsat TM imagery. Comparison of drainage network interpreted from TM imagery via the Lamprey Box v 1:50000 map details showed a 1.2km discrepancy (1.4%). Field checks would help to resolve the discrepancies one way or another, though errors are minimal.

A comparison was carried out using the Landsat TM interpretations i.e. via the Lamprey Box and on screen methods. The results of these comparisons are presented in Table 8.2 and Figure 8.3.

Table 8.2 Stream interpretation discrepancies for Landsat TM imagery.

	Length (km)	Total length (km)	% of total length
Streams interpreted from TM imagery via Lamprey Box but not on screen method	22.95	88.75	26%
Streams interpreted from TM imagery by on screen method but not via Lamprey Box	17.85	85.58	21%

The figures in Table 8.2 show that there was a significant difference in the streams interpreted by the author using the Lamprey Box and on screen interpretation methods. Approximately one quarter of the streams interpreted were different in each case. Examination of Figure 8.3 reveals that the differences in interpretations were almost invariably of first order streams or parts of first order streams. The author interpreted the imagery via the two methods some years apart and feels the differences are due more to subjectivity than methodology.

It was thought profitable to relate stream widths with their presence or absence on the channel network delineated from the Landsat imagery. This was carried out using the stream width measurements collected during the field survey (see Section 3.7). Stream widths of streams delineated on the 1:50000 OS map were compared with drainage details delineated from the Landsat TM imagery (see Figure 8.4).

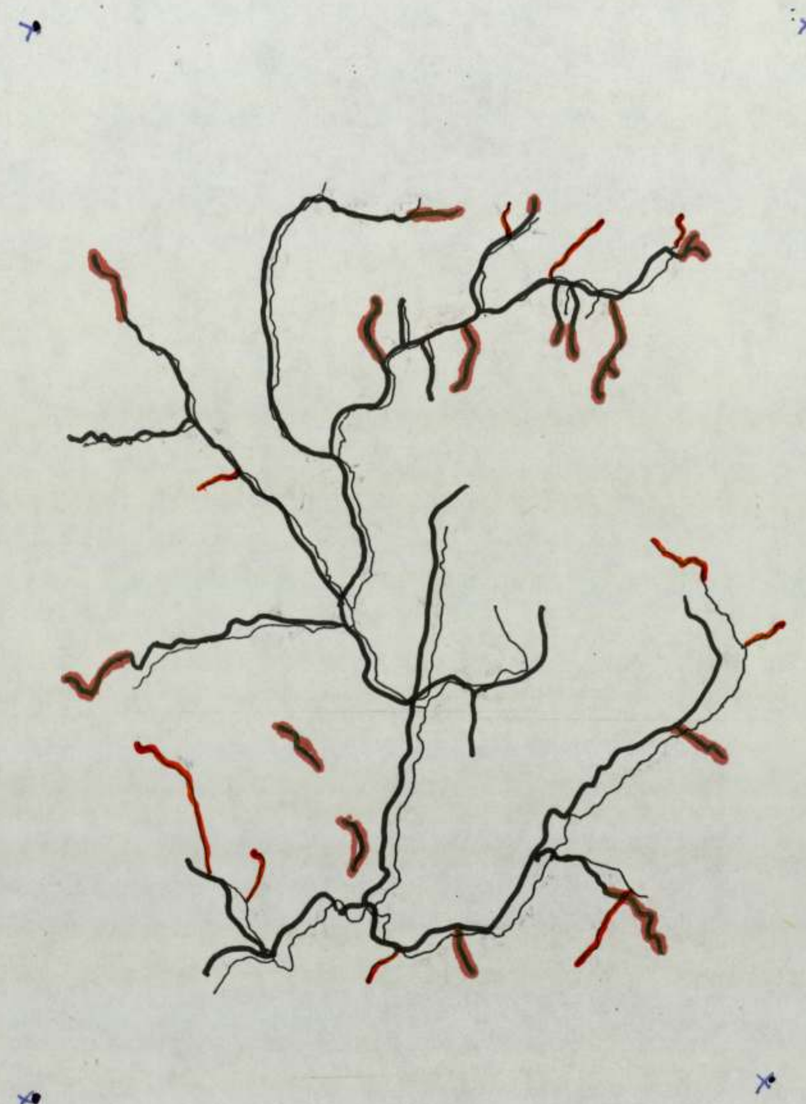

Figure 8.3 Discrepancies between Landsat TM drainage network interpretations via Lamprey Box and On Screen methods (overlay) - discrepancies are denoted in red.

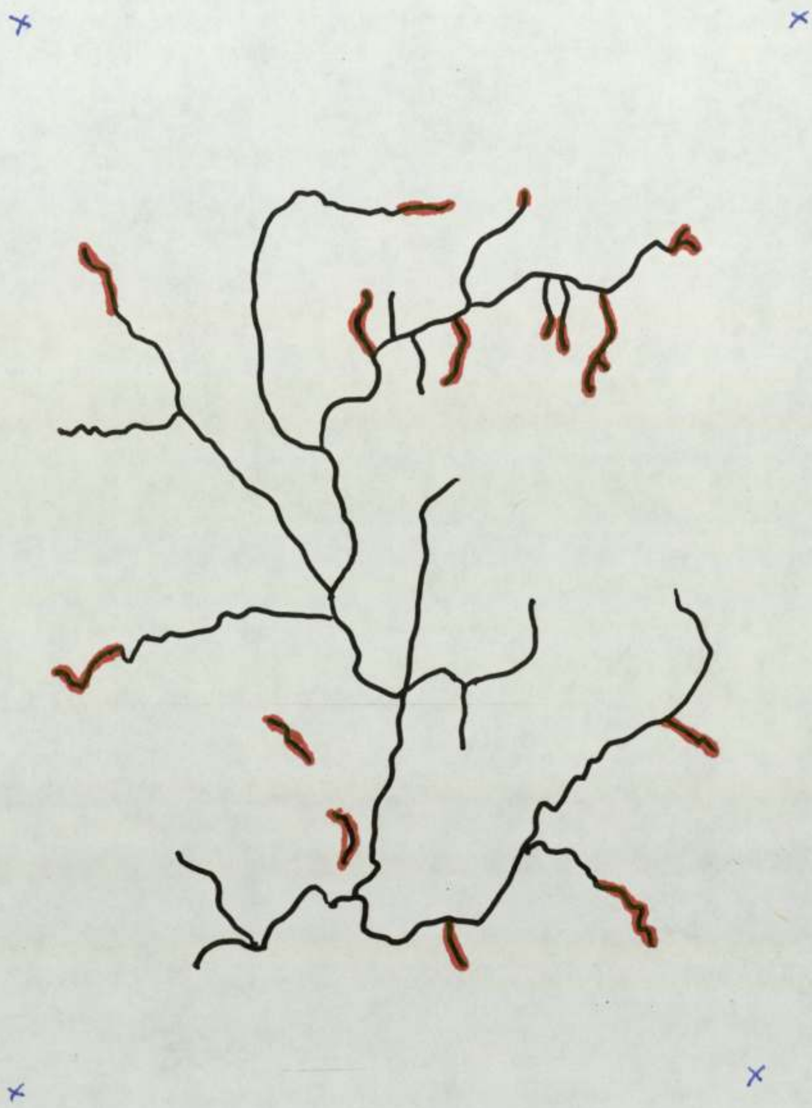

Figure 8.3 Discrepancies between Landsat TM drainage network interpretations via Lamprey Box and On Screen methods (overlay) - discrepancies are denoted in red.

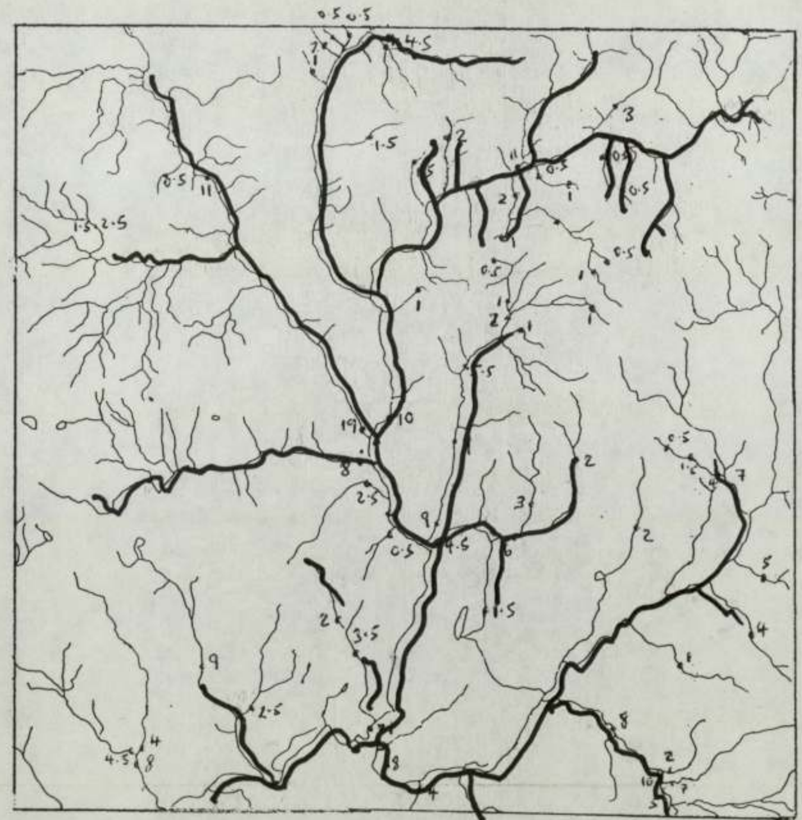

Figure 8.4 Stream width location map. Figures represent the stream width in metres at the point indicated. Grid references of the points can be found by referring to Figure 3.8 and Table 3.4. Overlay shows the Landsat TM delineated drainage details.

From this examination it was evident that a large part, probably over half, the drainage network outlined on the OS 1:50000 map in this area consisted of streams less than 3 metres in width.

Using the stream width data it was interesting to see how many of the streams could be identified on the Landsat TM imagery using the Lamprey Box method. The width

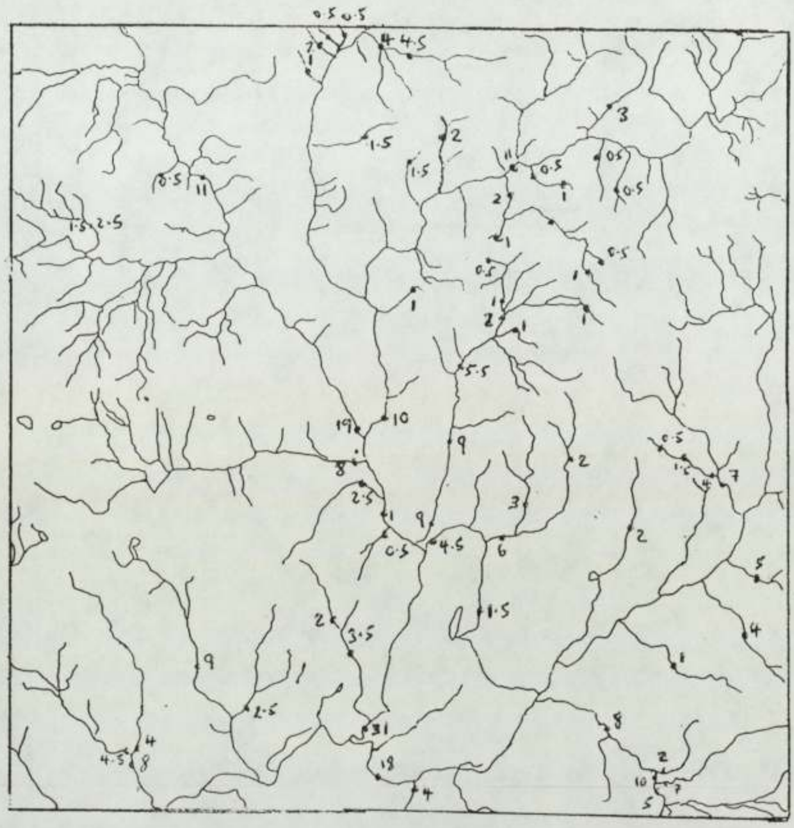

Figure 8.4 Stream width location map. Figures represent the stream width in metres at the point indicated. Grid references of the points can be found by referring to Figure 3.8 and Table 3.4. Overlay shows the Landsat TM delineated drainage details.

From this examination it was evident that a large part, probably over half, the drainage network outlined on the OS 1:50000 map in this area consisted of streams less than 3 metres in width.

Using the stream width data it was interesting to see how many of the streams could be identified on the Landsat TM imagery using the Lamprey Box method. The width intervals chosen were between 3 and 5 metres wide and over 5 metres wide. The stream widths can be found in Table 3.4 and results of the categorisation are presented in Table 8.3.

Table 8.3 Stream width details of streams identified from Landsat TM imagery.

	Number in field	No. identified from TM imagery	Correctly Identified
Streams over 5 metres wide	28	26	92%
Streams 3-5 metres wide	43	36	83%

The results in Table 8.2 indicate that Landsat TM is reliable in identifying significant drainage channels in the area. The main drainage channels were easily determined on the enhanced Landsat TM imagery (see figure 8.4). Many smaller streams, some only 0.5 metres wide could also be identified using the Landsat TM imagery. However, there was great inconsistency of results at these widths, identifiable streams frequently being associated with minor tributary valleys a few metres deep. Landsat MSS enhancements were only consistent in delineating stream widths of 10 metres or more (of which there are few in this area). Some streams as narrow as 3 or 4 metres appear sporadically on the MSS, see Figure 7.6.

Vicary (1987) also worked on the same imagery using similar methods to interpret drainage details. Table 8.4 presents a comparison of the results of France and Vicary, and Figure 8.5 shows the differences graphically.

Table 8.4 Comparison of drainage delineation results from France and Vicary.

Imagery Type	Landsat MSS	Landsat TM	Air Photos	1:50000 OS Map
France	25.21	88.75	121.5	272.4
Vicary	32.42	83.22	111.32	273.61
% Difference(France =100%)	+28.6	-6.2	-8.4	+0.1

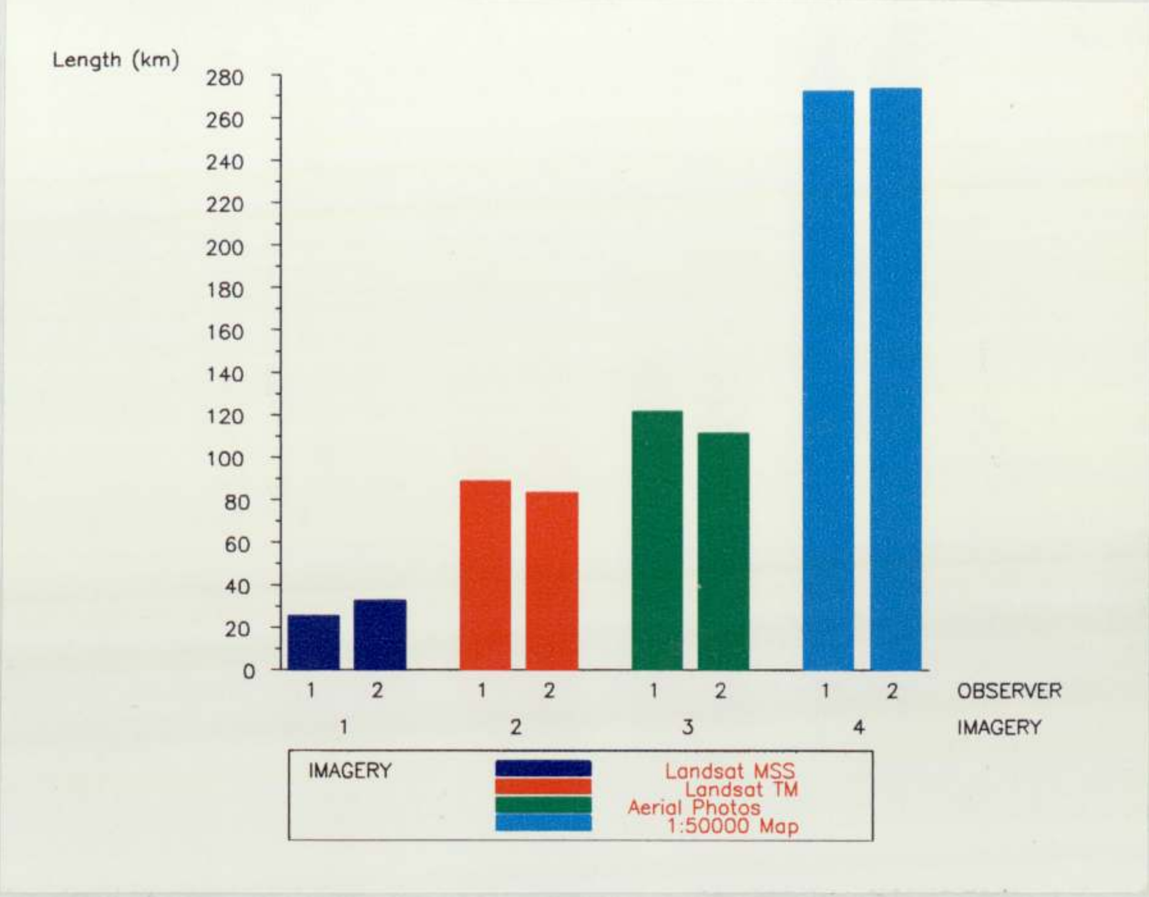

Observer 1 = France   Observer 2 = Vicary

Figure 8.5 Comparison of drainage delineation results from France and Vicary.

From Table 8.4 and Figure 8.5 it can clearly be seen that the results for interpretation of drainage features from the Landsat TM imagery and the aerial photography showed little variation between the interpreters, the Landsat MSS results showing a somewhat larger relative discrepancy.

Clark (1986) and Evans (1986) also examined the colour transparencies of the Landsat TM imagery. Again the Lamprey Box methodology was used. They used the imagery for delineation of drainage features and also for discrimination of landcover types. Details of drainage features were digitised from the 1:50000 OS sheet for comparison. Table 8.5 gives the results of Clark, Evans, Vicary and France, these are also presented graphically in Figure 8.6.

The surprising feature of the results presented in Table 8.5 is the discrepancy of channel lengths digitised from the 1:50000 OS map. Two pairings of results are seen, those of France and Vicary and those of Clark and Evans. The drainage details were denoted on the OS map by thin blue lines in the case of minor streams, followed by

Table 8.5 Interpretation of Drainage Networks from Landsat TM Colour Transparencies and 1:50000 OS Map.

	Data Type	
Interpreter	Landsat TM Channel Length (km)	1:50000 OS Map Channel Length (km)
France	89	272
Vicary	83	274
Clark	97	303
Evans	74	303

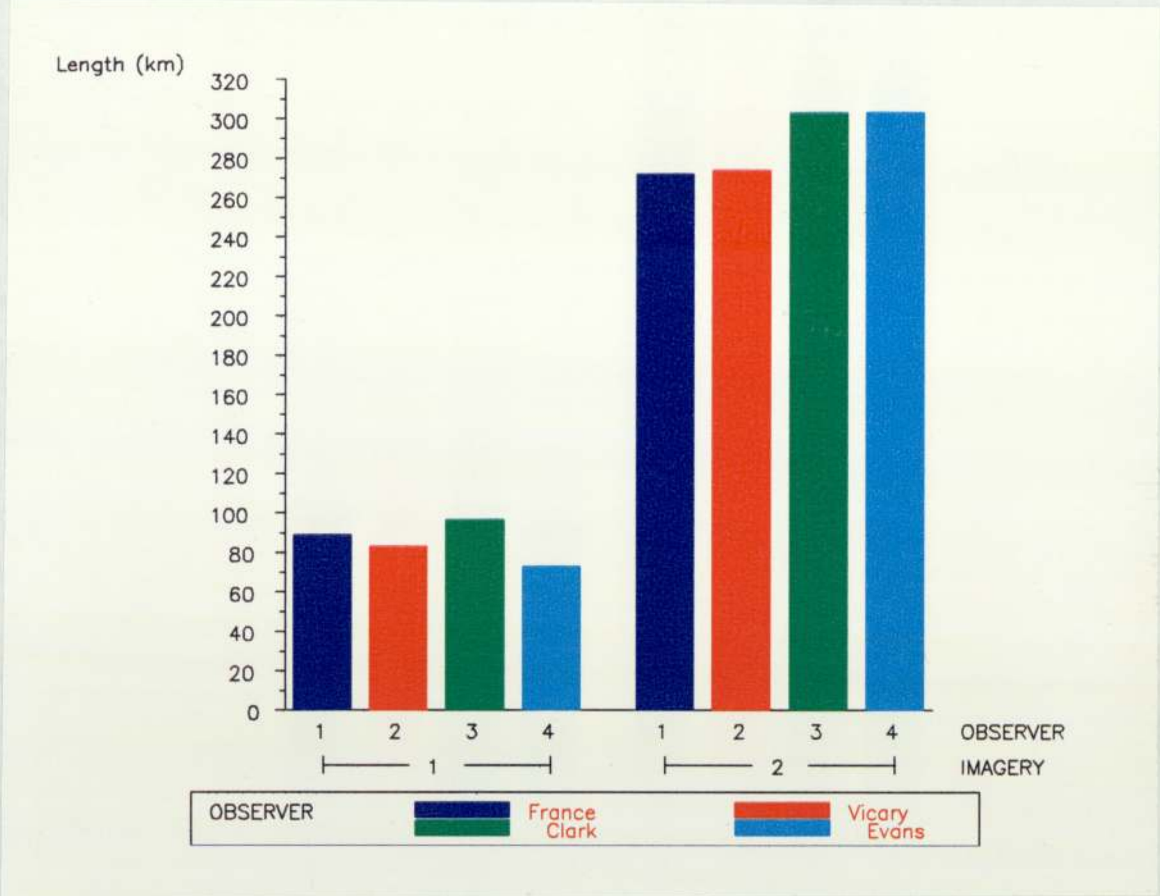

Imagery 1 = Landsat TM   Imagery 2 = 1:50000 OS map

Figure 8.6 Interpretation of drainage networks from Landsat TM colour transparencies and 1:50000 OS map.

slightly thicker blue lines for wider streams and then thin blue lines separating a blue coloured zone for the representation of rivers. The boundary of the research area was clearly marked on the map used by all the interpreters, and the digitising equipment and software applied was the same in each case and yet a difference of around 10% in results has occurred. Unfortunately no network maps were available for Vicary, Clark or Evans to enable direct comparisons, however the ordering figures presented in Table 8.12 indicate that the discrepancies arose in the measuring of minor streams i.e. first order. The results for channel delineation using the Landsat TM imagery are encouragingly all of the same order showing a maximum variation from the mean 85.5km) of around 15%.

It should be noted that the figures for stream length interpretation from Landsat TM imagery given for Clark and Evans in Table 8.4 are less than their initial interpretations. Clark originally interpreted 259km of stream lengths, of which only 97km were found to be streams after comparison with 1:50000 OS map details. Evans initially interpreted 96km of drainage features, of which 74km were consistent with the 1:50000 OS map details. Confusion was found to arise between rivers, roads and tree lines. Vicary comments on the difficulties of interpretation but does not quantify any errors found.

8.2.2 Drainage Network Ordering

The stream networks derived from each imagery type and the OS map data were used to produce stream ordering statistics. Each stream segment was ordered according to the system devised by Horton and modified by Strahler (as outlined in Section 2.2). It should be noted that this ordering was done on streams delineated for the research area for comparative purposes, and not on specific catchment areas as is required in practical application of the theory. Figures 8.7a,b & c show respectively the ordering for Landsat TM, aerial photography and 1:50000 map. Landsat MSS was not included for ordering since only a very limited network delineation was possible in this area, as illustrated in Figure 7.6. The quantitative ordering statistics are given in Table 8.6 and graphically illustrated in Figure 8.8.

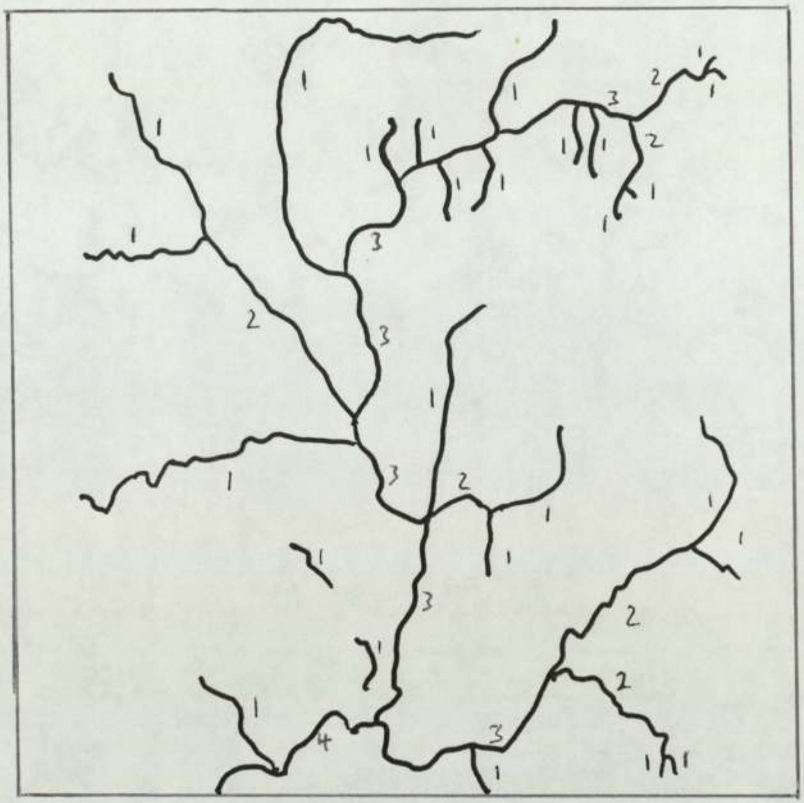

Figure 8.7a Stream ordering for Landsat TM derived network (via Lamprey Box).

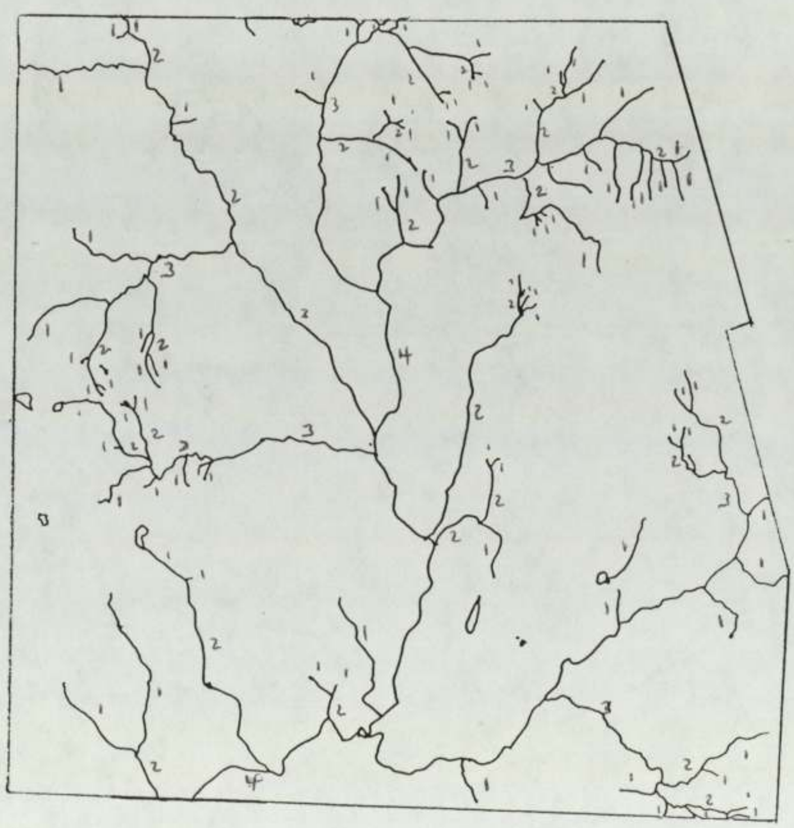

Figure 8.7b Stream ordering for aerial photographic derived network.

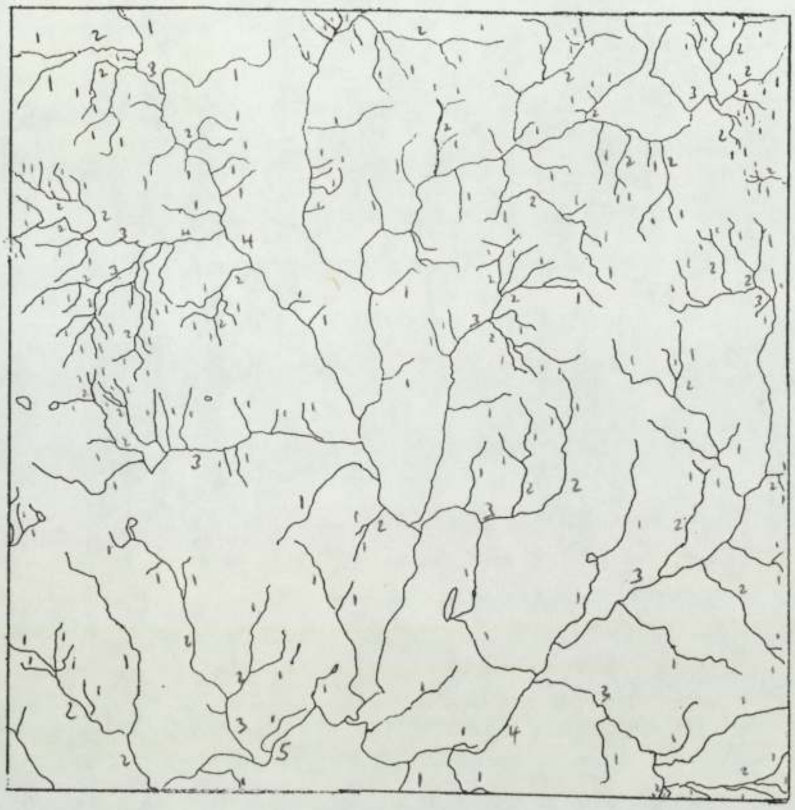

Figure 8.7c Stream ordering for 1:50000 map derived network.

Table 8.6 Streams orders interpreted from Landsat TM, aerial photos and 1:50000 map.

	Stream Order				
Data Type	1	2	3	4	5
Landsat TM	33	6	2	1	-
Aerial Photos	72	16	5	1	-
1:50000 OS Map	156	36	15	3	1

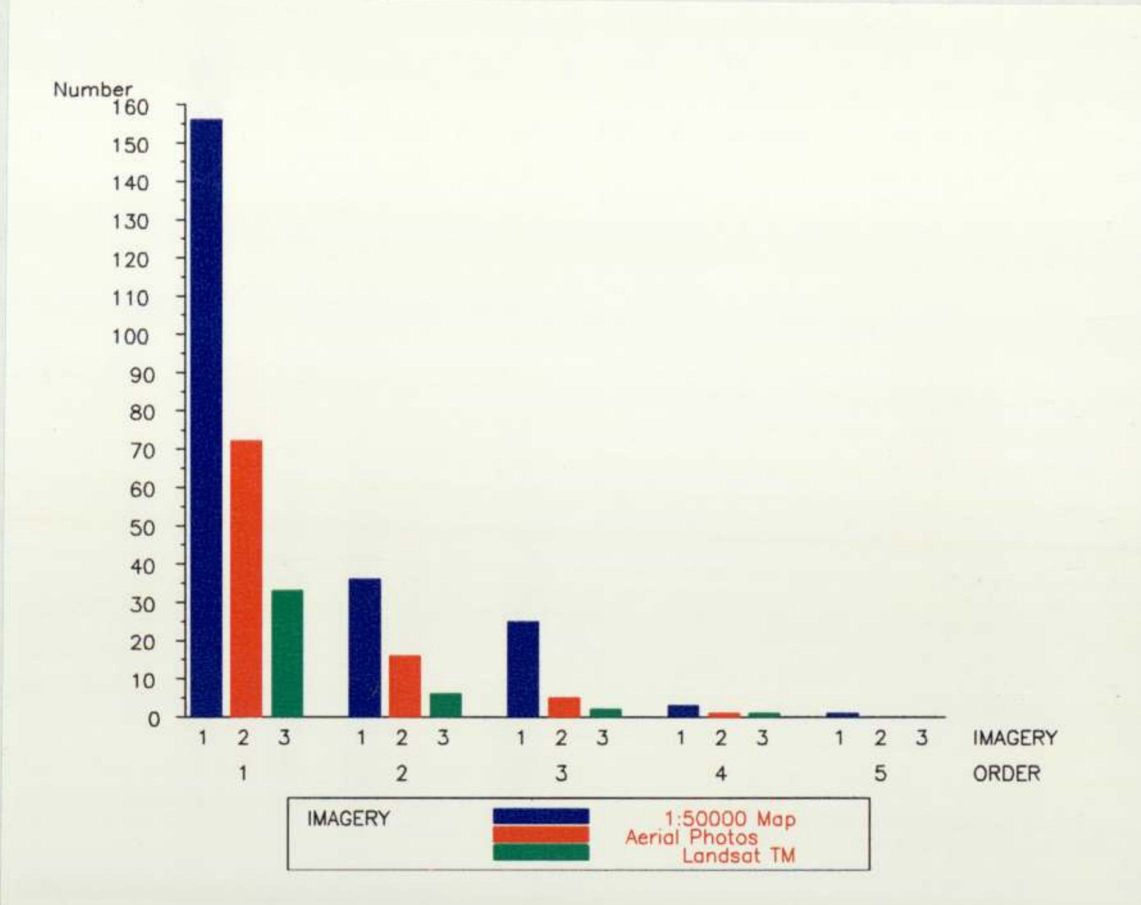

Figure 8.8 Stream ordering of imagery types using Strahler's ordering scheme.

Table 8.6 shows a variation in number of stream orders between the 1:50000 map and the satellite and aerial imagery. The fifth order stream on the map corresponds to the fourth order stream on the satellite and aerial imagery. It is at the first order where most discrepancies occur (as illustrated in Figures 8.2a and b), and these have an effect on subsequent stream orders. As discussed in Chapter 2, the drainage network on the 1:50000 map is derived from 1:10000 maps, which for mountain areas such as this are in turn interpreted from 1:10000 scale aerial photography. Many first order streams only 0.5 or one metre wide are included in this interpretation as evidenced by field work in the area. Some of these very minor tributaries can be delineated from the aerial photography of 1:50000 scale but few from the Landsat TM imagery.

Using the ordering statistics it was possible to derive the bifurcation ratio, as outlined in Section 2.2. Figure 8.9 shows the bifurcation ratios obtained for each type of imagery. Under normal basin conditions the gradient of the graphs should fall within the range 3-5 (Smart, 1972). All three graphs lie within this range, their values being 3.51 for the 1:50000 map, 3.16 for the Landsat TM imagery and 4.03 for the aerial photography. However there is some difference between the values and suggests that further areas need analysing in a similar manner to gain a more definitive view.

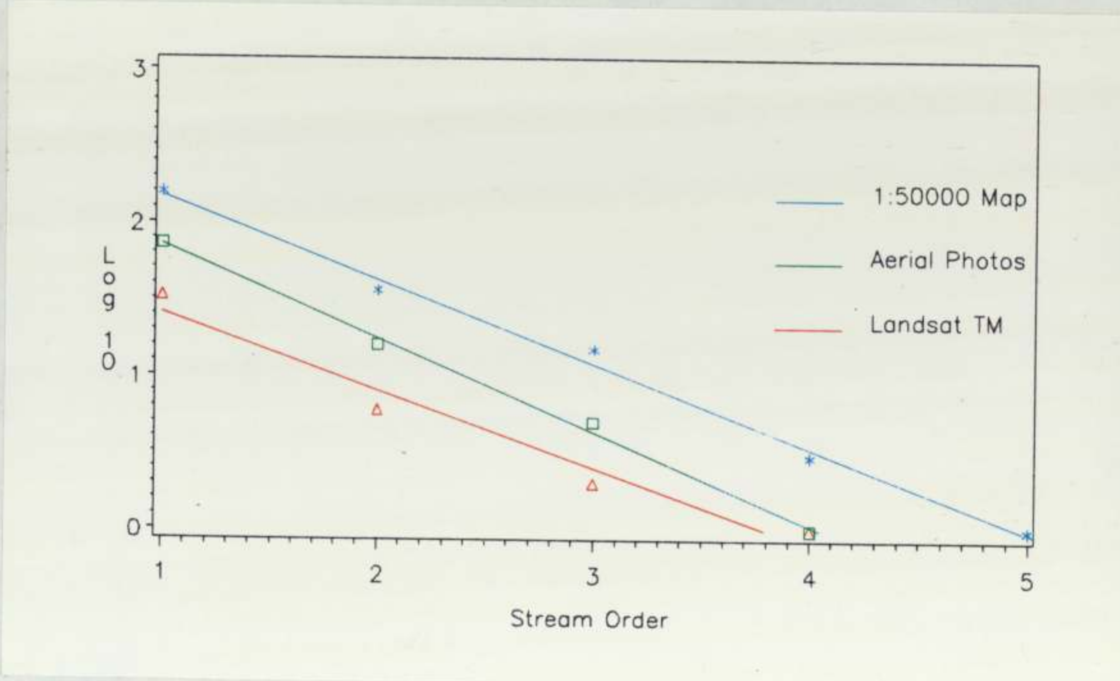

Figure 8.9 Bifuraction ratios derived from image interpretation of the drainage networks.

Clark (1986), Evans (1986) and Vicary (1987) also examined networks and stream orders from their image interpretations. Clark and Evans examined only the Landsat TM imagery, with Vicary examining the aerial photography networks in addition. Figures 8.10 - 8.12 show respectively, a comparison of France's and Vicary's results; a comparison of all four interpreters Landsat TM results and a comparison of their OS map results. Tabular results from these comparisons can be found in Appendix E.

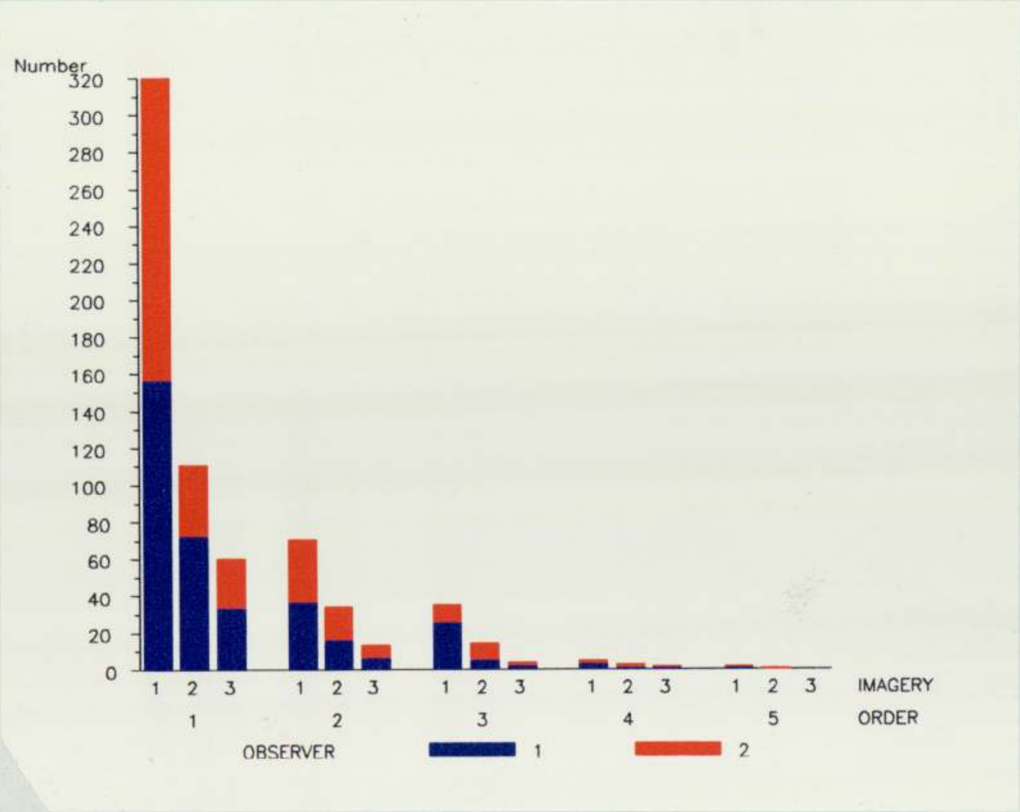

Observer 1 = France   Observer 2 = Vicary

Figure 8.10 Comparison of France and Vicary's network results.

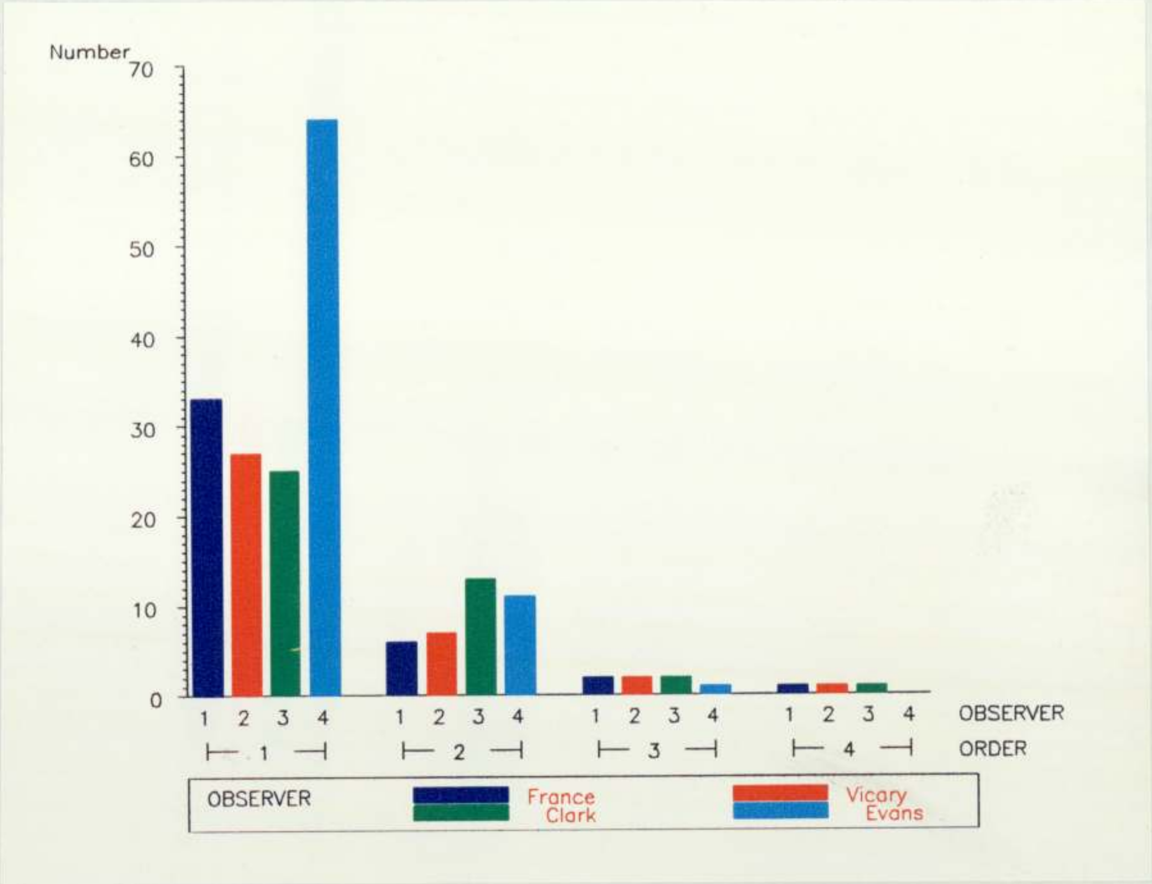

Figure 8.11 Comparison of stream order interpretation from Landsat TM imagery.

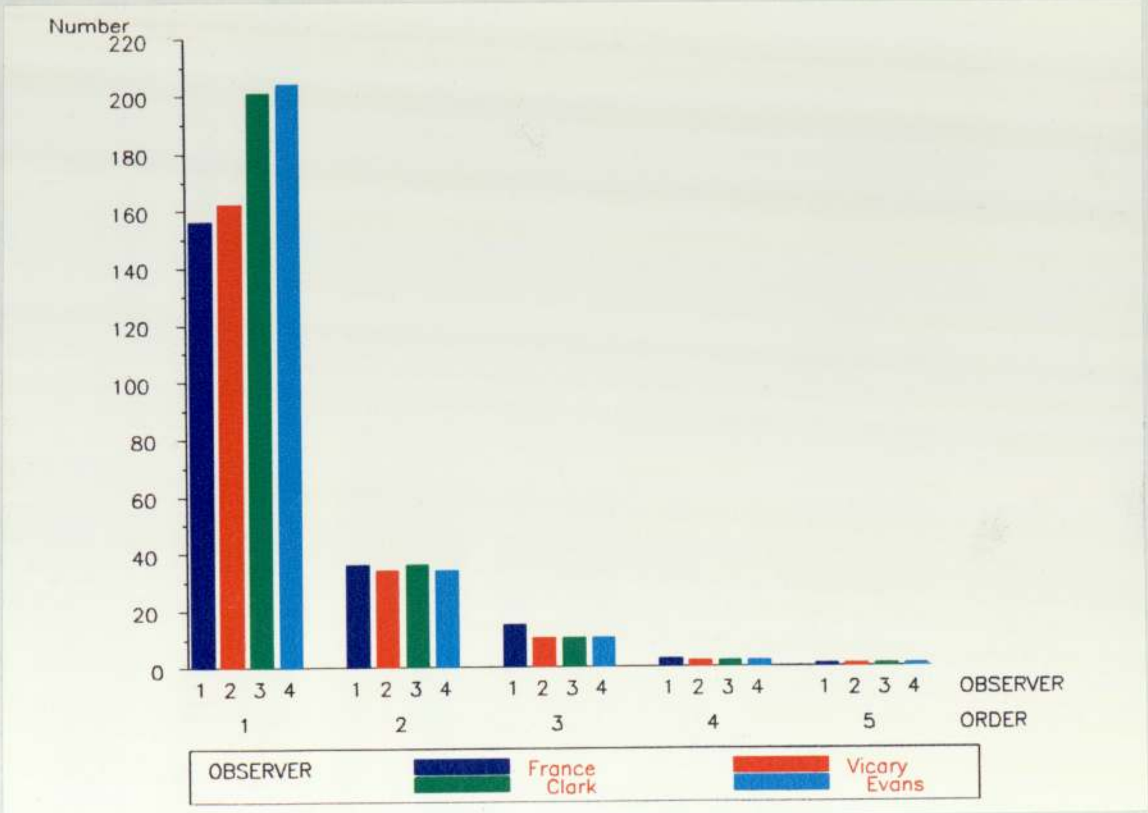

Figure 8.12 Comparison of stream order interpretation from 1:50000 OS map.

Examination of Figures 8.10 and 8.11 reveals that first order TM interpretations are similar, Evans apart. Second order TM interpretations show two groups of results; those of France and Vicary and those of Evans and Clark. Third and fourth order results are similar, though Evans has no fourth order stream. Suprisingly, interpretation of 1:50000 map drainage details (Fig 8.12) showed significant discrepancy at the first order level between the results of France and Vicary as opposed to those of Evans and Clarke. Subsequent order interpretations showed little variation between interpreters.

8.2.3 Catchment specific drainage network details

These results refer to the extended research area with statistics for seven or six catchment areas in the case of Landsat TM data and the Map data, and five catchment areas for the aerial photographic coverage as illustrated in Figures 7.9b, 7.11 and 7.3 respectively. The catchments are illustrated in Figure 8.13. The Mawddach catchment encompasses all other catchments except Cwm-Mynach.

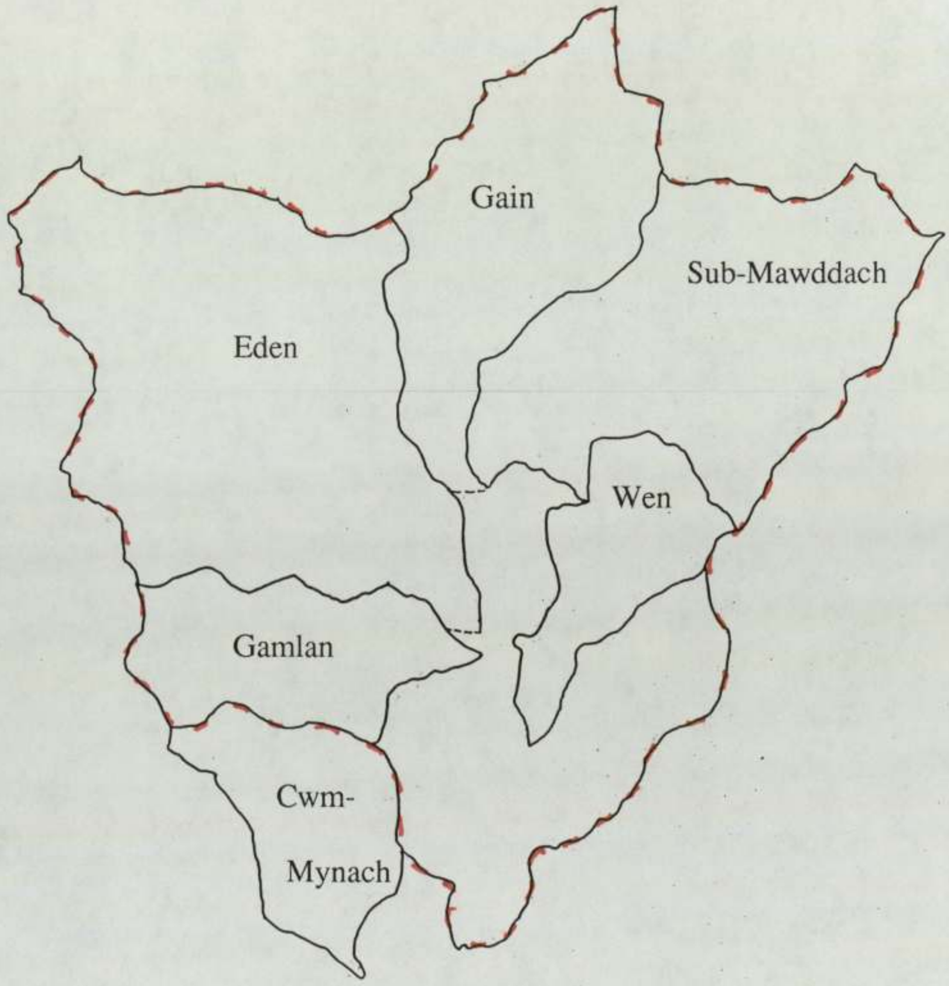

Figure 8.13 Illustration of the catchments used in analysis. — = boundary of Mawddach catchment.

Table 8.7 Stream lengths interpreted from Landsat TM, Aerial Photography and 1:50000 and 1:25000 OS Maps.

Catchment	Landsat TM (km)	1:50000 Map (km)	1:250000 Map (km)	Aerial Photos (km)
Wen	3.75	18.25	6.45	6.40
Cwm-mynach	6.65	11.35	5.70	5.50
Gamlan	3.40	20.65	7.80	12.25
Gain	9.20	34.15	10.80	32.45
Sub-Mawddach	16.42	49.70	18.30	-
Eden	10.62	60.30	30.00	27.45
Mawddach	55.49	216.75	91.05	-

The drainage lengths interpreted from each imagery type for each catchment are presented in Table 8.7. It can be seen from the table that the drainage delineated using the Landsat TM imagery and the aerial photography is considerably less than that marked on the map. For the Gamlan catchment where there was considerable cloud cover in the July 1984 TM image, the details were extracted from the September 1985 image. Linear regression analysis was applied to see if any significant correlations exist. Figure 8.14 shows linear regression of the Landsat TM figures and map figures for the seven catchments, with 95% confidence limits depicted.

For the seven catchments r^2=0.973 which is significant at the 1% level. The value of the large catchment of Mawddach is given high importance in this correlation, so regression was applied using six catchments, with Mawddach excluded. This is illustrated in Figure 8.15. Here an r^2 value of 0.593 was obtained which shows some correlation but is not significant at the 5% level (0.811).

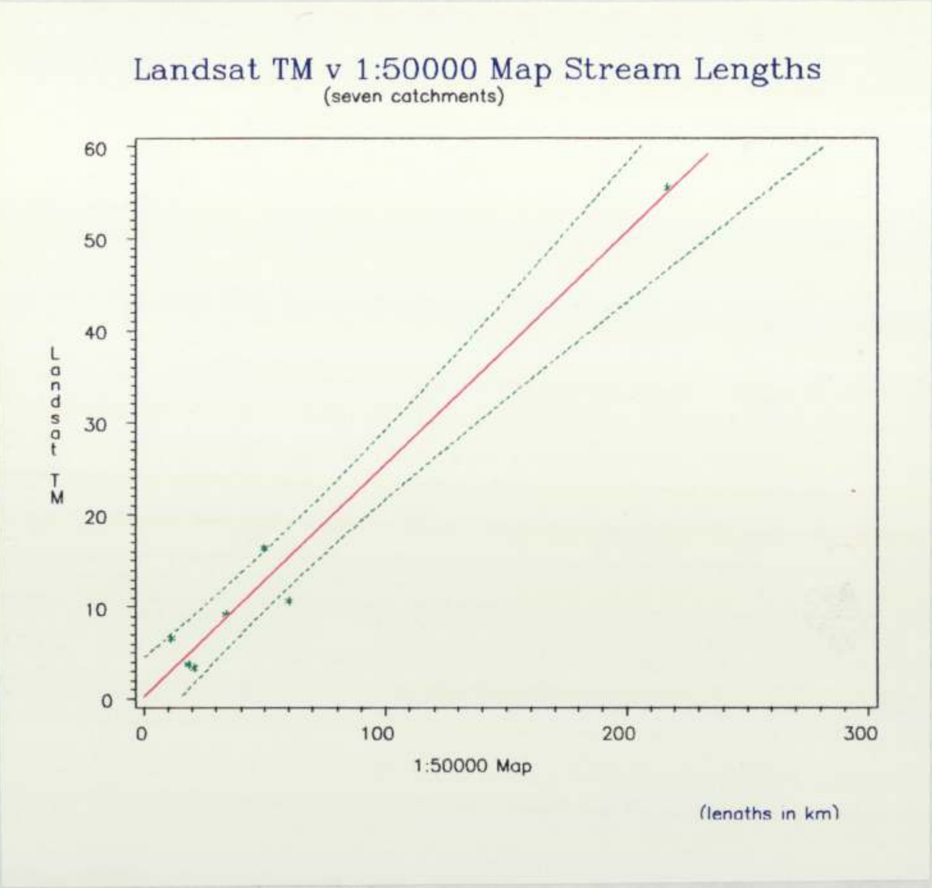

Figure 8.14 Regression analysis: Landsat TM v 1:50000 OS map drainage length details for all seven catchments.

For the aerial photography the r^2 value obtained was 0.630, which again is not sufficient for significant correlation (0.878 at 5%).

Ideally a larger number of catchments (30 or more) should be used to infer greater statistical significance to the results. This applies to all the regression analysis results presented in the following pages.

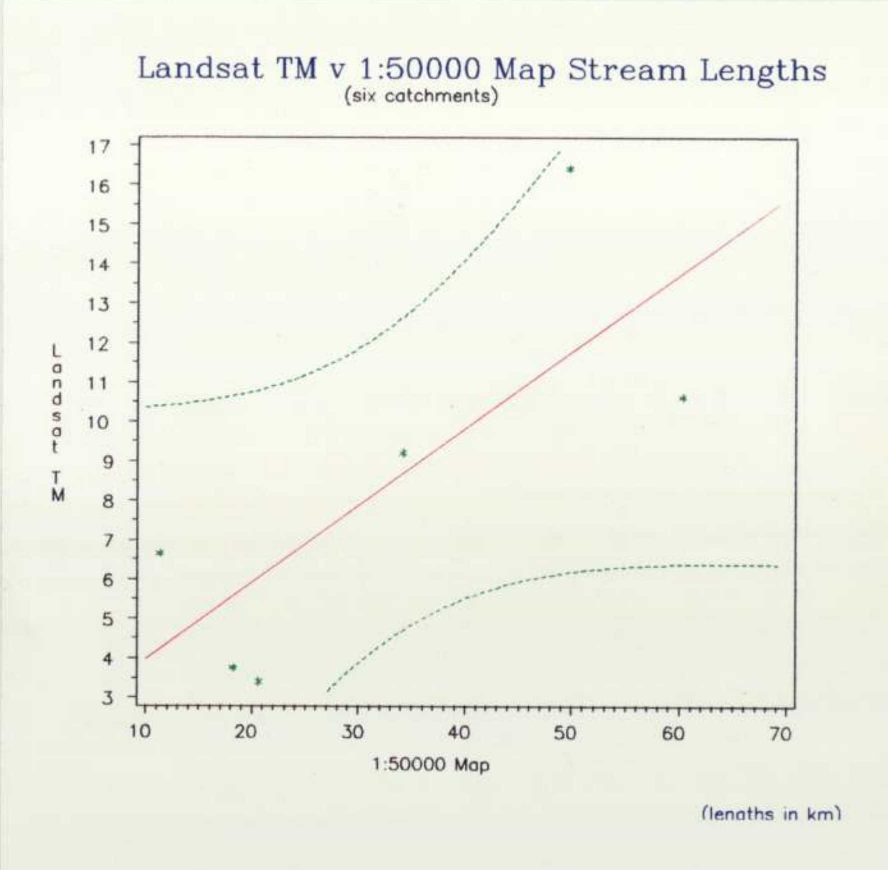

Figure 8.15 Regression analysis: Landsat TM v 1:50000 OS map drainage length details for all catchments except Mawddach.

Following on from work by several authors (see Section 2.2) using mainstream length to estimate catchment area, the mainstream lengths were measured for each catchment. High correlation (r^2=0.921) was shown for all seven catchments using the Landsat TM imagery. The standard estimate of error (S.E.E) was 1.94km. The figure for six catchments was, r^2=0.663 which shows some correlation but is not significant at the 5% level. High correlation was shown between the aerial photos and map data for mainstream length, r^2=0.951, which is significant at the 1% level (see Figure 8.16). Here the S.E.E. was 1.04km.

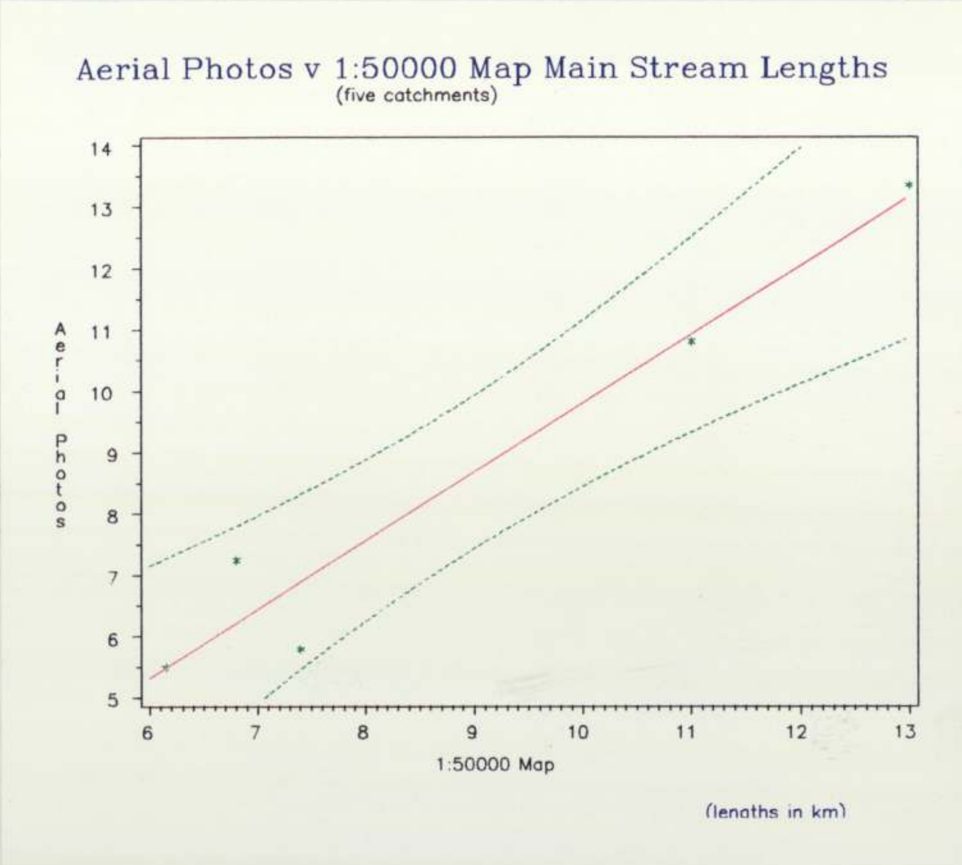

Figure 8.16 Regression analysis: Mainstream lengths of Aerial Photography v 1:50000 OS map details for 5 catchments.

Measurements of basin length using the method suggested by Newson (1975) (see Section 2.2) showed significant correlation between TM values and 1:50000 OS map values. A figure of r^2=0.969 was obtained for all seven catchments (S.E.E = 0.88km) with r^2=0.891 for six catchments (S.E.E = 1.01km)(see Fig. 8.17), both being significant at the 95% level. A very high correlation was seen for the aerial photos and 1:50000 map details (r^2=0.998), with an S.E.E. of 0.17km, as illustrated in Figure 8.18.

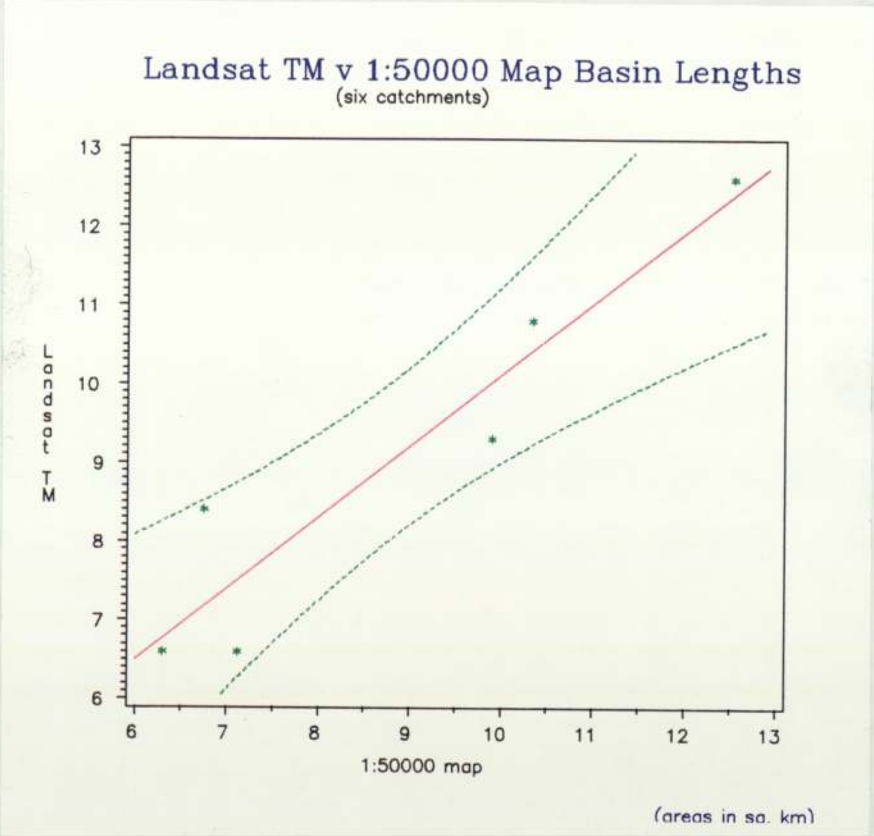

Figure 8.17 Regression analysis: Basin lengths of Landsat TM v 1:50000 OS map details for all catchments except Mawddach.

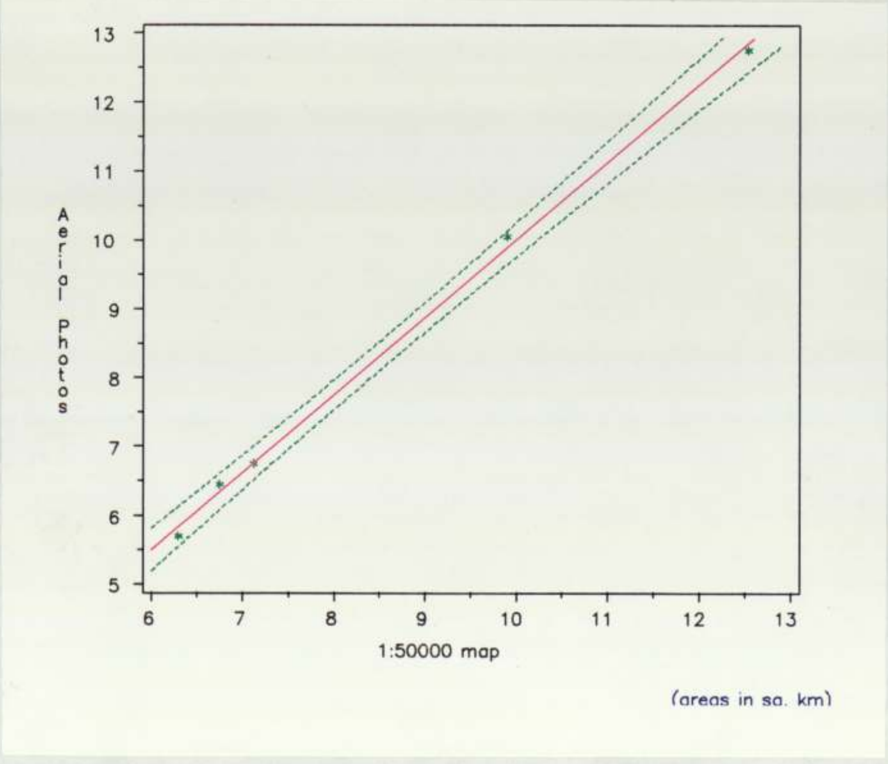

Figure 8.18 Regression analysis: Basin lengths of Aerial Photography v 1:50000 OS map details for 5 catchments.

8.2.4 Areal Morphometric Parameters

As previously mentioned, catchment area is a key factor in hydrological analysis. An attempt was made to delineate catchments using Landsat TM imagery with the on screen methodology, which is described in Section 7.4 and illustrated in Figure 7.9. Aerial photography was also used in the analysis. Landsat MSS was not used for this purpose as the stream network delineated was insufficient to gain meaningful boundaries on an area the size of the research area (235km^2). The catchments delineated were compared with areas obtained for the same catchments using interpretation of catchment boundaries from the 1:50000 OS map. Comparison was on an area v area basis rather than absolute locational assessment. The catchments used for this analysis were illustrated in Figure 8.13 and the quantitative results are presented in Table 8.8.

Table 8.8 Comparison of catchment areas from Landsat TM imagery and 1:50000 scale OS Map.

Catchment	Area interpreted on Landsat TM imagery (km^2)	Area interpreted on 1:50000 scale OS Map (km^2)	Area interpreted on Aerial Photos (km^2)
Wen	11.41	15.63	10.45
Cwm-Mynach	13.88	12.11	10.77
Gamlan	11.51	14.35	15.88
Gain	22.74	24.83	24.78
Sub-Mawddach	39.56	35.73	-
Eden	46.51	50.06	49.22
Mawddach	175.74	164.48	-

Linear regression was applied to the results of catchment areas for Landsat TM v

1:50000 map values, as illustrated in Figure 8.19. A very high correlation of $r^2=0.996$ was obtained for the seven catchments with an S.E.E of 4.55km^2.

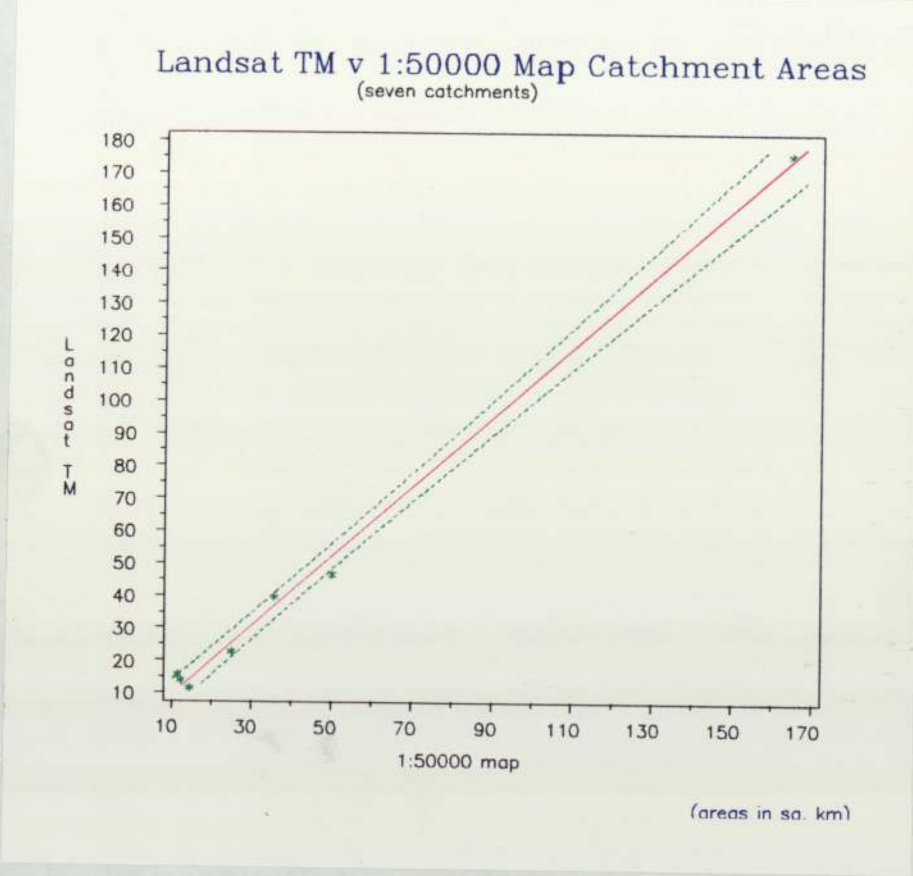

Figure 8.19 Regression analysis: Landsat TM v 1:50000 OS map interpreted catchment areas for all 7 catchments.

A regression was implemented for the six smaller catchments and again a high correlation was obtained ($r^2=0.951$)(S.E.E = 4.18km^2). This exhibits significance at the 1% level ($r^2=0.917$), and is illustrated in Figure 8.20.

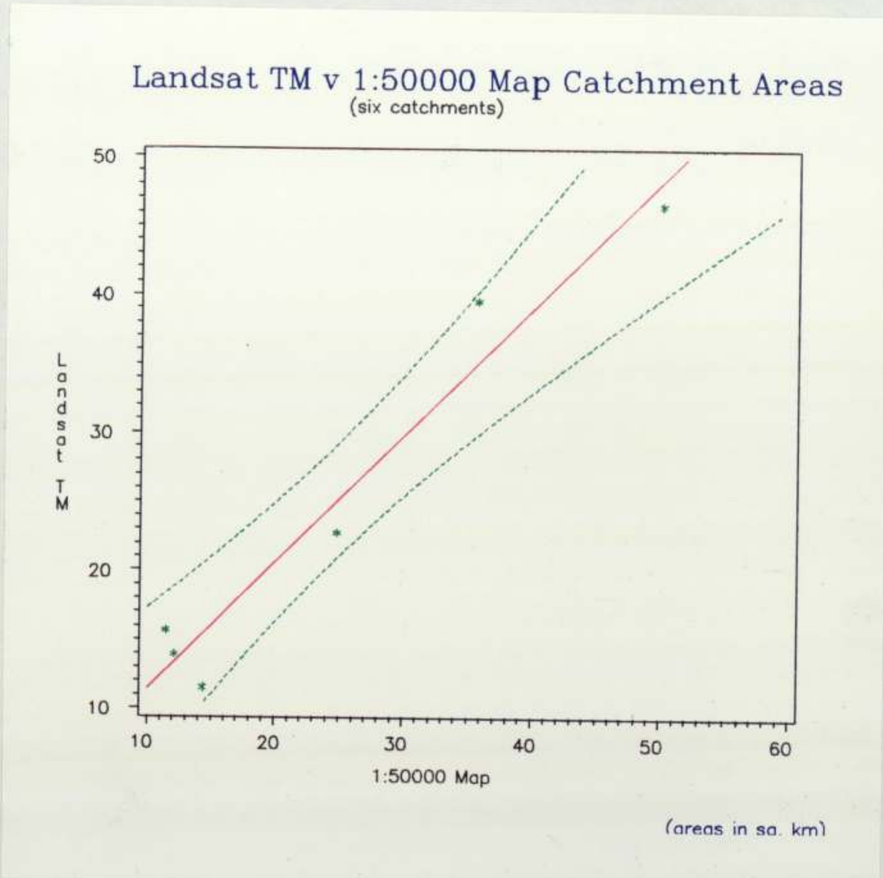

Figure 8.20 Regression analysis: Landsat TM v 1:50000 OS map for interpreted catchment areas, excluding Mawddach.

Linear regression of areal values obtained using the aerial photography v map values was also examined. A correlation of r^2=0.995 was produced with significance at the 1% level (r^2=0.959). The regression of this is illustrated in Figure 8.21. The S.E.E was 1.53km^2.

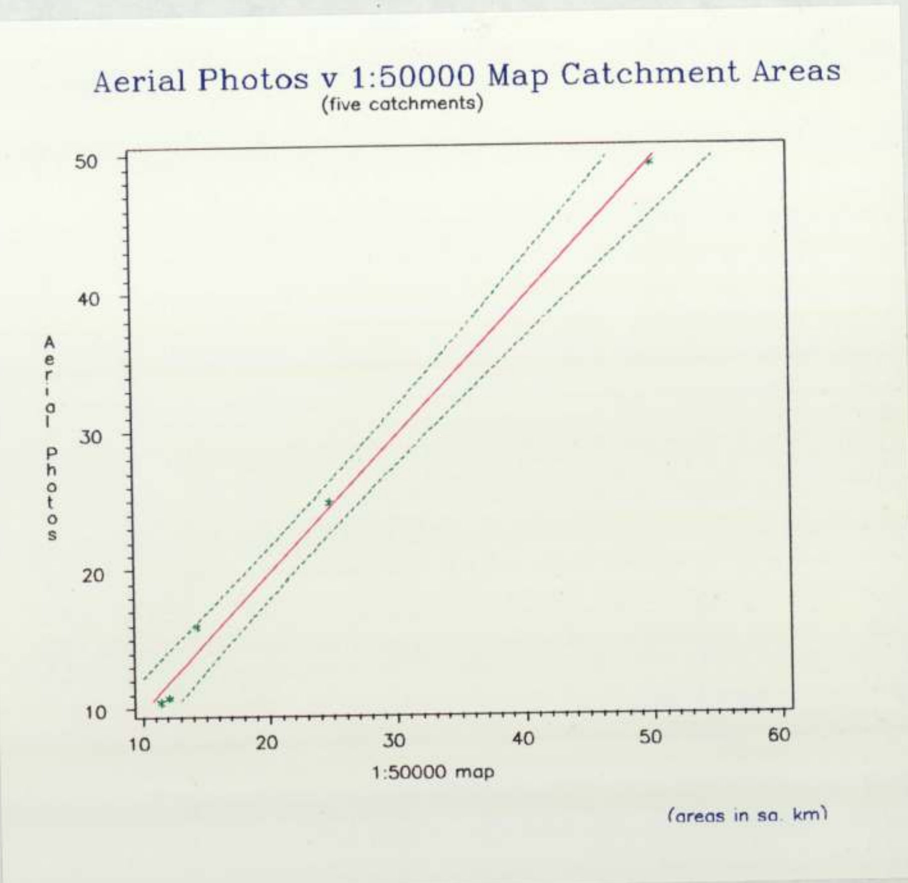

Figure 8.21 Regression analysis: Aerial Photos v 1:50000 OS map interpreted areas for 5 catchments.

Drainage density figures calculated from the interpretations are presented in Table 8.9. These figures are important in that they indicate the distance to the nearest channel i.e. overland flow length. This can have significant effects on peak flow characteristics.

Table 8.9 Drainage Densities interpreted from Landsat TM, Aerial Photography and 1:50000 OS Map.

Catchment	Landsat TM (km/km^2)	Map (km/km^2)	Aerial Photos (km/km^2)
Wen	0.329	1.168	0.612
Cwm-mynach	0.479	0.937	0.511
Gamlan	0.295	1.439	0.771
Gain	0.405	1.375	1.310
Sub-Mawddach	0.415	1.391	-
Eden	0.228	1.205	0.558
Mawddach	0.316	1.318	-

Regression analysis of Landsat TM and Aerial Photographic derived drainage densities v 1:50000 map details showed poor or no correlation. The results obtained were r^2=0.115 and r^2=0.103 for Landsat TM v 1:50000 map details for 7 and 6 catchments respectively. The r^2 value for the five aerial photography v 1:50000 map catchments was 0.432.

Stream frequency, the commonly used alternative to drainage density measurements (see Section 2.2) are presented in Table 8.10. Both stream segment and number of junctions are given. Regression analysis of stream junctions interpreted from Landsat TM imagery plotted against 1:50000 OS map values showed high correlation for all 7 catchments (r^2=0.933) but poor correlation for six catchments (without Mawddach)

(r^2=0.537) and no correlation for aerial photography v map (r^2=0.102).

Table 8.10 Stream Frequencies expressed as segments and junctions interpreted from Landsat TM, Aerial Photography and 1:50000 OS Map.

Catchment	Landsat TM		1:50000 Map		Aerial Photos	
	Segments	Junctions	Segments	Junctions	Segments	Junctions
Wen	1	1	27	14	7	4
Cwm-mynach	3	2	11	17	2	2
Gamlan	1	1	31	15	17	10
Gain	5	3	36	19	59	30
Sub-Mawddach	15	7	95	46	-	-
Eden	5	3	97	48	26	14
Mawddach	33	16	315	155	-	-

The relationship of overland flow to drainage density is approximately 1/2, showing direct proportionality and therefore the same map correlation as drainage density.

Shape Factors :

Interpreted catchment parameters were used to derive shape the factors for basin circularity (R_c), the basin elongation ratio (R_e) and lemniscate k (k).

Basin Circularity: R_c

Basin circularity was calculated for each catchment using Landsat TM (on screen results), aerial photography and 1:50000 OS map. Linear regression analysis of Landsat TM v 1:50000 Map showed poor correlation ($r^2=0.276$). Regression of aerial photo derived values v map values resulted in an higher correlation, $r^2=0.764$.

Table 8.11 R_c values derived from Landsat TM, Aerial Photography and 1:50000 OS Map.

Catchment	Landsat TM	Aerial Photos	1:50000 Map
Wen	1.48	0.99	1.17
Cwm-mynach	1.59	1.48	1.47
Gamlan	1.29	1.48	1.33
Gain	1.29	1.16	1.21
Sub-Mawddach	1.31	-	1.21
Eden	1.81	1.28	1.36
Mawddach	1.41	-	1.17

Basin Elongation Ratio: R_e

The values calculated for R_e from the image interpretations are presented in Table 8.12. No correlation was found between Landsat TM and map values ($r^2=0.041$), and between aerial photo and map values only limited correlation was exhibited ($r^2=0.506$).

Table 8.12 R_e values derived from Landsat TM, Aerial Photography and 1:50000 OS Map.

Catchment	Landsat TM	Aerial Photos	1:50000 Map
Wen	0.47	0.55	0.63
Cwm-mynach	0.70	0.57	0.62
Gamlan	0.71	0.57	0.56
Gain	0.51	0.40	0.51
Sub-Mawddach	0.62	-	0.58
Eden	0.84	0.63	0.59
Mawddach	0.72	-	0.66

Lemniscate k: k

Values of lemniscate k were calculated from the interpreated image parameters and are given in Table 8.13. Regression of Landsat TM and 1:50000 map values showed poor correlation (r^2=0.422), with aerial photo v map correlation showing increased correlation with r^2=0.784.

Table 8.13 k values derived from Landsat TM, Aerial Photography and 1:50000 OS Map.

Catchment	Landsat TM	Aerial Photos	1:50000 Map
Wen	3.02	3.03	2.86
Cwm-mynach	2.81	2.33	2.32
Gamlan	3.05	2.19	2.57
Gain	2.53	2.95	2.87
Sub-Mawddach	1.98	-	2.83
Eden	2.17	2.22	2.32
Mawddach	1.33	-	1.57

8.3 Landcover Information

This section presents the results of landcover classification using the methodologies outlined in Chapter 7 . A comparison with the coverage percentages is made between the Landsat TM classifications by visual interpretation and those obtained by automatic classification methods as discussed in Chapter 6.

General classification of landcover into six classes was decided upon for hydrological purposes (see discussion in Section 3.5). The classes selected were woodland/forest; lowland pasture/agriculture; moorland; urban; water; (cloud/cloud shadow). The results of visual interpretation described in Chapter 7 are given in Table 8.14 and Figure 8.22.

Table 8.14 Landcover - Visual Interpretation Results
(all areas as % of total)

Methodology	Data Types			
	Landsat TM	Landsat TM	Landsat MSS	Aerial Photos
	Lamprey Box	On Screen	Lamprey Box	Stereoscope
Forest/ Woodland	19.4	22.1	16.5	21.7
Moorland	43.2	43.0	52.3	46.9
Lowland Agriculture	34.3	31.9	26.9	30.3
Water	0.1	0.4	1.3	0.3
Urban	0.2	0.3	0.1	0.3
Cloud/Shadow	2.5	2.7	3.3	0.0
Unclassified	0.0	0.0	0.0	0.0

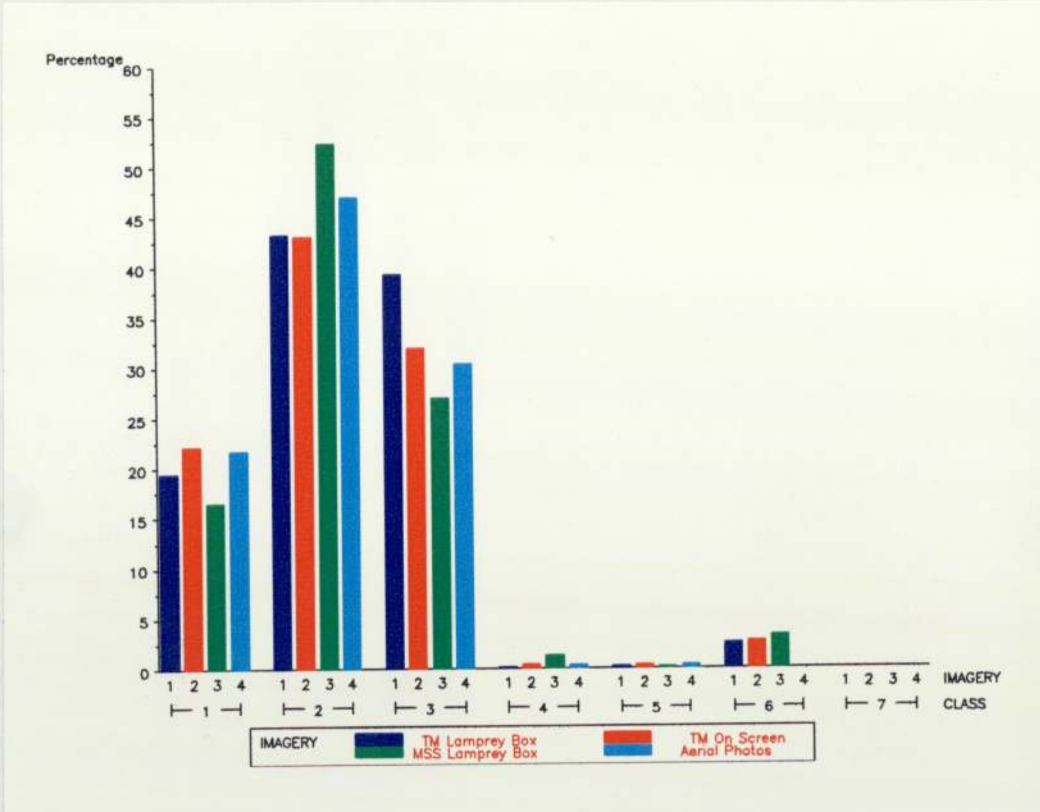

Classes
1 = Forest/Woodland 2 = Moorland 3 = Lowland Agriculture
4 = Water 5 = Urban 6 = Cloud/Shadow 7 = Unclassified

Figure 8.22 Graph of Landcover visual interpretation results.

It can be seen that forest/woodland, moorland and lowland agriculture constitute the vast majority of the land area. There is considerable similarity between the results obtained using the different data types and methods. The Landsat MSS result shows more moorland and correspondingly less lowland agriculture. The area covered by the aerial photography is smaller, though still represents 95% of the research area. From examination of the TM imagery and field knowledge the majority of the area not imaged by the aerial photography is moorland, with a little forest. The unclassified class is included in Table 8.14 to emphasise the contrast with the automatic classification results (see Table 8.15).

Table 8.15 presents results obtained by the author, together with those from other interpreters with little or no knowledge of the area. The table also includes results from automatic classification as detailed in Chapter 6. Figure 8.23 is a graphical representation of the results, with supervised classification results for the Band 3,4,5,7 combination and unsupervised results from the 10 class option.

Table 8.15 Comparison of Landsat TM Landcover Classifications (all figures are percentage values).

	Methodology					
	Lamprey Box	On Screen	Lamprey Box	Lamprey Box	Supervised	Unsupe-rvised
Interpreter	France	France	Clark	Evans	-	-
Forest/ Woodland	19.4	22.1	17.9	14.1	16.1	16.0
Moorland	43.2	43.0	52.7	56.4	44.8	43.7
Lowland Agriculture	34.3	31.9	28.8	24.5	32.4	34.9
Water	0.1	0.4	-	0.3	0.04	0.0
Urban	0.2	0.3	0.4	0.4	0.1	0.0
Cloud/ Shadow	2.5	2.7	-	4.6	0.05	0.0
Unclassified	0.0	0.0	0.0	0.0	6.5	4.5

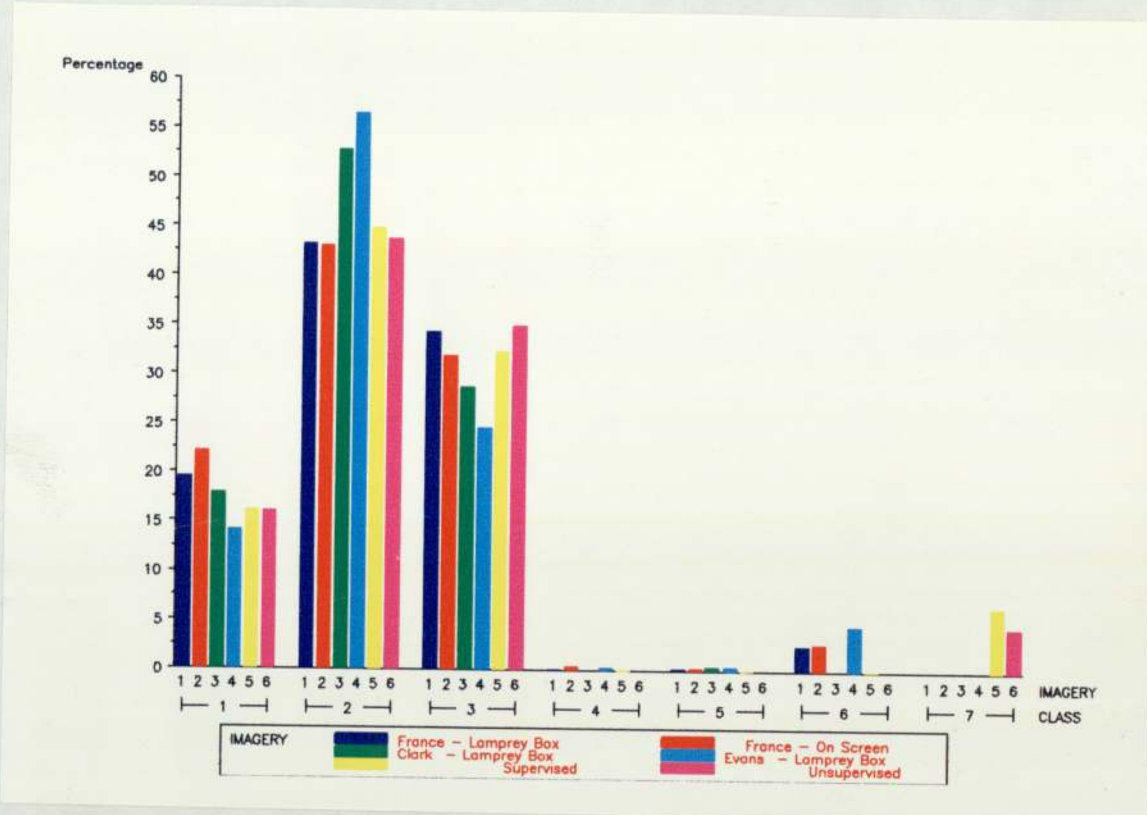

Classes
1 = Forest/Woodland 2 = Moorland 3 = Lowland Agriculture
4 = Water 5 = Urban 6 = Cloud/Shadow 7 = Unclassified

Figure 8.23 Graph of Landsat TM landcover results.

The classification results in Table 8.15 and Figure 8.23 exhibited a considerable degree of similarity between methods and to a lesser extent between interpreters. Results obtained by the author (France) showed consistency between Lamprey Box and on screen visual interpretation methods and those from by supervised and unsupervised automatic classification methods. The automatic classification methods showed some unclassified areas which on examination of the coloured classifications was seen to be mainly the cloud/cloud shadow area.

A comparison of Landsat TM and Landsat MSS supervised classification results is given in Table 8.16

Table 8.16 Comparison of Landsat TM and Landsat MSS supervised classification results (all figures are % values).

	Landsat TM	Landsat MSS
Forest/Woodland	16.1	19.3
Moorland	44.8	47.9
Lowland Agriculture	32.4	31.6
Water	0.04	0.04
Urban	0.1	0.05
Cloud/Shadow	0.05	0.0
Unclassified	6.5	0.6

The comparison in Table 8.16 shows good agreement between the Landsat TM and Landsat MSS supervised classifications.

8.4 Classification Accuracy

As mentioned in Section 6.7 only sufficient ground data was collected for supervision of the automatic classifier. A comprehensive accuracy assessment was thus not possible. However, part of the area ($130km^2$ 55%) was covered by a vegetation survey. The vegetation classes were interpreted from soil maps at 1:50000 scale (Robertson, 1982). The boundary details from this map were digitised using a

Summagraphics digitising tablet attached to the I^2S. These digitised boundaries were then used to from a polygonised output file in a similar manner to that described for on screen landcover interpretation (see Section 7.4). Figure 8.24 and Table 8.17 show the vegetation classes interpreted interpreted from the soil classes, together with forest areas (see also Figure 9.6).

Table 8.17 Vegetation classification from soil types.

Class No. in Figure 8.24	Soil Classes	Robertson's vegetation classes	Broad Landcover Categories L=Lowland M=Moorland
1	713e - Cegin	Arable and permanent pasture	L
2	811d - Conway 851b - Dovey	Permanent and ley grassland	L
3	611a - Malvern 611g - Manod	Dry acidic grassland	L
4	654b - Hafren 654c - Bodafon	White bent (Nardus) grassland	M
5	721a - Wilcocks 721e - Wilcocks	Flying bent (Molinia) grassland	M
6	311e - Revidge 311a - Bangor Preseli 313e - Powys	Dry heather moor	M
7	1011b - Winterhill 1013a - Crowdy	Bog	M

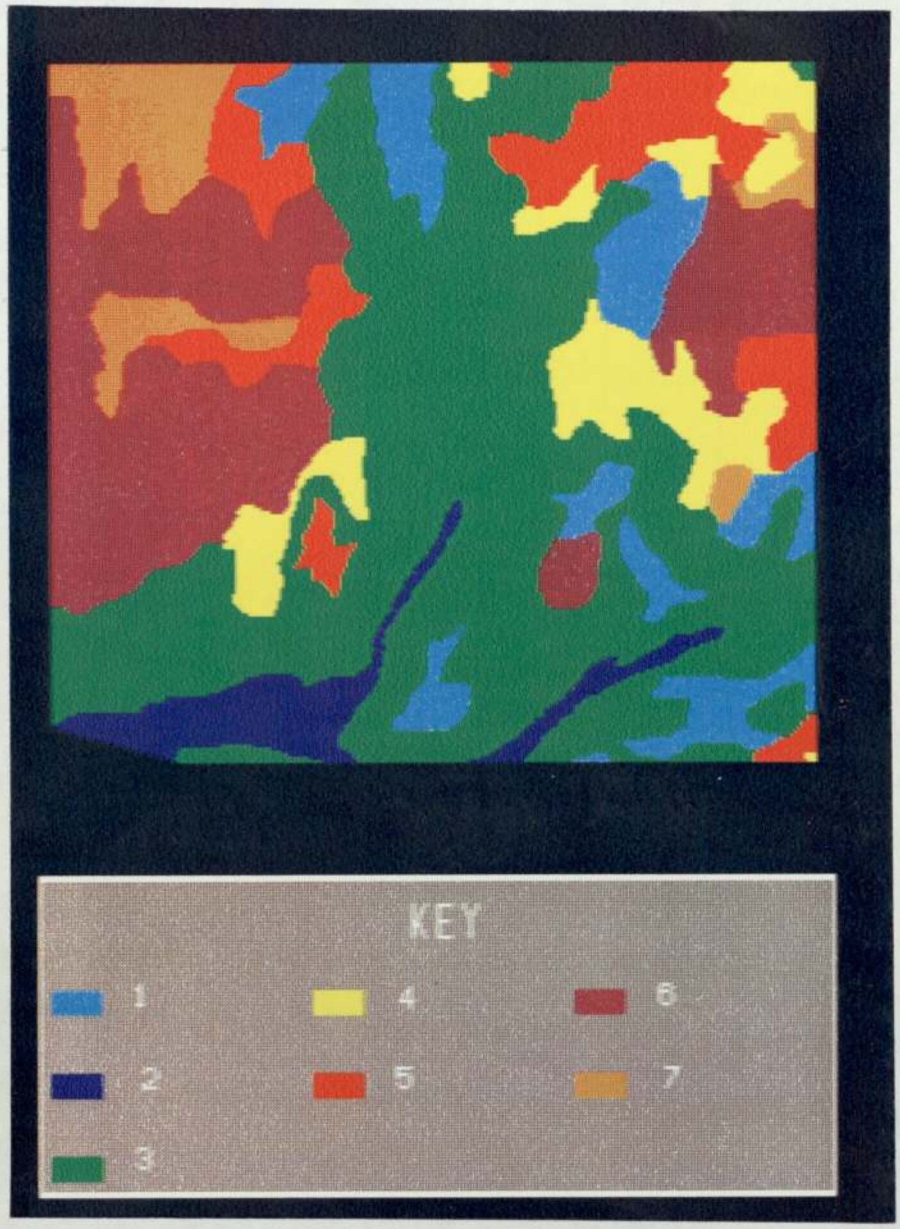

Figure 8.24 Robertson's soil derived landcover classification - for class Nos. refer to Table 8.17 (adapted from Robertson, 1982).

Further merging of the vegetation classes was carried out by the author to enable comparison with the broad classes interpreted from the aerial and satellite imagery. These classes can be seen in Table 8.17. To facilitate comparison, areas of water, cloud or urban as delineated from the on screen interpretation of the Landsat TM imagery were removed from the comparison. The final vegetation classification used for comparison is illustrated in Figure 8.25.

Figure 8.25 Broad landcover classification - for class derivation see Table 8.17.

The resulting image was then warped, with a 30m output pixel size, to geometrically register with the geocorrected Landsat TM classifications. In the case of Landsat MSS georegistration an output pixel size of 50m was used. Image to image comparisons were then carried out with urban areas, water areas and cloud areas removed from the

Landsat classifications. The Landsat TM classifications which were tested were the on screen visual interpretation, the band 3457 supervised classification and the unsupervised classification (from 10 classes). The supervised Landsat MSS classification was also examined. The results from these comparisons are presented as confusion matrices in Tables 8.18 a,b, c & d.

Table 8.18a Confusion matrix for Landsat TM on screen classification v Soil survey derived landcover classification.

		Soil Survey derived Vegetation Categories		
		Forest	Moorland	Lowland
Landsat TM on screen classes	Forest	0.774	0.049	0.155
	Moorland	0.071	0.818	0.111
	Lowland	0.155	0.133	0.734

Table 8.18b Confusion matrix for Landsat TM supervised classification v Soil survey derived landcover classification.

		Soil Survey derived Vegetation Categories		
		Forest	Moorland	Lowland
Landsat TM supervised classification	Forest	0.523	0.015	0.051
	Moorland	0.103	0.666	0.371
	Lowland	0.310	0.280	0.524
	Unclassified	0.064	0.039	0.054

Table 8.18c Confusion matrix for Landsat TM unsupervised classification v Soil survey derived landcover classification.

		Soil Survey derived Vegetation Categories		
		Forest	Moorland	Lowland
Landsat TM unsupervised classification	Forest	0.519	0.019	0.007
	Moorland	0.189	0.731	0.264
	Lowland	0.267	0.238	0.647
	Unclassified	0.025	0.012	0.082

Table 8.18d Confusion matrix for Landsat MSS supervised classification v Soil survey derived landcover classification.

		Soil Survey derived Vegetation Categories		
		Forest	Moorland	Lowland
Landsat MSS supervised classification	Forest	0.509	0.204	0.055
	Moorland	0.208	0.673	0.193
	Lowland	0.275	0.114	0.743
	Unclassified	0.008	0.009	0.009

An examination of the classification results on the basis of correct commission produced accuracy levels of 77.5% for the on screen visual interpretation, 57.1% for the supervised Landsat TM classification, 63.3% for the unsupervised Landsat TM classification, and 64.2% for the supervised Landsat MSS classification. It should be remembered when examining these figures that the test data was a vegetation classification on the basis of soil type and not a detailed field survey.

From the field survey carried out, it was recognised that vegetation types in the natural and semi-natural moorland areas can vary considerably from one type to another within a few metres. This spatial heterogeneity is not reflected in the soil classification derived vegetation types which tends to be a generalistation. If the classification and comparisons were carried out with a greater number of classes a clearer picture of capabilities would ensue.

8.5 Identification of Small lakes using Landsat TM imagery

Figure 8.26 illustrates the 34 small lakes delineated from the 1:50000 OS map of the area. This was used for assessing the capabilities of Landsat TM for the detection of small water bodies. Table 8.19 indicates the size of each lake and whether or not the lake was interpreted from the Landsat TM imagery via either the Lamprey Box or on screen methods. The table shows consistency of results using either of the ineterpretation methods. The sizes of lakes which proved identifiable indicates that Landsat TM imagery could be used to identify water bodies as small as 0.3 hectares in areas of open moorland, however an overall figure of 0.6 hectares is more realistic due to difficulty in identifying small water bodies within forested areas. This compares with figures of 2.4 hectares for Landsat MSS and a suggested value of 0.5 hectares for SPOT in multispectral mode i.e. with a 20 metre spatial resolution (Chidley and Drayton, 1986). Using aerial photographs the spectral contrast between water bodies and other terrain features was sufficient to enable lakes of 0.2 hectares and smaller to be identified. The comparative results are summarised in Table 8.20.

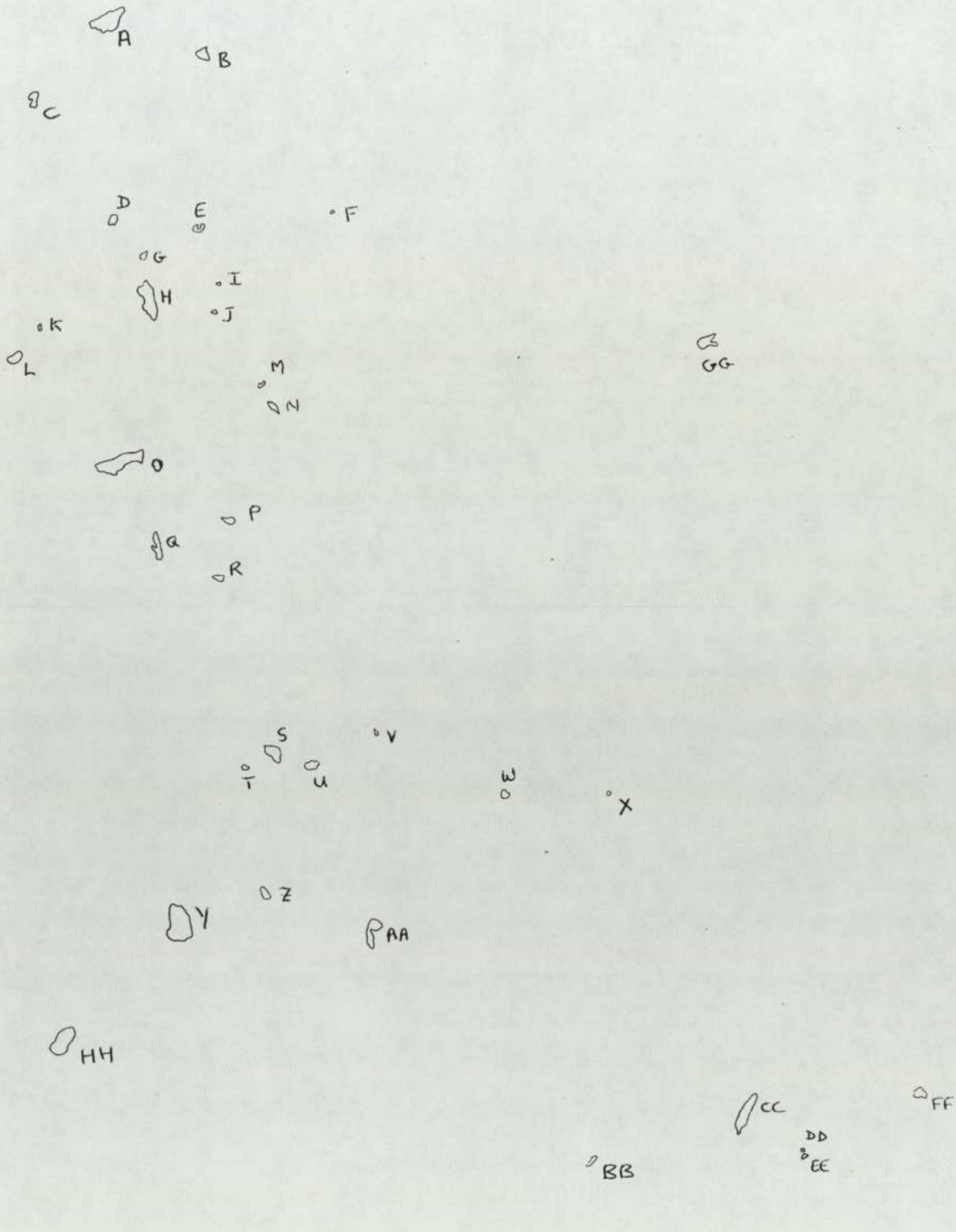

Figure 8.26 Map of small lakes for interpretation using Landsat TM. Lakes delineated from 1:50000 OS map. Scale =1:150000.

Table 8.19 Identification of small lakes from Landsat TM imagery via Lamprey Box and on screen methods.

Lake	Grid Ref.	Size (ha)	Identified via Lamprey Box	Identified on screen
A	2638 3383	13.5	Y	Y
B	2655 3377	3.0	Y	Y
C	2629 3370	2.8	Y	Y
D	2641 3351	2.5	Y	Y
E	2659 3348	1.4	Y	Y
F	2670 3351	1.1	Y	Y
G	2646 3345	0.3	Y	Y
H	2646 3337	13.0	Y	Y
I	2657 3340	0.2	N	N
J	2656 3336	0.4	N	N
K	2629 3334	0.5	Y	Y
L	2626 3338	2.9	Y	Y
M	2664 3324	0.8	Y	Y
N	2665 3321	1.5	Y	Y
O	2640 3321	15.0	Y	Y
P	2657 3303	2.0	Y	Y
Q	2647 3299	3.5	Y	Y
R	2656 3294	1.9	Y	Y
S	2663 3267	8.0	Y	Y
T	2659 3264	1.0	Y	Y
U	2670 3265	3.0	Y	Y
V	2680 3269	0.4	Y	Y
W	2700 3258	1.6	Y	Y
X	2716 3258	0.2	N	N

Table 8.19 continued

Lake	Grid Ref.	Size (ha)	Identified via Lamprey Box	Identified on screen
Y	2628 3238	21.0	Y	Y
Z	2663 3244	2.3	Y	Y
AA	2677 3237	6.8	Y	Y
BB	2713 3201	1.0	Y	Y
CC	2737 3207	14.0	Y	Y
DD	2742 3202	0.2	N	N
EE	2742 3201	0.4	N	N
FF	2760 3210	3.8	Y	Y
GG	2735 3327	4.5	Y	Y
HH	2630 3223	11.5	Y	Y

Table 8.20 Identification of small lakes from remotely sensed imagery.

Imagery Type	Spatial Resolution	Minimum area of water body consistently identifiable
Landsat TM	30m	0.6ha
Landsat MSS	80m	2.4ha
SPOT XS	20m	<0.5ha
Air Photos	1:50000 scale	<0.2ha

8.6 Summary

Drainage details

Landsat MSS was only useful for delineating the largest channels in this area i.e rivers over 10m wide, of which their are few. Landsat TM showed significant improvement with a recognisable network of approximately a third of the 1:50000 map detail. The indications are that the vast majority of 5m streams are identifiable either directly or by inference. This also applies to most of the 3m streams. The 1:50000 panchromatic aerial photography showed approximately 50% more detail than the Landsat TM, with marginally more on the 1:250000 map. The 1:50000 map showed much greater detail than any of the other data sources examined.

Two important factors to recognise in the interpretation process are experience and subjectivity. A large number of incorrect stream interpretations were made by inexperienced image interpreters. The attribution of experiential and subjective misinterpretations is a difficult division to make. However, from the series of results obtained it would appear that the former accounts for a much larger proportion of errors. The author's misinterpretation of Landsat TM drainage details was between 4 and 8% of the network delineated, on the assumption that the 1:50000 map details were 100% correct.

On a positive note it is interesting to see the great similarity of network interpretation lengths from TM imagery by different interpreters, after removal of errors.

Network ordering

Network ordering results showed some promise with the derivation of bifurcation ratios. However, further work is required to assess this area more fully. Some significant differences were seen between the results of different interpreters, particularly in first order interpretations which can have significant consequent effects on the overall ordering of the network topology.

Catchment parameters

The correlation of morphometric catchment parameters between Landsat TM imagery and 1:50000 OS map data, and between the 1:50000 aerial photography and 1:50000 map data showed considerable variation. A summary of the results is presented in Table 8.21. Catchment area, the most significant parameter, showed strong correlation both for Landsat TM v 1:50000 map and aerial photography v 1:50000 map. Basin length also showed strong correlations, with mainstream length slightly less. No other parameter measurements revealed significant correlations between Landsat TM derived parameters and 1:50000 map derived parameters. Aerial photography exhibited reasonable, though not significant (at 95% confidence level) correlations with 1:50000 map derived parameters of basin circularity and Lemniscate k. Statistics for a greater number of catchments (30 or more if possible) would increase confidence in the results obtained.

The lack of relief parameter measurements from Landsat TM and Landsat MSS imagery is a significant limitation when compared to aerial photography

Table 8.21 Summary of Morphometric Parameter Correlations with 1:50000 OS map derived parameters. * = significant correlation (*) = reasonable correlation.

Morphometric Parameter	Landsat TM imagery	1:50000 Aerial Photography
Stream Length	-	-
Mainstream Length	(*)	*
Basin Length	*	*
Catchment Area	*	*
Drainage Density	-	-
Stream Frequency	-	-
Basin Circularity (Rc)	-	(*)
Basin Elongation Ratio (Re)	-	-
Lemniscate k	-	(*)

<u>Landcover</u>

Landcover classification was done on a global basis for the whole area with no catchment specific information. The classes used were broad categorisations. Landcover interpretations from the aerial photography were possible for the categories considered, though colour would have aided the process. Results for visual interpretation of the Landsat TM imagery, aerial photography and Landsat MSS by the author revealed some differences between the former two and the latter. Minor differences were seen in the Landsat TM results obtained by different interpreters. The supervised and unsupervised automatic Landsat TM classification results showed similarity with the visual results for the major classes. A problem arose with the failure of the unsupervised classification to denote any areas as urban or water.

Supervised classification of the Landsat MSS data produced similar results to the Landsat TM supervised classification, with some small areas of discrepancy.

Classification accuracy was carried out with visual interpretation exhibiting most agreement with the test data. The accuracy assessment provides only a broad indication of the overall situation. An extensive field campaign would be required for a full accuracy assessment.

Water bodies

Consistency of results for the interpretation of small lakes from Landsat TM imagery was seen using the Lamprey Box and on screen methods. Some lakes as small as 0.3 hectares were identifiable, however a figure of 0.6 hectares is more appropriate for consistent recognition irrespective of adjacent landcover.

CHAPTER NINE: **THE USE OF GEOGRAPHICAL INFORMATION SYSTEMS**

9.1 Introduction

Along side the computer developments that have enabled digital image processing and enhancement, contemporaneous advances have occurred in the development of other spatial data systems. The most important related development is that of Geographic Information Systems (GIS). These can be described as computer data storage and analysis systems for spatial data. Reference was made in Chapter 2 to the increased use of these systems in hydrological applications.

Much of the World's cartographic and thematic data is currently, and increasingly so, being stored in geographic information systems that are designed to accept large volumes of spatial data derived from a variety of sources. The organisation of these systems allows for the incorporation of data derived from remote sensing, which can then be analysed further in relation with other spatial information. This has been recognised for some time as a potential use of remotely sensed data (Shelton and Estes, 1981; Short, 1982). In fact Simonett *et al.* (1977) suggest that the real utility of remotely sensed data is intimately linked to whether or not the data can be associated with other spatial information, usually stored in a GIS format.

It is the increasing importance of GIS and its application in hydrology using remotely sensed inputs (Trevett, 1990; Walsh *et al.*, 1990) which led to the inclusion of this chapter. The chapter examines some of the basic principles of GIS and how information from remotely sensed data and other sources can be used within the framework of a GIS to model parts of the hydrological cycle.

In the past one of the major stumbling blocks to the integration of remotely sensed data with other data types in a GIS has been one of data types. Many GIS operate using data stored in vector format, whereas remotely sensed data is stored in raster format as pixels. The overlaying of vector data with so-called raster backdrops is a fairly recent development on several GIS. However, there is a problem of complex data analysis with data types in different formats. Many GIS manufacturers are currently addressing this issue. The current solution is one of format conversion which was carried out in this instance on the remotely sensed classification and is discussed in Section 9.4. In this research the ARC/INFO vector-based GIS was used.

9.2 Hydrology and GIS

The questions which now need answering are, which data of hydrological relevance do we require as inputs to the GIS, and for what purposes? A useful illustration of GIS is one of overlying layers, as depicted in Figure 9.1. The layers of hydrological relevance may include: rainfall (as point data or interpolated zones), catchment boundaries, drainage networks, landcover types, topography, evapotranspiration - as a Digital Elevation Model (DEM), soil types, soil moisture, drift deposits, solid geology. The relevance of each parameter will depend on the analysis under consideration. The complex interelationships existing in the hydrological cycle have already been mentioned in this research.

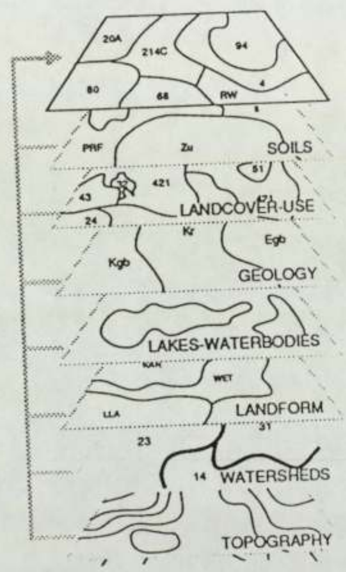

Figure 9.1 Depiction of a GIS as a series of layers (after ESRI, 1987).

Once the required data types have been decided upon, their source must be determined and subsequently the data input to the GIS. It is interesting to examine which of these data can currently be obtained using remote sensing. In Chapter 2 it was mentioned that rainfall information can now be interpreted using weather satellites and radar remote sensing, additional or alternative information being point source data from raingauge networks. Catchment boundaries and drainage networks can be interpreted from remotely sensed imagery as described in Chapters 7 and 8, the alternative sources being map data, stereo aerial photography or SPOT satellite stereo pairs, or DEM's derived from the latter three data types. Topographic details of slope and aspect are most easily obtained usng a DEM from the any of the sources just listed.

Landcover information of hydrological relevance can be obtained using remotely sensed data, as described in Chapters 6,7 and 8, or from maps where available. Soil types can in some areas of the world be interpreted using satellite imagery and are frequently interpreted from aerial photography (Mulders, 1987). Soil moisture interpretation has been attempted, with limited success using optical sensed remotely sensed data. Radar remote sensing is thought to have more potential for quantitative assessment of this parameter.

Interpretation of geological features from remotely sensed imagery is often dependent on the type of vegetation cover and also the topographic features of the surface. As mentioned in Section 3.3 aerial photography has been used for many years in this area and satellite imagery has been used with much success in arid and semi-arid areas of the globe. For the research area geological maps of both drift deposits and solid geology exist at 1:50000 scale.

Using the remotely sensed data the author has derived catchment boundaries, drainage network details and landcover distribution information, as described in Chapters 5, 6 7 and 8. One of the most important parameters required for much hydrological modelling is a description of the topography of catchments. This can be used to measure surface and channel slopes. A Digital Elevation Model (DEM) was created for use in hydrological evaluation of the research area. The other coverages entered into the GIS by digitisation were soil and vegetation types.

9.3 Creation of a Digital Elevation Model (DEM)

The source data used for creation of a DEM for the research area was elevation information from the 1:50000 Ordnance Survey map of the area. The map was placed on a A0 size Calcomp digitising table, which was connected to a VAX cluster on which the ARC/INFO software had been installed. Contours at 25 metre intervals were digitised, together with spot height information (see Figure 9.2).

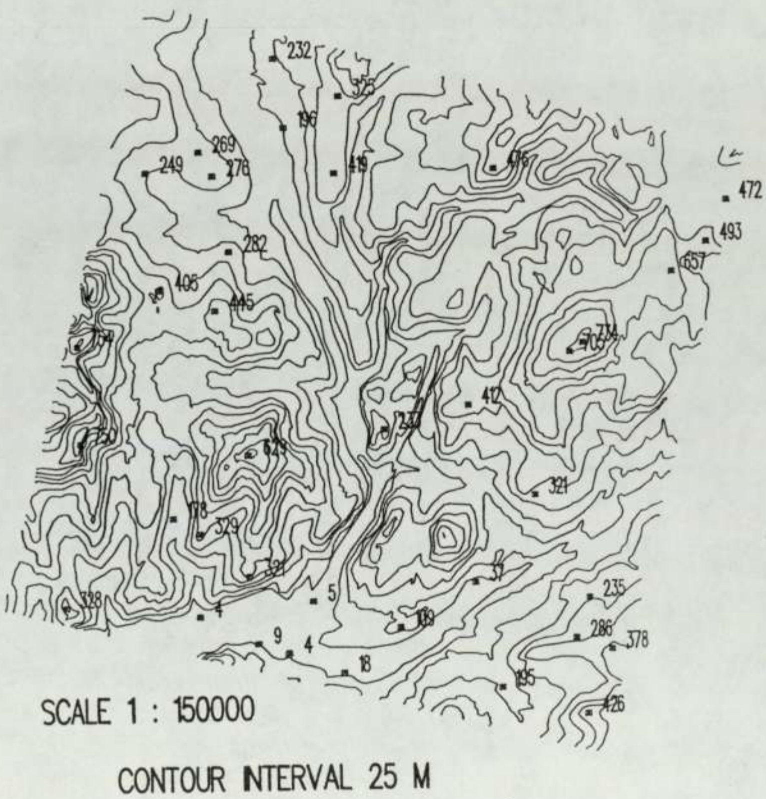

Figure 9.2 Contour and spot height information from the 1:50000 OS map.

This was then checked for errors and edited as appropriate using the ARCEDIT software routines. The resulting data was used as input to the TIN modelling software of ARC/INFO. These routines use a Triangulated Irregular Network (TIN) to describe surfaces, in this case a topographic surface. Further information on TIN structures can be found in ESRI (1987). TIN and other frequently used surface interpolation models are described in Moore *et al.* (1991). Figure 9.3 illustrates the TIN structure derived for the research area.

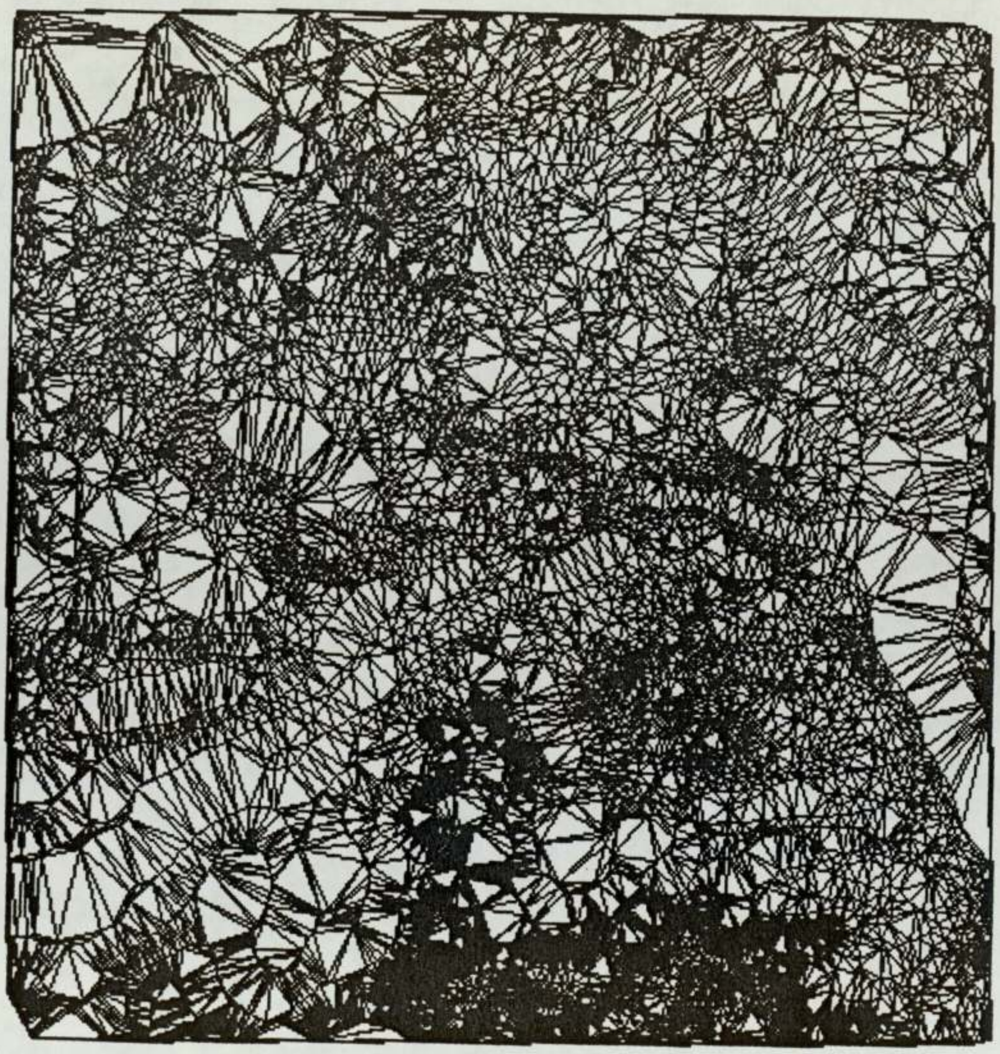

Figure 9.3 TIN structure derived for the research area.

Once a TIN structure has been created this can then be used to interpolate a Digital Elevation Model. The DEM derived for the research area is shown in Figure 9.4. Slope categories were defined for the DEM and used to create the slope map illustrated in Figure 9.5. This could be used together with catchment boundary details and other information (e.g. soil type, vegetation type) to define zones for input to hydrologic models.

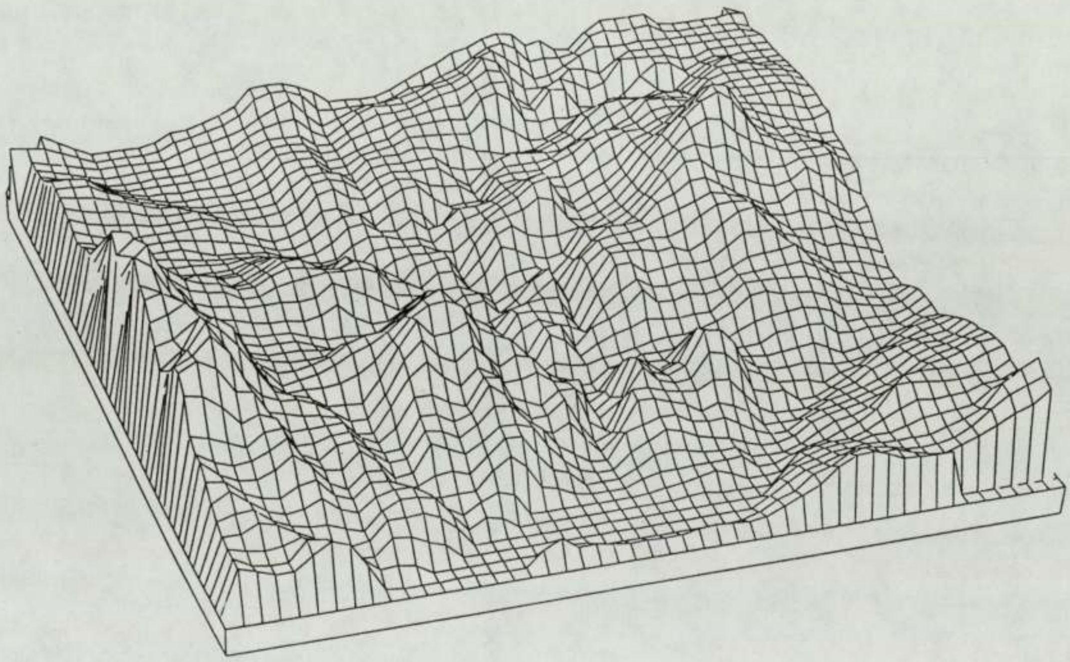

Figure 9.4 Surface interpolation using the TIN to form a DEM.

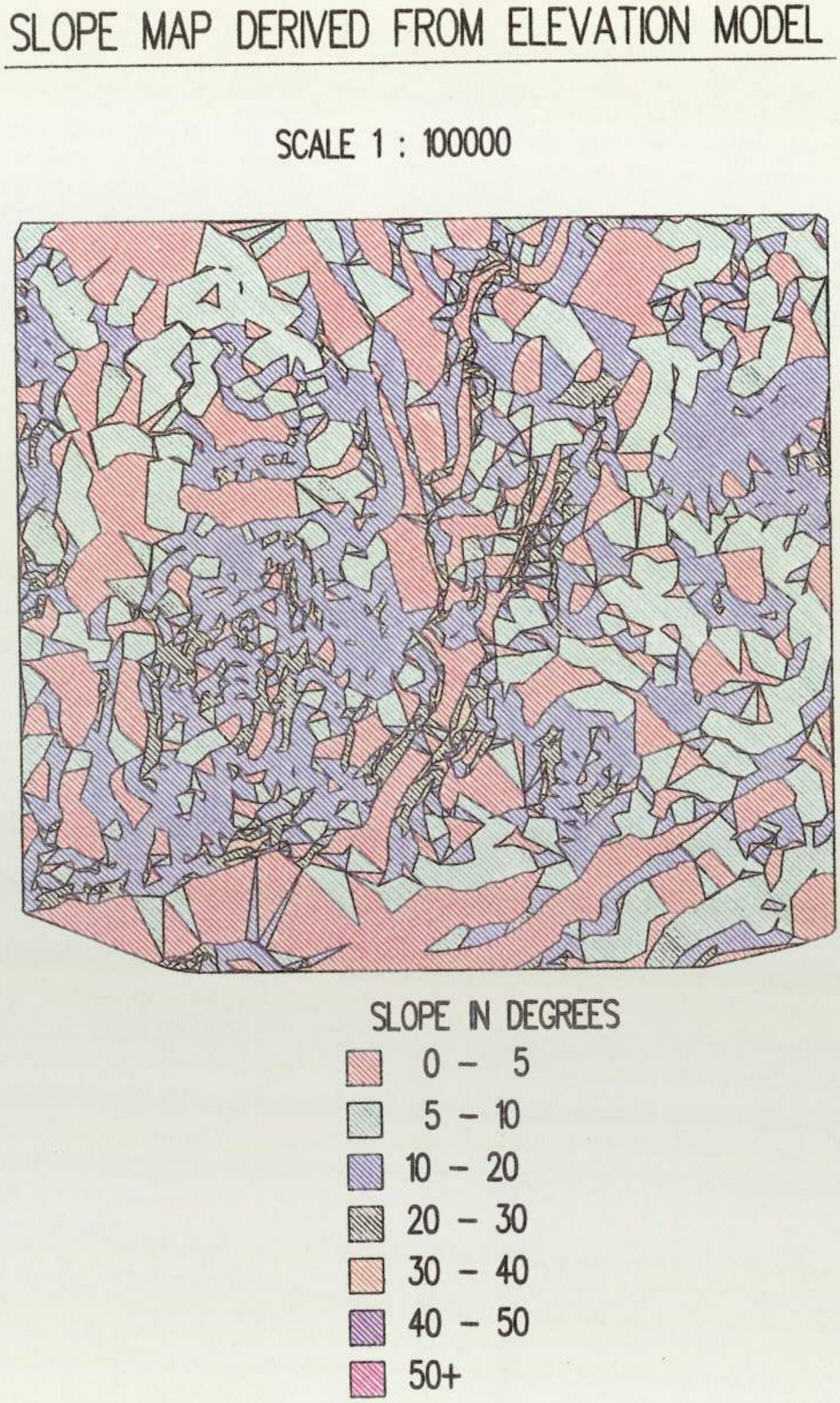

Figure 9.5 Categorised slope map of the research area.

9.4 Soil and Vegetation Types

Polygonal vector data sets of the soil and vegetation types were created from an ECO/TOPO experimental map at 1:50000 scale (Robertson, 1982). The boundaries were digitised using the setup described in Section 9.3. The data sets or "coverages" created were edited before creation of polygon topology again using ARC/INFO software routines. The coverages created are illustrated in Figures 9.6 and 9.7.

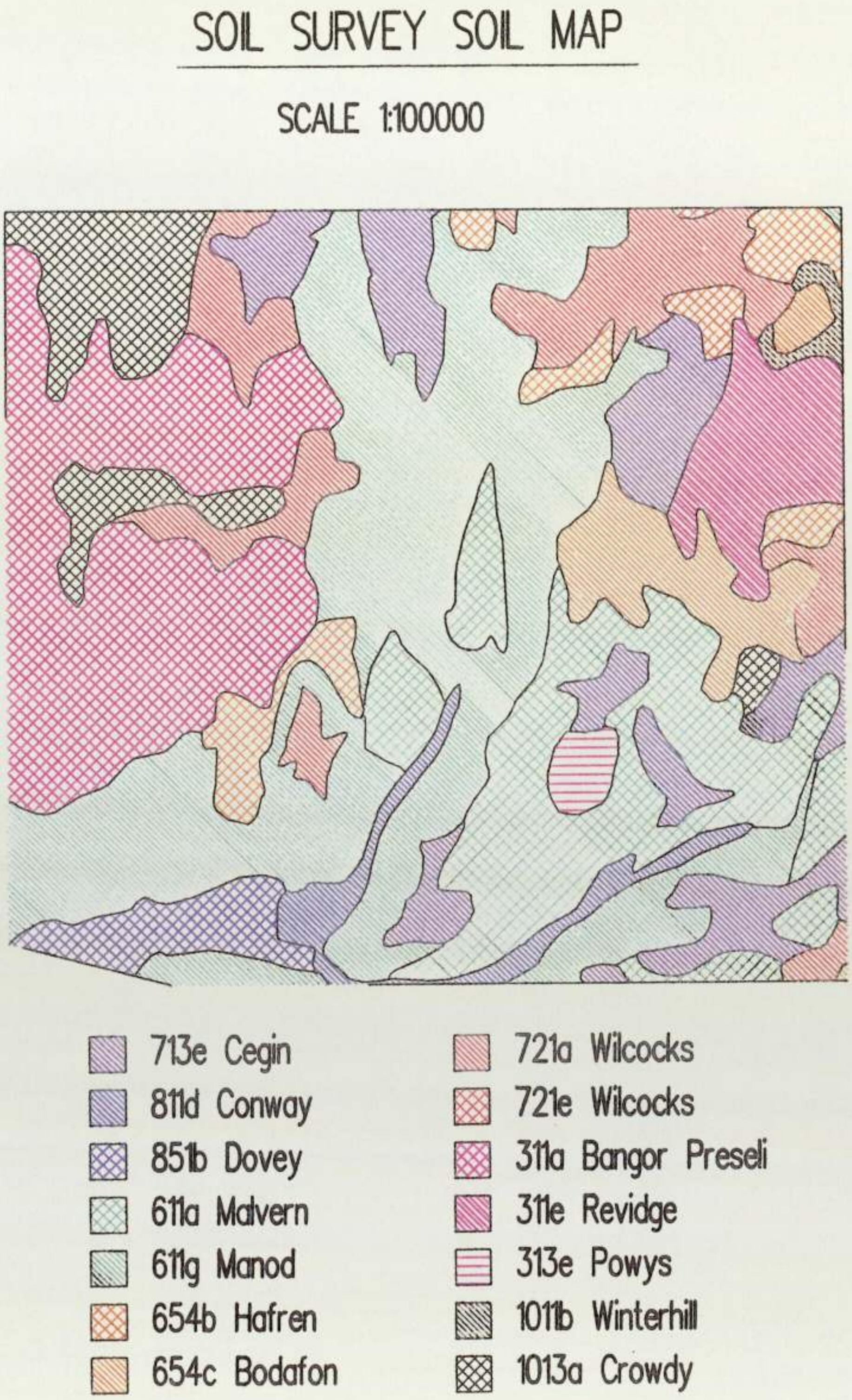

Figure 9.6 Soil types for part of the research area (adapted from Robertson, 1982).

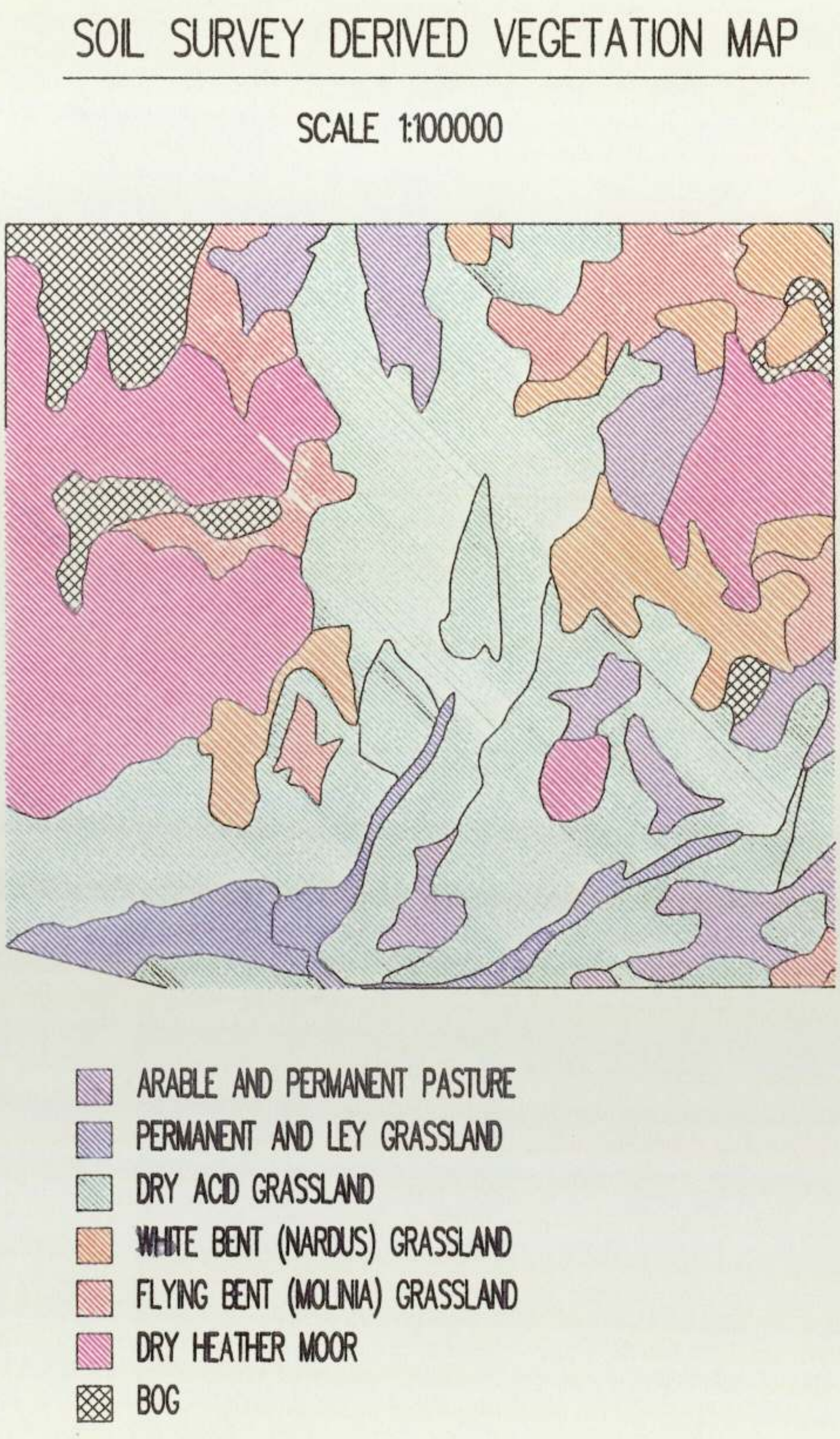

Figure 9.7 Vegetation classes derived from soil types, for part of the research area (adapted from Robertson, 1982).

9.5 Satellite derived Landcover Classes

The aim in this part of the research was to transfer classified satellite data from the image processing system to the GIS for analysis. A landcover classification from the Landsat TM data in System 600 format on the I^2S image processing system was converted to a Single Variable File for input to the ARC/INFO system, using procedures developed by France and Carboni (Boarelli and France, 1989). For analysis the data required further conversion to a polygon topology. This process using the GRIDPOLY function available in ARC/INFO took several hours on a relatively powerful VAX cluster. The final output contained 4714 polygons, and is illustrated in Figure 9.8.

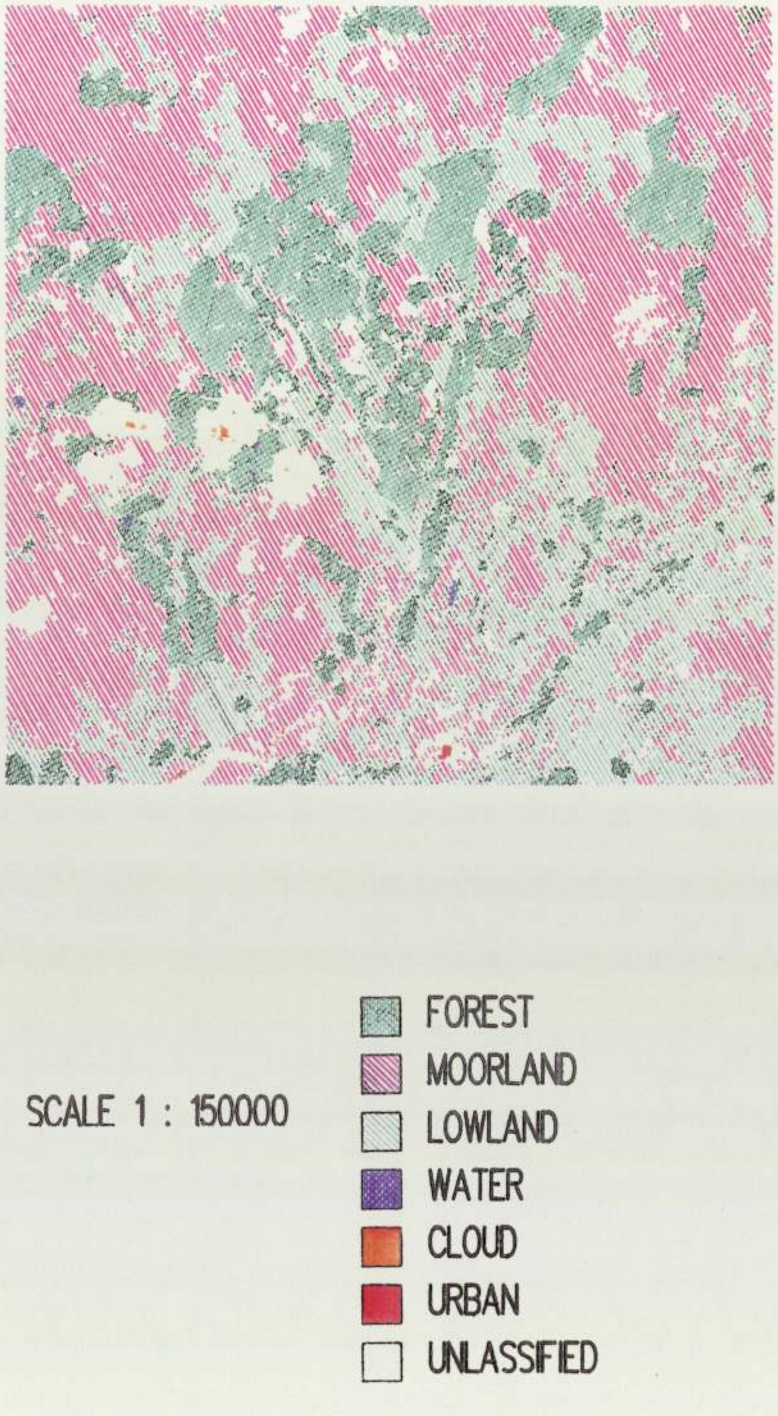

Figure 9.8 Polygonised landcover classification.

A further aim was to digitise the catchment boundaries to facilitate the calculation of each landcover type in each catchment. This was not possible due to the loss of access to ARC/INFO. The author has however used the same procedure for defining landcover classes within comuni (parish) boundaries for part of Northern Italy (Boarelli and France, 1989) using the REPORT function in INFO to list all areas.

9.6 Summary

The use of GIS for data storage, manipulation and analysis has only recently been possible. This chapter has provided only a brief introduction to the many capabilities of GIS. In this research various data types were input to a GIS. These included elevation information with the subsequent creation of DEM and slope classes. Further refinement of this technique is required to smooth the slope classes. Transfer of Landsat TM classifications to the GIS and vectorisation for analysis with other data types was carried out. Hydrologic models can be adapted to take inputs from GIS or whole new models created, based on a GIS. With full raster-vector integration imminent, the opportunities for using remotely sensed data within GIS will be numerous.

CHAPTER TEN: **DISCUSSION, CONCLUSIONS AND RECOMMENDATIONS**

10.1 Discussion

This chapter draws together the results and main points from the preceding chapters. Additional relevant information for making appropriate decisions with regard to remote sensing projects is also included.

The subject of data types was broached in chapter 4, where the differences between the studied data types were highlighted. It should be remembered that all the data types give only a generalisation of the ground reality. In the following chapters the effect of these variations on their usefulness was investigated. Some general questions one must then ask are:

Firstly, will the data type meet the requirements of the application under consideration, and is the user aware of all the potential data types available?

Is the data available for an appropriate time or could it be acquired, maybe for a specific time window. What differences will a different time make e.g. shadow problems, or highlights such as catchment boundaries with a low elevation winter sun?

Have we the equipment for the interpretation, or access to it?

Will the equipment allow all that we want e.g. precise photogrammetric measurements, geocorrection of large images or merging of images?

Have we the experience necessary to carry out the interpretation/image proceesing required? especially with regard to interpreter differences, mis-classification errors.

Which hardcopy type is suitable?

What do we want to do with the results? use them alone or input to a GIS and/or modelling system?

What are the costs involved in each option?

A detailed breakdown of possible costs is given in the report by Aston Unviversity, Civil Engineering Department (Aston, 1987). Broadly speaking the costs can be broken down into acquisition, processing (if required), interpretation, measurement and presentation.

Main results from the data types examined

Some general comments on each of the data types precede specific results. Examination of the aerial photography requires only simple equipment, though for very precise quantitative work a stereoplotter (contourplotter) is needed. For examination of digital data types, in this work the Landsat MSS and Landsat TM data, an image processing system is a pre-requisite. This can be expensive (tens of thousands of pounds) though with increasing processing power/cost ratios many functions can be adequately performed by systems costing less than £10000. Map data can be extracted/input through scanning, frame grabbing or time-consuming manual digitising, depending on the detail required for a particular application.

Stream lengths and networks

For the research area ($235km^2$) in this region of high relief (by British standards) little of the network was discernable from Landsat MSS imagery. Thus, Landsat MSS was of very limited use in this area for network interpretation, with only the major rivers clearly discernable. Sporadic appearances of other smaller streams were insufficient for significant network delineation. A significant network was visible on the Landsat TM, with ground data indicating a majority of 3-5m streams identifiable with even greater recognition over 5m. The aerial photography was useful for delineating more detail than the Landsat TM, even at this relatively small photographic scale. Drainage networks from the Ordnance Survey 1:50000 map showed considerably more drainage detail than any of the other data types.

Landsat TM was useful for the delineation of a fourth order network. The aerial photography also enabled delineation of a fourth order network, with many minor streams. 1:50000 scale map data provided the most comprehensive network details with a fifth order network. The bifurcation ratios derived from the Landsat TM, aerial photography and 1:50000 map showed a degree of similarity but insufficient to draw firm conclusions.

Morphometric catchment parameters

Catchment areas were seen to have a strong correlation both between Landsat TM and

1:50000 map data and between the 1:50000 aerial photos and map data. Very good agreement was seen between the photographically derived catchments and the map data. Basin length and mainstream length values derived from both Landsat TM and the aerial photography also exhibited correlation with 1:50000 map derived values. No correlations were found when examining shape parameters for Landsat TM v map data. Some correlation was seen between map results and the photographically derived basin circularity and lemniscate k parameters.

Rango *et al.* (1975) suggest minimum catchment size of $78km^2$ for interpretation using Landsat MSS data, whereas Drayton *et al.* (1986b) suggest $200km^2$, which seems more appropriate from the experience of this research. For Landsat TM data I would venture to suggest a figure of $30km^2$, for this type of area i.e. with similar topography and vegetation.

Landcover Classes

The panchromatic aerial photography enabled discrimination of the classes under consideration, with stereoscopy aiding the moorland/lowland class division. Colour photography would be preferred for vegetation discrimination where available.

The Landsat TM landcover classifications showed a fair degree of similarity between visual and automatic classification methods, with some minor discrepancies between interpreters. Landsat MSS classifications showed agreement with the Landsat TM results, apart from some small areas of discrepancy. Results of accuracy checking revealed visual interpretation to be the most successful method of classification with 77.5% accuracy. However, more specific ground data are required for a full determination of accuracy using each method.

The author is involved in on-going collaborative work on landcover classification. This has entailed examining three of the Institute of Hydrology's experimental catchments, two upland and one lowland catchment using Landsat TM and Multispectral SPOT data. Results using a greater number of landcover classes than in this research have proved very positive (Roberts, France and Robinson (in press); Roberts *et al.* (in press)).

10.2 Conclusions

For drainage network interpretation at least one near infrared band should be selected. If the interpretation is carried out using a single band then Landsat MSS band 7 or Landsat TM bands 4 or 5 should be used. For colour interpretations several Landsat TM band combinations were seen to be appropriate for interpretation, namely bands 5,4,1; 4,5,3; 5,4,3 and 4,3,2. For Landsat MSS, bands 7,6,5 were found to be more suitable for drainage detail interpretation than the usual 7,5,4 band combination which was used for visual interpretation of vegetation classes. High pass filtering was found to aid in the interpretation of drainage features.

The Landsat MSS data was not suitable for network delineation in this area, since only a small part of the network was delineated. Landsat TM enabled the interpretation of a considerable network though less than the aerial photography. A degree of subjectivity was evident in the interpretation of first order streams on the Landsat TM imagery. Errors of mis-classification of linear features such as roads and tree lines or hedgerows with rivers were considered mainly attributable to lack of experience in photo-interpretation techniques.

Catchment area interpretations from Landsat TM imagery were seen to have high correlation with 1:50000 scale map data. This is consistent with findings for Landsat MSS data by previous workers. Strong correlations were also seen for the basin length and mainstream length parameters. Landsat TM derived stream length and basin shape parameters exhibited no correlation with map derived parameters. The aerial photography showed some correlation for the shape parameters in addition to area, basin length and mainstream length. Landsat TM imagery appears suitable for the interpretation of catchments to a minimum size of around $30km^2$ in areas with relatively high topographic variation and well developed drainage networks, however the examination of similar types of area is required to confirm this.

No significant differences were found in visual interpretation of imagery using either colour transparencies via the Lamprey Box or interpreting directly from the image analysis monitor using the on screen method. Interactive landcover discrimination using a trackball is not recommended due to the excessive time involved.

Landcover classifications for the broad categories considered generally showed good agreement, though some discrepancies were encountered. Results for the visual interpretation and automatic classification of the Landsat TM imagery were very similar, with the exception of small areas of water and urban class in the unsupervised classification of Landsat TM. Landsat TM visual interpretations compared well with the aerial photogaphic photo-interpretation, but showed some differences with the Landsat MSS visual interpretation. Minor differences were seen in the visual interpretation of Landsat TM by different interpreters, though this may be partly due to inexperience.

For the automatic classification of landcover types near infrared and visible bands were employed with success for either Landsat TM or Landsat MSS imagery. In both supervised and unsupervised classification procedures operator decisions with regard to training area selection, band selection, confidence limits or the merging of output classes were seen as critical to the outcome of the classifications. Classification using vegetation indices for hydrological modelling is an area worth further investigation.

On examination of 34 lakes in the area, the Landsat TM imagery was found suitable for discriminating some lakes as small as 0.3 ha, though for consistent identification a figure of 0.6ha is suggested.

The transfer of raster Landsat classifications to vector GIS is possible, with subsequent vectorisation for integrated analysis with other data types.

10.3 Recommendations and future possibilities

The success of Landsat TM in delineating drainage details in an upland area needs comparison in a lowland area, especially with regard to the estimation of catchment area. Absolute locational accuracies of the interpreted areas requires quantitative assessment either manually or in a spatial analysis system such as a GIS. Further work is also needed on the assessment of drainage network variation.

Examination of a Landsat TM spectrascan print of a band 5,4,1 FCC with high pass filtering would enable comparison between the hard copy types examined in this research and a common interpretation media, which the author was unable to examine during this research.

Drainage details interpreted from Landsat TM imagery or aerial photography and input to GIS systems could be used in the assessment of morphometric parameters. The assessment of relationships between morphometric drainage details and other data, such as elevation information (DEM), vegetation type, soil type, geology, precipitation could also be carried out in such an environment.

One step further is the use of these data sets for hydrological modelling under a finite element scenario. With information from satellite and ground-based radar on precipitation, antecedent moisture conditions (possibly from microwave sensors on ERS-1), a DEM, a Landsat TM derived vegetation classification, soil type and geological information also possibly from remote sensing sources. The author is currently involved in applying remote sensing and GIS techniques for the provision of parameter requirements in the Institute of Hydrology Distributed Model (Roberts, Calver and France, 1990).

The potential of Landsat TM data for landcover identification has led to the commencement of a landcover mapping project for Great Britain using Landsat TM, which is due for completion in 1992 (Jones, pers. comm.). This data source will then be available for use in digital modelling.

Proposals for Landsat 7 include an along-track stereoscopic capability with topographic accuracy of 20m or better (Colvocoresses, 1990). Gerard Brachet (1990) refers to the development of along-track steroscopic coverage with 5m spatial resolution in satellites after SPOT 4. These proposals indicate the possibility of extensive topographic mapping from satellite data, with the creation of DEM's. This has been possible with current SPOT satellites but on a limited scale with off-nadir viewing.

It certainly seems that the future offers much scope for the use of remote sensing, geographic information systems and digital elevation models in many areas of hydrology.

REFERENCES

Abbott, M.B., Bathurst, J.C., Cunge, J.A., O'Connell, P.E. and Rasmussen, J. (1986). An introduction to the European Hydrological System-Systeme Hydrologique Europeen, "SHE", 1: History and philosophy of a physically-based, distributed modelling system. J. Hydrol., 87: 45-59.

Abrahams, A.D. (1972). Drainage densities and sediment yields in eastern Australia. Australian Geographical Studies 10, 19-41.

Allewijn, R. (1990). Remote Sensing and Runoff Modelling in Alpine areas. A Landsat-supported conceptual semi-distributed rainfall-runoff model, applied to the N-Italian Alps. Ph D thesis, Free University of Amsterdam.

Allord, G.J., Scarpace, F.L. (1979). Improving streamflow estimates through use of Landsat. In Satellite Hydrology, 5th Annual William T. Pecora Memorial Symp. on Remote Sensing, American Water Resources Association, Minneapolis, MN, 284-291.

Ambaruch, R., Simmons, J.W. (1973). Application of remote sensing to hydrology. NASA Report No. CR 120278.

Anderson, M.G., Burt, T.P. (1985)(Eds.). Hydrological Forecasting. Wiley & Sons, Chichester, UK. 604pp.

Anuta, P.E. (1977). Computer-assisted analysis techniques for remote sensing data interpretation. Geophysics, Vol. 42, 468-481.

ASAE (American Society of Agricultural Engineers) (1982). Hydrologic modeling of small watersheds. ASAE Monograph No. 5, Haan, C.T., Johnson, H.P., Brakensiek, D.L. (Eds.). 533pp.

Astaras, T., 1985. Drainage network analysis of Landsat images of the Olympus-Pieria mountain area, northern Greece. Int. Jour, Remote Sensing, Vol. 6, No. 5, 673-686.

Astaras, T., Lambrinos, N., Soulakellis, N. (1990). A drainage system analysis evaluation of, and comparison between, Landsat-3 RBV, Landsat-5 TM and SPOT PA imageries covering the Central Macedonia district, Greece. Int. Jour. Remote Sensing, Vol. 11, No. 9, 1549-1559.

Aston University, (1987). An assessment of currently available Satellite and Aerial imagery in evaluating Water Resources and Landcover. A report by Aston University Civil Engineering Department for National Remote Sensing Centre, RAE, Farnborough, UK.

Atkinson, P. (1988). The interrelationship between resampling method and information extraction technique. Proceeding of IGARSS '88 Symposium, Edinburgh, Scotland, 13-16 Sept. 1988. ESA SP-284 (IEEE 88CH2497-6). ESA Publications Division. 521-527.

Baker, J.R., Briggs, S.A., Gordon, V., Jones, A.R, Settle, J.J, Townshend, J.R.G., Wyatt, B.K. (1991). Advances in classification for land cover mapping using SPOT HRV imagery. Int. Jour. Remote Sensing, Vol. 12, No. 5, 1071-1085.

Barrett, E.C., Herschy, R.W. (1985). A European perspective on satellite remote sensing for hydrology and water management. Hydrologic Applications of Space Technology (Proceedings of the Cocoa Beach Workshop, Florida, August 1985). IAHS Publ. No. 160, 1986.

Belward, A.S., Taylor, J.C., Stuttard, M.J., Bignal, E., Mathews, J., Curtis, D (1990). An unsupervised approach to the classification of semi-natural vegetation from Landsat Thematic Mapper data. Int. Jour. Remote Sensing, Vol. 11, No. 3, 429-445.

Benson, M. (1959). Channel slope factor in flood frequency analysis. Proc. Amer. Soc. Civ. Engrs, 85 (HY4), 1-19.

Beven, K.J., Kirkby, M.J. (1979). A physically based, variable contributing area model of basin hydrology. Hydrological Sciences Bull., 24, 43-69.

Billingsley, F.C. (1983) (ed.). Data processing and reprocessing. Chapter 17 in The Manual of Remote Sensing 2nd edn., R.N. Colwell (ed.), The American Society of Photogrammetry and Remote Sensing, Vol. 1, 719-792.

Blyth K., Rodda, J.C. (1973). A stream length study. Water Resources Research Vol. 9, No. 5.

Blyth, K. (1981). Remote Sensing in Hydrology. Institute of Hydrology, Wallingford, Oxon. UK, Report No. 74.

Boarelli, G., France, M.J. (1989). Progetto Territorio Analisi del Territorio, Sviluppo Metodologie. Unpublished report by Telespazio Spa. Rome, Italy.

Boorman, D.B., Hollis, J.M. (1990). Hydrology of soil types. A hydrologically-based classification of the soils of England and Wales. MAFF Conference of River and Coastal Engineers, Loughborough University, 1990.

Brachet, G. (1990). SPOT programme status: medium term and long term planning on the basis of market requirements. Remote Sensing Society Bulletin, June 1990, 1067-1071.

Brown, H.E. (1970). Man shapes the earth. Geographical Jour. 136, 74-84.

Chavez, P.C., Bauer, B. (1982). An Automatic Optimal Kernel-Size Selection Technique for Edge Enhancement. Remote Sensing of Environment, Vol.12, 22-38.

Chavez, P.C., Guptill, S.C., Bowell, J.A. (1984). Image Processing Techniques for Thematic Mapper Data. Technical Papers, 50th Annual Meeting of the American Society of Photogrammetry, Vol. 2, 728-743.

Chidley, T.R.E, Drayton, R.S. (1986a). Visual interpretation of standard satellite images for the design of water resources schemes. Hydrologic Applications of Space Technology (Proceedings of the Cocoa Beach Workshop, Florida, August 1985). IAHS Publ. No. 160, 1986.

Chidley, T.R.E, Drayton, R.S. (1986b). The use of SPOT-simulated imagery in hydrological mapping. Int. Jour. Remote Sensing, Vol. 7, No. 6, 791-799.

Chorley, R.J, Malm, D.E.A., Pogorzelski, H.A. (1957). A new standard for estimating drainage basin shape. Amer. Jour. Sci., 255, 138-141.

Chorley, R.J. (1969). The drainage basin as the fundamental geomorphic unit. In Water, Earth and Man, a synthesis of hydrology, geomorphology and socio-economic geography, Chorley, R.J. (Ed.) pp 77-99. Methuen, London.

Chow, V.T. (1964). Handbook of Applied Hydrology. McGraw-Hill.

Clark, C. (1986). Assessing the accuracy of Landsat TM in determining parameters for use in hydrological models. Final year Undergraduate project. Aston University, Civil Engineering Dept.

Clayden, B., Hollis, J.M. (1984). Criteria for differentiating soil series. Soil Surv. Tech. Monogr. No.17.

Colvocoresses, A.P. (1986). Image mapping with the Thematic Mapper. Phot. Engrg. and Rem. Sens. Vol. 52, No. 9, 1499-1505.

Colvocoresses, A.P. (1990). An operational earth mapping and monitoring satellite system: a proposal for Landsat 7. Phot. Engrg. and Rem. Sens. Vol. 56, No. 5, 569-571.

Cooper, S., Beck P., Harowitz, J., Toran, D. (1975). The use of ERTS imagery in reservoir management and operation. Final report of Corps of Engineers, Waltham, Massachusetts. March 1975.

Crawford, N.H., Linsley, R.K. (1966). Digital simulation in Hydrology: Stanford Watershed Model IV. Technical report 39, Dept. of Civil Engineering, Stanford University, U.S.

Crist, E.P., Cicone, R.C. (1984a). Comparisons of the Dimensionality and features of simulated Landsat-4 MSS and TM data. Remote Sens. of Environ. Vol. 14, 235-246.

Crist, E.P., Cicone, R.C. (1984b). Application of the Tasseled Cap Concept to Simulated Thematic Mapper Data. Phot. Eng. & Rem. Sens., Vol. 50, No.3, 3443-352.

Curran, P.J. (1985). Principles of Remote Sensing. Longman, London & New York.

Drayton, R.S., Chidley, T.R.E. (1985). Hydrologic modelling using satellite imagery. International conference on Advanced technology for monitoring and processing global environmental data, Remote Sensing Society and CERMA. Publ. Remote Sensing Society. 219-225.

Drayton, R.S., Kidd, C.H.R, Mandeville, A.N., Miller, J.B. (1980). A regional analysis of river floods and low flows in Malawi. Institute of Hydrology, Wallingford, Oxon, UK. Report No. 72.

Drayton, R.S., Chidley, T.R.E., Rees, S.W., Pritchard, A.J. (1986a). Visual interpretation of satellite imagery for the estimation of key parameters in hydrologic models. Institute of British Geographers Annual Conference, Reading University, January 1986.

Drayton, R.S., Chidley, T.R.E., Collins, W.G. (1986b). International seminar on Photogrammetry and Remote Sensing for the Developing Countries, ISPRS< New Delhi, 1986.

Drayton, R.S., Chidley T.R.E, Collins, W.G. (1986c). Simple classifiers of satellite data for hydrologic modelling. Symposium on Remote Sensing for Resources Development and Environmental Management, Enschede, Netherlands. Balkema, Rotterdam. 709-711.

Drury, S.A. (1987). Image interpretation in Geology. Allen and Unwin, London.

Duda, R.O., Hart, P.E. (1973). Pattern classification and scene analysis. John Wiley, N.Y.

Dunne, T., Dietrich, W.E. (1980). Experimental investigation of Horton overland flow on tropical hillslopes - 2. Hydraulic characteristics and hillslope hydrographs. Zeitschrift fur Geomorphologie, Supplement 35, 60-80.

Eagleson, P.S. (1970). Dynamic Hydrology, McGraw-Hill, New York.

Engman, E.T. (1986). Hydrologic research before and after AgRISTARS. IEEE Trans. on Geosc. and Rem. Sens., Vol. GE-24, No. 1, 5-11.

Engman, E.T, Gurney, R.J. (1991). Remote Sensing in Hydrology. Chapman and Hall.

ESRI, (1987). Introduction to TIN. Environmental Systems Research Institute, Redlands, California.

Evans, D. (1986). Assessing the accuracy of Landsat TM in determining parameters for use in hydrological models. Final year Undergraduate project. Aston University, Civil Engineering Dept.

Farnsworth, R.K., Barrett, E.C., Dhanju, M.S. (1984). Application of remote sensing to hydrology including groundwater. Technical Documents in Hydrology, UNESCO, Paris, 122pp.

Fett, W., Neumann, P., Schultz, G.A. (1990). Hydrological model based on satellite imagery and GIS. International Symp. on Remote Sensing and Water Resources, Enschede, Netherlands, 20-24 Aug. International Assoc. of Hydrogeologists and Netherlands Society for Remote Sensing. 347-357.

Fortin, J.P., Villeneuve, J.P, Guillot, A., Seguin, B. (1986). Development of a modular hydrological forecasting model based on remotely sensed data, for interactive utilization on a microcomputer. Hydrologic Applications of Space Technology, IAHS Publ. No. 160, 307-319.

France, M. J.; Hedges P. D. 1986. A hydrological comparison of Landsat TM, Landsat MSS and black & white aerial photography. International Society for Photogrammetry and Remote Sensing Comission VII, Enschede, Netherlands, 24-29 August 1986, 717-720.

France, M. J.; Chidley, T.R.E.; Collins, W.G., 1986. Extraction of hydrological parameters from Landsat Thematic Mapper imagery. Twentieth International Symposium on Remote Sensing of Environment, Nairobi, Kenya, 4-10 December 1986, 1165-1174.

France, M.J., Hedges, P.D., 1988. The appropriate use of remotely sensed satellite data for water resource assessment and modelling. Remote sensing for operational applications. The Remote Sensing Society Annual Conference, University of Bristol, Bristol. 147-153.

Friedman, S.Z. (1980). Mapping Urbanized Area Expansion through Digital Image Processing of Landsat and Conventional Data, Pasadena, Calif.: Jet Propulsion Laboratory Publication, 79-113.

Fuller, R.M. (1981). Aerial photographs as record of changing vegetation patterns. In Ecological Mapping from Ground, Air and Space, Symp. Nov. 25-27. Institute of Terrestrial Ecology, NERC, Monks Wood, Abbots Ripton, Huntingdon.

Gardiner, V. (1982). Stream networks and digital cartography. In perspectives in alternative cartography: cartographic computing technology and its applications. Cartographica, Vol. 19, No. 2, 38-44.

Goldberg, M., Schlien, S. (1978). A clustering scheme for multispectral images. IEEE Transactions on Systems, Man and Cybernetics, SMC-8, 86-92.

Gray, D.M. (1961). Interrelationships of watershed characteristics. Jour. Geophys. Res., 66, 1215-1223.

Gregory, K.J., Walling, D.E. (1973). Drainage Basin Form and Process, A geomorphological approach. Edward Arnold, London.

Groves, J.R., Ragan, R.M., Clapp, R.B. (1983). Development and testing of a remote sensing based hydrological model. Hydrological Applications of Remote Sensing and Remote Data Transmission (Proceedings of the Hamburg Symposium, August 1983). IAHS Publ. No. 145. 601-612.

Hack, J.T. (1957). Studies of longitudinal stream profiles in Virginia and Maryland, US Geological Survey Prof. Paper No. 294-B.

Hall, D.G.M., Reeve, M.J., Thomasson, A.J., Wright, V.F. (1977). Water retention, porosity and density of field soils. Soil Surv. Tech. Monogr. No. 9. Soil Survey England and Wales.

Haralick, R.M., Fu, K. (1983). Pattern recognition and classification. Chapter 18 in The Manual of Remote Sensing 2nd edn., R.N. Colwell (ed.), The American Society of Photogrammetry and Remote Sensing, Vol. 1, 793-805.

Hodgson, J.M. (1976). Soil survey field handbook. Soil Surv. Tech. Monogr. No. 5.

Horton, R.E. (1932). Drainage basin characteristics. Trans. Am. Geophys. Union, Vol. 13, 350-361.

Horton, R.E. (1945). Erosional development of streams and their drainage basins: hydrophysical approach to quantitative morphology. Bull. Geol. Soc. Am., Vol. 56, 275-370.

Hyatt, E.C., Cox, J.J, Collins, W.G. (1988). Advances in computerized retrieval in remote sensing. Int. Jour. Remote Sensing, Vol. 9, Nos. 10 and 11, 1739-1750.

Jackson, T.J., Ragan, R.M., Fitch, W.N. (1977). Test of Landsat-based urban hydrologic modelling. ASCE J. Resour. Plann. Manage. Div. 103, No. WR1, Proc. Paper 12950, 141-158.

Jensen, J.R. (1986). Introductory digital image processing - a remote sensing perspective. Prentice-Hall, Englewood Cliffs, New Jersey.

Kauth, R.J., Thomas, G.S. (1976). The Tasseled Cap - A graphic description of the Spectral - Temporal Development of Agricultural Crops as seen by Landsat. Proceedings of Symposium on Machine Processing of Remotely Sensed Data. West Lafayette, Ind.: Laboratory for the Applications of Remote Sensing, 41-51.

Kennedy, J.B., Neville, A.M. (1976). Basic statistical methods for engineers and scientists, 2 edn. Harper & Row, New York.

Khorram, S., Brockhaus, J.A., Geraci, A (1991). A regional assessment of land-use/land-cover types in Sicily with TM data. Int. Jour. Remote Sensing, Vol. 12, No.1, 69-78.

Knighton, D. (1984). Fluvial forms and processes. Edward Arnold, London, 218pp.

Kokelaar, B.P. (1977). Tremadoc to Llanvirn volcanism on the south east side of the Harlech Dome (Rhobell Fawr), North Wales. In The Caledonides of the British Isles - reviewed. Harris, A.L., Holland, C.H., Leake, B.E. (Editors). Spec. Publ. Geol. Soc. London, No. 8, 591-596.

Kudritskii, D.M., Popov, I.V., Romanova, E.A. (1966). Hydrographic interpretation of aerial photographs. Oldbourne press.

Landegrebe, D.A. and staff (1975). A study of the utilization of ERTS-1 data from the Wabash River Basin, Laboratory for the Applications of Remote Sensing, Purdue University, Western Lafayette, Indiana, Information Note 052375.

Luthin, J.N. (1957). Drainage of agricultural lands. American Society of Agronomy. Madison, Wisconsin.

Manual of Remote Sensing, 2 Edn. (1983). American Society of Remote Sensing, Falls Church, Virginia.

Mather, P.M. (1987). Computer processing of remotely-sensed images - an introduction. Wiley and Sons.

Mauser, W. (1984). Calculation of flood hydrographs using satellite-derived land-use information in the Dreisam watershed/S-W Germany. Proc. IGARSS '84 Symp., ESA-SP-215, 301-304.

Melton, M.A. (1957). An analysis of the relations among elements of climate, surface properties and geomorphology. Office of Naval Research, Geography Branch, Project NR 389-042, Tech. Rep. 11.

Melton, M.A. (1958). Correlation structure of morphometric properties of drainage systems and their controlling agents. Jour. Geol., 66, 442-460.

Meteorological Office, (1967). Map of Rainfall: Annual average 1916-1950. Publ. Ordnance Survey.

Miller, V.C. (1953). A quantitative geomorphic study of drainage basin characteristics in the Clinch Mountain area, Virginia and Tennesee. Office of Naval Research, Geography Branch, Project NR 389_042, Tech. Rep. 3.

Mogorovich, P. (1987). Integrating TM and Cartographic data. Proc. of Workshop on "Earthnet Pilot Project on Landsat Thematic Mapper Applications", Frascati, Italy, Dec. 1987. ESA SP-1102 - ISBN 92-9092-000-9 May 1989. 323-331.

Moik, J.G. (1980). Digital processing of remotely sensed images. NASA, Washington DC.

Moore, I.D., Grayson, R.B., Ladson, A.R. (1991). Digital terrain modelling: A review of hydrological, geomorphological and biological applications. Hydrological Processes, Vol. 5, 3-30.

More, R.J. (1969). The basin hydrological cycle. In Water, Earth and Man. Methuen, London.

Mulders, M.A. (1987). Remote Sensing in Soil Science. Devlopments in Soil Science No. 15. Elsevier.

Naef, F. (1981). Can we model the rainfall-runoff process today? Hydrological Sci. Bull., Vol. 26, No. 3, 281-289.

NASA, (1976). Landsat data users handbook. NASA document 76SDS4258 Goddard Space Flight Center, Washington, DC.

NASA, (1984). Earth Observing System, Working Group Report, Vol. 1, NASA/Goddard Space Flight Center, Greenbelt, MD.

NERC, (1975). Flood Studies Report. Natural Environment Research Council, Swindon.

NERC, (1985). Hydrometric Yearbook 1981. NERC, Swindon.

NERC, (1986). Hydrometric Yearbook 1984. NERC, Swindon.

Newson, M. (1975). Mapwork for flood studies, Part 1: Selection and derivation of Indices. Institute of Hydrology, Wallingford, Oxon, UK. Report No. 25 (Part 1).

Newson, M. (1976). Mapwork for flood studies, Part 2: Analysis of indices and re-mapping. Institute of Hydrology, Wallingford, Oxon, UK. Report No. 25 (Part 2).

Ongley, E.D. (1968). Towards a precise definition of drainage basin axis. Australian Geogr. Stud., No. 6, 84-88.

Parde, M. (1955). Fleuves et Rivieres (3 Edn.), Armand Colin, Paris.

Palero, M.M. (1990). The unit hydrograph approach based on morphological parameters determined with air photographs, Landsat Multi Spectral Scanner and Thematic Mapper data. In Proc. Int. Symp. on Remote Sensing and Water Resources, Enschede, Netherlands, 20-24 Aug. International Assoc. of Hydrogeologists and Netherlands Sociey for Remote Sensing. 427-432.

Peck, E.L., Keefer, T.N., Johnson, E.R. (1981). Strategies for using remotely sensed data in hydrologic models. NASA Rep. No. CR-66729, Goddard Space Flight Center, Greenbelt, MD.

Penman, H.L. (1948). Natural evaporation from open water, bare soil and grass. Proc. Royal Soc. A, Vol. 193, 120-145.

Penning-Rowsell, E.C. (1969). The morphometric analysis of drainage basins from maps. Occasional Paper No. 1. Department of Geography, University College, London.

Rakhmanov, V.V. (1966). Role of forests in water conservation, Israel Program for Scientific Translations, Jerusalem.

Rango , A. (1975). Applications of remote sensing to watershed management. In Guidelines for Watershed Management, FAO Conservation Guide, FAO, Rome, Italy. 37-50.

Rango, A. (1990). Remote sensing of water resources: accomplishments, challenges and relevance to global monitoring. In Proc. Int. Symp. on Remote Sensing and Water Resources, Enschede, Netherlands, 20-24 Aug. International Assoc. of Hydrogeologists and Netherlands Society for Remote Sensing. 3-16.

Rango, A., Foster, J., Salomonson, V.V., (1975). Extraction and utilization of space acquired physiographic data for water resources development. Water Res. Bull., Vol. 11, No. 6, 1245-1255.

Richardson, A.J., Wiegand, C.L. (1977). Distinguishing vegetation from soil background information. Photogr. Eng. and Remote Sensing, Vol. 43, No. 2, 207-216.

Rodda, J.C. (1969). The flood hydrograph: in Water, Earth and Man (Ed. Chorley, R.J.). Methuen, 405-418.

Roberts, G., Calver, A., France, M. (1990). The use of remote sensing and geographic information systems for providing the parameter requirements of the Institute of Hydrology Distributed Model. XV General Assembly, European Geophysical Society, Copenhagen, 23-27 April, 1990.

Roberts, G., France, M., Robinson, M. Computing the water balance of a small agricultural catchment in southern England by consideration of different land-use types. I. Land classification using remotely sensed imagery. Jour. Agricultural Water Management (in press).

Roberts, G., France, M., Johnson, R.C., Law, J.T. The analysis of remotely-sensed images of the Balquhidder area of Scotland for estimating percentages of land cover types in the Kirkton and Monachyle catchments. Journal of Hydrology (in press).

Robertson, J.S., (1982). Map published with paper by Bickmore, D.P. - Mapping the Vegetation of Britain. In Perspectives in the Alternative Cartography: Cartographic Computing Technology and its Applications. Cartographica, Vol. 19, No.2, 100-106.

Robinson, G.S. (1977). Edge detection by compass gradient masks. Computer graphics and image processing, Vol. 6, 492-501.

Rosenfeld, A., Kak, A.C. (1976). Digital picture processing. Academic press, New York.

Rosenfeld, A., Kak, A.C. (1982). Digital picture processing. Second edition, Vol. 1, Academic Press, N.Y.

Rouse, J.W., Haas, R.H, Schell, J.A., Deering, D.W. (1973). Monitoring vegetation systems in the great plains with ERTS; 3rd ERTS Symp. NASA SP-351, I:309-317.

Rouse, J.W., Haas, R.H, Schell, J.A., Deering, D.W., Harlan, J.C. (1974). Monitoring of the vernal advancement and retroradiation (greenwave effect) of natural vegetation. Report No. RSC 1978-4, Remote Sensing Center, Texas A&M Univ., College, Satation, TX.

Rudeforth, C.C. (1967). Upland soils from Lower Palaeozoic sedimentary rocks in Mid-Wales. Rep. Welsh Soils Discussion Group No. 8. 42-51.

Rudeforth, C.C. (1970). Soils of north Cardiganshire. Mem. Soil Surv. Gt. Br.

Rudeforth, C.C., Thomasson, A.J. (1970). Hydrological properties of soils in the River Dee catchment. Soil Survey Spec. Surv. No. 4.

Sabins, F.F. (1987). Remote Sensing Principles and Interpretation (2 edn). Freeman, New York.

Salomonson, V.V., Ambaruch, R., Rango, A., Ormsby, J.P, (1975). Remote sensing requirements as suggested by watershed model sensistivity analyses. Proc. 10th Symp. on Remote Sensing of Environment, Ann Arbor, MI, Environmental Research Institute of Michigan , Ann Arbor, MI, 1273-1284.

Schowengerdt, R.A. (1983). Techniques for Image Processing and Classification in Remote Sensing. Academic Press, N.Y.

Schumm, A.C. (1954). Evolution of draiange systems and slopes in badlands at Perth, Amboy, New Jersey. Office of Naval Research, Project NR 389-042, Tech. Rep. 8.

Scheidegger, A.E. (1965). The algebra of stream-order numbers, USGS Prof. Paper, No. 525-B, 187-189.

Schultz, G.A. (1988). Remote Sensing in Hydrology. Jour. of Hydrol., 100: 239-265.

Schultz, G.A. (1989). Remote Sensing of Watershed Characteristics and Rainfall Input. In Unsaturated Flow in Hydrologic Modeling Theory and Practice. Kluwer Academic. 301-323.

Shelton, R.C., Estes, J.E. (1981). Remote Sensing and geographical information systems: an unrealised potential. Geo-Processing 1: 395-420.

Short, N.M. (1982). The Landsat Tutorial Workbook: Basics of Satellite Remote Sensing. NASA Reference Publ. 1078, Washington DC.

Simonett, D.S., Smith, T.R., Tobler, W., Marks, D.G., Frew, J.E., Dozier, J.C. (1977). Geobase Information System Impacts on Space Image Formats. Santa Barbara Remote Sensing Unit Technical Report 3. University of California, Santa Barbara.

Slater, P.N. (1980). Remote sensing: optics and optical systems. Addison-Wesley, Reading, Massachusetts.

Smart, J.S., Surkan, A.J. (1967). The relation between Mainstream length and Area in Drainage Basins. Water Resources Research, Vol. 3, No. 4 963-974.

Smart, J.S. (1972). Channel Networks in Advances in Hydroscience, Vol. 8., 305-344. Academic Press, N.Y.

Steube, M.M., Johnston, D.M. (1990). Runoff volume estimation using GIS techniques. Water Resources Bull. Vol. 26, No. 4. 611-620.

Strahler, A.N. (1950). Equilibrium theory of erosional slopes approached by frquency distribution analysis. Amer. Jour. Sci., 248, 673-696; 800-814.

Strahler, A.N. (1952). Dynamic basis of geomorphology. Bull. Geol. Soc. Amer., 63, 923-938.

Strahler, A.N. (1958). Dimensional analysis applied to fluvially eroded landforms, Bull. Geol. Soc. Am., 69, 279-300.

Strahler, A.N. (1964). Quantitative geomrphology of drainage basins and channel networks, Section 4-II, in V.T. Chow (Ed.), Handbook of Applied Hydrology, McGraw-Hill. 4-39 to 4-76.

SSEW, (1984). Soils and their use in Wales. Soil Survey of England and Wales, Bulletin No. 11. SSEW, Harpenden, England.

Szekielda, K.H. (1988). Satellite monitoring of the Earth. John Wiley, N.Y. 326pp.

Thomasson, A.J. (1975). Soils and field drainage. Soil Surv. Tech. Monogr. No. 7.

Townshend, J.R.G., Cushnie, J.N., Hardy, J.R., Wilson, A. (1988). Thematic Mapper Data - Characteristics and Use. NERC, Swindon.

Townshend, J.R.G. (1984). Agricultural landcover discrimination using thematic mapper spectral bands. Int. Jour. Remote Sensing, Vol. 5, 681-698.

Trevett, W. (1990). Remote Sensing and Geographical Information Systems, their role in Hydrology and Environmental Planning and Management. Unpubl. Paper presented at Remote Sensing and Water Resources, Enschede, Netherlands, 20-24 Aug. 5pp.

Tucker, C.J. (1979). Red and photographic infrared linear combinations for monitoring vegetation. Remote Sensing of Environment, Vol. 8, 127-150.

US Agency for International Development (1973). Techniques for assessing hydrological potentials in Developing Countries. US AID, Washington D.C., Report No. 215149.

US Army Corps of Engineers (1976). Urban storm water runoff, "STORM". Computer program 723-L2520, Hydrologic Engineering Center, Davis, CA.

US Army Constr. Eng. Res. Lab. (1988). Geographical Resource Analysis Support System (GRASS) reference manual. Campaign III.

US Department of Agriculture, (1972). Soil Conservation Service. National Engineering Handbook, section 4, Hydrology US Government Printing Office, Washington DC.

USDA (1986). US Department of Agriculture Soil Conservation Service. Urban hydrology for small watersheds. Tech. Release 55(210-VI-TR-55), 2nd Edition.

Verstappen, H.Th., (1977). Remote Sensing in Geomorphology. Elsevier, Amsterdam.

Verstappen, H.Th., (1983). Applied Geomorphology. Elsevier.

Vicary, C. (1987). Remote sensing and its potential for hydrological modelling. Final year undergraduate project, Aston University, Civil Engineering Dept.

Vieux, B.E., Bralts, V.F, Kittleson, K. (1986). Hydrologic modelling using remote sensing and Geographic Information Systems and the Finite Element Method. Proc. 20th Int. Symp. on Remote Sensing of Environment, Nairobi, Kenya, 4-10 Dec. 20pp.

Walsh, S.J., Cooper, J.W., Essen, I.E., Gallager, K.R. (1990). Image enhancement of Landsat Thematic Mapper Data and GIS data integration for evaluation of resource characteristics. Photogr. Eng. and Remote Sensing, Vol. 56, No.8, 1135-1141.

Ward, R.C. (1975). Principles of Hydrology 2nd Edn. McGraw-Hill.

White, L.P. (1977). Aerial photography and remote sensing for soil survey. Clarendon press.

Wiltshire, S.E., Hewson, A.D. (1983). A conversion factor for stream frquency derived from Second series 1:25000 scale maps. Institue of Hydrology, Wallingford, Oxon, Report No. 84.

WMO (1975). Intercomparison of conceptual models used in operational hydrological forecasting. WMO Operational Hydrology Report No. 7.

Wood, E.F., O'Connell, P.E. (1985). Real-time forecasting, in Hydrological Forecasting (Anderson, M.G., Burt, T.P. (1985)(Eds.)). Wiley & Sons, Chichester, UK. 505-558.

Zevenbergen, A.W., Rango, A., Ritchie, J.C., Engman, E.T., Hawkins, R.H. (1988). Rangeland runoff curve numbers as determined from Landsat MSS data. Int. Jour. Rem. Sens. Vol. 9, No. 3, 495-502.

Zuidam, R.A. (1985). Aerial Photo-Interpretation in Terrain Analysis and Geomorphologic Mapping. ITC, Enschede, Netherlands. Publ. Smits, The Hague.

Appendix A Remote sensing parameter requirements for hydrology

1. Salomonson et al. (1975)

TABLE 2. SUMMARY OF SENSITIVITY ANALYSIS RESULTS AND REMOTE SENSING REQUIREMENTS

(1)	(2) TOWN CREEK, ALABAMA WATERSHED (365 KM^2)		(3) ALAMOSA CREEK, COLORADO WATERSHED (277 KM^2)		(4)	(5)
WATERSHED MODEL INPUT PARAMETER	REFERENCE VALUE	INPUT VARIATION GIVING ± 5% VARIATION IN RUNOFF	REFERENCE VALUE	INPUT VARIATION GIVING ± 5% VARIATION IN RUNOFF	REMOTE SENSING CAPABILITY REQUIRED FOR 40 KM^2 WATERSHED	REMARKS
Fraction of Impervious Area (FIMP)	36.5 KM^2	± 20%	27.7 KM^2	± 10%	0.4-0.8 KM^2 Area 130-180 Meter resolution	$e = \frac{rK}{\sqrt{A}}$ (Castruccio, 1974) r = Spatial resolution
Fraction of Water Surface Area (FWTR)	36.5 KM^2	± 20%	27.7 KM^2	± 10%	0.4-0.8 KM^2 Area 130-180 Meter resolution	A = Area K = Data processing factor = 0.5 e = Acceptable error, ± 10%
Forested Fraction of Watershed (FFOR)			0.40	±10%	± 0.04	Value applies during period with snow on ground (Winter-Spring)
Maximum Volume of Interception (VINTMR)	0.4 CM	Very Insensitive > ± 100%	0.4 CM	Very Insensitive -80% = +5% R.O.	Ability to distinguish grassland, moderate forest cover, and heavy forest cover	Appears possible with LANDSAT
Overland Flow Roughness Coefficient (OFMN)	0.05	± 40%	0.35	No sensitivity to storm runoff	Level II Land use	Some categories are possible with LANDSAT. High altitude aircraft data are applicable
Overland Flow Surface Length (OFSL)	473 M	± 40%	314 M	No sensitivity to storm runoff	± 10-20 Meters	High altitude aircraft or Skylab Earth Terrain Camera
Overland Flow Surface Slope (OFSS)	0.062	± 50%	0.34	No sensitivity to storm runoff	Percent slope, ± 3%	Stereo photography or radar altimetry
Fraction of Incident Radiation Reflected by Snow (FIRR)			0.60 (snow)	± 3.5%	± 2-3% Albedo	Requires anisotropy model and reflectance versus albedo relationships
Lower Zone Capacity – Soil Moisture (LZC)	10 CM	± 7-8%	15 CM	± 6-8%	± 1 CM or ± 7%	Microwave offers a possibility or thermal infrared
Precipitation			3-8 CM per storm	± 10%	± 0.3-0.8 CM	Cloud type identification or radar along with ground-based benchmark observations
Evaporation			50 CM/YR	± 20%	± 10 CM/YR	A heat balance approach or an empirical evaporation to land use and vegetation type, density and stress approach may be successful

2. Blyth (1981)

TABLE 4A TYPICAL MEASUREMENT REQUIREMENTS OF HYDROLOGICAL VARIABLES

Hydrological Element	*Resolution (metres)			Accuracy	Frequency		
	A	B	C				
DRAINAGE BASIN CHARACTERISTICS							
Drainage area	30	30	100	(±1% of watershed area)		(every 10 years)	
Channel dimensions and patterns	30	30	100	(±5% of length)		(every 5 years or after major flood event)	
Overland flow length	30	30	100	(±5% of length)		(every 5 years)	
Surface slope	30	30	100	(±5% hor. ±5 cm vert.)		(every 5 years)	
Land cover type	100	100	100	(±1% of watershed area)		(every year)	
Albedo	100	300	1,000	(5%)		(6 hourly)	
SURFACE WATER					A	B	C
Areal extent	10	30	100	(5%)	(daily)	(daily)	(4 days)
Saturated soil area	10	30	100	(5%)	(daily)	(daily)	(4 days)
Flood extent	10	30	100	(5%)	(1 hour)	(12 hrs)	(1 day)
Flood plain boundaries	10	10	10	(5%)	(5 yrs) (& after major flood events)	(5 yrs)	(5 yrs)
Lake or river stage	-	-	-	±1 cm	(10 min) (30 min)	(15 min) (1 hour)	(1 hr) (4 hrs)
WATER QUALITY							
Turbidity	30	100	1,000	(±0.5 FTU)		(daily)	
Suspended sediment	30	100	1,000	(±10 ppm)		(daily)	
Colour	30	100	1,000	(±10 mg Pt/1)		(daily)	
Aglae bloom	30	100	1,000	-		(2-3 days)	
Surface film detection	30	100	1,000	-		(daily)	
Surface water temperature	30	100	1,000	(±0.03°C in 0-1° range) ±0.1°C in 1-4 range otherwise ±1°C)		(6 hours)	
Temperature profile	-	1,000	10,000	(±0.25°C)		(2-3 days)	
PRECIPITATION	100	1,000	5,000	±2 mm if <40mm ±5% if > 40 mm		6-hourly	
EVAPORATION OR EVAPOTRANSPIRATION	100	1,000	5,000	±0.5 mm		daily	

* Estimates for drainage basins of the following sizes:-

A - < 100 km^2

B - 100 - 1,000 km^2

C - >1,000 km^2

TABLE 4B TYPICAL MEASUREMENT REQUIREMENTS OF HYDROLOGICAL VARIABLES

Hydrological Element	*Resolution			Accuracy	Frequency
	A	B	C		
SNOW					-
Snowline	30	100	1,000	-	(Daily)
Snow cover	300	1,000	10,000	(± 5% of snow area)	(Daily)
Water equivalent	100	300	1,000)	± 2 mm if <2cm	Daily
Free water content	100	300	1,000)	±10% if >2cm	
Snow surface temperature	100	300	1,000	+ 1°C	(6-hourly)
Surface albedo	100	300	1,000	(5%)	(6-hourly)
GROUNDWATER DETECTION					
Aquifer mapping	100	100	100	-	(5 years)
Location of discharge to rivers	30	30	30	-	(weekly)
Location of discharge to lakes	100	100	100	-	(weekly)
Location of springs	30	30	30	-	(5 years)
GROUNDWATER LEVEL	300	1,000	1,000	(1 cm)	(daily)
SOIL TYPE	100	1,000	1,000	-	(5 years)
UNSATURATED ZONE					
Moisture content profile	100	300	1,000	10% of field capacity	(daily)
Temperature profile	100	300	1,000	(0.5°C)	(daily)
Infiltration/Percolation	100	300	1,000	(10%)	(daily)
Depth of seasonal frost	100	300	1,000	(10%)	(weekly)

* Estimates for drainage basins of the following sizes:-

A - < 100 km^2
B - 100 - 1,000 km^2
C - >1000 km^2

TABLE 4C DATA REQUIREMENTS FOR LARGE SCALE ATMOSPHERIC WATER BALANCE ESTIMATION

Hydrological Element	Resolution	Accuracy	Frequency
Precipitation	100 km	± 2 mm if < 40 mm ± 5% if > 40 mm	6-hourly
Evaporation, Evapo transpiration	100 km	(± 5%)	(6-hourly)
Atmospheric Moisture Storage	100 km	(± 5%)	(6-hourly)
Atmospheric Moisture Flux divergence	100 km	(± 5%)	(6-hourly)

3. Barrett and Herschy (1985)

TABLE 2: Hydrological and water management observational requirements
(summary giving main headings of table in Final Report)

PARAMETER	RESOLUTION			FREQUENCY			ACCURACY		
	MAX	MIN	OPT	MAX	MIN	OPT	MAX	MIN	OPT
A Precipitation	100m	$\boxed{\text{10km}}$	1km	5min	$\boxed{\text{1M}}$	$\boxed{\text{1h}}$	10%	30%	20%
B Snow depth	30m	$\boxed{\text{10km}}$	1km	12h	$\boxed{\text{1M}}$	$\boxed{\text{24h}}$	2cm	$\boxed{\text{10cm}}$	$\boxed{\text{5cm}}$
C Ice cover	10m	$\boxed{\text{1km}}$	25m	$\underline{\text{12h}}$	$\boxed{\text{7d}}$	$\underline{\text{24h}}$	1%	$\boxed{\text{20\%}}$	$\boxed{\text{10\%}}$
D Glaciers -dimensions	$\boxed{\text{10m}}$	$\boxed{\text{500m}}$	$\boxed{\text{25m}}$	$\boxed{\text{1y}}$	$\boxed{\text{10y}}$	$\boxed{\text{2y}}$	$\underline{\text{1\%}}$	$\boxed{\text{5\%}}$	$\boxed{\text{2\%}}$
E Surface water areal extent	10m	$\boxed{\text{100m}}$	30m	12h	$\boxed{\text{7d}}$	24h	1%	5%	3%
F Groundwater -aquifer maps	50m	1km	100m	1y	5y	3y	5m	30m	10m
G Evaporation	$\underline{\text{100m}}$	$\boxed{\text{10km}}$	$\boxed{\text{1km}}$	$\boxed{\text{12h}}$	$\boxed{\text{10d}}$	$\boxed{\text{1d}}$	$\underline{\text{10\%}}$	$\boxed{\text{30\%}}$	$\boxed{\text{20\%}}$
H Water quality -turbidity	$\underline{\text{30m}}$	$\boxed{\text{300m}}$	$\underline{\text{100m}}$	$\underline{\text{3h}}$	$\boxed{\text{24h}}$	$\underline{\text{6h}}$	$\underline{\text{10\%}}$	$\boxed{\text{50\%}}$	$\boxed{\text{20\%}}$
I Drainage -drainage area	10m	$\boxed{\text{100m}}$	$\underline{\text{20m}}$	$\boxed{\text{3y}}$	$\boxed{\text{10y}}$	$\boxed{\text{5y}}$	0.1%	1%	0.5%

LEGEND

FREQUENCY: h = hour; d = day; M = month, y = year.

FEASIBILITY $\boxed{}$ = Requirement can be generally met by existing satellite(s)

$\underline{}$ = Requirement should be generally met by near future satellite(s)

Note: where a value is neither boxed nor underlined the observational requirement cannot generally be met either by existing or firmly expected future satellites, given the present state of the art.

Appendix B Sample Landsat Processing data

```
****  THEMATIC MAPPER CCT REPORT  ****

==========================================

== LANDSAT  5  TRACK- 193  FRAME 29 QUADRANT  1        == PRODUCT                               BSQ   6250
== SCENE ACQUIRED AT- FUCINO-ON       86  7  15        == PROCESSED AT ITA - FUCINO ON          88   3  30
== INPUT SCENE CENTRE LAT            44.6166538        == PROCESSED SCENE CENTRE LAT        45.3244973
== INPUT SCENE CENTRE LON             9.8723578        == PROCESSED SCENE CENTRE LON         9.5710053
== SOFTWARE RELEASE-NUMBER         TMFR-CCT-012

              ** RADIOMETRIC SENSOR CALIBRATION APPLIED **

== INTERNAL CALIBRATION SOURCE              N          == PRE-FLIGHT DATA                              Y
== HISTOGRAM EQUALIZATION                   N          == SUN ELEVATION CORRECTION                     N

                  ** GEOMETRIC CORRECTIONS APPLIED **

== FORWARD/REVERSE ALIGNMENT                Y          == DETECTOR PLACEMENT AND DELAY                 Y
== MIRROR SCAN PROFILE                      Y          == LINE LENGTH INFORMATION                      Y
== GYRO DATA                                Y          == ANGULAR DISPLACEMENT SENSOR (ADS) DATA       Y
== ATTITUDE CORRECTION SYSTEM (ACS) DATA    Y          == EPHEMERIS DATA                               Y
== SCAN GAP                                 Y          == EARTH ROTATION                               Y
== SENSOR ALTITUDE AND PANORAMIC DISTORTION Y          == PCD USED FOR CORRECTION                      Y

                  ** RESAMPLING ALGORITHM APPLIED **

== TWO-DIMENSIONAL RESAMPLING               Y          == RESAMPLING ALGORITHM CODE  NEAREST NEIGHBOUR
```

Appendix C Geocorrection statistics

1. Landsat TM

Minimum Vector:

55.000	17.000	12.000
8.000	5.000	.000

Maximum Vector:

254.000	218.000	251.000
217.000	254.000	172.000

Mean Vector:

69.419	29.255	25.906
88.245	72.297	25.091

Standard Deviations:

16.225	9.475	11.829
21.605	24.024	11.401

Covariance Matrix for 6 bands:

1	263.251
	147.792
	183.738
	88.466
	231.937
	142.022
2	147.792
	89.783
	109.733
	73.142
	154.595
	88.670
3	183.738
	109.733
	139.931
	59.764
	195.021
	115.578
4	88.466
	73.142
	59.764
	466.767
	278.542
	75.575
5	231.937
	154.595
	195.021
	278.542
	577.131
	250.456
6	142.022
	88.670
	115.578
	75.575
	250.456
	129.992

Correlation Matrix for 6 bands:

	1	1.000	.961	.957	.252	.595	.768
	2	.961	1.000	.979	.357	.679	.821
	3	.957	.979	1.000	.234	.686	.857
	4	.252	.357	.234	1.000	.537	.307
2.	5	.595	.679	.686	.537	1.000	.914
	6	.768	.821	.857	.307	.914	1.000

Eigen Values Eigen Vectors:

.679	-.374	-.238	-.289	-.418	-.672	-.307
.219	.392	.182	.301	-.826	.011	.200
.094	-.541	-.269	-.249	-.356	.644	.177
.005	.615	-.370	-.512	-.070	.237	-.402
.002	.186	-.301	-.344	.091	-.279	.819
.001	-.029	.781	-.619	-.057	.019	.046

2. Landsat MSS

Minimum Vector:

1.000 .000 2.000
.000

Maximum Vector:

101.000 122.000 127.000
56.000

Mean Vector:

22.349 22.919 55.006
28.392

Standard Deviations:

2.969 4.380 13.422
8.408

Covariance Matrix for 4 bands:

1	8.814
	10.065
	9.968
	4.622
2	10.065
	19.184
	16.743
	7.869
3	9.968
	16.743
	180.140
	111.019
4	4.622
	7.869
	111.019
	70.700

Correlation Matrix for 4 bands:

1	1.000	.774	.250	.185
2	.774	1.000	.285	.214
3	.250	.285	1.000	.984
4	.185	.214	.984	1.000

Eigen Values Eigen Vectors:

.901	-.048	-.081	-.846	-.525
.085	-.516	-.844	.019	.147
.010	.852	-.523	.007	-.010
.005	.070	.091	-.533	.838

Appendix D Landsat TM and Landsat MSS data statistics

1. Landsat TM

Control Point Statistics

Order Index of Mapping is 1

#	Output Control Points		Input Control Points		Predicted Input Points	
1	331.763	271.221	121.938	54.938	120.944	54.997
2	319.209	271.682	244.938	454.063	244.670	453.785
3	323.499	267.863	84.063	349.063	84.739	349.207
4	316.682	276.634	425.938	491.938	425.694	491.942
5	329.239	277.136	331.938	85.063	332.873	84.769
6	323.563	278.463	425.063	255.063	424.774	255.372
7	323.764	272.681	237.063	298.938	237.243	298.990

#	Coordinate Error		Point RMS error
1	-.993	.060	.995
2	-.268	-.277	.386
3	.676	.144	.691
4	-.243	.005	.243
5	.936	-.293	.981
6	-.289	.310	.423
7	.181	.053	.188
Maximum Errors:	.993	.310	.995
Signed Mean:	.000	.000	.558
Absolute Mean:	.512	.163	.558
RMS Error:	.605	.202	.638

2. Landsat MSS

Control Point Statistics

Order Index of Mapping is 1

#	Output Control Points		Input Control Points		Predicted Input Point	
1	130.000	119.000	115.000	210.000	115.001	210.106
2	97.000	230.000	118.000	282.000	118.094	282.155
3	212.000	291.000	229.000	298.000	228.900	297.783
4	337.000	128.000	287.000	178.000	287.084	178.201
5	206.000	44.000	157.000	152.000	156.921	151.756

#	Coordinate Error		Point RMS error
1	.001	.106	.106
2	.094	.155	.182
3	-.100	-.217	.239
4	.084	.201	.217
5	-.079	-.244	.257
Maximum Errors:	.100	.244	.257
Signed Mean:	-.000	.000	.200
Absolute Mean:	.072	.185	.200
RMS Error:	.080	.191	.207

Display image dec deleted
Display image fc deleted